

Polymer-Immobilised Ionic Liquid Phase: Designing New Tools for Catalysis

Jack Robert Ellison



A thesis submitted for the degree of
Doctor of Philosophy in Chemistry

School of Chemistry
Newcastle University
September 2015

DECLARATION

This thesis is submitted to Newcastle University for the degree of Doctor of Philosophy. The research detailed within was performed between the years 2011-2014 and was conducted in Newcastle University laboratories under the supervision of Dr Simon Doherty and Dr Julian G. Knight. I certify that all material is original except where acknowledged by reference and that none of the material offered in this thesis has been previously submitted by me for a degree or any other qualification at this or any other university.

ABSTRACT OF THE DISSERTATION

Ionic liquids (ILs) have been paid particular interest in the field of catalysis over the past 2 decades, offering not only enhancements in catalyst performance but also the ability to heterogenise molecular species and effectively combine the benefits homogenous and heterogeneous catalysis. Although advantageous, significant limitations remain, particularly with respects to leaching and mass transport. As a result the heterogenisation of IL moieties, in the form of the Supported Ionic Liquid Phase (SILP), has been widely investigated to avoid these issues. By extension of the SILP concept, polymer materials can offer additional benefits through the well-defined, controllable nature of polymer chemistry. The work presented herein focuses on the application of pre-fabricated ionic liquid tagged monomers to prepare well-defined polymer supports under mild, controllable conditions, termed the Polymer Immobilised Ionic Liquid Phase (PIILP). These well-defined materials were then used to support various homogeneous catalytic species as a means to give highly active, recyclable systems which effectively combine the positive aspects of homogeneous and heterogeneous catalysis with the enhancement effects associated with ionic liquids. Chapter 1 discusses the use of ionic liquids, SILP and PIILP-type systems in catalysis across the literature, before briefly assessing common polymerisation methods in order to determine the most suitable means to prepare PIILP materials. The initial evaluation of the PIILP methodology is discussed in chapter 2, wherein a linear pyrrolidinium-functionalised support was prepared by ring-opening metathesis polymerisation (ROMP). The resulting material was used to immobilise a peroxophosphotungstate species to give a heterogeneous catalyst which was highly active in epoxidation, alcohol oxidation and sulfoxidation reactions under relatively mild conditions with H_2O_2 as the oxidant. Chapter 3 discusses the implementation of the PIILP-catalysed sulfoxidation chemistry under continuous flow conditions, with the promising performance highlighting the potential application of PIILP in the preparation of pharmaceutical intermediates and in the purification of crude oil. In chapter 4 cross-linked polystyrene-based PIILP materials are shown to be effective supports in asymmetric Diels-Alder and Mukaiyama-Aldol reactions, with PIILP supports giving enhancements in *ee* compared to analogous IL and SILP systems. Similarly, in chapter 5 polystyrene-based supports are effectively used to immobilise Pd nanoparticles whilst also investigating the effect of heteroatom donating co-monomers. Although moderately promising catalytic performance was observed in a range of Suzuki Miyaura couplings, no clear trends with regards to nanoparticle size and catalyst performance were noted. The results obtained throughout this thesis highlight the vast potential of the PIILP methodology in heterogeneous catalysis, however the incredibly complex nature of the relationship between the catalyst, support and substrate makes it difficult to fully rationalise performance trends. As such, further, more extensive studies into the support properties will be required to realise PIILP to its fullest potential.

ACKNOWLEDGEMENTS

First and foremost, I would like to thank Dr Simon Doherty for his constant supervision, guidance and support both in and out of the lab throughout the past years, ensuring that the project goes as smoothly and productively as possible.

Dr Julian Knight for providing advice when all other sources of knowledge seem to fail and for ensuring that I both continue to learn and do not forget what I already know through his problem solving sessions in group meetings.

I would also like to thank my past colleagues, Hamid Mehdi-Zodeh and Nico Ward for their help whilst starting out and Ashley Clemmet and Einas Abood who were also working on PIILP at different stages throughout my time in Newcastle.

Dr Michael Carroll for allowing us use of his FlowSyn apparatus, without which chapter 3 would not have been possible, as well as all the MAC group for their help getting set up on the system.

Prof Chris Hardacre, Dr Pete Goodrich and Dr Leanne Hall at Queen's University Belfast for their work throughout our collaboration providing characterisation of the polymers and supported catalyst and, in particular, for their contributions to chapter 4.

Prof Ian Fairlamb and his research group for offering advice regarding nanoparticle chemistry as well as allowing the use of their characterisation apparatus.

I of course owe many thanks to all my friends and family for their support over the past 4 years, in particular my ever patient girlfriend Natalie for tolerating me during the writing up process.

TABLE OF CONTENTS

Chapter 1: Ionic Liquid, Supported Ionic Liquid and Polymer-Immobilised Ionic Liquid Phase Catalysis

Table of Contents	2
2.1. Abstract	3
2.2. Introduction	3
2.3. Ionic Liquids	4
2.4. Supported Ionic Liquid Phase Catalysis	18
2.5. Polymer-Immobilised Ionic Liquid Phase Catalysis	23
2.6. Polymerisation Methods	26
2.6.1. <i>Step Polymerisation</i>	27
2.6.2. <i>Radical Polymerisation</i>	28
2.6.3. <i>Living Radical Polymerisation</i>	31
2.6.4. <i>Ionic Polymerisation</i>	34
2.6.5. <i>Ring-Opening Polymerisation</i>	37
2.7. Conclusions	39
2.8. References	40

Chapter 2: PIILP Tungsten-based Polyoxometalate Oxidation Catalysis

Table of Contents	48
2.1. Abstract	49
2.2. Introduction	49
2.3. Results and Discussion	51
2.3.1. <i>Polymer and Catalyst Design and Synthesis</i>	51
2.3.2. <i>Epoxidation Catalysis</i>	59
2.3.3. <i>Alcohol Oxidation Catalysis</i>	63
2.3.4. <i>Sulfoxidation Catalysis</i>	65
2.3.5. <i>Polymer Support Comparisons</i>	69
2.3.6. <i>Ionic Liquid Functionality Comparisons</i>	75
2.4. Conclusions	79
2.5. Experimental	81
2.6. References	93

Chapter 3: PIILP Continuous Flow Oxidation Chemistry

Table of Contents	98
3.1. Abstract	99
3.2. Introduction	99
3.3. Results and Discussion	101
3.3.1. <i>Batch Optimisation</i>	101
3.3.2. <i>Segmented Flow Experiments</i>	105
3.3.3. <i>Continuous Flow, Scale Up and Sequential Reactions</i>	114
3.4. Conclusions	119
3.5. Experimental	121
3.6. References	124

Chapter 4: PIILP Lewis Acid Catalysed Carbon-Carbon Bond Formation

Table of Contents	128
4.1. Abstract	129
4.2. Introduction	129
4.3. Results and Discussion	130
4.3.1. <i>Polymer and Catalyst Synthesis</i>	130
4.3.2. <i>Copper Bis(oxazoline) Catalysed Diels-Alder Reactions</i>	132
4.3.3. <i>Copper Bis(oxazoline) Catalysed Mukaiyama-aldol Reactions</i>	140
4.4. Conclusions	142
4.5. Experimental	144
4.6. References	151

Chapter 5: PIILP Palladium Nanoparticle Catalysed Carbon-Carbon Bond Formation

Table of Contents	155
5.1. Abstract	156
5.2. Introduction	156
5.3. Results and Discussion	160
5.3.1. <i>Polymer Design and Synthesis</i>	160
5.3.2. <i>Suzuki-Miyaura Cross-Couplings</i>	171
5.4. Conclusions	185
5.5. Experimental	187
5.6. References	197

Appendices

A.1. Segmented Flow Oxidation of Thioanisole with Varying H ₂ O ₂ Concentrations	203
A.2. Kinetic Plots for the Oxidation of Thioanisole Using 20 Equivalents of H ₂ O ₂ at 30°C	206
A.3. Conversion-Selectivity Profiles for Segmented Flow Sulfoxidations	207
A.4. Kinetic Plots for PIILP Catalysed Suzuki Miyaura Cross-Couplings	210

LIST OF FIGURES

Chapter 1: Ionic Liquid, Supported Ionic Liquid Phase and Polymer-Immobilised Ionic Liquid Phase Catalysis

- Figure 1.1* Number of articles in the field of chemistry with “ionic liquids” as the topic (Source: Web of Science 21/11/2014)
- Figure 1.2* Commonly used cations and anions for ionic liquids
- Figure 1.3* Representation of the different types of interactions present in imidazolium-based ILs reported by Olivier-Bourbigou *et al*
- Figure 1.4* An ideal IL-based liquid-liquid biphasic catalytic system
- Figure 1.5* Imidazolium-tagged and untagged bis(oxazoline) ligands used in asymmetric Diels-Alder reactions
- Figure 1.6* Example schematic of continuous flow homogeneous catalysis using a scCO₂-IL biphasic system
- Figure 1.7* Schematic representation of Supported Ionic Liquid Phase (SILP) for catalysis
- Figure 1.8* Illustration of the four main categories of SILP-based catalyst materials: A) immersion method; B) and C) covalent anchoring methods; D) solid catalyst with ionic liquid layer
- Figure 1.9* Surface functionalization of CNT materials with imidazolium-based IL fragments used by Serp *et al* in the immobilisation of Rh hydrogenation catalysts
- Figure 1.10* Examples of functionalised polymers used as catalyst supports taken from the literature
- Figure 1.11* Common commercially available ion-exchange resins
- Figure 1.12* Basic principle behind Polymer-Immobilised Ionic Liquid Phase (PIILP) catalysts
- Figure 1.13* Examples of PILs prepared through step growth polymerisation methods
- Figure 1.14* General Schrock-type and 1st and 2nd generation Grubbs catalysts

Chapter 2: PIILP Tungsten-based Polyoxometalate Oxidation Catalysis

- Figure 2.1* Hydrogen peroxide-mediate degradation of the Keggin structure phosphotungstic acid to give the corresponding Venturello peroxometalate
- Figure 2.2* Poly(ethylene oxide-pyridinium) matrix developed by Yamada *et al* for the immobilisation of phosphotungstic acid

- Figure 2.3* Imidazolium mesylate-functionalised homopolymer prepared by Dyson *et al* through ROMP used as a support for active gold nanoparticle catalysts
- Figure 2.4* Molecular structure of **2.4** confirming the stereochemistry of initial cycloaddition. Hydrogen atoms, the water molecule of crystallisation and the bromide counterion have been removed for clarity
- Figure 2.5* Different modes of catalyst deactivation associated with the ring-opening metathesis polymerisation of *endo*-substituted norbornene monomers illustrated using **2.4**
- Figure 2.6* TGA and DSC curves for IP-**2.1** taken with a heating rate of 5 °C min⁻¹
- Figure 2.7* Solid state ³¹P NMR spectrum of POM-**2.1** and corresponding assignments in agreement with work conducted by Hill and co-workers
- Figure 2.8* High resolution transmission electron spectroscopy images of prepared catalyst POM-**2.1**
- Figure 2.9* Conversions with respect to time for successive hydrogen peroxide-mediated epoxidations of *cis*-cyclooctene using recycled POM-**2.1**
- Figure 2.10* High resolution transmission electron microscopy images of POM-**2.1** taken after 4th recycle
- Figure 2.11* Solid state ³¹P NMR spectrum of POM-**2.1** taken after 4th recycle
- Figure 2.12* TGA curve for POM-**2.1** taken with a heating rate of 10 °C min⁻¹
- Figure 2.13* Conversion and sulfoxide selectivity profiles as a function of subsequent catalyst recycles for the oxidation of thioanisole with 2.5 equivalents of hydrogen peroxide catalysed by POM-**2.1**
- Figure 2.14* IPs **2.2 – 2.5** used to investigate the effect of different polymer support structure on catalyst performance in H₂O₂-mediated oxidations. In each case the ionic loading (mmol g⁻¹) is shown
- Figure 2.15* TGA curve for POM-**2.5** taken with a heating rate of 10 °C min⁻¹
- Figure 2.16* Polystyrene-based IPs **2.5 – 2.8** used to illustrate the effect of IL group functionality on catalyst performance in H₂O₂-mediated sulfoxidations. In each case the ionic loading (mmol g⁻¹) is shown
- Figure 2.17* Conversion and selectivity profiles for the oxidation of various sulfides catalysed by POM-**2.5 – 2.8** under reaction conditions outlined in tables 2.5 and 2.8
- Figure 2.18* Graphical summary of the performance of POM-**2.1** in the H₂O₂-mediated oxidation of aryl alkyl sulfides in MeCN and MeOH solvents

Chapter 3: PIILP Continuous Flow Oxidation Chemistry

- Figure 3.1* Representation of the increasing surface area to volume ratio present in microfluidic systems
- Figure 3.2* Influence of reaction conditions on the selectivity for methyl phenyl sulfone in the hydrogen peroxide-mediated oxidation of thioanisole catalysed by 0.5 mol% POM-**2.1**. Influence of (a) temperature at a reaction time of 15 min (b) reaction time at 45 °C. Reaction conditions: 1 mmol thioanisole, 5 mmol 35% H₂O₂, 3 mL solvent.
- Figure 3.3* PIILP-immobilised peroxometalate catalyst POM-**2.1**
- Figure 3.4* Schematic representation of the Uniqsis FlowSyn set-up used in the segmented and continuous flow sulfoxidation reactions catalysed by a cartridge of POM-**2.1** mixed in silica
- Figure 3.5* Schematic representation of the modes of mixing observed in segmented and continuous laminar flow conditions
- Figure 3.6* Conversion-selectivity profile as a function of reaction temperature in the segmented flow oxidation of thioanisole catalysed by POM-**2.1** in MeCN and MeOH solvents
- Figure 3.7* Conversion-selectivity profile as a function of residence time (Rt) in the segmented flow oxidation of thioanisole catalysed by POM-**2.1** in MeCN and MeOH solvents
- Figure 3.8* Equations 1-5 used to estimate rate constants through pseudo steady state analysis for consecutive elementary reactions
- Figure 3.9* Kinetic plots obtained through equations 1-3 for the oxidation of thioanisole with 12 eq H₂O₂ in MeCN and MeOH
- Figure 3.10* Comparison of the conversion-selectivity profiles obtained in the segmented flow oxidation reactions conducted in MeCN and MeOH with and without doping with an extra equivalent of H₂O
- Figure 3.11* Conversion-selectivity profile as a function of residence time for the segmented flow sulfoxidation of thioanisole in MeOH-H₂O (1 : 1, v/v) at 30 °C with 3 equivalents of H₂O₂ catalysed by POM-**2.1**
- Figure 3.12* Conversion-selectivity profile as a function time for an 8 hour continuous flow sulfoxidation of thioanisole catalysed by POM-**2.1** at 30 °C with a residence time of 4 minutes in (a) MeCN, (b) MeCN with replenishment of the H₂O₂ reagent stream after 4 hours (*), (c) MeOH and (d) MeOH with replenishment of the H₂O₂ reagent stream after 4 hours (*)
- Figure 3.13* Conversion-selectivity profile as a function time for an 8 hour continuous flow sulfoxidation of thioanisole catalysed by POM-TBA at 30 °C with a residence time of 4 minutes in (a) MeCN and (b) MeOH with replenishment of the H₂O₂ reagent stream after 4 hours (*)
- Figure 3.14* (a) Conversion-selectivity profile at residence times of 5 and 15 minutes for segmented flow POM-**2.1** catalysed consecutive sulfoxidation of three different

substrates using the same catalyst cartridge. (b) Conversion-selectivity profile at residence times of 5 and 15 minutes for segmented flow POM-2.1 catalysed consecutive sulfoxidation of three different substrates using fresh catalyst

Figure 3.15 Proposed continuous flow setup for the PIILP catalysed oxidative desulfurization of crude oils

Chapter 4: PIILP Lewis Acid Catalysed Carbon-Carbon Bond Formation

Figure 4.1 IPs 4.2-4.5 used in the immobilisation of Cu(II)-bis(oxazoline) catalysts for the asymmetric Diels-Alder reaction. In each case the degree of cross-linking and ionic loading (mmol g^{-1}) is shown

Figure 4.2 The commercially available IPs 4.6 and 4.7 used in the immobilisation of Cu(II)-bis(oxazoline) catalysts for the asymmetric Diels-Alder reaction. In each case the degree of cross-linking and ionic loading (mmol g^{-1}) is shown

Figure 4.3 Possible geometries of catalyst B based on those proposed by G. Desimoni *et al.* for Mg(II) bis(oxazoline) complexes

Figure 4.4 IR spectrum of IP-4.2, IP-4.2-catalyst A, and IP-4.2-catalyst A after use in a Diels-Alder reaction

Figure 4.5 Proposed structures of potential PEG-functionalised cationic monomers based on compounds 2.4 and 2.8

Chapter 5: PIILP Palladium Nanoparticle Catalysed Carbon-Carbon Bond Formation

Figure 5.1 Schematic representation of Ostwald ripening

Figure 5.2 Schematic representation of the stabilisation of metal nanoparticles using different types of protective groups: (A) ligands; (B) ionic species such as salts or surfactants; and (C) polymers

Figure 5.3 Chromatogram obtained at a wavelength of 254 nm for the SEC conducted on a sample of IP-5.2. Unreacted monomer was observed in the fractions taken around the 300 mL mark and after 400 mL

Figure 5.4 Solid state ^{13}C NMR spectra for (a) IP-5.2 and (b) IP-5.2-PdCl₄. Signals corresponding to CH₂-CN highlighted for clarity. A shift downfield from 23.753 to 24.218 ppm was observed upon the introduction of Pd

Figure 5.5 XPS spectra and corresponding peak fits for (a) IP-5.1-Pd⁰ and (b) IP-5.2-Pd⁰, assignments based on those recently published by Lemke *et al*

Figure 5.6 TEM images and corresponding size distributions for IP-5.1-Pd⁰ ((a) to (c)) and IP-5.2-Pd⁰ ((d) to (f))

- Figure 5.7* TEM image and corresponding nanoparticle size distribution for IP-5.1-Pd⁰ taken after catalysis in the Suzuki coupling of 3-bromonitrobenzene and phenylboronic acid
- Figure 5.8* Mechanism of the Pd nanoparticle-catalysed Suzuki cross-coupling involving both homogeneous and heterogeneous pathways proposed by Pérez-Lorenzo
- Figure 5.9* TEM images and corresponding size distribution for nanoparticles generated from IP-5.1-PdCl₄ ((a) and (c)) and IP-5.2-PdCl₄ ((b) and (d)) in the presence of phenylboronic acid under catalytic conditions
- Figure 5.10* Effect of (a) solvent volume and (b) catalyst loading on the Suzuki Miyaura coupling of 4-bromotoluene with phenylboronic acid catalysed by IP-5.1-Pd⁰ and IP-5.1-PdCl₄
- Figure 5.11* Reaction profiles for the Suzuki Miyaura coupling of (a) 2-bromotoluene and (b) 4-bromobenzonitrile with phenylboronic acid catalysed by IP-5.1-Pd⁰ and IP-5.1-PdCl₄
- Figure 5.12* Effect of stirring the catalyst with Hg poison before reaction for the Suzuki coupling of 4-bromotoluene with phenylboronic acid catalysed by IP-5.1-Pd⁰ and IP-5.1-PdCl₄, results obtained without Hg are shown for reference

LIST OF TABLES

Chapter 1: Ionic Liquid, Supported Ionic Liquid Phase and Polymer-Immobilised Ionic Liquid Phase Catalysis

<i>Table 1.1</i>	General comparison of organic solvents with ionic liquids outlined by Plechkova and Seddon
------------------	--

Chapter 2: PIILP Tungsten-based Polyoxometalate Oxidation Catalysis

<i>Table 2.1</i>	Comparison of the relative reactivities of different transition metal carbene metathesis catalysts
<i>Table 2.2</i>	Epoxidation of allylic alcohols and alkenes with hydrogen peroxide in acetonitrile catalysed by POM-2.1 and POM-TBA
<i>Table 2.3</i>	Oxidation of aliphatic alcohols to corresponding carbonyls with hydrogen peroxide in acetonitrile catalysed by POM-2.1
<i>Table 2.4</i>	Oxidation of thioanisole catalysed by POM-2.1 with varying equivalents of H ₂ O ₂
<i>Table 2.5</i>	Selective oxidation of sulfides to sulfoxides with hydrogen peroxide catalysed by POM-2.1
<i>Table 2.6</i>	Conversion and sulfoxide selectivity values obtained for subsequent catalyst recycles in the oxidation of thioanisole in MeOH catalysed by POM-2.1
<i>Table 2.7</i>	Comparison of the catalytic performance of the different prepared PIILP catalysts in select hydrogen peroxide-mediated epoxidations, alcohol oxidations and sulfoxidations
<i>Table 2.8</i>	Selective oxidation of sulfides to sulfoxides with hydrogen peroxide catalysed by POM-2.1 and POM-2.5

Chapter 3: PIILP Continuous Flow Oxidation Chemistry

<i>Table 3.1</i>	Oxidation of thioanisole catalysed by POM-2.1 conducted in varying solvents
<i>Table 3.2</i>	Selective oxidation of sulfides to sulfones with hydrogen peroxide catalysed by POM-2.1
<i>Table 3.3</i>	Conversion and sulfoxide selectivity values obtained for subsequent catalyst recycles in the oxidation of thioanisole in MeOH catalysed by POM-2.1 and POM-TBA immobilised on silica
<i>Table 3.4</i>	Estimated rate constants for the formation of methyl phenyl sulfoxide (k_a) and methyl phenyl sulfone (k_b) in MeCN and MeOH
<i>Table 3.5</i>	Summary of the optimum sulfoxide and sulfone selectivity for the segmented flow oxidations of selected aryl sulfides catalysed by POM-2.1

Chapter 4: PIILP Lewis Acid Catalysed Carbon-Carbon Bond Formation

- Table 4.1* Comparison of the Diels-Alder reaction between *N*-acryloyloxazolidinone and cyclopentadiene catalysed by 10 mol% Cu(OTf)₂/bis(oxazoline) complexes in Et₂O, CH₂Cl₂ and [C₂mim][NTf₂] under homogeneous conditions and on SiO₂, CNT- and polystyrene-SILP under heterogeneous conditions
- Table 4.2* Comparison of the Diels-Alder reaction between *N*-acryloyloxazolidinone and cyclopentadiene catalysed by 10 mol% Cu(OTf)₂/bis(oxazoline) complexes immobilised onto a range of polymer supports and polymer-IL supports
- Table 4.3* Recycle of the Diels-Alder reaction between *N*-acryloyloxazolidinone and cyclopentadiene using catalyst **A** immobilised on IPs and SiO₂ with and without additional IL
- Table 4.4* Mukaiyama-aldol reaction between 1-phenyltrimethoxysilane and methylpyruvate using catalyst **A** under homogeneous, SILP and PIILP conditions

Chapter 5: PIILP Palladium Nanoparticle Catalysed Carbon-Carbon Bond Formations

- Table 5.1* Solvent effect in the Suzuki-Miyaura coupling of 4-bromoacetophenone and phenylboronic acid catalysed by IP-5.1-Pd⁰
- Table 5.2* Effect of water content in the IP-5.1-Pd⁰-catalysed Suzuki coupling of 4-bromoacetophenone and phenylboronic acid in EtOH
- Table 5.3* Effect of base in the IP-5.1-Pd⁰-catalysed Suzuki coupling of 4-bromoacetophenone and phenylboronic acid
- Table 5.4* Suzuki-Miyaura cross-couplings of arylbromides with phenylboronic acid catalysed by PIILP catalysts based on IP-5.1 and IP-5.2

LIST OF SCHEMES

Chapter 1: Ionic Liquid, Supported Ionic Liquid Phase and Polymer-Immobilised Ionic Liquid Phase Catalysis

- Scheme 1.1* General routes used to synthesise imidazolium-based ionic liquids
- Scheme 1.2* Proposed mechanism of formation of the active Ru species in the hydrogenation of arenes in the presence of [C₄mim][OTf] and water
- Scheme 1.3* Lewis acid-catalysed alkenylation of benzene with 1-phenyl-1-propyne and proposed ion exchange between the metal catalyst and [C₄mim][SbF₆] ionic liquid medium
- Scheme 1.4* Pd-catalysed Heck arylation to give a mixture of regioisomers
- Scheme 1.5* Lewis acid-catalysed Diels-Alder reaction between *N*-acryloyloxazolidinone and cyclopentadiene
- Scheme 1.6* Initiation, propagation, termination and disproportionation steps of free-radical polymerisation
- Scheme 1.7* Different modes of chain-transfer in free radical polymerisation
- Scheme 1.8* Basic representation of atom-transfer radical polymerisation (ATRP)
- Scheme 1.9* Reversible-addition-fragmentation chain-transfer (RAFT) process between a propagating polymer chain and a dithioester RAFT agent
- Scheme 1.10* Initiation steps in anionic polymerisations
- Scheme 1.11* Initiation with Lewis acids and Friedel-Crafts catalysts in cationic polymerisations
- Scheme 1.12* Termination and chain transfer steps in cationic polymerisations
- Scheme 1.13* General mechanism of ring-opening metathesis polymerisation (ROMP) catalysed by Grubbs Ru-carbene catalyst

Chapter 2: PIILP Tungsten-based Polyoxometalate Oxidation Catalysis

- Scheme 2.1* Catalytic cycle involved in Ring-Opening Metathesis Polymerisation (ROMP) facilitated by the Ru carbene Grubbs catalysts
- Scheme 2.2* Synthesis of the pyrrolidinium bromide-functionalised norbornene monomer **2.4**
- Scheme 2.3* Ring-Opening Metathesis Polymerisation of **2.4** and *cis*-cyclooctene catalysed by Grubbs 1st generation catalyst and subsequent removal of Ru end groups from polymer chains. Ionic loading (mmol g⁻¹) is shown

- Scheme 2.4* Mechanism for the epoxidation of allylic alcohols involving coordination to an adjacent tungsten centre modified from the mechanism proposed by Stapleton *et al*
- Scheme 2.5* Oxidation of thioanisole with hydrogen peroxide catalysed by POM-**2.1**
- Scheme 2.6* Synthesis of the imidazolium bromide-functionalised norbornene monomer **2.6**
- Scheme 2.7* Synthesis of the pyrrolidinium bromide-functionalised styrene monomer **2.8** and subsequent free radical initiated polymerisation to give IP-**2.5**

Chapter 4: PIILP Lewis Acid Catalysed Carbon-Carbon Bond Formation

- Scheme 4.1* Synthesis of norbornene-based ionic monomers and ring-opening metathesis polymerisation catalysed by Grubbs 2nd generation catalyst to yield IP-**4.1**, ionic loading (mmol g⁻¹) is shown
- Scheme 4.2* Synthesis of styrene-based ionic monomers **4.3.NTf₂** and **4.5.NTf₂**
- Scheme 4.3* Diels-Alder reaction between *N*-acryloyloxazolidinone and cyclopentadiene catalysed by 10 mol% Cu(OTf)₂/bis(oxazoline) complexes
- Scheme 4.4* Mukaiyama-aldol reaction between 1-phenyl-1-trimethylsiloxyethene and methyl pyruvate catalysed by 10 mol% Cu(OTf)₂/bis(oxazoline) complexes
- Scheme 4.5* Hydrolysis and subsequent Mukaiyama-aldol reaction of 1-phenyltrimethoxysilane to yield 3-hydroxy-1,3-diphenyl-butan-1-one by-product

Chapter 5: PIILP Palladium Nanoparticle Catalysed Carbon-Carbon Bond Formation

- Scheme 5.1* Representative Pd-catalysed cross-coupling reactions to form carbon-carbon bonds
- Scheme 5.2* Synthesis of the norbornene-based imidazolium chloride monomer **5.5**
- Scheme 5.3* Synthesis of the norbornene-based co-monomer **5.6** and cross-linker **5.8**
- Scheme 5.4* Synthesis of functionalised styrene monomers **5.4**, **5.5**, and **5.7** from 4-vinylbenzyl chloride
- Scheme 5.5* Free-radical initiated polymerisation of **5.4** with functionalised and unfunctionalised co-monomers to give the cross-linked polymers IP-**5.1** and IP-**5.2**
- Scheme 5.6* Pd-catalysed Suzuki-Miyaura cross-coupling between aryl halides and aryl boronic acids in the presence of base
- Scheme 5.7* Suzuki-Miyaura cross-coupling between 4-bromoacetophenone and phenylboronic acid catalysed by IP-**5.1**-Pd⁰

Scheme 5.8 Catalytic cycle for Pd-catalysed Suzuki-Miyaura cross-couplings, proceeding through transmetallation via (A) direct attack of hydroxide to the boronic acid, and (B) by generation of a PdOH complex

LIST OF SYMBOLS AND ABBREVIATIONS

ADMET	acyclic diene metathesis
AIBN	azobisisobutyronitrile
BET	Brunauer-Emmett-Teller
BINAP	2,2'-bis(diphenylphosphino)-1,1'-binaphthyl
bistriflimide (NTf ₂)	bis(trifluoromethane)sulfonimide
Box	bis(oxazoline)
C ₂ mim	1-ethyl-3-methylimidazolium
C ₄ mim	1-butyl-3-methylimidazolium
CNT	carbon nanotubes
Cy	cyclohexyl
dba	dibenzylideneacetone
DBT	dibenzothiophene
DMC	dimethylcarbonate
dppm	1,1-bis(diphenylphosphino)methane
DVB	divinylbenzene
ee	enantiomeric excess
EG	ethylene glycol
FT-IR	Fourier Transform InfraRed
GC-MS	Gas Chromatography Mass Spectrometry
GPC	Gel Permeation Chromatography
HOMO	highest occupied molecular orbital
HPA	heteropolyacid
HPLC	High Performance Liquid Chromatography
ICP-OES	Inductively Coupled Plasma Optical Emission Spectrometry
IL	Ionic Liquid
IP	Ionic Polymer
L _n	ligand
LUMO	lowest unoccupied molecular orbital
M _n	number average molecular weight
M _w	weight average molecular weight
NHC	N-heterocyclic carbene
NOESY	Nuclear Overhauser Effect Spectroscopy
NUPHOS	1,4-bis(diphenylphosphino)-1,3-butadiene
PC	propylene carbonate
PDI	polydispersity index
PEEK	polyether ether ketone
PEG	polyethylene glycol
PIILP	Polymer-Immobilised Ionic Liquid Phase
PIL	polyionic liquid
ppm	parts per million
PS	polystyrene
PVA	poly(vinyl alcohol)
PVP	poly(<i>N</i> -vinyl-2-pyrrolidone)
RAFT	Reversible addition-fragmentation chain-transfer
ROMP	Ring-Opening Metathesis Polymerisation
R _t	residence time
scCO ₂	super critical carbon dioxide
SEC	Size Exclusion Chromatography
SEM	Scanning Electron Microscopy

SILP	Supported Ionic Liquid Phase
TBA	tetrabutylammonium
TEM	Transmission Electron Microscopy
TGA-DSC	Thermal Gravimetric Analysis – Differential Scanning Calorimetry
TOF	turnover frequency
TON	turnover number
triflate (OTf)	trifluoromethanesulfonate
TSIL	Task Specific Ionic Liquid
XPS	X-ray Photoelectron Spectroscopy

PUBLICATIONS

S. Doherty, J. G. Knight, **J. R. Ellison**, D. Weekes, R. W. Harrington, C. Hardacre, H. Manyar “An efficient peroxometalate-based polymer-immobilised ionic liquid phase (PIILP) catalyst for hydrogen peroxide-mediated oxidation”, *Green Chem.*, 2012, **14**, 925 – 929

S. Doherty, J. G. Knight, **J. R. Ellison**, P. Goodrich, L. Hall, C. Hardacre, M. J. Muldoon, S. Park, A. Ribeiro, C. A. N. de Castro, M. J. Lourenço and P. Davey, “An efficient Cu(II)-bis(oxazoline)-based polymer immobilised ionic liquid phase catalyst for asymmetric carbon-carbon bond formation”, *Green Chem.*, 2014, **16**, 1470 – 1479

S. Doherty, J. G. Knight, M. A. Carroll, **J. R. Ellison**, S. J. Hobson, S. Stevens, C. Hardacre and P. Goodrich, “Efficient and Selective Hydrogen Peroxide-Mediated Oxidation of Sulfides in Segmented and Continuous Flow using a Peroxometalate-Based Polymer Immobilised Ionic Liquid Phase Catalyst”, *Green Chem.*, 2015, **17**, 1559 – 1571

Chapter 1

Ionic Liquid, Supported Ionic Liquid and Polymer-Immobilised Ionic Liquid Phase Catalysis

Table of Contents:

2.1.	Abstract	3
2.2.	Introduction	3
2.3.	Ionic Liquids	4
2.4.	Supported Ionic Liquid Phase	18
2.5.	Polymer-Immobilised Ionic Liquid Phase	23
2.6.	Polymerisation Methods	26
	<i>2.6.1. Step Polymerisation</i>	27
	<i>2.6.2. Radical Polymerisation</i>	28
	<i>2.6.3. Living Radical Polymerisation</i>	31
	<i>2.6.4. Ionic Polymerisation</i>	34
	<i>2.6.5. Ring-Opening Polymerisation</i>	37
2.7.	Conclusions	39
2.8.	References	40

1.1. Abstract

The use of ionic liquids in catalysis has seen an extended growth phase over the past two decades due to their unique and tuneable physicochemical properties which can not only offer enhancements in catalyst performance but also act as a means to heterogenise catalytic species. Whilst the use of ionic liquids has been successfully applied across a wide variety of chemistry, in some cases on an industrial scale, there are clear limitations. In an attempt to address these, the concept of the Supported Ionic Liquid Phase (SILP) catalysis was developed which proved to be largely successful, particularly in fixed-bed gas-phase reactors. However, limitations still remained with regards to ionic liquid/catalyst leaching as well as unfavourable characteristics of the generally inorganic support materials. The incorporation of ionic liquid fragments into the architecture of polymeric materials, which we have termed Polymer-Immobilised Ionic Liquid Phase (PIILP), has become increasingly popular over the past few years as either a subset or an evolution of the SILP methodology. By using PIILP, leaching of the ionic liquid moieties is negated whilst the use of polymer chemistry affords materials with tuneable chemical and physical properties. As this work will focus on the development and use of PIILP the application and relative merits of ionic liquids, SILP and PIILP in catalysis are discussed, and ubiquitous polymerisation methods are assessed as a means to generate PIILP materials for the immobilisation of catalytic species.

1.2. Introduction

Efficient organic synthesis plays a key role across a broad spectrum of scientific disciplines ranging from chemistry to biology and materials. At present there is considerable drive to develop more environmentally benign, sustainable processes in accordance with parameters such as the “12 Principles of Green Chemistry”,¹ *E*-factor² and atom efficiency.³ Catalysis is an essential and vital tool in the development of “green” processes. The advantages of the use of molecular, homogeneous catalysts are well-established, including the use of a well-defined single active site that is markedly more active and selective than their heterogeneous counterparts. In this regard, the use of molecular catalysts has found widespread application across the chemical industry, including processes based on oxidation, metathesis, hydroformylation, carbonylation, hydrocyanation and oligomerisation.⁴ Major drawbacks occur with regards to separation and recycling of the catalytic species, with isolation of the active catalyst after reaction often difficult and potentially resulting in contamination of both the catalyst and products. This scenario often leads to expensive purification procedures which generally disagree with the aforementioned green principles as well as adding additional cost to the process. Whilst the use of heterogeneous catalysts negates this requirement and yields easily

recyclable systems, there is generally a pronounced reduction in catalyst performance due, in part, to the more ill-defined nature of the active sites; in fact, some of the listed industrial transformations above have no heterogeneous counterpart.

Further to the use of catalysis to improve the “green” credentials of processes, the solvents used are coming under increasing scrutiny. With regards to conventional volatile organic solvents, concerns arise from their volatility, flammability and lasting effect on the environment; for example, the use of solvents accounts for 50% of the post-treatment greenhouse gas emissions and 60% of the energy used in industrial pharmaceutical processes.⁵ In an attempt to address issues with organic solvents as well as immobilisation and recycling of homogeneous catalysts, numerous non-conventional reaction media have been investigated including water, supercritical carbon dioxide (scCO₂) and perfluorinated solvents.⁶ Generally, these alternate media form biphasic systems in which the product can be extracted either by solvent or by the gaseous reagent stream and have been successfully applied to a variety of transformations including hydrogenation, hydroformylation, metal-catalysed C-C bond coupling and oxidation.⁵ Despite their successes there are severe limitations to this approach including the solubility of the catalyst or reagent and, in the case of fluorinated solvent, the generation of hydrofluoric acid under harsh reaction conditions. Of all the non-conventional reaction media investigated it is ionic liquids, with their unique, tuneable physicochemical properties, which have received the most attention and have shown the greatest promise.

1.3. Ionic Liquids

Ionic liquids (ILs) are a fascinating class of solvent comprised entirely of anion and cation pairs which remain in the liquid state at low temperatures, conventionally below 100 °C, which have received widespread attention across a range of chemistry due to their low volatility, low vapour pressure and tuneable properties. ILs have been widely acknowledged to have been first reported in 1914 with observations made by Paul Walden about the physical properties of ethylammonium nitrate, mp 13-14 °C, which formed in the neutralisation of ethylamine with concentrated nitric acid.⁷ Despite this observation ILs received very little attention over subsequent decades; select examples include “liquefied quaternary ammonium salts”, which were reported to dissolve cellulose in 1934⁸, and mixtures of aluminium (II) chloride and alkylpyridinium halide salts that were reported in 1948⁹ and 1975.¹⁰ ILs, as they are understood today, were not truly realised until 1992 with the preparation and characterisation of a series of compounds based on the 1-ethyl-3-methylimidazolium cation with a range of different anions including [CH₃CO]⁻, [NO₃]⁻ and [BF₄].¹¹ Since this development, room-

temperature ILs have become more readily available as reaction media for synthetic chemistry. As opposed to previous iterations, which largely revolved around electrochemical applications, ILs have seen a meteoric rise in popularity over the past 20 years (figure 1.1). Most modern ILs are comprised from cations which bear a quaternary ammonium ion, preferably a substituted imidazolium, pyridinium, pyrrolidinium, or phosphonium

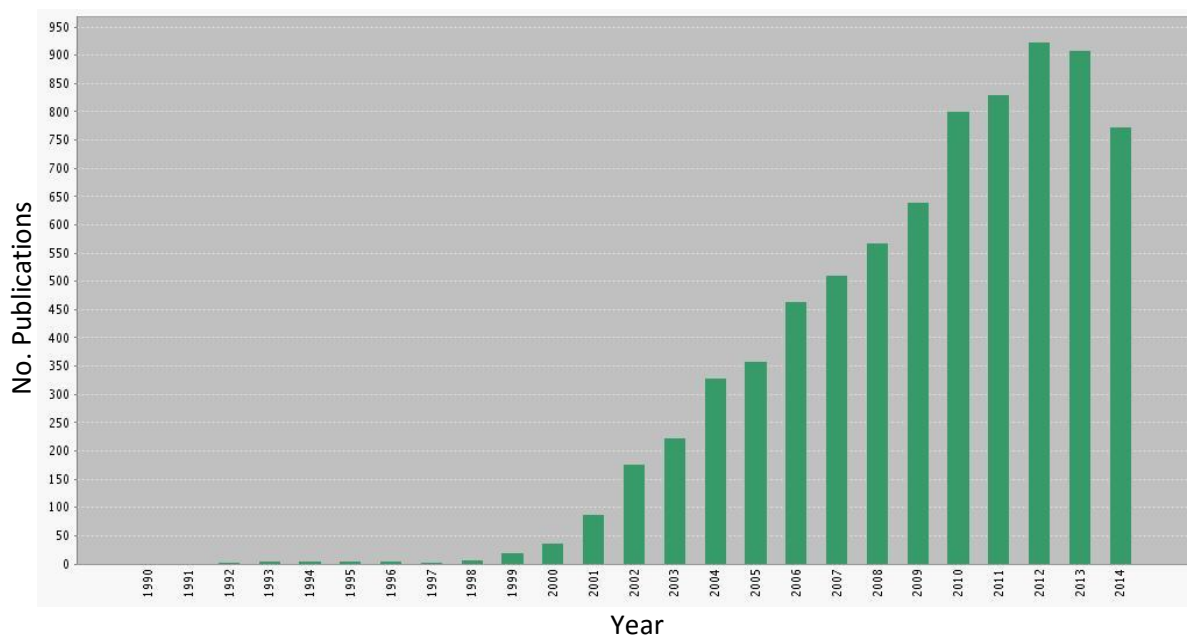


Figure 1.1 Number of articles in the field of chemistry with “ionic liquids” as the topic (Source: Web of Science 21/11/2014)

cation (figure 1.2). Unlike the early examples of ILs that heavily favoured the use of mixed chloroaluminate counterions (which exhibited varying properties as a result of mixed composition as well as a lack of stability towards hydrolysis¹²) a whole plethora of anions are now available to chemists, ranging from halides, to perfluorinated anions, to triflates, and bistriflimides. Through functionalization of both ions and by varying anion-cation pairings it is possible to generate an estimated 10^{18} different ILs.¹³ It is this incredible potential for structural diversity which gives rise to one of the most desirable aspects of the application of ILs: allowing for fine tuning of their physicochemical properties to fit a specific need. Generally, the cation is responsible for control over the ILs physical properties, such as melting point, viscosity and density, whilst the anion controls chemical properties and reactivity.¹⁴ The ability to fine tune physicochemical properties coupled with generally low volatility/vapour pressure has led to a wide range of application for ILs; however, it is estimated that over half of all publications involving ILs concern their use in synthesis and catalysis,¹⁵ and as such this section will focus solely on evaluating their use in this capacity.

Due to the incredibly diverse nature of ILs it can be difficult to make statements about their properties, as varying cation-anion combinations give rise to markedly different physicochemical properties; however general statements, as well as comparisons to conventional organic solvents,

can be made (table 1.1). One of the common properties amongst ILs is their negligible vapour pressure, although there are some examples of “distillable ionic liquids” which

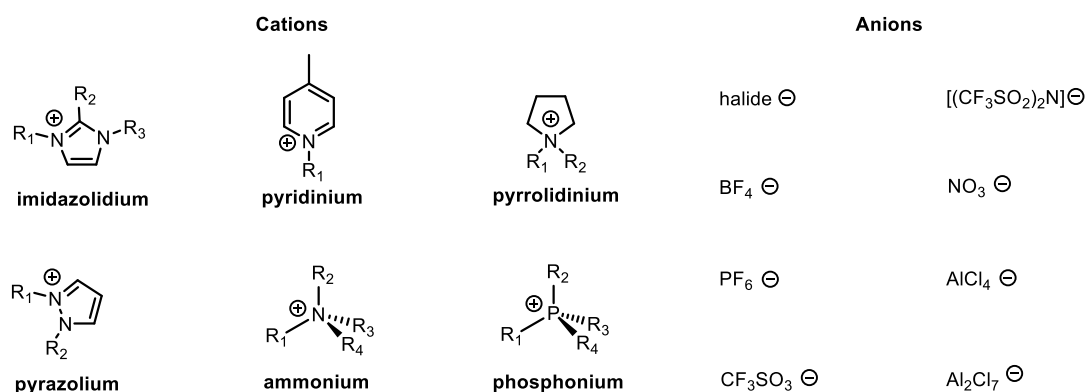


Figure 1.2 Commonly used cations and anions for ionic liquids

require high temperatures.¹⁶ This low vapour pressure limits exposure to toxic solvent vapour that is associated with conventional organic solvents whilst also allowing for effective immobilisation of the reaction solvent and a suitable thermally stable catalyst, which in turn allows the product to be isolated by distillation. The general lack of vapour pressure can also be advantageous in catalysis when employing the use of transition metal catalysts, which are often air- and moisture-sensitive,

Table 1.1 General comparison of organic solvents with ionic liquids outlined by Plechkova and Seddon¹⁷

Property	Organic solvents	Ionic liquids
Number of solvents	>1000	>1,000,000
Applicability	Single function	Multifunction
Catalytic ability	Rare	Common and tuneable
Chirality	Rare	Common and tuneable
Vapour pressure	Obeys the Clausius-Clapeyron equation	Negligible vapour pressure under normal conditions
Flammability	Usually flammable	Usually non-flammable
Solvation	Weakly solvating	Strongly solvating
Polarity	Conventional polarity concepts apply	Polarity concept questionable
Tuneability	Limited range of solvents available	Virtually unlimited range means “designer solvents”
Cost	Normally cheap	Typically between 2 and 100 times the cost of organic solvents
Recyclability	Green imperative	Economic imperative
Viscosity/cP	0.2-100	22-40,000
Density/g cm ⁻³	0.6-1.7	0.8-3.3
Refractive index	1.3-1.6	1.5-2.2

allowing for the straightforward removal of water impurities by heating the solvent under high vacuum prior to reaction.

As stated previously, the combination and functionalization of both anion and cation in ILs leads to an incredibly broad variation in their properties, possibly the most notable and important of which is polarity and, by extension, how the IL interacts with solutes. Due to the fully ionic nature of ILs it may be expected that they would behave as superpolar solvents, however ILs generally exhibit moderate polarities of a similar magnitude to acetonitrile and methanol, although there is no definitive way to accurately measure the polarity of the IL in question.^{18,19} Whilst straightforward Coulombic interactions of the ion pair play a considerable role, the inter- and intramolecular forces involved with ILs are considerably more complex. Taking the commonly used dialkylimidazolium type IL as an example (figure 1.3) it can be seen that multiple intermolecular forces are possible, including hydrogen-bond donation by the protons of the cation and acceptance by the anion, π -stacking from the aromatic ring of the imidazolium unit and possible Van der Waals interactions

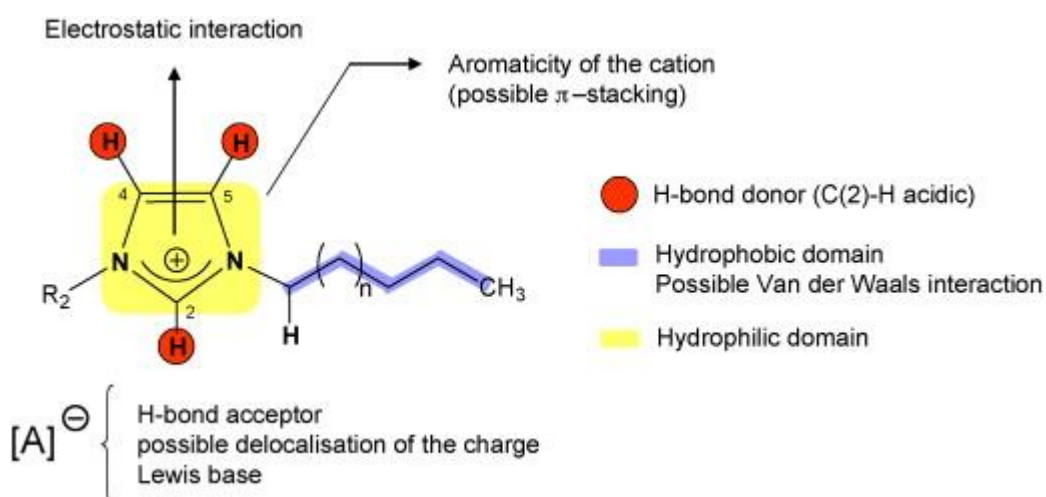


Figure 1.3 Representation of the different types of interactions present in imidazolium-based ILs reported by Olivier-Bourbigou *et al.*¹⁹

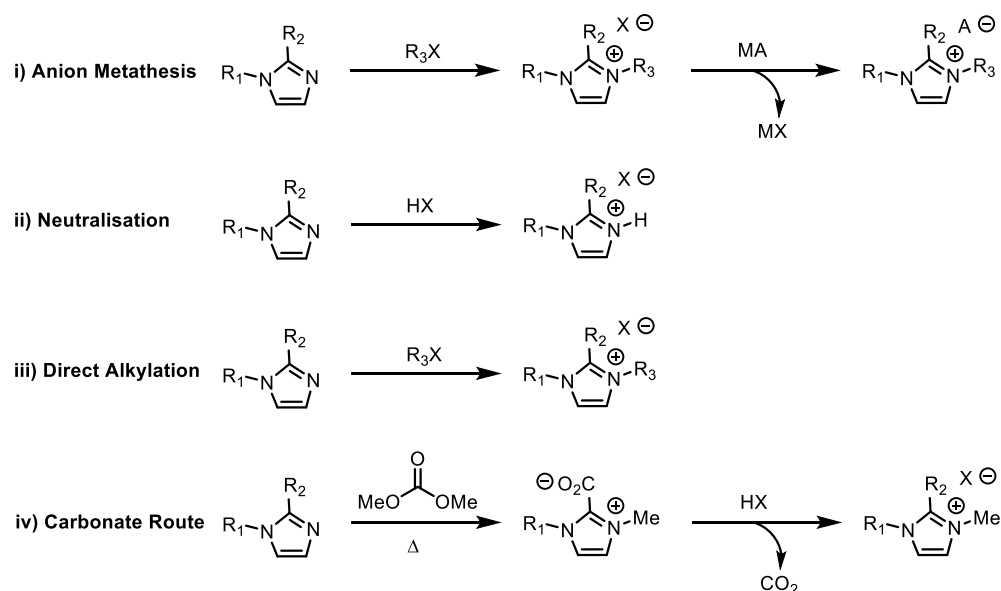
from the alkyl side chains. As a result, ILs have unique solubility properties, being able to dissolve polar and non-polar substrates through a combination of the interactions listed above. The complex combination of potential intermolecular forces at play also gives rise to complicated, sometimes ordered mesoscopic structures in bulk ILs. Again this effect can be difficult to quantify in general terms for all ILs; for example, there are several aspects to consider for imidazolium-based ILs with different anions such as the anion symmetry, its proximity with regards to the positively charged imidazolium delocalised, the strength of the anion-cation interaction, and the potential for H-bonding between ionic fragments.¹⁹ The bulk structural organisation of ILs can play a key role in the understanding of their role within a reaction. Three-dimensional, almost polymeric networks formed by H-bonding interactions with dialkylimidazolium chlorides have been observed through a number

of techniques including X-ray diffraction and NMR spectroscopy,²⁰ whilst a similar effect has also been observed by NOESY NMR for imidazolium salts with tetrafluoroborate ($[\text{BF}_4]^-$) and *bis*(trifluoromethanesulfonyl)amide ($[\text{NTf}_2]^-$) anions through π - π stacking interactions of the imidazolium cations.²¹ Such mesoscopic arrangements can give rise to both hydrophilic and hydrophobic domains from the ionic regions and alkyl side chains of the IL fragments, respectively. This presence of microdomains can have a profound effect on reactions conducted in ILs and how the solvent interacts with the solutes, potentially even directing reagents/mechanisms in a similar fashion to porous solid supports. For example, significant rate enhancements, as high as a 167% increase, were observed in bimolecular substitution reaction of *N*-(*p*-fluorophenyldiphenylmethyl)-4-picolinium chloride and various simple alcohols by varying the length of the alkyl side chain of the imidazolium IL solvent.²² The authors postulated that the rate enhancements were a direct result of pseudo-encapsulation of the reactants within the polar domains of the IL, essentially altering the effective concentration of the reagents. Similarly the presence of polar and non-polar domains can have a profound effect on the formation of catalytically active species. For example, a direct correlation exists between the alkyl side chain length, and hence size of the non-polar domains, and the size of *in situ* generated Ru nanoparticles from $[\text{Ru}(\text{cycloocta-1,5-diene})(\text{cyclooctatetrane})]$. In this regard the size of the forming nanoparticles is limited by the local concentration of the non-polar organometallic precursor, which in turn is determined by the size of the corresponding non-polar domains within the ionic liquid.²³

Whilst the complex nature of ILs can make it incredibly difficult to determine how a reaction will be influenced, it is possible to fine-tune the physicochemical properties in order to meet a specific need. For example, while the general definition of an IL states their melting point as $< 100\text{ }^\circ\text{C}$ it is often preferential to use ILs which remain liquid at room temperature and below, further expanding the scope of their application. For a particular cation, the choice of anion has been shown to have a profound effect on the melting point, with coordinating and hydrophilic anions such as halides yielding higher melting points, and weakly coordinating and hydrophobic anions such as triflates ($[\text{OTf}]^-$) and triflamides ($[\text{NTf}_2]^-$) giving lower melting points.²⁴ Further to this, fine-tuning of the length of the alkyl side chain can alter the melting point, with longer chains generally lowering the melting point.²⁴ Disruption of the ILs molecular symmetry can also lower the melting point of ILs by making crystallisation more difficult whilst a delocalisation of the positive charge has also been shown to have a similar effect.²⁵ In terms of viscosity ILs demonstrate one of their key drawbacks. Generally ILs will exhibit viscosities which are considerably higher than conventional organic solvents; this can have a strong deleterious effect on reactions with regard the dynamics and kinetics of a process. This effect is most profound when considering catalysis, with the rate-determining step often being the association of a reactant with the catalyst molecule. Mass transport limitations imposed by an ILs

high viscosity can significantly slow this, and hence the entire reaction quite considerably. Despite this it is possible to tune and lower the viscosity of an IL, with the choice of anion having the strongest effect, whilst the addition of small amounts of water, even as low as the parts-per-million range, can also significantly lower viscosity.²⁵ Although the presence of water is a less than ideal when considering catalysis in ILs it does highlight that it is possible to significantly alter an ILs properties relatively easily.

As illustrated previously (figure 1.2) numerous different types of IL architectures are available, however, of these the most frequently used are those based on the dialkylimidazolium cation. In this regard, there are essentially 4 synthetic pathways to yield the desired IL (scheme 1.1), each exhibiting both advantages and disadvantages. Often the most popular method of IL synthesis employs the use of quaternisation-metathesis sequences which utilises quaternisation of an



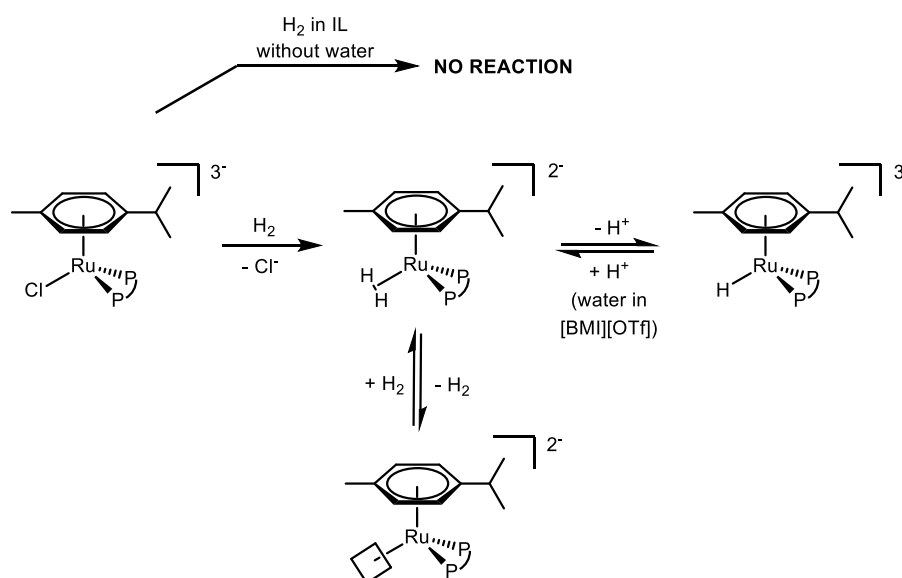
Scheme 1.1 General routes used to synthesise imidazolium-based ionic liquids

imidazole unit with an alkyl halide, followed by metathesis with a suitable metal-counter anion species (MA). While this chemistry is relatively simple, it severely reduces any 'green' credentials of the IL in question by the necessary generation of stoichiometric amounts of metal halide (MX) by-products which can often be difficult, time consuming and costly to remove. This can be especially problematic when considering hydrophilic ILs, as both filtration and aqueous extraction are rendered unusable as a means to remove the metal salt by-product. Despite this there have been recent breakthroughs which circumnavigate both the use of silver salts in the metathesis step and issues associated with the use of water, by preparing water miscible ILs in the melt of onium-halide salts in the presence of either the lithium or sodium salt of the desired anion; the resulting IL can then be extracted with either CH_2Cl_2 or THF.²⁶ Other common routes to synthesise ILs include neutralisation of a base with a Brønsted acid or by direct alkylation. Although these methods have attractive

features such as high atom efficiency, both the neutralisation and alkylation processes are often non-quantitative and form impurities which are difficult to remove, whilst the functionality of the final IL is limited by the reactivity and availability of the alkylating agent. The use of alkylhalides has also been negated in order to generate further ILs through the use of dimethylcarbonate (DMC) as an alternative green methylating agent. Subsequent anion exchange with either a suitable Brønsted acid or water can yield a wide variety of ILs with varied physicochemical properties whilst avoiding the use of metal-based reagents.²⁷ Numerous non-conventional procedures have also been reported for the synthesis of ILs; these employ the use of either microwave or ultrasound irradiation.¹⁹ For example, microwave activation has been used to achieve an efficient one-pot solvent-free synthesis of imidazolium and pyridinium ILs through an S_N2-metathesis sequence followed by either extraction or precipitation, with the use of microwave heating affording much higher yields than conventional heating under otherwise analogous conditions.²⁸ Whilst the use of such activation methods has been proven to be an efficient methodology in terms of both product yield and the energy requirements, many ILs are in fact unstable and prone to decompose under sonochemical conditions, and as such the scope of functionality is once again limited.²⁹

The purity of the IL used in catalytic processes has proven to be a crucial factor in performance. The presence of impurities such as inorganic halides, unreacted alkyl halides, and protic reagents (in particular water) can drastically alter both the physical and chemical properties of the IL and hence influence catalyst performance.³⁰ Whilst water is particularly problematic due to the generally hydroscopic nature of ILs, the rest of the impurities are artefacts arising during the IL synthesis. For example, the presence of halide ions in ILs has been shown to cause deactivation of an arene hydrogenation precatalyst [H₄Ru₄(η⁶-C₆H₆)₄][BF₄]₂³¹ as well as Cu(II)-bis(oxazoline)-based Lewis acid catalysts. While impurities often act as a catalyst poison, water has been shown to play a key role in the hydrogenation of arenes catalysed by [(*p*-cymene)RuCl(dppm)] under biphasic conditions.³² The key step in the mechanism of this reaction is dissociation of a chloride from the ruthenium; as such the ability of the IL medium to solvate Cl⁻ is an important factor. When the reaction is conducted in neat or dried 1-butyl-3-methylimidazolium triflate ([C₄mim][OTf]) no reaction was observed as a result of poor dissociation of chloride in the IL, rendering the precatalyst inactive; however, upon addition of water ([C₄mim][OTf] : H₂O 50 : 50), formation of the active hydride species is observed and the reaction proceeds *via* an entirely different mechanism (scheme 1.2). A similar effect can be observed with residual unreacted N-alkylimidazole impurities present after alkylation to yield dialkylimidazolium ILs. For example, unreacted N-methylimidazole has been shown to act as an effective base in several organic reactions,³³ in fact, it has been observed that the imidazole acts as a much more efficient base catalyst than L-proline or piperidine in Michael additions conducted in ILs.³⁴ In the synthesis of Au and PdAu nanoparticles, N-methylimidazole, even at incredibly low

concentrations, has also been shown to act as an effective base, stabilising the nanoparticles and preventing aggregation.³⁵ From these select examples it is clear that the purity of an IL plays a critical role in its performance when used as a catalyst, with the presence of impurities being both advantageous and detrimental under the right circumstances. This again highlights the complex nature of ILs as solvents and illustrates that an extensive understanding is required before their implementation. In this regard, numerous analytical protocols have been used to quantify the impurities in ILs including ¹H NMR spectroscopy,^{30, 36} electrochemical methods³⁷ and X-ray photoelectron spectroscopy.³⁸



Scheme 1.2 Proposed mechanism of formation of the active ruthenium species in the hydrogenation of arenes in the presence of [C₄mim][OTf] and water.³²

As stated previously, more than half of all publications concerning ILs revolve around their use in catalysis. In this regard the use of ILs as a bulk solvent can greatly simplify product isolation through their non-volatility and unique solubilities, allowing for either product extraction or distillation. In this sense, ILs effectively combine the benefits of homogeneous catalysis with the immobilisation benefits associated with heterogeneous catalysis. In a similar manner to the fluoros phase and aqueous phase-based approaches discussed above, it is also possible to pass a stream of gaseous reagents through an IL containing dissolved catalyst to give a highly efficient heterogeneous system. Further to this the unique, tuneable phase behaviour of ILs can be exploited to give bi- or even triphasic IL/water/organic systems as ILs can be fine-tuned to render them hydrophilic, completely hydrophobic or partially miscible with water. In an ideal liquid-liquid biphasic system (figure 1.4) the IL is able to dissolve the active catalytic species while also being partially miscible with the substrate, with the reaction product having limited solubility in the ionic phase; this would allow for simple decantation of the organic or aqueous layer. While appealing, the reality of these systems often requires subsequent extraction steps in order to enhance the obtained yields, increasing the

reliance on conventional volatile organic solvents. These extraction steps often highlight one of the major limitations of the use of IL-based liquid-liquid systems with regards to leaching of both the catalyst and the IL fragments into the extraction solvent, resulting in potential product contamination and loss of expensive designer solvents, catalysts and ligands. Liquid-liquid biphasic systems have also been shown to drastically alter reaction selectivity and alter product distributions due to solubility of products in processes such as the hydrogenation of dienes and olefin oligomerisation and metathesis. Again, in this sense, the tuneable nature of ILs allows for optimisation of performance with regards to catalyst retention, activity, selectivity and stability in a rational fashion. While this methodology has proven particularly effective for charged catalysts and catalyst precursors through efficient immobilisation by Coulombic interactions, neutral species are often much less soluble and are hence more prone to leaching during the extraction process. Even when the catalyst is charged, leaching of either the metal and/or ligand may still occur when the active species exists in an equilibrium between a bound and unbound metal centre, as is the case for copper(II)-bis(oxazoline)-catalysed Diels-Alder reactions.³⁹

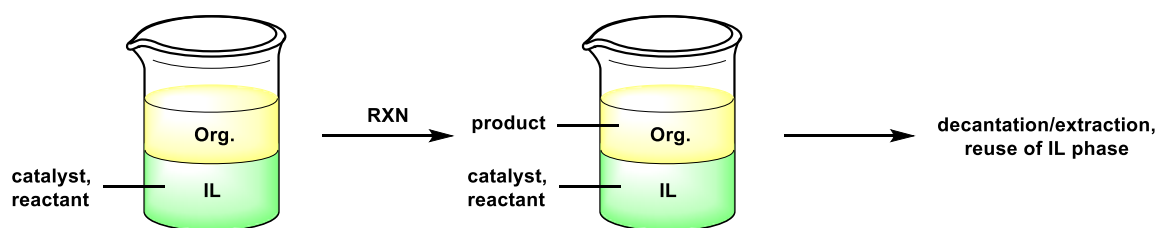


Figure 1.4 An ideal IL-based liquid-liquid biphasic catalytic system

In addition to simplifying product separation, the use of a liquid-liquid biphasic systems greatly also enables the catalyst to be recycled and reused. In principle, once the product has been removed either by decantation or extraction, the IL phase can be reused directly or after an additional drying/purification step. This is of particular benefit as often the catalyst and/or the IL used constitute the most costly aspect of a reaction. Unfortunately in many cases a drop in catalyst activity and selectivity is often observed upon successive reuse; again this is often associated with leaching of both the catalyst and ligand during the extraction or purification processes between catalytic cycles. In an attempt to further improve catalyst and ligand retention within the IL phase, the concept of tagged or task-specific ionic liquids (TSILs) was developed. In TSILs an IL fragment is functionalised with a remote ligand which will coordinate to a metal; this functionalization can be incorporated either onto the anion or cation. By incorporating an IL unit into the architecture of a catalyst, its miscibility with the IL media is vastly improved. Since the inception of this concept, tagged ligands, both chiral and achiral, have been applied to a wide variety of transition metal-catalysed reactions including hydroformylation, olefin metathesis, Suzuki-Miyaura cross-coupling, and transfer

hydrogenations, with more recent examples concerning the functionalization of organocatalysts such as L-proline.⁴⁰ Previous work by the Doherty group developed imidazolium-tagged bis(oxazoline) ligands for the use in Cu-catalysed Diels-Alder reactions (figure 1.5). The resulting functionalised catalyst was recycled 10 times without any loss in activity or enantioselectivity, which was a stark contrast to the conventional, uncharged ligand.⁴¹ This improved retention in the IL phase is consistent throughout the application of TSILs in catalysis, illustrating the practical benefit of tagging on catalyst retention, while appropriate functionalization of the IL fragments could also facilitate reaction mechanisms, further improving catalyst activity. In this regard the presence of an appropriate functional group could help stabilise the formation of a preferred transition state during a reaction, or provide ligand-type interactions with transition metal centres. Despite this, however, the additional expense and difficulty involved in the often incredibly complex synthesis of optimum tagged ligands for specific needs could potentially outweigh the benefits afforded by the use of ILs and as such should be considered a major limitation.

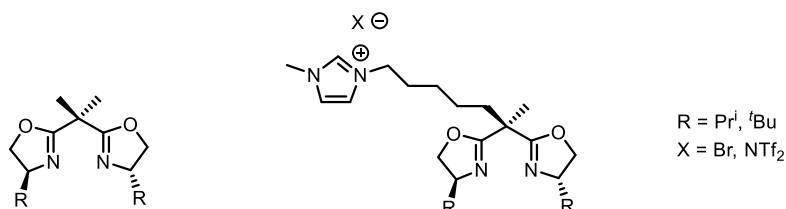


Figure 1.5 imidazolium-tagged and untagged bis(oxazoline) ligands used in asymmetric Diels-Alder reactions

As an extension of the use of ILs to give liquid-liquid biphasic conditions their unique, tuneable properties have been exploited to give systems in which the ILs miscibility with the co-solvent can be reversibly switched. At high temperatures the mixture of IL and co-solvent remains homogeneous which enables the reactant and catalyst to mix efficiently, while upon cooling the mixture separates to afford a biphasic system which allows the product-containing organic layer to be separated as described above. Select early examples include the use of a fluororous-tagged IL-toluene combination used in hydrosilylation⁴² and IL-water systems in hydrogenation,⁴³ while more recently polyether,⁴⁴ heteropolyanion⁴⁵ and dicationic Brønsted acid⁴⁶ based ILs have all exhibited thermoregulated biphasic properties when used in catalysis. The use of such thermoregulated systems can effectively avoid major mass transport limitations associated with conventional liquid-liquid biphasic systems.

While the use of conventional organic solvents to extract products and unreacted reagents has been largely successful in their application their use can significantly decrease the environmentally benign/green aspects of a liquid-liquid biphasic system. In this sense the alternate fluororous phase, aqueous and super critical carbon dioxide (scCO₂) solvents discussed in the introduction have all been used in conjunction with ILs in biphasic systems. The use of scCO₂ has

received considerable interest due to its non-toxic nature, easy recovery and ability to extract a wide range of substrates from ILs, as well as finding additional interest as a means of addressing environmental concerns by developing a practical for CO₂ generated in other areas of industry which would otherwise be released into the environment. The first successful example of the use of scCO₂ was demonstrated in the hydrogenation of 1-decene catalysed by rhodium species in 1-butyl-3-methylimidazolium hexafluorophosphate ([C₄mim][PF₆]) with extraction of products with scCO₂ allowing for efficient recycling and reuse of the IL-catalyst phase.⁴⁷ A later development demonstrated that the use of 1-ethyl-3-methylimidazolium-based IL ([C₂mim][PF₆]) in the iridium-catalysed asymmetric hydrogenation of imines gave an enhancement in the rate of reaction, attributed to the enhanced availability of H₂ in the IL phase.⁴⁸ The use of scCO₂ in conjunction with ILs also allows for the development of continuous flow processes (figure 1.6). For example, early work by Cole-Hamilton *et al.*, concerning the rhodium-catalysed hydroformylation of 1-octene, developed a system in which the catalyst was immobilised in a stationary IL phase whilst scCO₂ was used as the transport vector for the substrates and resulting products. The high solubility of scCO₂ in the IL media proved to be highly advantageous by resulting in a reduction in the IL viscosity. To this end the mass-transport limitations often encountered during catalysis in ILs were significantly reduced.⁴⁹

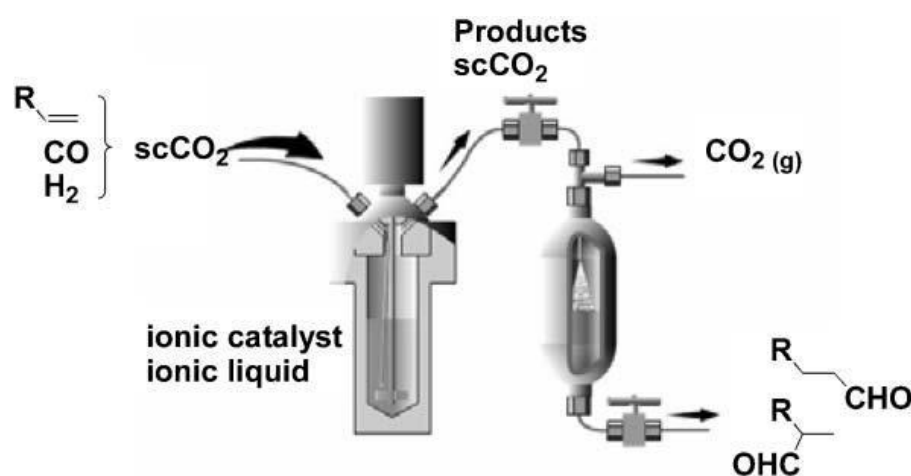
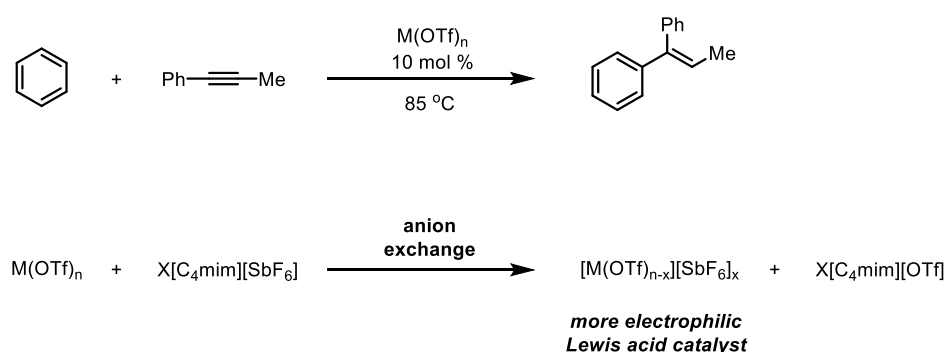


Figure 1.6 Example schematic of continuous flow homogeneous catalysis using a scCO₂-IL biphasic system⁵⁰

As stated previously, the incredibly diverse nature of ILs makes it difficult to categorise their effect on a reaction, with each IL often being specifically suited to a single reaction system. Despite this, the use of ILs in catalysis has demonstrated clear general advantages in a wide spectrum of ubiquitous catalytic processes. The clear advantages of catalyst immobilisation, stabilisation and ease of separation are often the driving force behind the application of ILs, however, numerous reports have documented considerable enhancements in both reaction rate and selectivity, in particular for Lewis acid carbon-carbon bond forming reactions.⁵¹ For example, the Sc(OTf)₃-catalysed Diels-Alder reaction between 2,3-dimethylbutadiene and 1,4-naphthoquinone and the related cyanosilylation of benzaldehyde both gave high conversion in relatively short reaction times in [C₄mim]-based ILs at low

catalyst loadings (0.1-0.2 mol%), while the same reaction in dichloromethane proceeded incredibly slowly. What is of particular interest is the enhancement in rate was also observed with just one equivalent of IL, demonstrating that the positive effects an IL can have on a reaction can sometimes be achieved when using the IL as an additive rather than as a bulk solvent.⁵² A similar effect is also observed in a more pronounced fashion in the Sc-catalysed Friedel-Crafts alkylation of benzene with 1-hexene, which proceeded to near quantitative conversion when conducted in the same IL at room temperature; the same system in organic solvents remained completely inactive.⁵³ The same effect was also observed for the alkylation of benzene with 1-phenyl-propyne catalysed by 10 mol% Sc(OTf)₃ or Hf(OTf)₄. Again, very high yields of the desired Z-alkenylation product were observed in just 4 h in IL whilst yields dropped below 30 % even after 96 h when the reaction was conducted in organic solvent. It was reported that the observed increase in activity could be attributed to an anion exchange process between the catalyst and the IL giving rise to an enhancement of the metal's Lewis acidity (scheme 1.3).⁵⁴ In addition to the formation of a highly Lewis acidic metal species there is also some evidence for the stabilisation of cationic vinyl and arenium reaction intermediates during Friedel-Crafts reactions in ILs which can

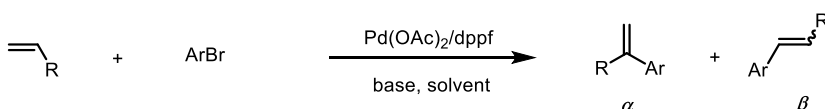


Scheme 1.3 Lewis acid-catalysed alkenylation of benzene with 1-phenyl-1-propyne and proposed ion exchange between the metal catalyst and [C₄mim][SbF₆] ionic liquid medium

further contribute to the rate enhancement.^{54a} Similar enhancements in rate have also been reported for a range of Lewis acid-catalysed reactions including Sc-catalysed Beckmann rearrangements⁵⁵ as well as the Cu-catalysed Diels-Alder⁵⁶ and the Mukaiyama-aldol reaction.⁵⁷ Enhancements in the rate of carbon-carbon bond forming reactions are not only limited to Lewis acid-catalysed processes, a similar profound effect has also been reported for palladium-catalysed reactions such as Heck, Stille and Suzuki-Miyaura couplings. In this regard, the enhancement in rate is thought to be associated with the formation of an electron-rich anionic species of the type [L_nPdX]⁻. This reactive species has been reported to be highly active towards oxidative addition⁵⁸ as well as giving a nucleophilic assistance effect for the transmetalation step in the case of Stille and Suzuki-Miyaura couplings. In these cases the anionic species promotes exchange by expanding the coordination sphere of the Sn (or B) reagent.⁵⁹ While these effects are often associated with nanoparticle-based catalysis it is

possible that an anion-cation pair or a TSIL could also afford similar optimisation for well-defined molecular complexes.

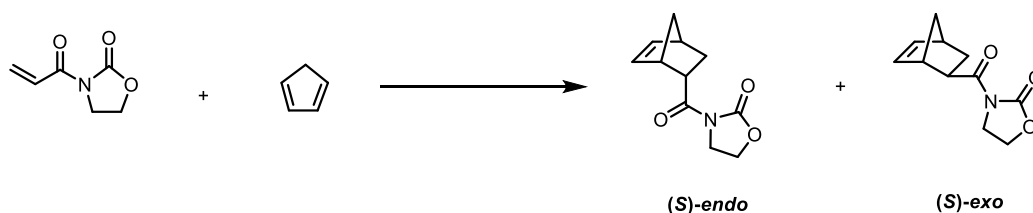
Further to enhancements in reaction rate, the use of ILs in catalysis has also been widely documented to yield dramatic improvements in reaction selectivity. One of the more profound examples is for the regioselectivity of the Heck arylation of electron-rich olefins (scheme 1.4). Generally, under standard conditions, electron rich olefins will give a mixture of regioisomers with very low selectivity in comparison to electron-withdrawing functionalised terminal olefins which give high yields of the β -regioisomer. Whilst it is possible to achieve high α -arylation selectivity when using either aryl triflates as the coupling partner, or by employing stoichiometric amounts of thallium or silver salts, both these approaches have clear drawbacks.⁶⁰ By using the IL [C₄mim][BF₄] as the solvent the α -selectivity for the Pd/dppf-catalysed arylation of electron-rich olefins was vastly improved compared to the same reaction in conventional organic solvents. Improvements were observed across a range of substrates and in some cases complete selectivity for the α -arylated product was achieved; the authors reasoned that the ionic environment afforded by the IL facilitated dissociation of halide to allow for an ionic reaction pathway, a route which is known to yield high α -selectivity through a combination of electrostatic and frontier orbital interactions.⁶¹ A similar enhancement in regioselectivity was also observed in the arylation of 4-bromotoluene with *trans*-ethyl cinnamate, in this case the improvement in selectivity was attributed to rapid intramolecular neutralisation of an olefin-coordinated Pd-H species by a metal bound acetate.⁶² Similar improvement in ILs with regards to enantioselectivity have also been well-documented



Scheme 1.4 Pd-catalysed Heck arylation to give a mixture of regioisomers

across a range of Lewis acid-catalysed reactions. Previous work by the group concerning the Diels-Alder reaction between *N*-acryloyloxazolidinone and cyclopentadiene (scheme 1.5) catalysed by either Cu(OTf)₂/bis(oxazoline) or Pt/diphosphine species reported significant enhancements in ee, as well as rate, when reactions were conducted in ILs.^{63,64} With regards to the latter example a comparison between BINAP/Pt and the conformationally more flexible NUPHOS/Pt complexes in both IL and dichloromethane was conducted, indicating that the enhancement in ee was attributed to a decrease in the rate of racemisation of the NUPHOS/Pt catalyst as well as an intrinsic solvent effect. When considering enhancements in ee the use of ILs also affords a more general advantage in that high ee's can be obtained at room temperature which avoids the use of low temperatures often required in organic solvents.

Due to their advantageous role in catalysis with regards to both catalyst immobilisation/product separation and potential enhancements in reaction performance, ILs have found application in new process technologies across all areas of the chemical industry, either at the pilot plant or fully commercialised scale.¹⁷ One of the more pronounced applications of ILs in industry is the isobutene/butane alkylation performed by PetroChina, China's largest oil producer, which tested a variety of acidic methylimidazolium and pyridinium IL catalysts up to a 1000 ton scale,⁶⁵ arguably the largest commercial usage of an IL.¹⁷



Scheme 1.5 Lewis acid-catalysed Diels-Alder reaction between *N*-acryloyloxazolidinone and cyclopentadiene

Despite the clear advantages afforded by the use of ILs there are several limitations that hinder their application, and as such these issues must be addressed in order to optimise ILs in catalysis. Common dialkylimidazolium-based ILs can often be incredibly expensive while the functionalised TSILs by merit of their more complex structures are even more costly, often prohibiting their large scale application. As such it is necessary to strive to develop more simplistic IL synthesis or develop methodologies which require the use of much less IL. With regards to the synthesis of ILs the purity of the end product can often be problematic as discussed above due to the non-quantitative nature of IL synthesis. Impurities such as unreacted imidazolium bases, inorganic salts and water can all have a profound effect on catalysis. Whilst this influence is not always negative it does highlight the necessary deep understanding of the IL being used and its purity when used in catalysis. Further issues arise with regards to the synthesis of ILs when considering their overall 'green credentials'. As ILs have found considerable interest largely as green alternatives to organic solvents, the sometimes protracted synthesis could potentially outweigh any positive effects. Whilst ILs are generally considered highly stable, the evaluation, and indeed application, of ILs is often conducted under Schlenk-type conditions, *i.e.* under vacuum or a nitrogen atmosphere. Under more harsh reaction conditions (such as high acidities, basicity and temperatures *etc.*) ILs, particularly the functionalised TSILs, may not be as stable as previously envisioned. The often high viscosity of ILs is arguably one of their more prominent drawbacks, imposing mass transport limitations on the system as discussed above. Whilst it is possible to minimise this problem through fine tuning of the ion pair or by functionalization, the added difficulty in this procedure does highlight that the use of ILs in the liquid phase, either as a bulk solvent or in a liquid-liquid biphasic system, is less than ideal. Further issues also arise with regards to the biphasic system due to the requirement of a co-solvent, again

potentially negating the ILs 'green credentials'. Whilst it is possible to recycle and reuse the catalyst/IL phase this process is by no means perfect with catalyst and IL leaching often occurring.

To conclude, ILs possess unique properties and scope in the usage of catalytic processes, allowing for improvement in catalyst performance as well as its recycle and reuse, while their diverse, tuneable nature allows for optimisation for almost any conceivable system. However, their role and effect on a reaction system is often incredibly complex, making predictions very difficult. It is easy to consider ILs simply providing an "ionic environment", however the multiple possible inter- and intra-molecular forces, as illustrated in figure 1.3, illustrate the need for a more in-depth understanding of the ILs physicochemical properties and the role it plays in a reaction mechanism. While clearly advantageous under the correct conditions, the sometimes severe limitations of ILs, in particular their high viscosity and high cost, has led to considerable drive within the chemical community to develop new, different methodologies for their usage.

1.4. Supported Ionic Liquid Phase Catalysis

The major concerns evident when using ILs in homogeneous catalysis are most predominantly product isolation as well as the large quantities required, particularly when processes are conducted on a large scale. With regards to the latter point, the large quantities of IL required can be disadvantageous due primarily to the prohibitively high cost of the IL, as well as the potential toxicological concerns which arise from the lack of understanding of their long term stability. As such there has been a considerable drive to reduce the amount of IL used whilst still maintaining the positive influences in homogeneous catalysis; this led to the concept of the Supported Ionic Liquid Phase (SILP). In a typical SILP system (figure 1.7)⁶⁶ a small amount of IL is dispersed through a high surface area material, such as silica, alumina or an activated carbon, resulting in a high surface area thin film of IL. The catalyst of choice is then dissolved in the thin layer of IL to give what is essentially a homogeneous catalyst that can react in the same fashion described above; as such SILP effectively combines the positive properties of homogeneous and heterogeneous catalysis by providing a solid, insoluble material which can be easily isolated and reused but has the favourable performance of a homogeneous system. Further advantages of SILP over catalysis in bulk IL phases arises from the incredibly thin IL film on the support surface, which generally falls in the range of 10-50 Å.⁶⁷ As a result, the dissolved catalyst within the IL layer is close to the reaction interface, drastically reducing diffusion pathways and negating potential problems which arise from viscosity when using bulk or biphasic ILs. As such the use of SILP can often lead to enhanced rates when compared to the use of bulk ILs.

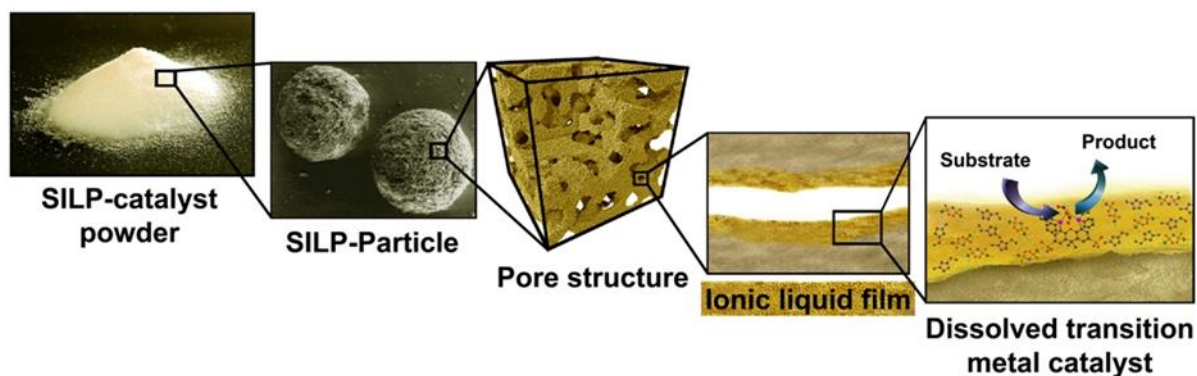


Figure 1.7 Schematic representation of Supported Ionic Liquid Phase (SILP) materials for catalysis⁶⁶

Early examples of the application of SILP include the impregnation of silica with pre-formed Lewis acidic ILs, most commonly consisting of aluminium chloride derivatives, which catalysed a range of Friedel-Crafts reactions.⁶⁸ As with their IL forbear, SILP materials have become increasingly popular, and as such, much more diverse in subsequent years, incorporating a variety of ILs, catalyst and support materials. In this regard there are essentially four main methodologies in the preparation of SILP materials (figure 1.8). The immersion method (figure 1.8 A) is arguably

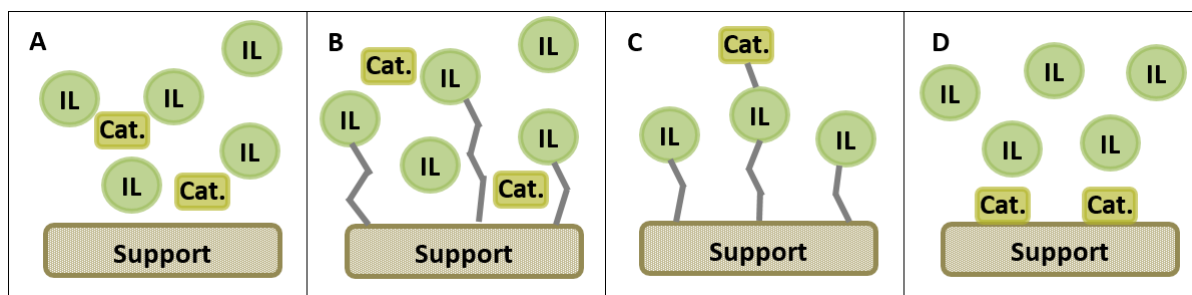


Figure 1.8 Illustrations of the four main categories of SILP-based catalyst materials: A) immersion method; B) and C) covalent anchoring methods; D) solid catalyst with ionic liquid layer

the most straightforward means of generating a SILP catalyst and is by far the most commonly used, particularly for the immobilisation of a homogenous metal complex. Preparation occurs by simple impregnation of the support material with a pre-prepared solution of the catalyst or precatalyst in IL, often in the presence of a suitable organic solvent (wet impregnation). Following the impregnation process the non-volatile nature of the IL allows for the organic solvent to be removed *in vacuo* leaving the desired dry SILP material. The use of highly porous silica gels (*c.a.* surface area of 300-500 m²g⁻¹)⁶⁹ as the support material appears to be the most prevalent choice by far, though mesoporous silica as well as silica-alumina systems such as zeolites have also been used.⁷⁰ The use of other inorganic materials, such as alumina, are much less frequently used due to their lower pore volume but may be favoured under certain conditions due to their greater tolerance to pH. Organic materials, such as the chiral polymer chitosan,⁷¹ and more advanced materials such as membranes,⁷² carbon nanotubes

and sintered metal fibres⁷³ have all found use. Materials generated through the immersion method have been well-documented in applications across a wide variety of catalysis including hydroformylation, olefin metathesis, carbonylation and hydroamination, as well as metal-catalysed carbon-carbon coupling.^{67,69,74} As stated previously the use of SILP materials affords advantages over bulk ILs with regards to ease of catalyst isolation and reuse as well as improved reaction rates due to the thickness of the IL being close to the reaction interface. However, unexpected effects can also occur upon confinement to the support material. For example, early work concerning Rh-catalysed hydroformylations on silica-based SILP materials showed that the organometallic complex formed in solution was also formed within the thin IL layer, with such an ordering effect leading to drastically reduced mobility of both the IL fragments and metal complex, which in turn resulted in unusual properties in the supported complexes.⁷⁵ A more profound example can be found in immobilisation of copper bis(oxazoline) complexes dissolved in [C₄mim][PF₆] on the layered, charged silicate Laponite. Proximity of the chiral metal complex to the support surface imposed rotational restrictions on the catalyst, giving what was essentially a two-dimensional nanoreactor which was suggested to be the cause of the reversal in enantioselectivity for cyclopropanation reactions compared to their homogenous counterparts.⁷⁶ The use of immersion-prepared SILP catalysts has been particularly successful in gas phase fixed-bed reactors, for example silica-immobilised Rh-catalysed hydroformylation⁷⁷ and methanol carbonylation,^{70b} whilst the use of scCO₂ as the transport vector has also been used in continuous enantioselective hydrogenations.⁷⁸ The use of such continuous processes has clear advantages with regard to catalyst reuse, an increased turnover frequency, and vastly improved space time yields as well as the potential for different reaction activities and selectivities. Despite the successful application of these SILP materials in continuous processes, examples are severely limited to gas phase processes, with the use of the liquid phase generating clear issues with regards to leaching of the IL and the immobilised catalyst.

In order to address the prevalent issues with leaching in SILP materials the covalent anchoring method (figure 1.8B) was established. In this methodology the surface of the support of choice is modified by either covalent attachment of a monolayer of an appropriate functionalized IL fragment or by sol-gel synthesis.⁷⁹ The desired catalyst, with or without additional 'free' IL, can then be immobilised on the material through wet impregnation. Numerous examples of this methodology have investigated the immobilisation of the organocatalyst L-proline on the surface of modified silica.⁸⁰ The application of these materials to the aldol reaction between acetone and several aldehydes gave good activity and enantioselectivity when compared to the homogeneous counterpart and, more importantly, was easily isolated and recyclable with only a minor drop in performance. A similar effect was also observed with the immobilisation of Mn III salen complexes on imidazolium-functionalised silica while also giving an enhancement in enantioselectivity.⁸¹

Functionalization of the support surface with an IL monolayer has also been extended to other support materials, for example carbon nanotubes (CNT) have been investigated due to their good mechanical strength, high chemical stability and high surface area-to-volume ratio.⁸² Functionalization of the surface of CNTs (figure 1.9) increases the material's affinity for [C₄mim][PF₆] and allows for high loadings of IL up to 55 wt% to be achieved with no detectable leaching. Immobilisation of Rh complexes afforded a material which proved to be highly active for the hydrogenation of 1-hexene, drastically outperforming analogous oxide-based support materials whilst fully retaining the Rh/IL phase upon recycle.

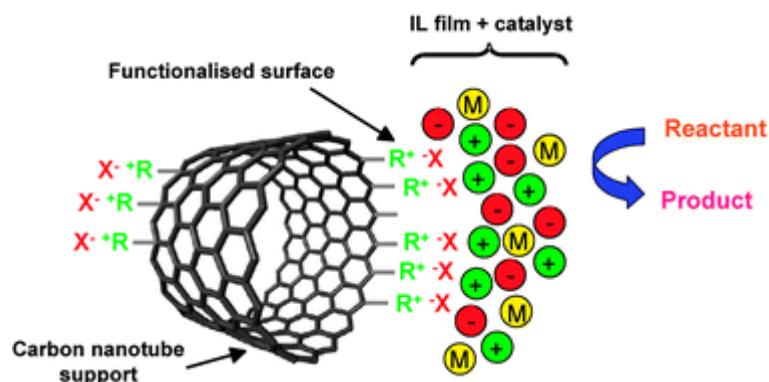


Figure 1.9 Surface functionalization of CNT material with imidazolium-based IL fragments used by Serp *et al* in the immobilisation of Rh hydrogenation catalysts⁸²

The use of covalent anchoring within SILP materials is not limited to tethering of the IL. In this regard, the ligand or the catalyst can also be covalently bound to the IL fragments (figure 1.8C). For example, work by Karimi and Enders functionalised the surface of silica with pendant methylimidazolium IL fragments. The resulting immobilised ILs were able to form N-heterocyclic carbenes upon addition of Pd(OAc)₂; the resulting material was highly active in the Heck reaction of various haloarenes whilst also exhibiting high thermal stability and promising recycle properties.⁸³

The final SILP methodology (figure 1.8D) involves the coating of a preformed heterogeneous catalyst with a thin layer of IL in a similar fashion to the immersion method; by using a heterogeneous catalyst leaching of the active species can be avoided. This type of methodology, generally referred to as “solid catalyst with ionic liquid layer” (SCIL),^{74, 84} has been applied to a range of chemistry, with the presence of the IL film giving enhancements in catalytic performance. For example, the use of a covalently immobilised Sc catalyst on silica for the aqueous phase Mukaiyama-aldol reaction gave a marked improvement in activity when a thin film of hydrophobic IL was introduced.⁸⁵ Whilst the use of this methodology still suffers the same potential leaching issues with regards to the IL fragments the use of a preformed heterogeneous catalyst can be extremely attractive as it avoids complex functionalization of the insoluble material which occurs in other immobilisation methods. For example, Kernchen and co-workers reported the use of imidazolium-based ILs on a commercially

available Ni catalyst.⁸⁶ In the sequential hydrogenation of 1,5-cyclooctadiene to cyclooctene and cyclooctane the presence of the IL film facilitated a marked improvement in both activity and yield when compared to conventional biphasic systems, illustrating the promise and potential of this approach for application across a wider range of commercially available catalysts.

SILP catalysis has been widely demonstrated to successfully combine the attractive aspects of both heterogeneous and homogeneous catalysis whilst also offering additional advantages with regards to product separation and catalyst recycle when compared to IL-based liquid-liquid biphasic systems. In particular SILP catalysts are most successful when used in fixed bed reactors for continuous gaseous phase reactions and offer the potential to improve catalyst turnover and space time yields which would render such systems incredibly attractive for industrial processes. The use of alternative transport vectors, such as $scCO_2$, as well as covalent attachment of the ILs to the support material have, to an extent, circumnavigated the limitations of SILP imposed by leaching when used in liquid phase systems. Despite this, multiple limitations still remain; with regards to the former, high investment and operating costs as well as the limited solvating ability of $scCO_2$ can mar the advantages associated with its use, whilst the latter method suffers from the same added complexity issues as TSILs discussed previously.

Further complexities in the general application of the SILP methodology arise from the use of the support material, which can have a profound influence on the reaction. Considerations must be made about the effect the support has on catalyst performance as well as the interactions between the support material and the catalyst and IL; this makes SILP systems incredibly difficult to understand mechanistically and kinetically. Confinement of catalytic species in a thin layer of IL has proven to be a largely positive effect by overcoming mass transport limitations, however, it cannot be assumed that this will be the case for every support-IL-catalyst combination as confinement can also occasionally impose unexpected geometric constraints on organometallic complexes. Proximity of the catalyst to the support surface has been shown to also have a profound effect on chiral catalysts, drastically altering selectivity in sometimes unexpected ways. Further issues can arise with regards to the chemical stability of the support material under harsher reaction conditions. For example, in the Rh-catalysed hydroformylation of propene using silica-based supports, a significant drop in catalyst performance was associated with an irreversible reaction between the catalyst, ligand and the acidic silanol groups present on the silica surface. The study illustrated that partial dehydroxylation was essential to achieve efficient SILP catalysts under these conditions.⁸⁷

The complex nature of the relationship between support-IL-catalyst in SILP materials has led to less-defined fundamental understandings of numerous aspects of the systems, making it difficult to make broader, more general statements about SILP materials. Instead, an in-depth understanding

for each specific catalytic process will require detailed mechanistic studies as well as thorough investigation of the basic reaction kinetics. In this regard, the use of SILP methodologies is a constantly evolving field, with considerable emphasis on improving the fundamental understanding of the supported catalysts as well as developing novel materials which may address the limitations associated with SILP.

1.5. Polymer-Immobilised Ionic Liquid Phase Catalysis

As discussed previously, the concept of supported ionic liquid phase catalysis has been applied to a wide variety of different materials, which are predominately high surface area inorganic matrices. By extension of the application of SILP, organic polymers have also been explored as the support material,⁸⁸ essentially combining the advantages of SILP with the tuneable microstructure, ionic microenvironment, charge density and distribution, functionality and hydrophilicity/hydrophobicity of polymers. While there are examples of polymers being used in conventional SILP systems, such as the biopolymer chitosan for the immobilisation of Pd(OAc)₂ and [C₄mim] ILs for allylic substitution reactions,⁷¹ the majority of examples concern the use of covalent anchoring type materials. In this regard a suitably functionalised polymer can be tagged with an IL moiety in a manner similar to that discussed above or, more commonly, an IL fragment can be functionalised in to a suitable monomer and subsequently polymerised. The latter methodology has been extensively used in recent years to generate a subclass of polyelectrolytes dubbed poly(ionic liquid)s (PIL). Such materials have been well-documented and found applications in a range of different disciplines including electrochemical devices, sensor technology and in purification/scavenging systems.^{88c, 88d} The use of PILs in catalysis is dominated by vinylimidazolium and polystyrene-based polymers due to the relative ease of synthesis of suitable polymerisable ILs, often generated by the straightforward alkylation of an imidazole with a vinylbenzyl halide. Such systems have been applied to various different areas of catalysis, however, the scope of application again appears to be rather limited with most examples concerning the immobilisation of transition metal nanoparticles. For example, palladium immobilised on the imidazolium-tagged cross-linked polystyrene resin **1** (figure 1.10) has shown to be an active catalyst for the Heck arylation, acting as a reservoir to release and recapture the active palladium species.⁸⁹ Dubbed a gel-supported ionic liquid-like phase (g-SILP) by the authors, the system supports the Pd via a *N*-heterocyclic carbene functionality, giving an active catalyst which was both air- and moisture-stable and that could be recycled over 5 runs with very little Pd leaching or drop off in catalyst performance. This system also effectively demonstrates the importance of control of the support microenvironment with the catch and release mechanism being dominated by the ionic environment whilst the resulting metal nanoclusters were stabilised by additional imidazolium

cations. A high ionic loading (and hence charge density) caused a reduction in catalyst activity but increased the efficiency of recycle, while the anion of the IL had a profound effect on activity, with strongly coordinating anions reducing the activity and weakly coordinating anions, such as $[\text{SbF}_6]^-$ and $[\text{BF}_4]^-$, giving high catalyst activity but poorer recyclability. A similar fine tuning effect can be observed across numerous different polymer systems, through judicious choice of the anion and cation and by adjusting the ionic loading and morphology the properties of these materials, such as thermal stability, hydrophilicity, swelling and polarity can all be tuned in a rational manner, highlighting the advantages of using a polymer as the support material over other inorganic supports.⁹⁰ Similarly, Pd nanoparticles were produced through the complexation of PdCl_2 with linear main-chain viologen polymers and subsequent reduction.⁹¹ Through this procedure, ionically convoluted insoluble polymer matrices were obtained, with the interaction between polymer chains and the metal species providing effective cross-linking. These materials proved to be highly efficient, recyclable catalysts for the α -alkylation primary alcohols under mild, solvent free conditions. Systems such as these highlight the synergistic effect with regards to a material's physical properties which can be achieved between well-defined catalysts and polymer species.

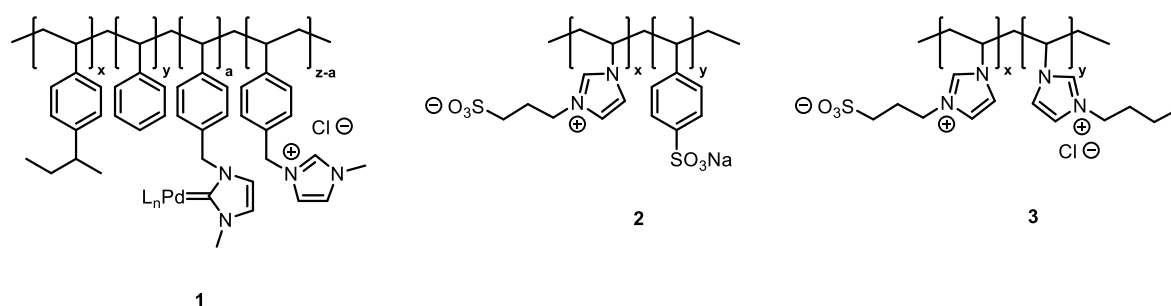


Figure 1.10 Examples of different functionalised polymers used as catalyst supports taken from the literature

Other examples of the application of polymer supports in SILP-type systems include a dual catalyst system comprised of Pd nanoparticles stabilised by the sulfonated, water-soluble polymers **2** and **3**, and a heteropoly acid (HPA).⁹² The resulting system was incredibly active and selective catalyst for the hydrogenation of phenol and gave cyclohexanone in almost quantitative yield (>99% selectivity). The combination of Pd and the HPA proved to be the most efficient catalyst, outperforming similar systems based on Pt, Ru and Rh nanoparticles, a Pd/C catalyst or when conducted in the absence of acid. The authors postulated that the ionic polymer was able to both stabilise the Pd nanoparticles and control the reaction selectivity through the creation of macromolecular cavities which were lined with ion pairs and the sulfonic acid groups. The presence of these cavities effectively concentrated the phenol through favourable hydrogen-bonding interactions whilst also displacing cyclohexanone before it could react further. The success of this system demonstrates the potential impact of control over the support microenvironment and

morphology on catalyst performance, and that the control of these factors through polymer modification could be a useful concept that could be applied across a range of reaction types.

The application of IL-tagged polymers to support catalysts has also been extended to commercially available materials. In this regard ion-exchange resins, commonly used in water purification, metal recovery/separation and chromatography applications, have been well documented as supports for catalytic applications.⁹³ The vast majority of ion-exchange resins, such as the sulfonic acid-functionalised Amberlyst® and the quaternary ammonium-functionalised Amberlite®, consist of a polystyrene network which is cross-linked to varying degrees bearing different ionic moieties (figure 1.11). As readily available insoluble materials, ion-exchange resins can be an attractive prospect when preparing heterogeneous catalysts, in particular, quaternary ammonium based anion exchange resins which can mimic the effects of IL on a catalyst centre. In this regard heterogeneous analogues of homogeneous catalysts can be prepared by simple ion exchange of the resin's counterion with a suitably charged precatalyst, negating the need for any prior material synthesis. Functionalization of the ionic sites on the resin can also be exploited to give suitable IL moieties which will have improved ionic affinity to the desired catalyst or even bind it covalently.⁹⁴ To this end, ion-exchange resins have been used to immobilise a wide variety of organometallic complexes which have been successfully applied to recyclable processes across a range of reactions including carbonylation,⁹⁵ hydroformylation,⁹⁶ hydrogenation⁹⁷ and oxidation.⁹⁸

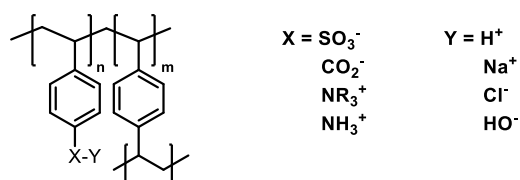


Figure 1.11 Common commercially available ion-exchange resins

As stated previously PILs, by merit of their unique, tuneable properties which can combine the attractive aspects of both ILs and polymers, have been receiving increasing interest across varying different chemical disciplines. However, despite the clear advantages offered by the ability to fine tune the microenvironment and morphology of support materials as well as the enormous range of functionalization possible, the use of PILs is somewhat more limited in scope when applied to the field of catalysis, which is often considered more of an upcoming field.^{88c, 88d} In this regard the use of IL-functionalised polymers is largely limited to the use of polystyrene-based systems which are most often used for the stabilisation of transition metal nanoparticles.^{88d, 99} As such the work presented in this thesis was undertaken to develop the use of IL-decorated polymers as general tools in the heterogenisation of homogeneous catalysts for use across the whole spectrum of synthesis. By exploring appropriate, well-defined polymer chemistry it will be possible to generate materials that possess chemical and physical properties which are both suitable for different reaction conditions

and can, in principle, be altered in a rational manner to fine tune the resulting materials to give optimum catalyst performance. As an evolution of the SILP methodology the materials developed in this work have are described as the Polymer-Immobilised Ionic Liquid Phase (PIILP) and can be defined as a polymer/co-polymer formed from one or more types of prefabricated ionic liquid-like monomer and, if required, an appropriate co-monomer, therefore they do not require post-polymerisation modification (figure 1.12). Following the preparation of a suitable support material, the desired catalyst can be immobilised via impregnation methods. By immobilising pre-formed homogeneous catalysts or their corresponding precursors in this manner, it will be possible to effectively combine the high activity and selectivity of homogeneous catalysts with the positive aspects of heterogeneous catalysis.¹⁰⁰ Through the use of a prefabricated IL-tagged monomer an additional degree of control over the final PIILP material can be achieved with regards to purity of the product as post-polymerisation modifications can often be difficult and non-quantitative. Although challenging it will be necessary to undertake detailed studies into the nature of the relationship between the polymer support and the catalyst if PIILP is to be utilized to its full potential, in this regard allowing for the rational alteration of the support material through controlled, operationally straightforward polymer chemistry to achieve optimum, highly efficient heterogeneous catalysts.

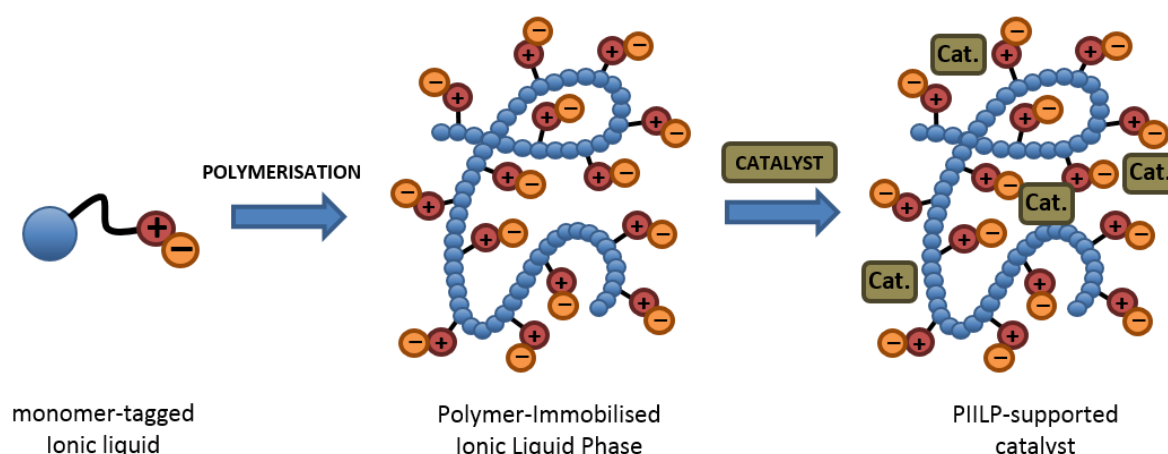


Figure 1.12 Basic principle behind Polymer-Immobilised Ionic Liquid Phase (PIILP) catalysis

1.6. Polymerisation Methods

Polymers decorated with ILs, particularly PILs, are largely well-documented and have been prepared through a range of different polymerisation methods.^{88c, 88d} However, as stated previously the use of these materials in a manner similar to the proposed PIILP is largely limited to radical-initiated polystyrene-based systems, which can not only limit the scope of functionalization possible in the final polymer material but often requires post-polymerisation modification. If the PIILP methodology is to be used to its full extent it will be necessary to consider different polymerisation methods to

achieve the broadest design potential possible, as such common polymerisation methods are briefly discussed and evaluated as tools of the synthesis of PIILP catalyst supports.

1.6.1. Step Polymerisation

Step polymerisation consists of successive conventional organic reactions between mutually reactive functional groups on the monomers to generate oligomeric materials and is ubiquitous in the production of everyday polymers. The majority of step polymerisations involve reactions between heteroatom-containing functional groups resulting in highly functionalised polymer backbones, for example polycondensation reactions to generate polyesters, polyethers and polyamides. Due to the nature of chain formation in step polymerisations incredibly high degrees of conversion are required to achieve long chain lengths, as such it is often difficult to obtain high molecular weight polymer molecules. The number and type of functional groups present in the monomers used is of key importance, with chain growth requiring two mutually reactive units on each monomer. The presence of three or more reactive groups on each monomer leads to polymer chain branching and cross-linking, while one group results in chain termination. As step polymerisation relies on the extent of a straightforward organic reaction the chain length, or degree of polymerisation, in linear systems is related to the reaction time. As such desired molecular weight products can be potentially obtained by quenching the reaction at an appropriate time. This method, however, can result in the isolation of polymers containing unreacted end groups and hence alterations in the desired chain lengths. In order to effectively control the chain length of a linear polymer the stoichiometry of the reacting monomers must be carefully controlled. In this sense one of the reagents is present in a slight excess to ensure that the other monomer is completely consumed, and that the chain ends therefore have the same functional group as the reagent in excess to prevent further polymerisation. Other methods include the addition of monofunctionalised monomers to essentially cap the growing polymer chain.⁹⁴

Polymers containing ILs prepared through step growth polymerisation have been prepared by various means (figure 1.13). The most direct method involves quarterisation of alkyldihilides with a suitable nitrogen-containing unit such as an imidazole to afford **4** which can be further modified by anion exchange to give the desired PIL.¹⁰¹ Ionic polyolefins such as **5** have also been prepared via acyclic diene metathesis polymerisation (ADMET)¹⁰² whilst hydroboration polymerisation of diallylimidazolium ILs lead to polymer **6**.¹⁰³ Polycondensation reactions have also been exploited to yield PIL materials such as polyimide **7**.¹⁰⁴ In each case these materials were used as solid electrolytes.

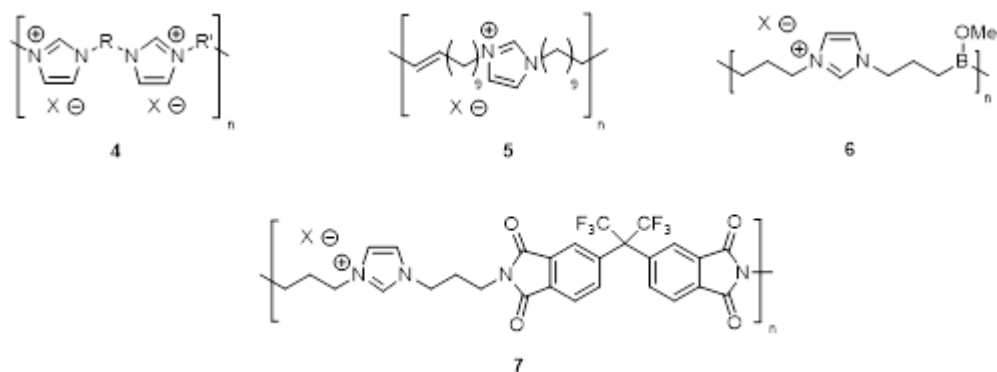


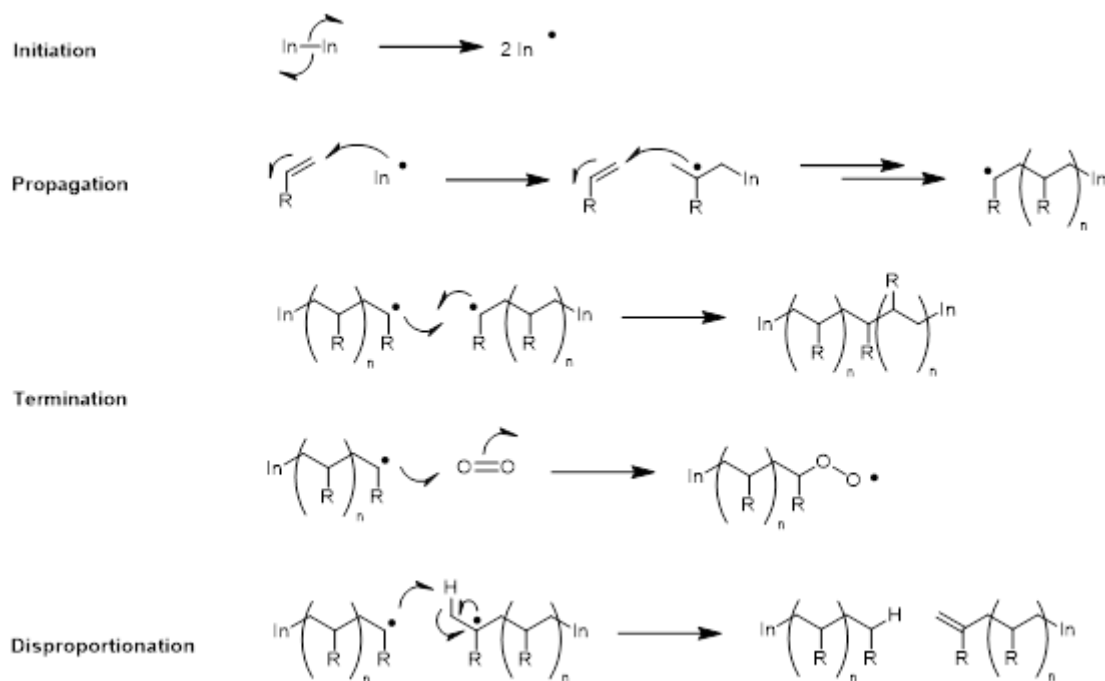
Figure 1.13 Examples of PILs prepared through step growth polymerisation methods

The use of step growth polymerisation methods to generate materials used in catalysis is largely unexplored, which is most likely an artefact of the reactive groups required to form the polymer backbones. The presence of heteroatoms and vinyl groups could potentially be attacked by the supported catalyst, which would alter the composition of the polymer and potentially affect catalyst performance upon recycle and reuse. The requirement for specific functionality in the monomers in order to achieve polymerisation also severely limits the scope of IL moieties which can be accessed, with more varied functionalities potentially leading to unwanted polymer branching/cross-linking or degradation of the IL fragment during polymerisation.

1.6.2. Radical Polymerisation

The use of radical polymerisation chemistry is by far the most commonly used and versatile method for polymerisation used across chemical disciplines. As with all chain-growth polymerisations, in which an unsaturated monomer adds to the active site of the growing chain, the use of free-radicals consists of 3 reaction steps, initiation, propagation and termination.¹⁰⁵ While there are numerous means to achieve initiation, most commonly an initiating molecule, such as a peroxide or azo-compound like azobisisobutyronitrile (AIBN), undergoes homolytic bond fission through either thermal decomposition or photolysis to generate an active radical species. The active species then attacks the π -bond of the unsaturated monomer (most commonly a C=C double bond) to generate

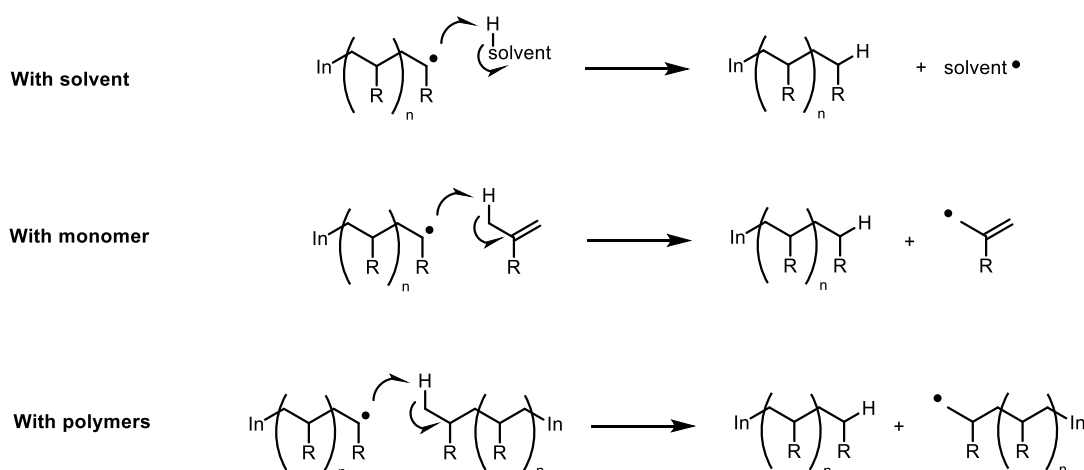
another active radical centre. Propagation of the polymer chain then proceeds via rapid sequential addition of the monomer to the active centre which repeats until the radical is terminated either by combination of two radical species, radical disproportionation (in which a hydrogen atom from one polymer chain is abstracted to another to give a saturated group) or by interaction with inhibitors, such as oxygen.¹⁰⁶ Termination type events are also possible in which only one radical centre is



Scheme 1.6 Initiation, propagation, termination and disproportionation steps of free-radical polymerisation

destroyed. Mechanistically these proceed in a similar manner to disproportionation, accompanied by a transfer of an active radical centre to another forming polymer chain (scheme 1.7). These chain-transfer events can occur with different components of the reaction mixture such as the initiator, unreacted monomer and solvent, meaning it is important to take careful considerations into account when preparing designer polymers which may require unsuitable solvents or other reagents. The presence of chain-transfer reactions can often be problematic with regards to reduction in polymer chain lengths as well as unwanted cross-linking. Whilst problematic, steps can be taken to avoid chain-transfer: for example the amount of chain-transfer which occurs with the solvent molecules is dependent on the amount of solvent present, allowing for a reduction by essentially increasing the reaction concentration, whilst the stability of the forming radical also increases the probability of chain-transfer. For example, halogen radicals are relatively stable¹⁰⁷ meaning that avoiding the use of halogenated solvents in polymer synthesis can reduce chain-transfer. This methodology may not be entirely appropriate for the preparation of functionalised PIILP-type materials due to limitations imposed by reactant solubility and functional group tolerance in the presence of free radicals.

The kinetics of free radical polymerisation are well understood and the rates of initiation, propagation, termination and chain-transfer can all be easily defined.¹⁰⁵ Under the steady state approximation the concentration of the reaction intermediate, in this case the growing polymer chain, remains constant. In this regard the rate of initiation and termination are the same, as a result there is little control over the polymer chain lengths present in the synthesised sample. A measure of the uniformity of chain lengths can be expressed by the polydispersity index (PDI), which is defined as the weight average molecular weight (M_w), the statistical mean molecular weight taking the weight fraction of each species in the sample into account, divided by the number average molecular weight (M_n), the statistical mean average molecular weight of all polymer chains in the sample. In the ideal, completely uniform sample, M_w will be equal to M_n giving a PDI value of 1. Due to the largely uncontrolled way in which chains propagate during free radical polymerisations there can be considerable variation in the average polymer chain length, as highlighted by the polystyrene standard used in gel permeation chromatography (GPC) which possess PDIs close to *c.a.* 1.2.¹⁰⁸

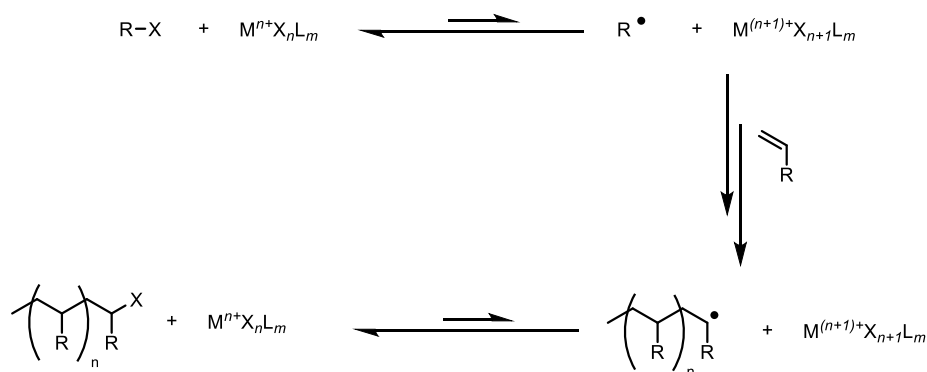


Scheme 1.7 Different modes of chain-transfer in free radical polymerisations

To conclude, although the free-radical polymerisation process, particularly utilizing styrene-based monomers, is well-documented and thoroughly understood, its application could potentially lead to issues in the production of PIILP materials. For instance, the requirement of radical initiators may not be compatible with all functionalities required for designer IL moieties whilst the largely uncontrolled nature of the polymerisation leads to non-uniformity within the sample through varied chain lengths as well as unwanted cross-linking through chain-transfer reactions. Due to the complex relationship between catalyst, IL and support material it is important to produce materials which are as well-defined as possible in order to assist in the rational understanding and eventual alteration of the support micro-environment to give optimum catalyst performance. Whilst these effects on polymer composition can be minimised through careful choice of reagent and solvent the potential imposition on reaction conditions required may also limit the overall design principle of PIILP.

1.6.3. Living Radical Polymerisation

As the use of standard free radical polymer chemistry can lead to somewhat ill-defined polymer samples with regards to uniformity of polymer chains, numerous methods have been developed to address this. In this sense, the desired effect is to remove the ability of the propagating polymer to undergo termination or chain-transfer reactions, resulting in systems in which the propagating chains grow at a much more consistent rate. With regards to radical systems, this generally involves the trapping and temporary deactivation of chain radicals.¹⁰⁵ Additional benefits can also be achieved by ensuring that the rate of initiation is much higher than the rate of propagation, further improving the uniformity between the growing polymer chains. Such systems are deemed living polymerisations as the lack of termination leaves the forming chains with active centres and polymerisation will continue as long as there is unreacted monomer present. The combination of the more uniform manner in which polymer chains propagate and the ability to control the chain length of the sample through the monomer stoichiometry/concentration makes living polymerisation highly desirable for the controlled synthesis of well-defined polymer materials. Numerous living systems have been explored; however, with regards to radical polymerisations two methodologies are most prominent. The first method, atom-transfer radical polymerisation (ATRP), is arguably the most documented and well developed. First introduced in 1995¹⁰⁹ ATRP (scheme 1.8) employs the use of transition metal catalysts which undergo single-electron transfers with organic halides, leading to homolysis of the R-X bond and the formation of an alkyl radical initiator. During this process the oxidation state of the metal centre is increased by 1 unit and subsequently the formed halide radical is trapped. During chain propagation the reverse of this process occurs which causes the oxidised transition metal to donate a halogen atom to the active centre on the chain thereby terminating the polymerisation through the formation of a new C-X bond and regeneration of the active metal centre. In this regard, chain growth proceeds through a series of activation-propagation-deactivation cycles. Through careful choice of the initiator, activator complex and reaction temperature it is possible to ensure that the equilibrium in these cycles favours capped polymer chains with no active centre. This results in rapid exchange and ensures that the concentration of active propagating chains is low, drastically reducing the probability of bimolecular termination reactions.



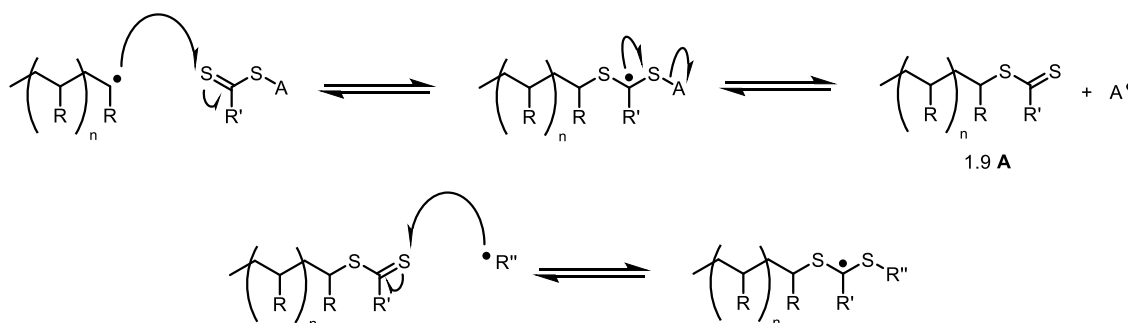
Scheme 1.8 Basic representation of atom-transfer radical polymerisation (ATRP)

The use of ATRP has proven to be incredibly useful in synthesis by showing good functional group tolerance, including amino-, hydroxy- and vinyl groups, whilst also employing the use of inexpensive, commercially available catalysts, often comprised of copper complexes in conjunction with pyridine-based ligands.¹⁰⁷ As such ATRP has been used to prepare different PILs, including various hydrophobic tetraalkylammonium-based PILs¹¹⁰ and the production of environmentally friendly, well-defined alkylammonium PILs for different purposes.¹¹¹

Although ATRP has been successfully used to generate a wide variety of polymers with narrow molecular weight distributions, whilst also exhibiting good functional group tolerance, some limitations still remain, in particular, with regards to the often high temperatures required to achieve reaction. Again this may not be entirely appropriate in the application of the PIILP methodology as some of the more complex functionalised IL moieties may be unable to tolerate harsher conditions.

The second common method of living radical polymerisation is reversible addition-fragmentation chain-transfer (RAFT), in which chain-transfer is exploited to achieve control over the growing polymer chains. First discovered in 1998, RAFT uses thiocarbonyl compounds as chain-transfer agents which fragment during the chain-transfer step to generate a new radical and a new dithioester species (scheme 1.9).^{105,107} In order for the chain-transfer reaction to be straightforward, the reactivity of the active radical centre in the forming chain and the radical generated by fragmentation of the thioester group must be similar, whilst still being reactive enough to activate the exchange process. Through this process, the active radical centre on the propagating chain is trapped by the dithioester RAFT agent to afford 1.9 **A** which remains inactive until another radical species adds to the resulting thioester end group. As with ATRP, the effective concentration of radical-containing propagating chains remain very low throughout the polymerisation with initiation and addition-fragmentation chain-transfer events with the dithioester agent being more dominant; this severely reduces the probability of bimolecular terminations. Unlike ATRP, in which the metal acting

as a single-transfer agent is catalytic, the RAFT agent will eventually be consumed with the thioester groups forming part of the polymer architecture.



Scheme 1.9 Reversible-addition-fragmentation chain-transfer (RAFT) process between a propagating polymer chain and the dithioester RAFT agent

Whilst RAFT shows very high functional group tolerance with regard to the monomers used (for example methacrylates, methacrylamide and acrylonitrile based monomers), the relative reactivity of the reacting components must be finely balanced in order to achieve effective reversible-addition-fragmentation chain-transfer. In this sense, the constituents on the RAFT agent are of particular importance as the R' has a dramatic influence on the stability of the C=S double bond as well as the subsequent adduct radical which forms after fragmentation. These in turn affect the position and rates of the equilibria throughout the polymerisation. The leaving radical **A** must be stable enough to push the equilibria shown in scheme 1.9 to the right yet reactive enough to reinitiate growth of a new polymer chain, as such the RAFT agent employed must be carefully tailored with consideration to both the monomers being used as well as the reaction temperature.

Due to its living nature, RAFT (as well as ATRP) can be exploited for the synthesis of block copolymers. In this regard, one monomer of choice is added to the reaction mixture and completely consumed to afford a homopolymer with a narrow molecular weight distribution and an active radical centre, addition of a second monomer continues the polymerisation to afford a block co-polymer. Through this procedure and careful control over reaction stoichiometry it is possible to generate well-defined block lengths within the copolymer. Although advantageous, the production of such block copolymers under RAFT conditions can prove challenging with regards to finding a RAFT agent which is compatible with two different monomer systems.¹¹² The use of multifunctional RAFT agents can also be used to generate highly branched materials such as star, brush and comb polymers. Thus, the combination of multifunctional raft reagents and living polymerisation could present an opportunity to prepare designer PIILP supports with functionalised channels within the matrix which could facilitate and direct reagents during a reaction. Again there are numerous examples of PILs produced through RAFT, including various imidazolium-based block copolymers.¹¹³

Whilst showing promise for the development of the PIILP methodology, the effective use of RAFT may prove somewhat challenging. Despite the relatively large functional group tolerance the use of a RAFT agent can still somewhat limit the potential for monomer functionalization, whilst the incorporation of thioester groups, albeit in very low concentrations, could potentially affect the performance of a supported catalyst, leading to the need for post-polymerisation chemical and physical purification steps. Again the ability of both ATRP and RAFT to form block copolymers could prove to be a highly desirable tool in the production of designer catalyst supports, however, a rational understanding of how these properties influence catalyst performance may prove to be difficult to obtain.

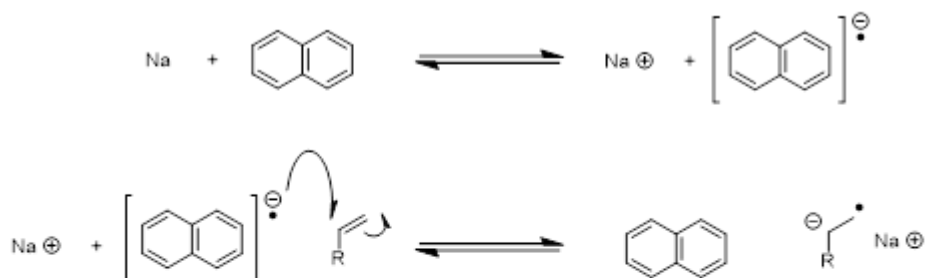
1.6.4. Ionic Polymerisation

Ionic polymerisations are chain growth polymerisations in which the active centres are comprised of either ions or ion pairs and can be considered an alternative to radical systems for olefinic monomers. Due to the presence of an ionic charge in the active centre, ionic polymerisations are much more monomer-specific than radical-initiated systems and require substituent functionality that can stabilise the active centre.

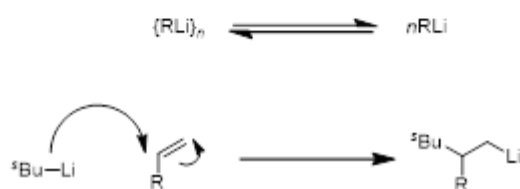
Anionic polymerisations have been studied since the early days of polymer chemistry, often employing a strong base as initiator in a solvent that allows chain transfer; however, these conditions severely limited the degree of polymerisation which could be achieved. Despite these limitations, anionic polymerisation has become ubiquitous in modern chemistry, for example, in the production of synthetic rubbers and elastomers.¹¹⁴ In modern anionic polymerisations the desired active carbanion is generated through two means, either single electron transfer from a suitable metal centre to give a monomeric radical-anion, or by reaction with an organometallic such as butyllithium.^{107,105} For the former, initiation occurs via a dicarbanion species which is formed from the organic radical-anion. Commonly this can be achieved through the use of alkali metals such as sodium with aromatic compounds such as naphthalene (scheme 1.10 a). The use of alkali metals can present issues related to the solubility of the electron-transfer complex, with heterogeneous conditions yielding incredibly slow initiation, as such the solvent choice is generally limited to ethers, such as THF. Initiation via the use of organolithium bases can negate this limitation as these compounds are often soluble in non-polar media. Although aggregation of the organolithium species can lead to a reduced activity the addition of a small amount of polar solvent can solvate lithium ions which is often sufficient to reduce this effect.¹⁰⁵ Increasing the polarity in this fashion favours the

disaggregation of the organolithium species, increasing the amount of free alkyllithium responsible for initiation (figure 1.10 b). As such an increase in initiation speed is observed.

a) Initiation by Electron Transfer



b) Initiation with Organolithiums

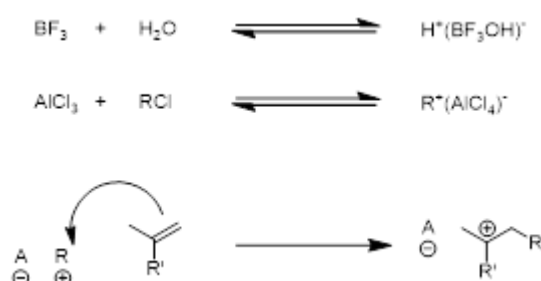


Scheme 1.10 Initiation steps in anionic polymerisations

One of the more favourable aspects of anionic polymerisation is the often absent termination process. Due to the charged nature of the active centre, bimolecular termination is not possible due to Coulombic repulsion. As such, anionic polymerisations are largely considered to be living processes with a high degree of control over chain formation and polydispersity. In order to fully utilise the lack of termination, anionic polymerisations must be conducted under high purity condition as trace amounts of oxygen, CO₂ and water all lead to termination. As such intentional termination can be achieved through the addition of alcohols, water or Brønsted acid which can also act as a chain transfer agent through neutralisation of the anionic active centre.¹¹⁵

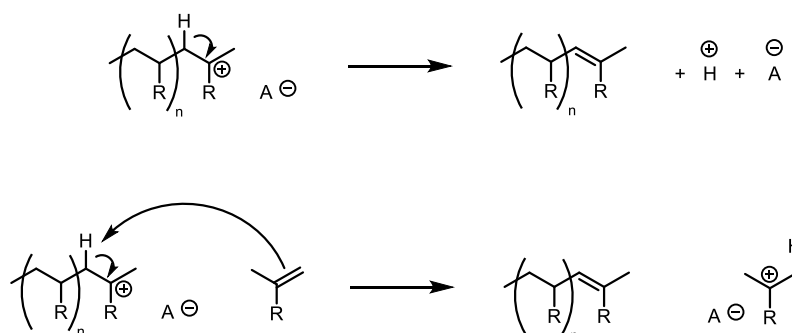
As with its anionic counterpart, cationic polymerisation has been extensively studied since the early days of polymer chemistry; however, due to the restricted range of monomers, with predominately olefinic and heterocyclic monomers reactive under these conditions, it has found relatively few applications.¹⁰⁵ In this regard, polymerisation occurs through highly reactive carbocations which have a strong tendency to undergo chain transfer and rearrangements, which severely limits the control available over chain length as well as the skeletal structure in the end product. Initiation in cationic polymerisation is commonly achieved through the use of strong acids, either classical protic or Lewis acids/Friedel-Crafts catalysts such as BF₃ or AlCl₃. With regards to the latter, a much faster rate of reaction is achieved using water, alcohols or even carbocation donors

such as esters and acid anhydrides as the cation source scheme 1.11). Functionality present in the initiator and monomer is clearly important for polymerisation process, for example halide-based acids such as HF are clearly unsuitable due to the ability of the counter-ion to rapidly combine with the generated carbocation. In a similar fashion the initiated monomer cannot bear any nucleophilic functionality as this too will instantly react with the carbocation active centre.



Scheme 1.11 Initiation with Lewis acids and Friedel-Crafts catalysts in cationic polymerisations

As in anionic polymerisation, the charge present on the active centre prevents bimolecular termination, however, unlike anionic polymerisation unimolecular termination events are possible. In this regard, termination occurs either by the generation of a terminal C=C bond by molecular rearrangement to release a proton or by chain transfer yielding a monomeric carbocation (scheme 1.12). In both cases the resulting electrophile is associated with a counter anion, beginning the growth of a new polymer chain; as such little change to the concentration of propagating species is observed. Terminal C=C bonds formed through termination of chain transfer are of very low activity due to the steric hindrance brought about by the 1,2-substitution and such bonds are unlikely to reinitiate for the rest of the polymerisation process. Again, chain transfer is also possible with the solvent or trace impurities in the reaction mixture such as water, meaning that the solvent of choice and purity is of the utmost importance.



Scheme 1.12 Termination and chain transfer steps in cationic polymerisations

The use of cationic polymerisation is a largely limited technique with respect to the scope of monomer functionality as well as limited control over the growing polymer chain length and branching features and as such is unlikely to be a viable method for use in the synthesis of PIILP supports. Whilst this aspect is somewhat improved in anionic systems, with the lack of any formal

termination step the presence of a charged active centre will clearly prohibit the use of preformed IL moieties as outlined in the initial PIILP method rationale; standard post-polymerisation procedures have to be employed to apply ionic polymerisation to the synthesis of polymer immobilised ionic liquids.

1.6.5. Ring-Opening Polymerisation

Ring-opening polymerisations are a subclass of polymerisation reactions in which the reaction is driven by the relief of bond-angle strain and/or steric repulsion in cyclic monomers. Commonly ring-opening polymerisations can proceed through sequential addition of cyclic monomer to an ionic centre in a similar fashion discussed above but with additional enthalpic driving forces, however, there are also non-ionic mechanisms which can also proceed through condensation or radical reactions.¹¹⁶ As such ring-opening polymerisations encompass a wide variety of cyclic monomers including alkanes and alkenes as well as heteroatom-containing species such as ethers, phosphates and siloxanes.¹¹⁶ Due to this, ring-opening polymerisation is considered a versatile polymer methodology, particularly with regards to the production of biopolymers.

Of particular note within ring-opening polymerisations is ring-opening metathesis polymerisation (ROMP), which utilises transition metal-based carbene complexes including W, Mo, Re, Ru and Ti, to give unsaturated polymers from strained olefin monomers.¹⁰⁷ Early ROMP catalysts were based on W and Mo-mixed alkylidene-imido complexes (figure 1.14A), however, more recently Ru-carbene containing Grubbs' catalysts (figure 1.14B-C) have evolved as powerful tool for the C-C bond formation; this methodology been applied in the agrochemical and pharmaceutical industries.¹¹⁷ Although Grubbs' catalysts are generally less active than the traditional Schrock-type metathesis catalysts they exhibit exceptional functional group tolerance and are air- and water-stable.¹⁰⁸ This is a direct result of the electron-rich ruthenium centre, as opposed to the electron-

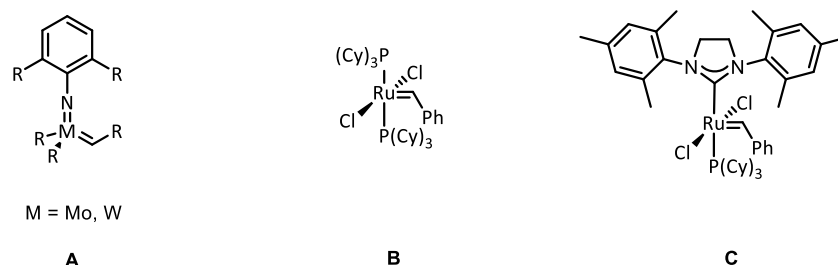
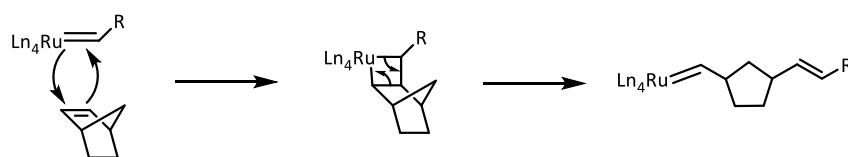


Figure 1.14 General Schrock-type and 1st and 2nd generation Grubbs metathesis catalysts

poor molybdenum and tungsten centres present in Schrock-type catalysts, which require catalyst preparation prior to use and an inert atmosphere whilst handling.¹¹⁸ Due to its soft nature, the ruthenium centre of Grubbs' catalysts will bind preferentially to soft Lewis bases and π -acids such as olefins over harder centres like N- and O-donors. By exploiting this functional group tolerance it is possible to use ROMP to generate functionalized polymers which contain the desired IL-like fragments simply by a judicious choice of monomer. Thus, the use of ROMP to directly incorporate the ionic fragments negates the need for post-polymerisation modification which is generally associated with the alternative polymerisation methods described above.

ROMP catalysed by Grubbs' catalyst proceeds via a cycloaddition reaction between the metal-carbene bond of the catalyst and a strained double bond of a cyclic olefin. The resulting metallocyclobutane intermediate reopens to reduce ring-strain to afford the first unit of polymer attached to the catalyst via a new metal carbene (scheme 1.13). Another unit of monomer then inserts into this newly formed metal-carbene to propagate the polymerisation. As the rate of initiation in ROMP is typically far greater than the rate of propagation the polymer chain grows at a consistent rate to afford a polymer with a very narrow mass distribution and of a desired molecular weight, based on the catalyst loading. Typically ROMP reactions using Grubbs' catalyst have been illustrated to be capable of achieving PDIs < 1.1 ¹⁰⁸; in contrast, the polystyrene standards used in gel permeation chromatography experiments to determine the weight and number molecular weight averages typically have a PDI of 1.2. As the metal-carbene responsible for propagation is present and relatively stable throughout the reaction¹¹⁸ ROMP is a living process; this allows the length of polymer chain, as well as the microstructure and ionic microenvironment, to be controlled directly by altering the concentrations of catalyst and functional co-monomers.



Scheme 1.13 General mechanism of ring-opening metathesis polymerisation (ROMP) catalysed by Grubbs Ru-carbene catalysts

Utilizing ROMP to generate suitable materials for PIILP catalysis requires monomers which contain strained cyclic systems. In this regard, bicyclic norbornene-based monomers have been polymerised efficiently using ROMP under relatively mild conditions and as such it is an ideal framework with which to introduce ionic liquid like fragments into a polymer.¹⁰⁸ Furthermore norbornene derivatives are readily prepared via a single step Lewis acid catalysed Diels-Alder cycloaddition between cyclopentadiene and a functional dienophile; the resulting adduct can be further modified/functionalised to afford a wide range of IL-based monomers. Previously Grubbs-catalysed ROMP has been exploited to prepare robust PIL-type cross-linked copolymers for the use

in fuel cell technology,¹¹⁹ whilst more recently Dyson and co-workers have prepared a water-soluble imidazolium-tagged homopolymer which was used to stabilise gold nanoparticle catalysts.¹²⁰

In conclusion, ring-opening polymerisation is often utilised as a means to prepare well-defined polymers, overcoming the difficulties often under standard methods by exploiting favourable enthalpic changes during ring opening. This approach has been particularly successful with the use of metal carbene catalysts in ROMP, particularly the Ru-based Grubbs catalyst. Although such catalysts are relatively expensive, which may be considered a limitation to their use for the synthesis of polymer immobilised ionic liquids, the potential benefits greatly outweigh this cost. In this regard, both the mild reaction conditions required for polymerisation and the high functional group tolerance coupled with modular and versatile synthesis of the ionic liquid-like monomers and co-monomers will allow for an incredibly broad design potential for PIILP materials. The well-behaved nature of living polymerisation will also allow the morphology and microenvironment of polymer immobilised ionic liquids to be modified in a rational manner in order to optimise catalyst performance.

1.7. Conclusions

In recent decades the use of ILs has developed into an invaluable tool across a range of chemical disciplines, particularly for developing efficient immobilised homogeneous catalysts. Whilst the nature of the relationship between catalyst, IL and substrate is often complex, the unique, tuneable physicochemical properties of ILs can allow for significant improvements in catalyst performance across a range of industrially relevant reactions. Additionally their application in biphasic systems allows them to be recycled and reused, which combines the benefits of homogeneous and heterogeneous catalysis. Despite the successes, the limitations imposed on the use of ILs as a reaction media with regards to leaching of the catalyst, ligand and IL upon recycle as well as mass transport issues renders them unviable for use on a larger scale. Whilst many of these issues have been effectively solved by use of SILP methodology, particularly the cost associated with large quantities of ILs and the mass transport limitations, broader applications can still be somewhat limited. Again the relationship between catalyst, IL, substrate and support material can be incredibly complex, making it difficult to make broader statements about materials as well as how exactly they will behave under particular reaction conditions. The use of various inorganic matrices as the support material has proven to be highly effective in SILP procedures, however successes are predominately limited to gas phase reactions with leaching remaining a major issue. Although modification of the support surface can improve this problem the process can often be synthetically complex and is often non-quantitative, leading to an extra aspect of ambiguity in an already complex systems. In this

regard, the use of living polymerisation to generate polymer supports should enable polymer properties and functionality to be modified in a rational manner in order to identify an optimum support-catalyst combination. Despite this, while numerous different methodologies have been used to prepare PILs for a variety of different applications, their use in catalysis appears to be viewed as a somewhat developing field. As such the use of IL-functionalised polymers as support materials remains somewhat limited in scope, with the area largely focused on the stabilisation of metal nanoparticles by polystyrene-based materials. Whilst the use of such polymer immobilised ionic liquids is by no means without its issues (for example, the incredibly complex nature of the interactions involved in these catalytic systems) the control afforded through the use of polymer chemistry should allow structure-performance relationship to be developed and an understanding of how these interactions influence catalyst efficiency.

Brief evaluation of common polymerisation methods indicates that the use of living radical-initiated systems, such as ATRP and RAFT, do show promise for the production of PIILP materials; however, the use of Grubbs metathesis catalyst to generate well-defined living polymers under mild conditions appears to offer the greatest degree of functional group tolerance, and hence maximises the overall design potential of any PIILP materials. As such, initial studies into the application of PIILP in catalysis will be undertaken using supports prepared via ROMP.

1.8. References

1. P. T. Anastas and M. M. Kirchhoff, *Acc. Chem. Res.*, 2002, **35**, 686-694.
2. R. A. Sheldon, *Green Chem.*, 2007, **9**, 1273-1283.
3. B. M. Trost, *Acc. Chem. Res.*, 2002, **35**, 695-705.
4. H. Olivier-Bourbigou, L. Magna and D. Morvan, *Appl. Catal., A*, 2010, **373**, 1-56.
5. S. Liu and J. Xiao, *J. Mol. Catal. A: Chem.*, 2007, **270**, 1-43.
6. P. Knochel, in *Top. Curr. Chem.*, Springer Berlin Heidelberg, 1999, vol. 206, pp. 1-152.
7. P. Walden, *Bull. Acad. Impér. Sci. St. Pétersbourg.*, 1914, **8**, 405-422.
8. *US Pat.*, 1943176, 1934.
9. a) F. H. Hurley and T. P. Wler, *J. Electrochem. Soc.*, 1951, **98**, 203-206; b) F. H. Hurley and T. P. Wler, *J. Electrochem. Soc.*, 1951, **98**, 207-212.
10. H. L. Chum, V. R. Koch, L. L. Miller and R. A. Osteryoung, *J. Am. Chem. Soc.*, 1975, **97**, 3264-3265.
11. J. S. Wilkes and M. J. Zaworotko, *J. Chem. Soc., Chem. Commun.*, 1992, 965-967.
12. T. Welton, *Chem. Rev.*, 1999, **99**, 2071-2084.

13. M. J. Earle, S. P. Katdare and K. R. Seddon, *Org. Lett.*, 2004, **6**, 707-710.
14. A. Stark and K. R. Seddon, in *Kirk-Othmer Encyclopedia of Chemical Technology*, ed. A. Seidel, John Wiley & Sons, Inc., Hoboken, New Jersey, 2007, vol. 26, pp. 836-924.
15. J. P. Hallett and T. Welton, *Chem. Rev.*, 2011, **111**, 3508-3576.
16. U. Kreher, A. Rosamilia, C. Raston, J. Scott and C. Strauss, *Molecules*, 2004, **9**, 387-393.
17. N. V. Plechkova and K. R. Seddon, *Chem. Soc. Rev.*, 2008, **37**, 123-150.
18. R. Giernoth, in *In situ NMR Methods in Catalysis*, eds. J. Bargon and L. Kuhn, Springer Berlin Heidelberg, 2007, vol. 276, ch. 16, pp. 1-23.
19. H. Olivier-Bourbigou, L. Magna and D. Morvan, *Appl. Catal. A*, 2010, **373**, 1-56.
20. J. Dupont, *J. Braz. Chem. Soc.*, 2004, **15**, 341-350.
21. a) M. Deetlefs, C. Hardacre, M. Nieuwenhuyzen, A. A. H. Padua, O. Sheppard and A. K. Soper, *J. Phys. Chem. B*, 2006, **110**, 12055-12061; b) A. Mele, G. Romanò, M. Giannone, E. Ragg, G. Fronza, G. Raos and V. Marcon, *Angew. Chem. Int. Ed.*, 2006, **45**, 1123-1126.
22. C. C. Weber, A. F. Masters and T. Maschmeyer, *Angew. Chem. Int. Ed.*, 2012, **51**, 11483-11486.
23. a) T. Gutel, J. Garcia-Anton, K. Pelzer, K. Philippot, C. C. Santini, Y. Chauvin, B. Chaudret and J.-M. Basset, *J. Mater. Chem.*, 2007, **17**, 3290-3292; b) T. Gutel, C. C. Santini, K. Philippot, A. Padua, K. Pelzer, B. Chaudret, Y. Chauvin and J.-M. Basset, *J. Mater. Chem.*, 2009, **19**, 3624-3631.
24. J. D. Holbrey, R. D. Rogers, R. A. Mantz, P. C. Trulove, V. A. Cocalia, A. E. Visser, J. L. Anderson, J. L. Anthony, J. F. Brennecke, E. J. Maginn, T. Welton and R. A. Mantz, in *Ionic Liquids in Synthesis*, Wiley-VCH Verlag GmbH & Co. KGaA, 2008, ch. 3, pp. 57-174.
25. P. Wasserscheid and W. Keim, *Angew. Chem. Int. Ed.*, 2000, **39**, 3772-3789.
26. H. Srour, H. Rouault, C. C. Santini and Y. Chauvin, *Green Chem.*, 2013, **15**, 1341-1347.
27. a) M. Smiglak, J. D. Holbrey, S. T. Griffin, W. M. Reichert, R. P. Swatloski, A. R. Katritzky, H. Yang, D. Zhang, K. Kirichenko and R. D. Rogers, *Green Chem.*, 2007, **9**, 90-98; b) M. Fabris, V. Lucchini, M. Noè, A. Perosa and M. Selva, *Chem. Eur. J.*, 2009, **15**, 12273-12282.
28. A. Aupoix, B. Pégot and G. Vo-Thanh, *Tetrahedron*, 2010, **66**, 1352-1356.
29. J. D. Oxley, T. Prozorov and K. S. Suslick, *J. Am. Chem. Soc.*, 2003, **125**, 11138-11139.
30. K. R. Seddon, A. Stark and M. J. Torres, *Pure Appl. Chem.*, 2000, **72**, 2275-2287.
31. P. J. Dyson, D. J. Ellis, W. Henderson and G. Laurenczy, *Adv. Synth. Catal.*, 2003, **345**, 216-221.
32. C. Daguenet and P. J. Dyson, *Organometallics*, 2004, **23**, 6080-6083.
33. M. Mečiarová, M. Cigáň, Š. Toma and A. Gáplovský, *Eur. J. Org. Chem.*, 2008, **2008**, 4408-4411.

34. M. Mečiarová and Š. Toma, *Chem. – Eur. J.*, 2007, **13**, 1268-1272.
35. P. Dash and R. W. J. Scott, *Chem. Comm.*, 2009, 812-814.
36. Y. Yasaka, C. Wakai, N. Matubayasi and M. Nakahara, *Anal. Chem.*, 2008, **81**, 400-407.
37. R. Ge, R. W. K. Allen, L. Aldous, M. R. Bown, N. Doy, C. Hardacre, J. M. MacInnes, G. McHale and M. I. Newton, *Anal. Chem.*, 2009, **81**, 1628-1637.
38. F. Maier, J. M. Gottfried, J. Rossa, D. Gerhard, P. S. Schulz, W. Schwieger, P. Wasserscheid and H.-P. Steinrück, *Angew. Chem. Int. Ed.*, 2006, **45**, 7778-7780.
39. J. M. Fraile, J. I. García, C. I. Herreras, J. A. Mayoral, O. Reiser and M. Vaultier, *Tetrahedron Lett.*, 2004, **45**, 6765-6768.
40. a) S.-g. Lee, *Chem. Comm.*, 2006, 1049-1063; b) R. Sebesta, I. Kmentova and S. Toma, *Green Chem.*, 2008, **10**, 484-496.
41. S. Doherty, P. Goodrich, C. Hardacre, J. G. Knight, M. T. Nguyen, V. I. Pârvulescu and C. Paun, *Adv. Synth. Catal.*, 2007, **349**, 951-963.
42. J. van den Broeke, F. Winter, B.-J. Deelman and G. van Koten, *Org. Lett.*, 2002, **4**, 3851-3854.
43. P. J. Dyson, D. J. Ellis and T. Welton, *Can. J. Chem.*, 2001, **79**, 705-708.
44. a) B. Tan, J. Jiang, Y. Wang, L. Wei, D. Chen and Z. Jin, *Appl. Organomet. Chem.*, 2008, **22**, 620-623; b) Y. Zeng, Y. Wang, J. Jiang and Z. Jin, *Catal. Comm.*, 2012, **19**, 70-73; c) Y. Zeng, Y. Wang, Y. Xu, Y. Song, J. Zhao, J. Jiang and Z. Jin, *Chin. J. Catal.*, 2012, **33**, 402-406; d) Y. Zeng, Y. Wang, Y. Xu, Y. Song, J. Jiang and Z. Jin, *Catal Lett*, 2013, **143**, 200-205.
45. Y. Leng, J. Wang, D. Zhu, X. Ren, H. Ge and L. Shen, *Angew. Chem. Int. Ed.*, 2009, **48**, 168-171.
46. H. Zhi, C. Lu, Q. Zhang and J. Luo, *Chem. Comm.*, 2009, 2878-2880.
47. F. Liu, M. B. Abrams, R. T. Baker and W. Tumas, *Chem. Comm.*, 2001, 433-434.
48. M. Solinas, A. Pfaltz, P. G. Cozzi and W. Leitner, *J. Am. Chem. Soc.*, 2004, **126**, 16142-16147.
49. M. F. Sellin, P. B. Webb and D. J. Cole-Hamilton, *Chem. Comm.*, 2001, 781-782.
50. P. B. Webb, T. E. Kunene and D. J. Cole-Hamilton, *Green Chem.*, 2005, **7**, 373-379.
51. J. W. Lee, J. Y. Shin, Y. S. Chun, H. B. Jang, C. E. Song and S.-g. Lee, *Acc. Chem. Res.*, 2010, **43**, 985-994.
52. a) C. E. Song, W. H. Shim, E. J. Roh, S.-g. Lee and J. H. Choi, *Chem. Comm.*, 2001, 1122-1123; b) B. Y. Park, K. Y. Ryu, J. H. Park and S.-g. Lee, *Green Chem.*, 2009, **11**, 946-948.
53. C. E. Song, W. H. Shim, E. J. Roh and J. H. Choi, *Chem. Comm.*, 2000, 1695-1696.
54. a) R. R. Deshmukh, J. W. Lee, U. S. Shin, J. Y. Lee and C. E. Song, *Angew. Chem. Int. Ed.*, 2008, **47**, 8615-8617; b) M. Y. Yoon, J. H. Kim, D. S. Choi, U. S. Shin, J. Y. Lee and C. E. Song, *Adv. Synth. Catal.*, 2007, **349**, 1725-1737.
55. J. Y. Shin, D. J. Jung and S.-g. Lee, *ACS Catal.*, 2013, **3**, 525-528.

56. a) I. Meracz and T. Oh, *Tetrahedron Lett.*, 2003, **44**, 6465-6468; b) C.-E. Yeom, H. W. Kim, Y. J. Shin and B. M. Kim, *Tetrahedron Lett.*, 2007, **48**, 9035-9039.
57. S. Doherty, P. Goodrich, C. Hardacre, V. I. Pârvulescu and C. Paun, *Adv. Synth. Catal.*, 2008, **350**, 295-302.
58. C. Amatore and A. Jutand, *Acc. Chem. Res.*, 2000, **33**, 314-321.
59. a) C. Chiappe, G. Imperato, E. Napolitano and D. Pieraccini, *Green Chem.*, 2004, **6**, 33-36; b) V. Calò, A. Nacci, A. Monopoli and F. Montingelli, *J. Org. Chem.*, 2005, **70**, 6040-6044.
60. a) W. Cabri, I. Candiani, A. Bedeschi, S. Penco and R. Santi, *J. Org. Chem.*, 1992, **57**, 1481-1486; b) W. Cabri, I. Candiani, A. Bedeschi and R. Santi, *J. Org. Chem.*, 1992, **57**, 3558-3563; c) W. Cabri, I. Candiani, A. Bedeschi and R. Santi, *J. Org. Chem.*, 1993, **58**, 7421-7426.
61. J. Mo, L. Xu and J. Xiao, *J. Am. Chem. Soc.*, 2004, **127**, 751-760.
62. V. Caló, A. Nacci, A. Monopoli, S. Laera and N. Cioffi, *J. Org. Chem.*, 2003, **68**, 2929-2933.
63. S. Doherty, P. Goodrich, C. Hardacre, J. G. Knight, M. T. Nguyen, V. I. Pârvulescu and C. Paun, *Adv. Synth. Catal.*, 2007, **349**, 951-963.
64. S. Doherty, P. Goodrich, C. Hardacre, H.-K. Luo, D. W. Rooney, K. R. Seddon and P. Styring, *Green Chem.*, 2004, **6**, 63-67.
65. Z. Liu, R. Zhang, C. Xu and R. Xia, *Oil Gas J.*, 2006, **104**, 52-56.
66. S. Werner, N. Szesni, A. Bittermann, M. J. Schneider, P. Härter, M. Haumann and P. Wasserscheid, *Appl. Catal. A*, 2010, **377**, 70-75.
67. Q. Zhang, S. Zhang and Y. Deng, *Green Chem.*, 2011, **13**, 2619-2637.
68. C. P. Mehnert, *Chem. – Eur. J.*, 2005, **11**, 50-56.
69. C. Van Doorslaer, J. Wahlen, P. Mertens, K. Binnemans and D. De Vos, *Dalt. Trans.*, 2010, **39**, 8377-8390.
70. a) A. Corma, H. García and A. Leyva, *Tetrahedron*, 2004, **60**, 8553-8560; b) A. Riisager, B. Jorgensen, P. Wasserscheid and R. Fehrmann, *Chem. Comm.*, 2006, 994-996; c) G. Roger, *Chem. Eng. Techn.*, 2006, **7**, 869.
71. J. Baudoux, K. Perrigaud, P.-J. Madec, A.-C. Gaumont and I. Dez, *Green Chem.*, 2007, **9**, 1346-1351.
72. E. Miyako, T. Maruyama, N. Kamiya and M. Goto, *Biotechnol. Lett.*, 2003, **25**, 805-808.
73. M. Ruta, I. Yuranov, P. J. Dyson, G. Laurency and L. Kiwi-Minsker, *J. Catal.*, 2007, **247**, 269-276.
74. Y. Gu and G. Li, *Adv. Synth. Catal.*, 2009, **351**, 817-847.
75. C. Sievers, O. Jimenez, T. E. Müller, S. Steuernagel and J. A. Lercher, *J. Am. Chem. Soc.*, 2006, **128**, 13990-13991.

76. M. R. Castillo, L. Fousse, J. M. Fraile, J. I. García and J. A. Mayoral, *Chem. – Eur. J.*, 2007, **13**, 287-291.
77. M. Haumann, K. Dentler, J. Joni, A. Riisager and P. Wasserscheid, *Adv. Synth. Catal.*, 2007, **349**, 425-431.
78. U. Hintermair, T. Höfener, T. Pullmann, G. Franciò and W. Leitner, *ChemCatChem*, 2010, **2**, 150-154.
79. M. H. Valkenberg, C. deCastro and W. F. Holderich, *Green Chem.*, 2002, **4**, 88-93.
80. M. Gruttadauria, S. Riela, C. Aprile, P. L. Meo, F. D'Anna and R. Noto, *Adv. Synth. Catal.*, 2006, **348**, 82-92.
81. L.-L. Lou, K. Yu, F. Ding, W. Zhou, X. Peng and S. Liu, *Tetrahedron Lett.*, 2006, **47**, 6513-6516.
82. L. Rodriguez-Perez, E. Teuma, A. Falqui, M. Gomez and P. Serp, *Chem. Comm.*, 2008, 4201-4203.
83. B. Karimi and D. Enders, *Org. Lett.*, 2006, **8**, 1237-1240.
84. C. Copéret and R. Van Santen, *Dalt. Trans.*, 2010, **39**, 8354.
85. Y. Gu, C. Ogawa, J. Kobayashi, Y. Mori and S. Kobayashi, *Angew. Chem. Int. Ed.*, 2006, **45**, 7217-7220.
86. U. Kernchen, B. Etzold, W. Korth and A. Jess, *Chem. Eng. Technol.*, 2007, **30**, 985-994.
87. a) A. Riisager, R. Fehrmann, M. Haumann and P. Wasserscheid, *Eur. J. Inorg. Chem.*, 2006, **2006**, 695-706; b) A. Riisager, R. Fehrmann, M. Haumann, B. S. K. Gorle and P. Wasserscheid, *Ind. Eng. Chem. Res.*, 2005, **44**, 9853-9859; c) A. Riisager, R. Fehrmann, S. Flicker, R. van Hal, M. Haumann and P. Wasserscheid, *Angew. Chem. Int. Ed.*, 2005, **44**, 815-819.
88. a) B. M. L. Dooos, I. F. J. Vankelecom and P. A. Jacobs, *Adv. Synth. Catal.*, 2006, **348**, 1413-1446; b) J. Lu, F. Yan and J. Texter, *Prog. Polym. Sci.*, 2009, **34**, 431-448; c) D. Mecerreyes, *Prog. Polym. Sci.*, 2011, **36**, 1629-1648; d) J. Yuan, D. Mecerreyes and M. Antonietti, *Prog. Polym. Sci.*, 2013, **38**, 1009-1036.
89. M. I. Burguete, E. García-Verdugo, I. Garcia-Villar, F. Gelat, P. Licence, S. V. Luis and V. Sans, *J. Catal.*, 2010, **269**, 150-160.
90. V. Sans, N. Karbass, M. I. Burguete, V. Compañ, E. García-Verdugo, S. V. Luis and M. Pawlak, *Chem. – Eur. J.*, 2011, **17**, 1894-1906.
91. Y. M. A. Yamada and Y. Uozumi, *Tetrahedron*, 2007, **63**, 8492-8498.
92. A. Chen, G. Zhao, J. Chen, L. Chen and Y. Yu, *RSC Adv.*, 2013, **3**, 4171-4175.
93. P. Barbaro and F. Liguori, *Chem. Rev.*, 2008, **109**, 515-529.
94. G. Odian, *Principles of Polymerization*, Wiley, 2004.

95. a) D. Jiang, X. Li and E. Wang, *Macromol. Symp.*, 1996, **105**, 161-166; b) R. J. Sowden, M. F. Sellin, N. De Blasio and D. J. Cole-Hamilton, *Chem. Comm.*, 1999, 2511-2512; c) N. De Blasio, M. R. Wright, E. Tempesti, C. Mazzocchia and D. J. Cole-Hamilton, *J. Organomet. Chem.*, 1998, **551**, 229-234; d) N. De Blasio, E. Tempesti, A. Kaddouri, C. Mazzocchia and D. J. Cole-Hamilton, *J. Catal.*, 1998, **176**, 253-259; e) R. S. Drago, E. D. Nyberg, A. El A'mma and A. Zombeck, *Inorg. Chem.*, 1981, **20**, 641-644.
96. a) D. E. Bryant and M. Kilner, *J. Mol. Catal. A*, 2003, **193**, 83-88; b) J. Balu  and J. C. Bay n, *J. Mol. Catal. A: Chem.*, 1999, **137**, 193-203; c) I. Toth, B. Hanson, I. Guo and M. Davis, *Catal Lett*, 1991, **8**, 209-214; d) B. Cornils and E. G. Kuntz, *J. Organomet. Chem.*, 1995, **502**, 177-186; e) Y. Huang, L.-e. Min, Y. Li, R. Li, P. Cheng and X. Li, *Catal. Comm.*, 2002, **3**, 71-75; f) M. M. Diwakar, R. M. Deshpande and R. V. Chaudhari, *J. Mol. Catal. A: Chem.*, 2005, **232**, 179-186.
97. a) P. Barbaro, C. Bianchini, G. Giambastiani, W. Oberhauser, L. M. Bonzi, F. Rossi and V. Dal Santo, *Dalton Trans.*, 2004, 1783-1784; b) P. Barbaro, *Chem. – Eur. J.*, 2006, **12**, 5666-5675; c) C. Moreno-Marrodan, F. Liguori, E. Mercade, C. Godard, C. Claver and P. Barbaro, *Catal. Sci. Technol.*, 2015, **5**, 3762-3772.
98. a) G. Blanco-Brieva, E. Cano-Serrano, J. M. Campos-Martin and J. L. G. Fierro, *Chem. Comm.*, 2004, 1184-1185; b) S. Kanemoto, H. Saimoto, K. Oshima and H. Nozaki, *Tetrahedron Lett.*, 1984, **25**, 3317-3320.
99. S. Doherty, in *Catalysis in Ionic Liquids: From Catalyst Synthesis to Application*, The Royal Society of Chemistry, 2014, pp. 44-308.
100. a) M. Jones, R. Raja, J. Meurig Thomas and B. G. Johnson, *Top. Catal.*, 2003, **25**, 71-79; b) P. McMorn and G. J. Hutchings, *Chem. Soc. Rev.*, 2004, **33**, 108-122.
101. a) F. Li, F. Cheng, J. Shi, F. Cai, M. Liang and J. Chen, *J. Power Sources*, 2007, **165**, 911-915; b) Y. Zhang, L. Zhao, P. K. Patra, D. Hu and J. Y. Ying, *Nano Today*, 2009, **4**, 13-20.
102. B. S. Aitken, M. Lee, M. T. Hunley, H. W. Gibson and K. B. Wagener, *Macromolecules*, 2010, **43**, 1699-1701.
103. N. Matsumi, K. Sugai, M. Miyake and H. Ohno, *Macromolecules*, 2006, **39**, 6924-6927.
104. P. Li, Q. Zhao, J. L. Anderson, S. Varanasi and M. R. Coleman, *J. Polym. Sci. Part A Polym. Chem*, 2010, **48**, 4036-4046.
105. R. J. Young and P. A. Lovell, *Introduction to Polymers, Third Edition*, Taylor & Francis, 2011.
106. C. P. Reghunadhan nair, M. C. Richou, P. Chaumont and G. Clouet, *Eur. Polym. J.*, 1990, **26**, 811-815.
107. J. M. K. G. Cowie and V. Arrighi, *Polymers: chemistry and physics of modern materials*, CRC Press, 2008.

108. P. Schwab, R. H. Grubbs and J. W. Ziller, *J. Am. Chem. Soc.*, 1996, **118**, 100-110.
109. a) M. Kato, M. Kamigaito, M. Sawamoto and T. Higashimura, *Macromolecules*, 1995, **28**, 1721-1723; b) J.-S. Wang and K. Matyjaszewski, *J. Am. Chem. Soc.*, 1995, **117**, 5614-5615.
110. P. Cardiano, P. G. Mineo, F. Neri, S. Lo Schiavo and P. Piraino, *J. Mater. Chem.*, 2008, **18**, 1253-1260.
111. N. V. Tsarevsky and K. Matyjaszewski, *Chem. Rev.*, 2007, **107**, 2270-2299.
112. G. Moad, E. Rizzardo and S. H. Thang, *Aust. J. Chem.*, 2009, **62**, 1402-1472.
113. a) K. Vijayakrishna, S. K. Jewrajka, A. Ruiz, R. Marcilla, J. A. Pomposo, D. Mecerreyes, D. Taton and Y. Gnanou, *Macromolecules*, 2008, **41**, 6299-6308; b) H. Mori, M. Yahagi and T. Endo, *Macromolecules*, 2009, **42**, 8082-8092; c) K. Tauer, N. Weber and J. Texter, *Chem. Comm.*, 2009, 6065-6067; d) K. Vijayakrishna, D. Mecerreyes, Y. Gnanou and D. Taton, *Macromolecules*, 2009, **42**, 5167-5174.
114. H. Hsieh and R. P. Quirk, *Anionic Polymerization: Principles and Practical Applications*, Taylor & Francis, 1996.
115. *PRINCIPLES OF POLYMERIZATION, 4TH ED*, Wiley India Pvt. Limited, 2007.
116. a) P. Dubois, O. Coulembier and J. M. Raquez, *Handbook of Ring-Opening Polymerization*, Wiley, 2009; b) O. Nuyken and S. Pask, *Polymers*, 2013, **5**, 361.
117. R. L. Pederson, I. M. Fellows, T. A. Ung, H. Ishihara and S. P. Hajela, *Adv. Synth. Catal.*, 2002, **344**, 728-735.
118. R. H. Grubbs, *Angew. Chem. Int. Ed.*, 2006, **45**, 3760-3765.
119. a) N. J. Robertson, H. A. Kostalik, T. J. Clark, P. F. Mutolo, H. D. Abruña and G. W. Coates, *J. Am. Chem. Soc.*, 2010, **132**, 3400-3404; b) T. J. Clark, N. J. Robertson, H. A. Kostalik, T. J. Clark, P. F. Mutolo, H. D. Abruña and G. W. Coates, *J. Am. Chem. Soc.*, 2009, **131**, 12888-12889.
120. I. Biondi, G. Lauenczy and P. J. Dyson, *Inorg. Chem.*, 2011, **50**, 8038-8045.

Chapter 2

PIILP Tungsten-Based Peroxometalate Oxidation Catalysis

This chapter is based on the publication:

S. Doherty, J. G. Knight, J. R. Ellison, D. Weekes, R. W. Harrington, C. Hardacre and H. Manyar “An efficient peroxometalate-based polymer-immobilised ionic liquid phase (PIILP) catalyst for hydrogen peroxide-mediated oxidation”, *Green Chem.*, 2012, **14**, 925 – 929.

Table of Contents:

2.1.	Abstract	49
2.2.	Introduction	49
2.3.	Results and Discussion	51
	<i>2.3.1. Polymer and Catalyst Design and Synthesis</i>	51
	<i>2.3.2. Epoxidation</i>	59
	<i>2.3.3. Alcohol Oxidation</i>	63
	<i>2.3.4. Sulfoxidation</i>	65
	<i>2.3.5. Polymer Support Comparisons</i>	69
	<i>2.3.6. Ionic Liquid Functionality Comparisons</i>	75
2.4.	Conclusions	79
2.5.	Experimental	81
2.6.	References	93

2.1. Abstract

Ring-Opening Metathesis Polymerisation (ROMP) was utilised to generate a well-defined linear polymer decorated with pyrrolidinium-based ionic liquid moieties through a modular synthetic route in a controlled manner and under relatively mild conditions. The resulting material underwent complete ion exchange with an in situ generated peroxophosphotungstate polyanion to afford the heterogeneous oxidation catalyst POM-2.1. This proved to be both highly efficient and recyclable in a range of different oxidation reactions under varying mild conditions, with hydrogen peroxide as the oxidant. Following this initial success, the effect of polymer composition on catalyst performance was investigated by the preparation of similar polymers of varying chain lengths and co-monomer ratio, as well as an analogous polystyrene-based analogue to be used under select oxidation reactions. Though these comparisons showed no clear relationship between the polymer composition and catalyst behaviour it was determined that the polystyrene backbone was comparable to the one generated through ROMP; as such the synthetically more straightforward approach offered by the former was exploited to generate a range of supports with varying ionic liquid groups as a means to determine their effect on catalysis. By investigating the rapid, mild oxidation of sulphides with these materials a more profound effect on performance was observed, indicating that for this particular catalyst it is the IL functionality which dominates its behaviour, rather than the composition of the polymer backbone.

2.2. Introduction

Oxidation reactions have been described as the cornerstone of synthetic chemistry, often yielding key intermediates in the synthetic process or offering a direct route to numerous valuable compounds. Through the years a diverse range of different catalysts and conditions have been employed to achieve this reaction; however, despite the ubiquitous nature of oxidation catalysis limitations do remain, in particular with regard to reaction selectivity and the 'green credentials' of the process, with classical oxidations often requiring incredibly harsh conditions, expensive catalysts and the generation of large quantities of by-product. As such, like all processes, there is constantly a drive to deliver catalytic systems which can perform well under the mildest possible conditions. In this regard, numerous different mild, selective catalysts have been used with ionic liquids, either as a solvent or under SILP-type conditions, often exploited to immobilise and stabilise the catalyst whilst also offering enhancements in its performance.^{1,2} Of this mild subclass of oxidation catalysts one of the most widely investigated areas is the use of polyoxometalates (POMs). POMs have received this considerable attention, as highlighted by the breadth of research covered in the entirety of Chemical

Reviews 1998 issue 1, as an architecturally and structurally diverse³ class of redox active anionic transition metal-oxygen-based materials which have proven to be effective Brønsted acid catalysts in a range of commercially important transformations.⁴ Further to this, POMs offer a number of additional advantages over other organometallic catalysts including their high oxidative stability and the access to various structural types through simple variation of reaction stoichiometry or pH during their synthesis.⁵

Amongst the commonly used POMs one of the most widely documented in catalysis is the commercially available phosphotungstic acid ($\text{H}_3\text{PW}_{12}\text{O}_{40}$), which is often employed in oxidation catalysis in combination with hydrogen peroxide as the sole oxidant, vastly improving its green credentials over other transition metal-based systems. Early studies monitoring the reaction between phosphotungstic acid and hydrogen peroxide by ^{31}P NMR spectroscopy identified the active species as the Venturello peroxometalate $[\text{PO}_4\{\text{WO}(\text{O}_2)_2\}_4]^{3-}$ which is formed by degradation of the initial polyacid (figure 2.1).⁶ Commonly, phosphotungstic acid and its derived peroxometalate are used in conjunction with quaternary ammonium-based counterions in order to avoid issues associated

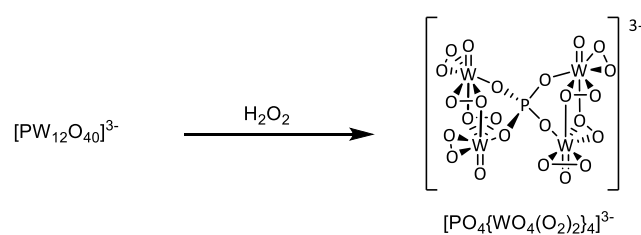


Figure 2.1 Hydrogen peroxide-mediated degradation of the Keggin structure phosphotungstic acid to give the corresponding Venturello peroxometalate.

with the acidity of the protons present. In this regard, such POMs have been extensively used in conjunction with ILs, for example recent studies in which guanidinium-based ILs were used in combination with either phosphotungstic acid or the derived peroxometalate and H_2O_2 to give an efficient epoxidation catalyst.⁷ Systems using ILs as both solvent and a source of cations as the counterion, rather than standard tetraalkylammoniums, consistently gave higher conversions and/or better recyclability. ILs have also been used for homogeneous catalytic systems based on phosphotungstic acid and H_2O_2 ; careful choice of the cation and fine tuning of the IL reaction medium allowed for a water soluble catalyst which could also accommodate lipophilic alkene substrates. Again the IL-based system gave high conversions and recycled efficiently over three cycles, however the eventual build-up of water in the IL-catalyst mixture yielded a biphasic system and partial precipitation of the catalyst.⁸ Various polymeric ammonium-containing supports have been successfully employed to immobilise heteropolyacids, for example a poly(ethylene oxide-pyridinium) matrix (figure 2.2)⁹ and an IL-modified polystyrene,¹⁰ whilst different solid supports have also been used to immobilise the active Venturello peroxometalate in various stages of the synthesis.¹¹ Taking

these considerations into account the peroxometalate $[\text{PO}_4\{\text{WO}_4(\text{O}_2)_2\}_4]^{3-}$ was identified as an ideal candidate to prepare new oxidation catalyst based on ammonium decorated polymer immobilised ionic liquids.

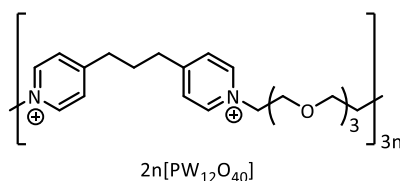


Figure 2.2 Poly(ethylene oxide-pyridinium) matrix developed by Yamada *et al* for the immobilisation of phosphotungstic acid

2.3. Results and Discussion

2.3.1. Polymer and Catalyst Design and Synthesis

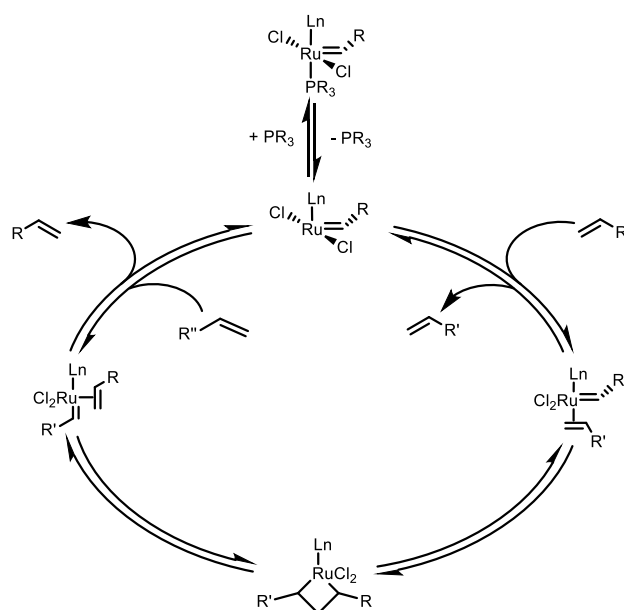
As discussed in chapter 1, ring-opening metathesis polymerisation (ROMP) was identified as the optimum polymerisation method for the preparation of our first generation PIILP materials due to a combination of the high degree of control during living polymerisation, as well as the mild reaction conditions and high functional group tolerance which yields the broadest possible design potential. As discussed in chapter 1, ROMP is generally facilitated by transition metal-based carbenes, the reactivity of which are summarised in table 2.1. Unlike the electron-poor tungsten and molybdenum centres utilised in more traditional Schrock-type metathesis catalysts, ruthenium-based Grubbs catalysts possess an electron-rich metal centre. It is this relatively soft reaction centre which affords Grubbs-catalysed ROMP both its high functional group tolerance and ease of handling, which make it an ideal tool for the incorporation of pre-made IL moieties into a polymer network.¹²

Table 2.1 Comparison of the relative reactivity of different transition metal carbene metathesis catalysts

Titanium	Tungsten	Molybdenum	Ruthenium	
Acids	Acids	Acids	Olefins	↑ Increasing Activity
Alcohols, Water	Alcohols, Water	Alcohols, Water	Acids	
Aldehydes	Aldehydes	Aldehydes	Alcohols, Water	
Ketones	Ketones	Olefins	Aldehydes	
Esters, Amides	Olefins	Ketones	Ketones	
Olefins	Esters, Amides	Esters, Amides	Esters, Amides	

The mechanism of ROMP catalysed by Grubbs catalyst (scheme 2.1) has been well documented and proceeds by initial dissociation of a ligated phosphine.¹³ This dissociation process can allow for fine-tuning of the activity of the metathesis catalyst through a combination of steric and electronic effects of the other ligands around the metal centre. For example, the tricyclohexylphosphine-functionalised 1st generation Grubbs catalyst is considered more electron-rich, therefore phosphine dissociation is rapid. In contrast, the 2nd generation catalyst, in which one

of the tricyclohexylphosphine ligands is replaced by a large N-heterocyclic carbene, yields a more electron-deficient metal centre and slower phosphine dissociation.¹⁴ As such Grubbs-type metathesis catalysts are constantly evolving with regard to the ligands surrounding the Ru centre as a means of fine tuning the catalyst activity to give optimum stability/functional group tolerance whilst also being sufficiently active to give good reaction rates. Following dissociation, the newly formed vacant site is occupied by coordination of the reacting olefin which subsequently undergoes cycloaddition with the metal carbene to form a metallocyclobutane intermediate which has been observed by NMR spectroscopy.¹⁵ The highly strained four-membered intermediate then reopens in order to relieve ring-strain to yield the first unit of the polymer chain attached to a newly formed metal carbene bond. The presence of this relatively stable metal carbene bond throughout the propagation process^{12b} lends ROMP its living nature which, when coupled with the typically faster rates of initiation than propagation, gives polymer chains of comparable length with a very narrow molecular weight distribution.



Scheme 2.1 Catalytic cycle involved in Ring-Opening Metathesis Polymerisation (ROMP) facilitated by the Ru carbene Grubbs catalysts

As ROMP is primarily driven by the relief of ring-strain, a fundamental feature of any monomer is the presence of a suitably strained cyclic system; in this regard several different olefin substrates have been investigated. Among these, the bicyclic norbornene has been shown to undergo polymerisation with remarkable efficiency and is thus one of the most commonly used monomers.^{12a} Further advantages of using norbornene as a framework for IL-tagged monomers under ROMP conditions arise from the Diels-Alder cycloaddition between a suitable dienophile and cyclopentadiene, as it is relatively straightforward to introduce functionality into the norbornene fragment that can be further modified to afford a range of different IL moieties. The use of such

systems has been successfully exploited to produce well-defined IL-tagged ROMP-based polymers; for example, the robust cross-linked alkylammonium-decorated copolymer used as an alkali anion exchange membrane in fuel cell technology,¹⁶ whilst more recently an imidazolium-tagged homopolymer was prepared by Dyson *et al.* to give a support for highly active water-soluble gold nanoparticle catalysts (figure 2.3).¹⁷

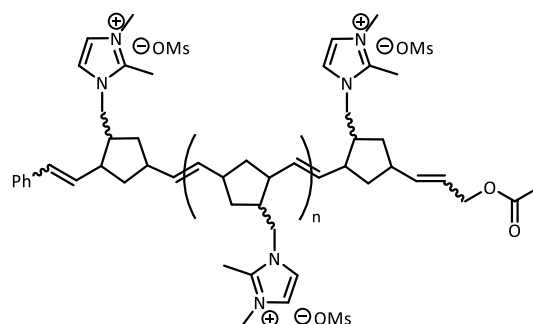
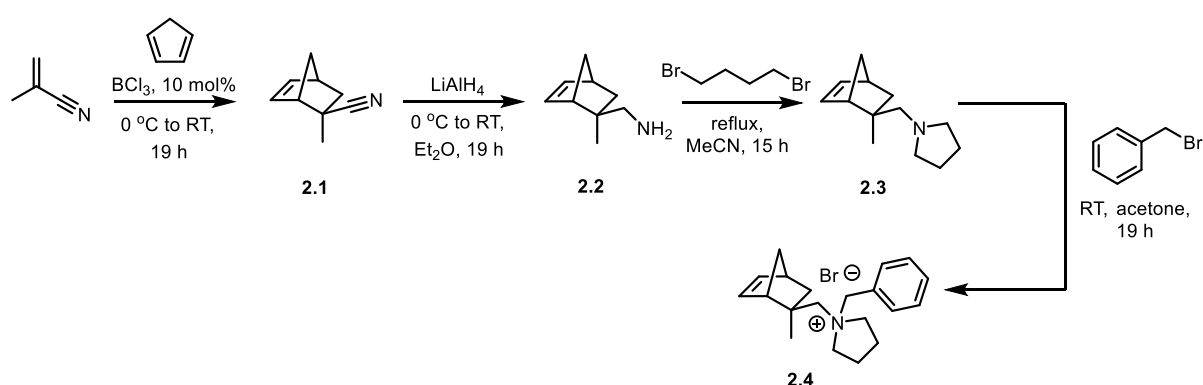


Figure 2.3 Imidazolium mesylate-functionalised homopolymer prepared by Dyson *et al.* through ROMP used as a support for active gold nanoparticle catalysts

Taking these successes into consideration, norbornene was identified as a suitable monomer and the pyrrolidinium-tagged compound **2.4** was proposed as an initial target. Pyrrolidinium bromide was selected as the initial IL-type functionality due to the synthetic ease by which it could be produced, and it was proposed that different counteranions could be easily obtained through ion exchange reactions if required. The methyl group present on the 2-position of the norbornene group, and the benzyl group used to quaternise the pyrrolidine centre, were incorporated to prevent unwanted β -elimination reactions which could occur if this system were used under broader catalytic conditions, adding an extra degree of chemical robustness to the monomer. The synthesis of **2.4** is shown in scheme 2.2 and begins with the BCl_3 -catalysed Diels-Alder cycloaddition between



Scheme 2.2 Synthesis of the pyrrolidinium bromide-functionalised norbornene monomer **2.4**

methacrylonitrile and freshly cracked cyclopentadiene in the absence of solvent to yield **2.1**. High *exo*-diastereoselectivity was achieved with a 89 : 11 mixture of *exo* and *endo* as confirmed by ^1H NMR spectroscopy in agreement with a previous synthesis.¹⁸ Following this **2.1** was reduced to by lithium aluminium hydride to give the corresponding primary amine **2.2**, a versatile intermediate in the synthesis of different onium-based monomers. The desired pyrrolidine ring was then generated

through an intramolecular dialkylation with 1,4-dibromobutane before subsequent quaternisation of the nitrogen atom using benzyl bromide in acetone to yield **2.4**, isolated as a spectroscopically and analytically pure white solid. Whilst the use of a four step linear synthesis to yield **2.4** may not be considered ideal with regard to minimising synthetic complexity, each step can be achieved without the need for purification by column chromatography; this significantly simplifies the overall process and reduces cost. By using a modular route, the overall design potential for monomers is greatly increased. For example, numerous different dienophiles could be employed in the initial Diels-Alder reaction to yield norbornene units with different functionalities which could be further modified to incorporate a range of IL moieties, whilst different chain lengths and chain types could be used in the dialkylbromide alkylation step to give rings with different architectures. The use of different quaternising groups could also be used to yield a library of structurally diverse IL groups.

The stereochemistry of **2.4** is determined in the initial Lewis acid-catalysed Diels-Alder reaction between methacrylonitrile and cyclopentadiene. Recently this reaction was reported to be highly *endo*-selective as a result of favourable secondary orbital interactions between the HOMO of cyclopentadiene and the LUMO of methacrylonitrile during the formation of the transition state.¹⁹ Despite this, previous assignments have reported the *exo*-diastereomer to be the major product.¹⁸ As a result of this apparent discrepancy in reported reaction selectivity, a single-crystal X-ray structure determination of **2.4** was undertaken in order to unequivocally establish which diastereoisomer was the major product. The molecular structure shown in Figure 2.4 confirms that the major diastereoisomer is the *exo*-isomer with the pyrrolidinium centre *anti*- to the norbornene bridge. The high yields obtained from each step in the synthesis of **2.4** rule out selective reactions of the minor

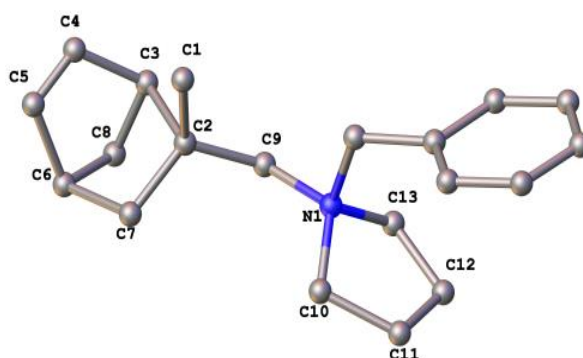
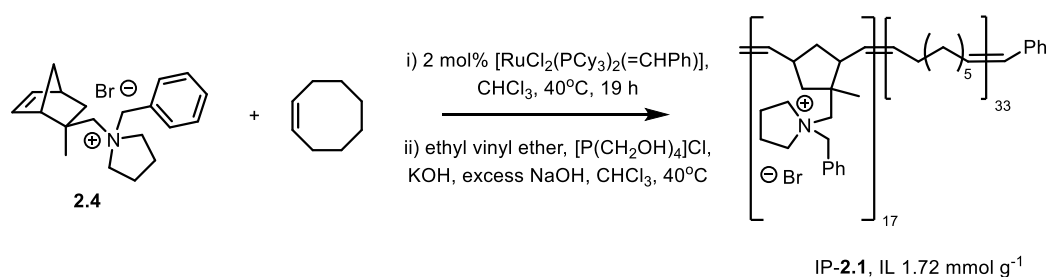


Figure 2.4 Molecular structure of **2.4** confirming the stereochemistry of initial cycloaddition. Hydrogen atoms, the water molecule of crystallisation and the bromide counterion have been removed from clarity

diastereoisomer (11% determined by ¹H NMR), as such the major diastereoisomer present in **2.4** can be assumed to be the same as in the initial Diels-Alder reaction to give **2.1**. This diastereoselectivity is believed to be attributed to steric effects during the formation of the transition state. Due to the linear nature of the nitrile group of methacrylonitrile, sufficient orbital overlap cannot occur between

the HOMO-LUMO pair in forming the *endo*-transition state, and as such there is not a sufficient reduction in energy to favour the *endo*-product.

Following the successful synthesis of **2.4** the initial target polymer IP-**2.1** was generated via ring-opening metathesis polymerisation according to scheme 2.3. Due to the charged nature the material it was elected to not produce a homopolymer as this would most likely be water-soluble and we required/desired an insoluble support material; in this regard, a co-monomer was selected. ROMP has been well documented to proceed with numerous different strained olefins; for the purpose of our initial study we chose to use *cis*-cyclooctene as co-monomer on the basis that it would act as a linear alkyl spacer and confer a high degree of hydrophobic character to the polymer material. Grubbs 1st generation catalyst was selected as the relative reactivity of two co-monomers towards ROMP and the linear nature of the forming polymer should not provide a particularly challenging environment for the catalyst. As such the much more reactive, and considerably more expensive metathesis catalysts such as the NHC-functionalised Grubbs 2nd generation catalyst, which are traditionally employed for more sterically congested and challenging systems, was not required.



Scheme 2.3 Ring-Opening Metathesis Polymerisation of **2.4** and *cis*-cyclooctene catalysed by Grubbs 1st generation catalyst and subsequent removal of Ru end groups from polymer chains. Ionic loading (mmol g⁻¹) is shown

After successful polymerisation under mild conditions of 40 °C overnight in chloroform, the reaction was quenched by addition of ethyl vinyl ether to remove the active Ru carbene from the propagating polymer chains. The cleaved Ru species was then removed by extraction with an aqueous solution of tris(hydroxymethyl)phosphine, in accordance with a procedure developed by Pederson *et al.*²⁰ Analysis of IP-**2.1** by ICP-OES indicated that the ruthenium content of the polymer sample was less than 0.001 wt%, showing that the Ru-based species in the material had been efficiently removed. Elemental analysis of IP-**2.1** gave a nitrogen content corresponding to an ionic loading of 1.72 mmol g⁻¹ and a co-monomer ratio of 1 : 2; combining this information with the stoichiometry of the polymerisation the average polymer chain consists of 17 units of ionic monomer and 33 units of alkyl co-monomer. As discussed above the ¹H NMR spectrum of **2.4** showed that the sample consists of approximately 11% of the *endo*- diastereomer, and although a minor component, this difference in stereochemistry within the monomer could have a profound effect on the polymer microenvironment by reducing the uniformity within the molecule. Previously, the relative rates of

reaction for both the *exo*- and *endo*-isomers have been extensively investigated, with a consensus that the *endo*- forms of norbornene-derived monomers are considerably less active during ROMP with different catalysts.²¹ In this regard, the difference in activity may be predominately associated with unfavourable steric effects arising from the reacting *endo*- isomer, which can occur through different modes (figure 2.4). During the ROMP process catalysed by Grubbs first generation catalyst, the formation of the metallacyclobutane ring is considered to be the rate-determining step.²² As the four-membered intermediate forms, a steric interaction between the protons on the newly formed sp³ centre and those on the pendant IL group may occur (figure 2.5 A). During the polymerisation process, the propagating species needs to favour a coordination which places the available coordination site of the catalyst over the terminal unit's cyclopentadiene ring in order to accommodate the steric bulk of the catalyst P(Cy)₃ ligand. In this instance the unfavourable steric interaction arises from proximity of the polymer chain's penultimate unit and the *endo* substituent of the approaching monomer (figure 2.4 B). Further interactions occur from the alkylidene formed during reaction of *endo* monomers, which have substituents of the cyclopentadiene ring in a *cis* relationship, again creating a highly congested area which could hinder approach of a monomer.^{21c} Further deactivation with *endo* isomers can occur through the formation of chelate-type interactions. In this regard, the pendant IL fragment could coordinate to the metal centre either upon monomer approach or after opening of the initial metallocyclobutane intermediate (figure 2.4 C). This chelating effect could slow the dissociation process and hence inhibit the approach of monomer.^{21c} ²³ Taking these mechanistic aspects into account it can be assumed that the minor *endo* form of **2.4** will react

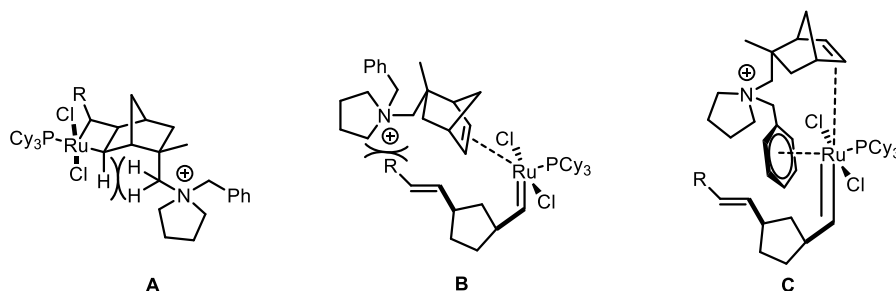
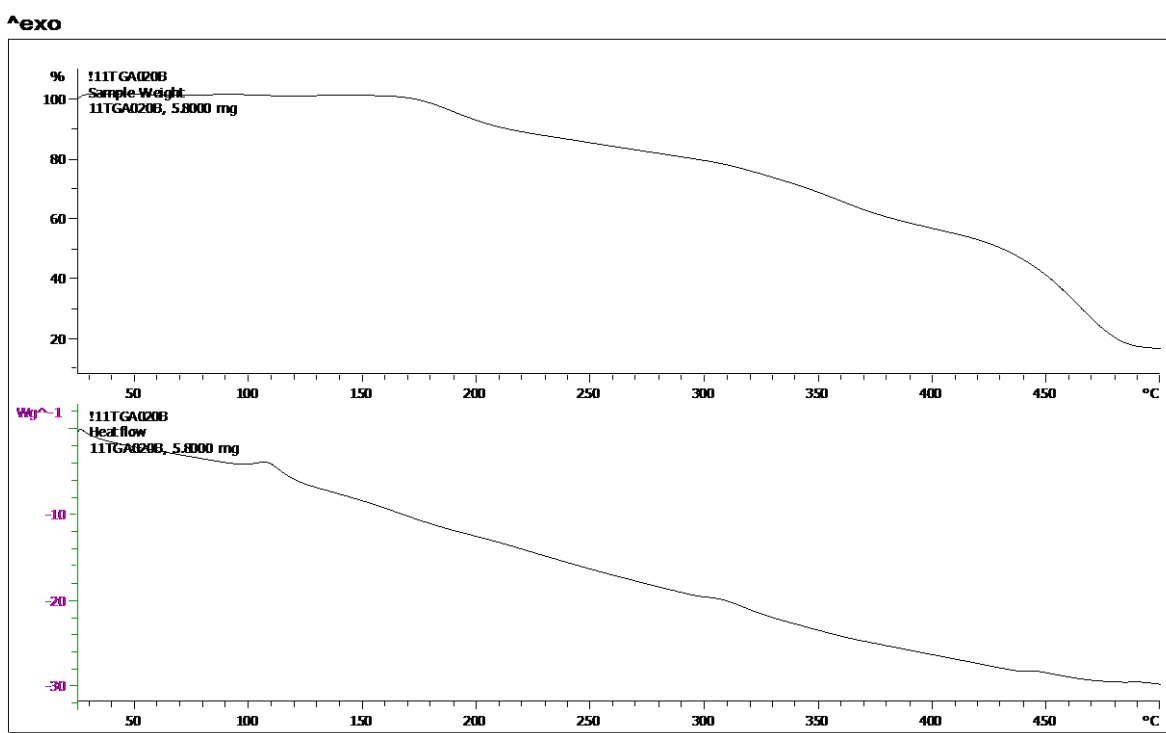


Figure 2.5 Different modes of catalyst deactivation associated with the ring-opening metathesis polymerisation of *endo*-substituted norbornene monomers illustrated using **2.4**

at a significantly reduced rate to the corresponding *exo* form, and as such its incorporation into the final structure of IP-**2.1** is likely to be negligible. In previous reports concerning the tacticity of polymers produced through ROMP, the resulting monomer geometries and stereochemistry within the polymer chain were determined by combinations of ¹H and ¹³C NMR experiments. Unfortunately due to the complex environment provided by the copolymer, the ¹H and ¹³C NMR spectra of IP-**2.1** consisted of very broad signals making formal assignment and overall confirmation of the assumptions about *endo/exo* incorporation as well as the ratio of *cis/trans* alkenes incredibly difficult.

As such it will be necessary to conduct more in depth studies into the ROMP process of **2.4** if these PIILP systems are to be fully understood and utilised to their full potential.

The thermal stability of IP-**2.1** was evaluated by thermogravimetric analysis and differential scanning calorimetry (TGA-DSC, figure 2.5); the TGA showed that there were two main degradation stages, also indicating that IP-**2.1** was thermally stable up to a temperature of 170°C, well above the reaction temperatures employed in liquid phase catalysis. Despite this apparent thermal stability, the heat flow plot (lower trace) clearly shows an endotherm at 100 °C; this could correspond to Hoffmann elimination with no loss in mass or polymorphic rearrangements. As such, it can be assumed that the architecture of IP-**2.1** may change through different degradation pathways at higher temperatures without necessarily losing mass. It will therefore be necessary to conduct further studies into the thermal stability and the degradation/decomposition pathways if materials like IP-**2.1** are to be used under more extreme conditions (*i.e.* >100 °C).



Lab: METTLER

STAR® SW 9.10

Figure 2.6 TGA and DSC curves for IP-**2.1** taken with a heating rate was 5 °C min⁻¹

As discussed in the introduction, the Keggin phosphotungstic acid and its associated active Venturello anion $[\text{PO}_4\{\text{WO}(\text{O}_2)_2\}_4]^{3-}$, were identified as ideal candidates for initial evaluation as oxidation catalysts for immobilisation on the newly developed PIILP materials. The H_2O_2 -mediated decomposition of phosphotungstic acid is well documented, with examples of support materials being used to stabilise the active anion at different stages in this decomposition. For the purposes of this exercise it was decided to first generate the active peroxometalate anion before immobilisation by ion exchange with IP-**2.1**, theorising that the ionic microenvironment provided by the PIILP support would sufficiently stabilise the active species over time. In this regard, phosphotungstic acid was

reacted with 200 equivalents of H_2O_2 before addition of the reaction mixture to a rapidly stirred solution of IP-**2.1** in EtOH, resulting in the immediate precipitation of the product as an amorphous white solid; this was isolated by filtration and dried under vacuum to afford PIILP-supported catalyst POM-**2.1**. The presence of $[\text{PO}_4\{\text{WO}(\text{O}_2)_2\}_4]^{3-}$ as the major species was confirmed by solid state ^{31}P NMR spectroscopy (figure 2.6), although the spectra clearly shows that POM-**2.1** consists of a number of different phosphorous-containing compounds. This observation has previously been reported during a study into the formation, reactivity and stability of $[\text{PO}_4\{\text{WO}(\text{O}_2)_2\}_4]^{3-}$.^{6e} ICP-OES analysis of POM-**2.1** showed that the sample consisted of 26.0 wt% tungsten, indicating that both complete anion exchange with the polymer bromide had occurred and that the proposed formulation was correct.

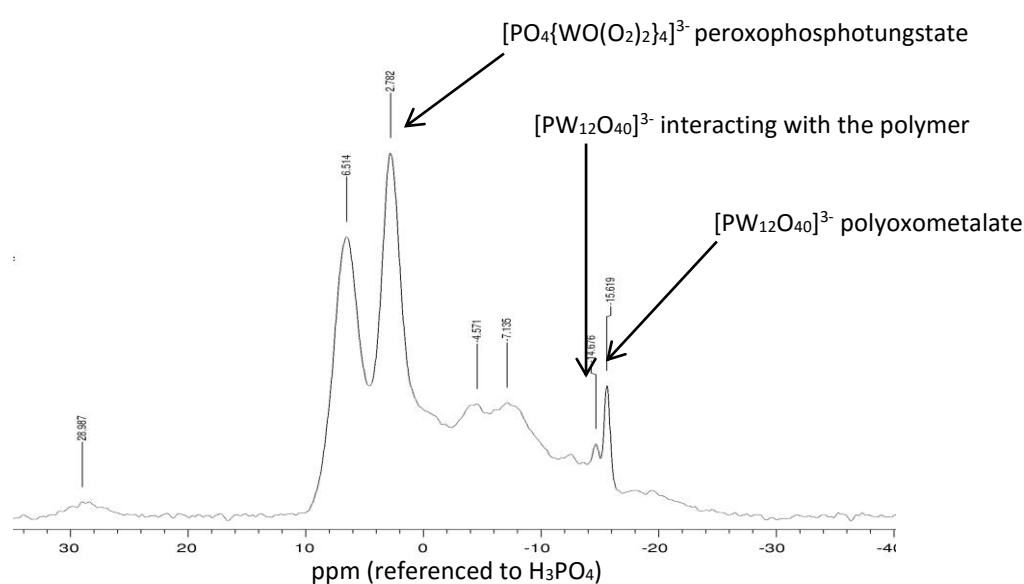


Figure 2.7 Solid state ^{31}P NMR spectrum of POM-**2.1** and corresponding assignments in agreement with work conducted by Hill and co-workers^{6e}

As the morphology and porosity of the catalytic species will have a distinct effect on the reaction outcome, nitrogen sorption analysis was conducted on POM-**2.1**. A Brunauer-Emmett-Teller (BET) plot gave a total surface area of $42 \text{ m}^2 \text{ g}^{-1}$ whilst pore size distribution curves calculated by the Barret-Joyner-Halenda (BJH) method indicated an average pore size of 8.3 nm and an average pore volume of $0.15 \text{ cm}^3 \text{ g}^{-1}$. For comparison, similar polyoxometalate-based polyammonium cation decorated meoporous materials reported previously exhibited comparable surface areas of $27 - 51 \text{ m}^2 \text{ g}^{-1}$ but with smaller pore sizes of just 3.6 nm.²⁴ Further investigation into the morphology of POM-**2.1** by transmission electron microscopy (TEM) showed highly contrasting features approximately $<1 \text{ nm}$ in size, corresponding to the peroxophosphotungstate surrounded by the poorly contrasting polymer material which appears granular in nature (figure 2.8).

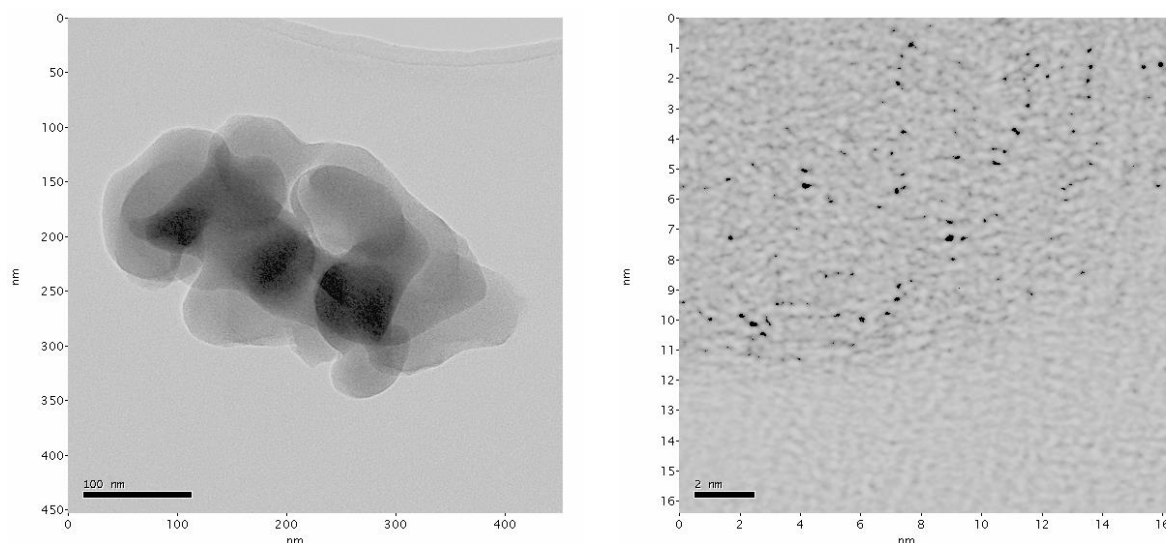


Figure 2.8 High resolution transmission electron microscopy images of prepared catalyst POM-2.1

2.3.2. Epoxidation Catalysis

The efficiency of the newly produced catalyst POM-**2.1** as an oxidation catalyst was first investigated for the epoxidation of allylic alcohols and alkenes. As a route to versatile synthetic precursors, the green oxidation to give epoxides has gained considerable interest and, in this regard, heterogeneous polyoxometalate catalyst has been used in conjunction with hydrogen peroxide as the sole oxidant. For example, a broad range of alkenes have been oxidised by $[\{W(=O)(O_2)_2(H_2O)\}_2(\mu-O)]$ immobilised on imidazolium IL-functionalised silica to give selectivity values and yields that compared favourably to the corresponding homogeneous analogue in acetonitrile.²⁵ As discussed previously $[PO_4\{WO(O_2)_2\}_4]^{3-}$ has also been successfully used in conjunction with various different polymer-based supports.¹¹ As such the efficiency of POM-**2.1** was evaluated across a range of different allylic alcohols and olefins, and compared against an analogous homogeneous catalyst POM-TBA, prepared by the anion exchange of $[PO_4\{WO(O_2)_2\}_4]^{3-}$ with tetrabutylammonium bromide (table 2.2). Initial evaluation of both catalysts focused on the epoxidation of *trans*-hex-2-en-1-ol using two equivalents of hydrogen peroxide, 0.5 mol% catalyst and a temperature of 50 °C in acetonitrile (entries 1 and 2). Interestingly under these conditions POM-**2.1** gave a conversion of 99% after just 4 hours whilst the homogenous analogue POM-TBA gave just a yield of 74% in the same time, implying that the porous, charged nature of POM-**2.1** could be providing a positive synergistic effect during catalysis; for example the porous nature of the material could direct and trap substrates in close proximity to active centres, enhancing the reaction rate. Gratifyingly this enhancement between the two catalysts was observed across the range of substrates summarised in table 2.2, with the heterogeneous POM-**2.1** giving comparable performance, and often even outperforming its homogeneous counterpart. Whilst clearly highly active, it is also possible to achieve a high degree of selectivity with both

peroxometalate catalysts. For example, the epoxidation of geraniol (entries 7 and 8) occurred with complete regioselectivity for the allylic alcohol to give the 2,3-epoxy alcohol as the sole product in high yield. Mechanistically, as with all the allylic substrates, this effect can be attributed to initial coordination

Table 2.2 Epoxidation of allylic alcohols and alkenes with hydrogen peroxide in acetonitrile catalysed by POM-2.1 and POM-TBA^a

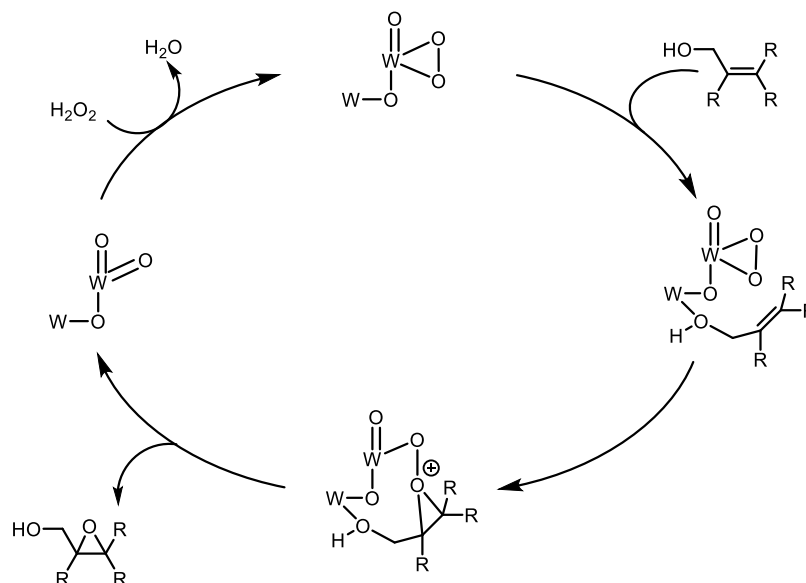
entry	substrate	Catalyst	Time	Conversion ^b	Isolated yield
1		POM-2.1	4	>99 (94)	94
2		POM-TBA	4	74 (66)	66
3		POM-2.1	4	89 (81)	81
4		POM-TBA	4	87 (74)	74
5		POM-2.1	4	>99 (92)	92
6		POM-TBA	4	94 (86)	86
7		POM-2.1	4	96 (91)	91
8		POM-TBA	4	97 (89)	89
9		POM-2.1	12	88 (81)	81
10		POM-TBA	12	82 (71)	71
11		POM-2.1	4	98 (91)	91
12		POM-TBA	4	74 (68)	68
13		POM-2.1	4	89 (79)	79
14		POM-TBA	4	80 (71)	71
15		POM-2.1	4	81(72)	72
16		POM-TBA	4	98 (89)	89
17		POM-2.1	12	76 ^c	--
18		POM-TBA	12	79 ^c	--

^aReaction conditions: 0.5 mol% catalyst, 1 mmol substrate, 2 mmol 35% H₂O₂, 3 mL MeCN, 50 °C. ^bDetermined by GC of reaction mixture using n-decane as an internal standard. ^cDetermined by ¹H NMR.

of the alcohol oxygen to one of the tungsten centres which holds the allylic C=C double bond in close proximity to the active O-O group of the catalyst (scheme 2.4). This coordination effect also explains the relative reactivity of both catalysts towards homoallylic substrates, with both catalysts giving much slower reaction rates (entries 9 and 10). In this regard the increased distance between the C=C double bond and the alcohol leads to suboptimal coordination of the double bond to the active peroxy-bridge of the catalyst upon coordination of the alcohol group to an adjacent tungsten. Despite this effect good conversions could still be achieved with both catalysts by increasing reaction times. Encouragingly, the conversion achieved for *cis*-cyclooctene using POM-2.1 approached that reported for the same heterogeneous peroxometalate polyanion immobilised within an organic dendrimer matrix²⁶ as well as peroxometalate-based room temperature IL systems.²⁷

Reasoning that the PIILP support of POM-2.1 would effectively retain and stabilise the active peroxometalate species, the recyclability and reusability of POM-2.1 was explored to assess the longevity of the catalyst. *Cis*-cyclooctene was selected as the test substrate and the catalyst reusability was studied up to four cycles, details of which are shown in figure 2.8. After each cycle the

catalyst was isolated by centrifugation of the crude reaction mixture, siphoning off of the liquid phase and washing with diethyl ether; the recovered catalyst was then used directly with no make-up quantity of fresh catalyst added for subsequent cycles. The reaction profiles obtained for POM-2.1



Scheme 2.4 Mechanism for the epoxidation of allylic alcohols involving coordination to an adjacent tungsten centre modified from the mechanism proposed by Stapleton *et al*²⁸

show that the catalyst recycles effectively, with the reaction reaching completion within each cycle, however minor reduction in reaction conversion of approximately 6% occurred upon each successive recycle. Analysis of the reaction solvent by ICP-OES after each filtration and recovery of the catalyst revealed that the tungsten content was below the detection limit of 1 ppm. As such it was determined that negligible leaching of the peroxophosphotungstate occurred during the recycling process and that the active catalyst was effectively retained within the polymer framework of the PIILP support. The observed gradual decrease in catalyst performance was instead attributed to attrition during filtration and recovery of the catalyst. TEM images of POM-2.1 obtained after the 4th recycle showed some aggregation of the peroxometalate (figure 2.9); however, the solid state ³¹P NMR spectrum obtained for the same sample indicated that the tetranuclear $[\text{PO}_4\{\text{WO}(\text{O}_2)_2\}_4]^{3-}$ anion is stable and remains the major phosphorous-containing species (figure 2.10), in agreement with earlier studies by the Ishii and Venturello groups.⁶ Due to the polyolefin backbone of IP-2.1 concerns were raised with regards to the oxidation of the PIILP material under the reaction conditions, which could alter the morphology and physical properties of the support material. Whilst the TEM images obtained for the recycled catalyst showed no obvious visual changes to the morphology of the support material, additional testing was required. Fourier transform infrared (FT-IR) spectroscopy of a recycled sample of POM-2.1 showed no signals corresponding to either epoxide ($\nu = 1280 - 1230, 950 - 815$ and $880 - 750 \text{ cm}^{-1}$) or alcohol ($\nu = 3550 - 3200 \text{ cm}^{-1}$) functionalities, implying that the alkene groups within the polymer backbone did not react under the mild reaction conditions. FT-IR spectroscopy also

confirmed the observations from the TEM images and ^{31}P NMR spectrum of recycled POM-2.1 that the active peroxophosphotungstate remained largely unchanged under the reaction conditions.

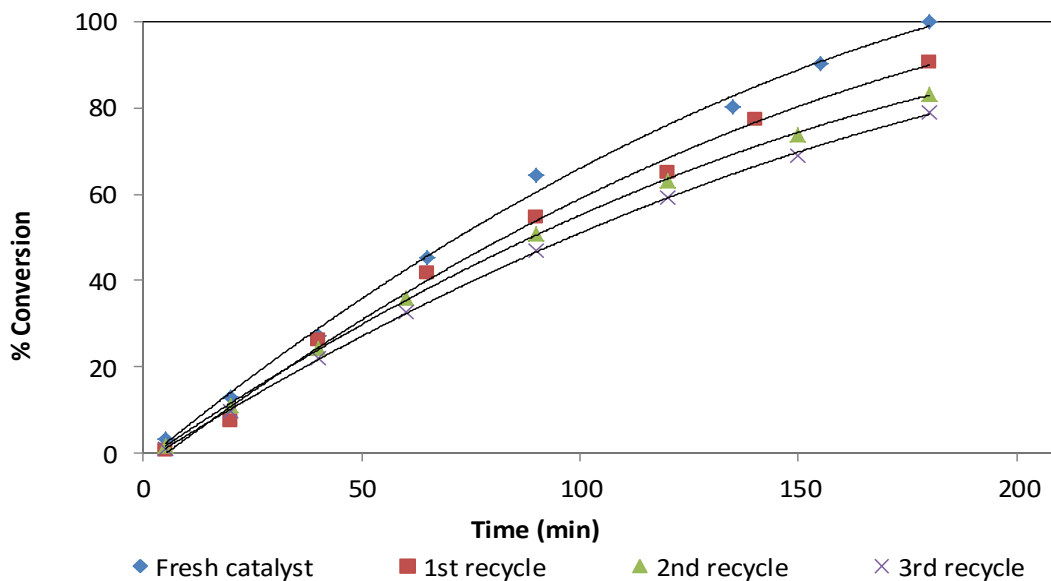


Figure 2.9 Conversions with respect to time for successive hydrogen peroxide-mediated epoxidations of *cis*-cyclooctene using recycled POM-2.1

As discussed above the tendency of POM-2.1 to outperform its homogeneous counterpart POM-TBA would imply that the microenvironment provided by the PIILP support helps facilitate the epoxidation. Although it would be incredibly difficult to achieve, these initial results suggest that the elucidation of catalyst activity-polymer structure relationships combined with the controlled, modular polymer synthesis utilised in this work would be an effective means to design and develop

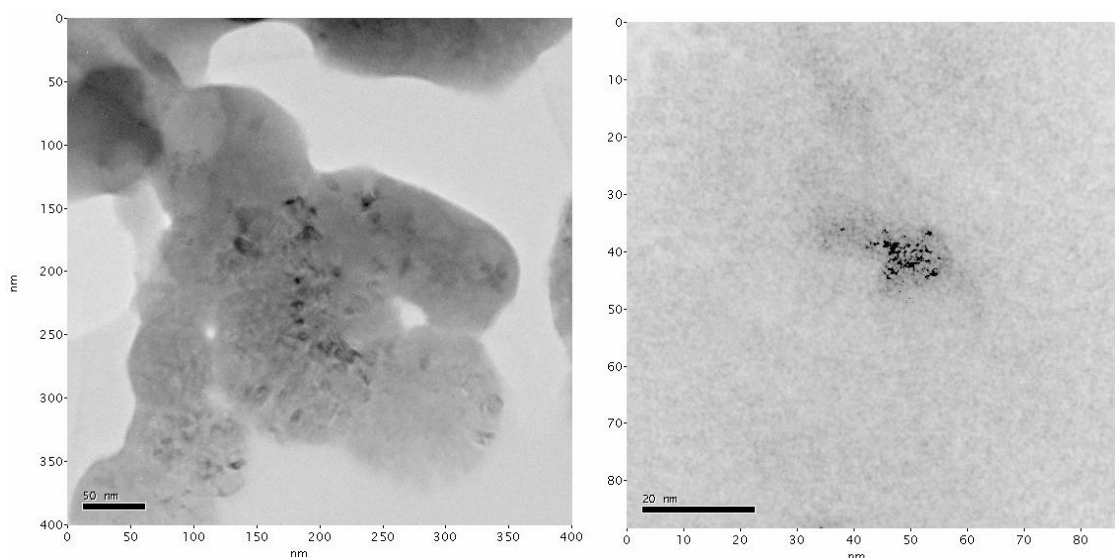


Figure 2.10 High resolution transmission electron microscopy images of POM-2.1 taken after 4th recycle

highly active, well-defined heterogeneous catalysts. The results summarised in table 2.2 show that the positive aspects of catalysis in IL can be successfully harnessed through PIILP materials, whilst the

catalyst longevity study clearly shows that PIILP supports can effectively retain polyionic transition metal catalysts and recycle efficiently with negligible leaching and little change to the materials morphology under mild reaction conditions.

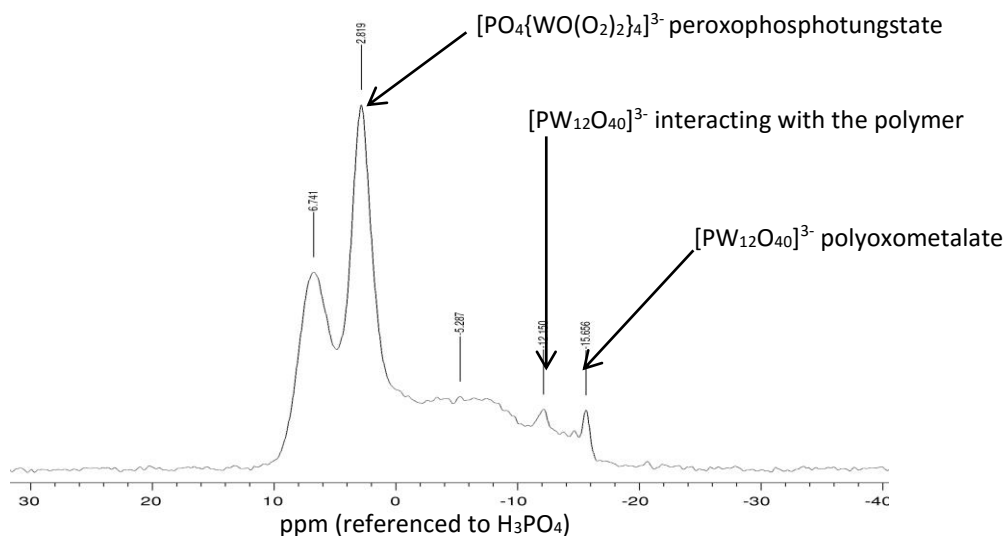


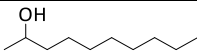
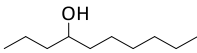
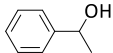
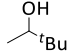
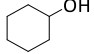
Figure 2.11 Solid state ^{31}P NMR spectrum of POM-2.1 taken after 4th recycle

2.3.3. Alcohol Oxidation

As with the oxidation of alkenes the oxidation of aliphatic alcohols has received considerable interest over the past few decades in an attempt to move away from traditional, harsher oxidants towards greener alternatives. In this regard, ILs have again been extensively investigated as a means to achieve these green credentials. Again this paved the way for efficient heterogeneous catalysis under SILP conditions and, like their epoxidation counterparts discussed above, the oxidation of alcohols to afford ketones or aldehydes catalysed by immobilised polyoxometalates has been previously investigated with PIILP-type supports, including polycationic dendrimers,^{26b} IL-modified polystyrene²⁹ as well as a poly(ethylene oxide-pyridinium) matrix.⁹ With this in mind and in order to more extensively evaluate the efficiency of POM-2.1 as an oxidation catalyst, further studies were conducted with a range of aliphatic alcohols (table 2.3). The much higher reaction temperature and time required to achieve high degrees of conversion make this transformation less viable for wider applications such as continuous flow processes. However, the evaluation of POM-2.1 under these harsher conditions will further illustrate the robustness of the PIILP-peroxophosphotungstate catalyst. Under the reported reaction conditions the selection of benchmark secondary alcohols gave excellent conversions using POM-2.1 as the catalyst. Despite these high yields, the rates of reaction reported for the same peroxometalate catalyst supported on different materials, including the IL-modified silica¹⁰ and poly(ethylene oxide-pyridinium) matrix⁹ mentioned previously, are significantly higher even when using reduced catalyst loadings and fewer equivalents of hydrogen peroxide. While

it was possible to achieve good conversions for the oxidation of 2-phenylethanol to acetophenone with lower temperatures and a catalyst loading of just 0.5 mol% a large excess of hydrogen peroxide and prolonged reaction time was required. The reduced activity of POM-2.1 under these reaction

Table 2.3 Epoxidation of aliphatic alcohols to corresponding carbonyls with hydrogen peroxide in acetonitrile catalysed by POM-2.1^a

entry	substrate	Conversion ^b
1		97
2		98
3		>99
4		94
5		98

^aReaction conditions: 2 mol% catalyst, 1 mmol substrate, 6 mmol 35% H₂O₂, 3 mL MeCN, 80 °C, 24 h.

^bDetermined by ¹H NMR.

conditions when compared to similar heterogeneous catalysts could, in part, be attributed to the deposition of the catalyst material on to the reaction vessel through the course of the reaction. This process could essentially cause the active [PO₄{WO(O₂)₂]₄]³⁻ to become much less accessible to the substrate. This observation is further vindicated by the fact that incredibly poor degrees of conversion in the range of 15-40% were obtained across all substrates if the sample POM-2.1 used was not sufficiently dispersed upon initial addition to the reaction mixture, indicating a strong dependence on catalyst accessibility. The TGA curves obtained for POM-2.1 (figure 2.12) demonstrated that there was no significant loss of mass or notable endotherms until a temperature of ~170 °C was reached, implying that the catalyst is structurally stable under the reaction conditions. As such the limitations observed for POM-2.1 under these reactions conditions might be mechanical in nature. In this regard, the deposition effect discussed above could be significantly improved by appropriate modification of the polymer structure and microenvironment. It is also possible that the pore size offered by POM-2.1 may not be compatible with large substrates such as 1-decanol and 2-decanol. Again appropriate modification of the polymer morphology could negate this effect. Due to the clear limitations encountered with the use of POM-2.1 for alcohol oxidation the polymer support structure was deemed inappropriate for this particular reaction, as such it was not investigated further with this catalyst. The results obtained also highlight the necessity to achieve an understanding about how the

polymer microenvironment will change under harsher conditions, for example, through polymer swelling, which may render the pore structure of the catalyst inappropriate for reaction.

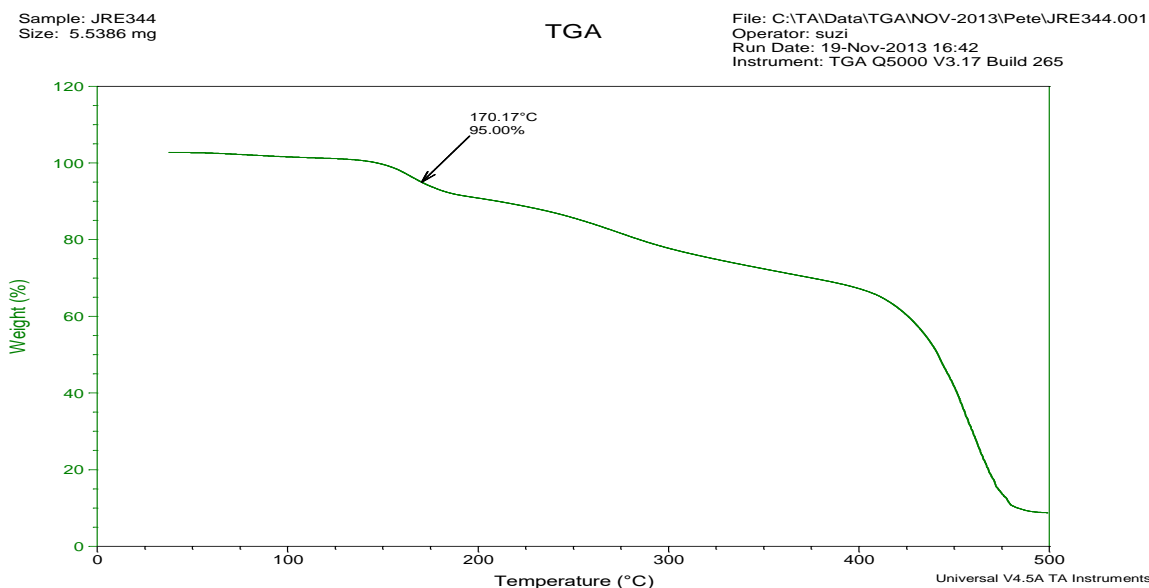


Figure 2.12 TGA curve for POM-2.1 taken with a heating rate of 10 °C min⁻¹

2.3.4. Sulfoxidation Catalysis

The selective oxidation of sulfides to yield sulfoxides or sulfones has received considerable interest over recent years due to the importance of both products as intermediates across a range of important chemistry including fine chemical, agrochemical and pharmaceutical production,³⁰ as chiral auxiliaries^{30b} and, more recently, as ligands in transition metal-catalysed asymmetric synthesis.³¹ The oxidation of sulphur-based impurities in crude oil also provides a more environmentally benign, milder means of removing the impurities when compared to more traditional catalytic hydrodesulfurisation methods.³² As a result the crux of research has again generally focused on moving away from more traditional, harsher oxidation systems towards more environmentally benign and milder reagents, such as hydrogen peroxide, whilst maintaining high activity and selectivity. To this end the application of IL-based systems, either as a bulk solvent or under SILP conditions, has significantly aided this aim. For example, peroxotungstate catalysts immobilised on a supported IL brush silica-based SILP system are highly active catalysts which exhibit high selectivity towards sulfoxides using aqueous hydrogen peroxide as the oxidant.³³ With this in mind, sulfoxidation catalysis was identified as an ideal means to further evaluate the POM-2.1-H₂O₂ system, particularly with regard to aspects of potential product selectivity. Initial investigation focused on the benchmark substrate thioanisole as this substrate has recently been oxidised by peroxometalate-based systems immobilised on the surface of IL-modified silica,^{33,34} IL-based POM salts,³⁵ temperature responsive

phase transfer catalysts,³⁶ tungstate-loaded SBA-15³⁷ and poly(ionic) liquid immobilised magnetic nanoparticles.³⁸ Initially the effect of product selectivity as a function of H₂O₂ : sulphur ratio was investigated in MeCN (table 2.4). Using 0.5 mol% of POM-2.1 moderate conversions and high sulfoxide selectivities of 96% were achieved at room temperature with either one or two equivalents of H₂O₂, while complete conversion was achieved with 3 equivalents, albeit at a slightly lower sulfoxide selectivity of 80% (entries 1 to 4). Previous reports have noted a profound effect of solvent choice on the selectivity of the oxidation, with protic solvents favouring the formation of the sulfoxide through favourable hydrogen-bond forming capabilities. This effectively solvates and stabilises the

Table 2.4 Oxidation of thioanisole catalysed by POM-2.1 with varying equivalents of H₂O₂^a

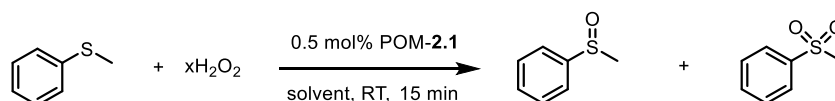
entry	solvent	eq. H ₂ O ₂	% Conv. ^b	% sulfoxide ^b	% sulfone ^b	Sulfoxide selectivity ^{b,c}
1	MeCN	1.0	54	52	2	96
2	MeCN	2.0	68	65	3	96
3	MeCN	2.5	88	74	14	84
4	MeCN	3.0	100	80	20	80
5	MeCN	5.0	100	53	47	53
6	MeOH	1.0	70	70	0	100
7	MeOH	2.0	90	88	2	98
8	MeOH	2.5	95	91	4	96
9	MeOH	3.0	100	95	5	95
10	MeOH	5.0	100	85	15	85
11	MeCN ^d	2.5	100	5	95	5
12	MeOH ^d	2.5	100	93	7	93
13	MeCN ^e	2.5	2.2	--	--	--
14	MeOH ^e	2.5	0	--	--	--

^aReaction conditions: 0.5 mol% catalyst, 1 mmol substrate, 35% H₂O₂, 3 mL solvent, room temperature, 15 min.

^bDetermined by ¹H NMR. ^cSulfoxide selectivity = [%sulfoxide / (%sulfoxide + %sulfone)] x 100%. ^dReactions conducted under same conditions using 0.5 mol% POM-TBA. ^eReactions conducted under same conditions using 0.5 mol% IP-2.1.

sulfoxide formed from the initial oxidation of thioanisole which could significantly slow the second oxidation to the corresponding sulfone.³⁹ As such a parallel study was conducted using MeOH as the solvent under the same reaction conditions in order to investigate the influence of solvent on selectivity. High sulfoxide selectivities were maintained even at high conversion when MeOH was used as the solvent (entries 8-9) in stark contrast to analogous reactions in MeCN (entries 3-4). Sulfoxide selectivity also seems to decrease at a much more dramatic rate as a function of increasing H₂O₂ concentration in MeCN compared to MeOH (entries 5 and 10). This solvent effect is much more evident for the homogeneous analogue of POM-2.1 in which sulfoxidation proceeds to completion with just 2.5 equivalents of H₂O₂ with both solvents giving almost complete selectivity for opposite products (entries 11-12). The heterogenisation of the [PO₄{WO(O₂)₂]₄]³⁻ anion appears to significantly reduce the catalyst's activity, essentially giving an inversion of reaction selectivity to favour the sulfoxide rather than sulfone. Despite this, high yields of sulfone can still be obtained using POM-2.1 with an excess of H₂O₂, higher temperatures and/or longer reaction times. Gratifyingly POM-2.1

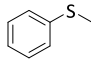
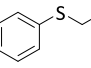
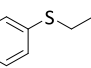
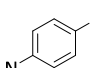
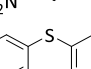
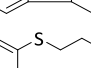
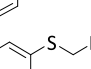
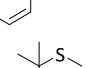
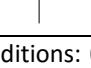
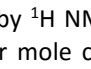
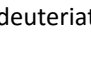
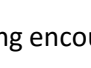
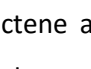
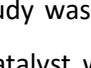
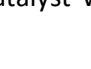

appears to give comparable performance to analogous heterogeneous oxidation catalysts published in the literature; for example Merrifield resin-supported peroxomolybdenun (VI) compounds⁴⁰ and polymer-immobilised peroxotungstates⁴¹ can achieve high sulfoxide and sulfone selectivities under similar mild conditions and low catalyst loadings. In comparison, peroxotungstates immobilised on multi-layer IL brushes-modified silica⁴² or IL-modified silica³⁷ and Keggin heteropolyacids⁴³ require much higher reaction temperatures, higher catalysts loadings and considerably longer reaction times to achieve similar performance, highlighting the highly efficient nature of POM-2.1 under relatively mild conditions. Due to the mild reaction conditions required to achieve oxidation, blank experiments were conducted in the absence of the $[\text{PO}_4\{\text{WO}(\text{O}_2)_2\}_4]^{3-}$ anion in order to determine the extent, if any, of background reaction in presence of IP-2.1. Reassuringly only very minor amounts of sulfoxide (2%) were observed when the reaction was conducted in MeCN while no reaction was observed in MeOH (entries 13-14), illustrating that the peroxometalate is required for reaction.



Scheme 2.5 Oxidation of thioanisole with hydrogen peroxide catalysed by POM-2.1

Encouraged by the high reactivity of thioanisole under relatively mild conditions and the potentially useful solvent dependent selectivity the evaluation of POM-2.1 was extended to a range of aryl alkylsulfides, using 2.5 equivalents of H_2O_2 as the optimum amount of peroxide with regards to achieving high conversion and sulfoxide selectivity (table 2.5). High conversions were obtained across the full scope of substrates tested and the same solvent dependent selectivity was seen for the different sulfides with sulfoxide selectivity significantly higher for MeOH, ranging from 89-98% compared to just 58-98% in acetonitrile. Complete chemoselectivity was observed for oxidation of the sulphur in allylphenyl sulfide and homoallylphenyl sulfide with no evidence for epoxidation of the double bond, most likely as a result of the mild reaction conditions and short reaction times (entries 5-6 and 11-12).^{44,37,41} The poor performance of POM-2.1 in the oxidation of dibenzothiophene (entry 9) is consistent with the electrophilic reaction mechanism previously reported, as a decrease in nucleophilicity of the sulfide results in a slower rate of oxidation.^{36,41,39d} Despite this limitation a high conversion could be achieved by increasing the reaction temperature to 65 °C, albeit at the cost of sulfoxide selectivity which was only 19% (entry 10). Unfortunately the preference for sulfoxide selectivity in MeOH solvent could not be exploited due to the limited solubility of dibenzothiophene.

Table 2.5 Selective oxidation of sulfides to sulfoxides with hydrogen peroxide catalysed by POM-2.1^a

entry	substrate	solvent	% Conv. ^b	% sulfoxide ^b	% sulfone ^b	Sulfoxide selectivity ^{b,c}	TOF ^d
1		MeCN	88	74	14	84	704
2		MeOH	95	91	4	96	760
3		MeCN	92	74	18	80	736
4		MeOH	92	86	6	93	736
5		MeCN	98 ^e	64 ^e	34 ^e	65 ^e	784
6		MeOH	99 ^e	97 ^e	2 ^e	98 ^e	792
7		MeCN	89	78	11	88	712
8		MeOH	56	53	3	95	448
9		MeCN	24	21	3	88	192
10		MeCN ^f	95	18	77	19	760
11		MeCN	98	58	40	58	792
12		MeOH	62	56	6	90	456
13		MeCN	99	75	24	76	792
14		MeOH	92	90	2	98	736
15		MeCN ^g	59	58	1	98	472
16		MeOH ^g	99	77	22	78	792

^aReaction conditions: 0.5 mol% POM-2.1, 1 mmol substrate, 2.5 mmol 35% H₂O₂, 3 mL solvent, RT, 15 min.

^bDetermined by ¹H NMR. ^cSulfoxide selectivity = [%sulfoxide / (%sulfoxide + %sulfone)]. ^dTOF = moles sulfide consumed per mole catalyst per hour. ^eDetermined by ¹³C NMR. ^fReaction conducted at 65 °C. ^gReactions conducted in deuteriated solvent for 2 minutes and monitored by ¹H NMR.

Taking encouragement from the positive recycle experiments conducted for the epoxidation of cis-cyclooctene and the efficient catalyst performance across the range of sulfides a catalyst longevity study was conducted using thioanisole (figure 2.13). Again the reaction was completed before the catalyst was isolated by centrifugation, washed with Et₂O and reused for another cycle.

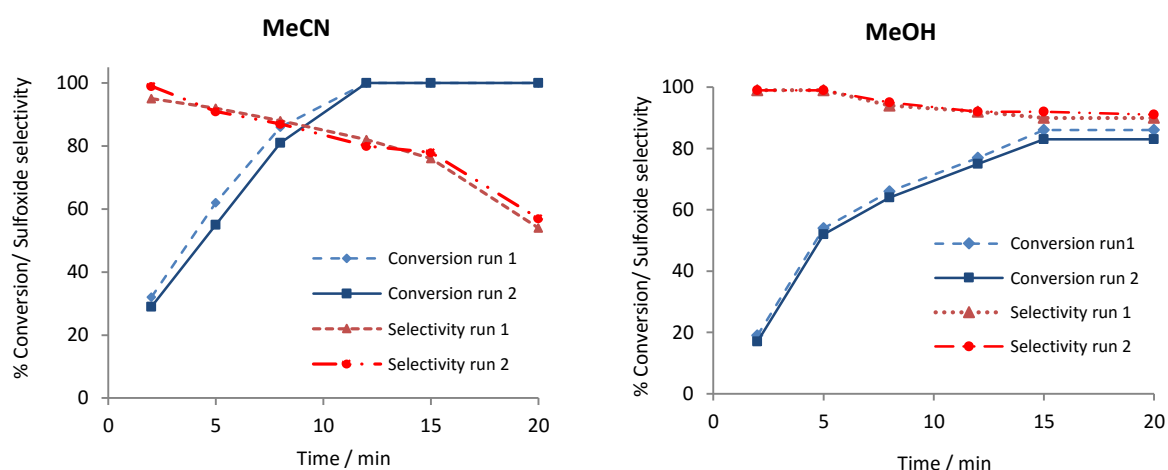


Figure 2.13 Conversion and sulfoxide selectivity profiles as a function of time for subsequent catalyst recycles in the oxidation of thioanisole with 2.5 equivalents hydrogen peroxide catalysed by POM-2.1

Reassuringly analysis of the reaction composition over time gave profiles which showed almost no decrease in catalyst performance with regard to conversion and sulfoxide selectivity between successive runs, implying that the catalyst is effectively stabilised within the PIILP support in both solvents investigated. As MeOH has been shown to give a much high sulfoxide selectivity and may be

considered the more environmentally benign solvent of the two a more thorough recycle study was conducted (table 2.6). Again no notable decrease in catalyst performance was observed, with both conversion and selectivity decreasing by just 4% over six successive cycles. Analysis of the MeOH solvent after the isolation and reuse of the catalyst from the first two runs of the experiment again showed that the tungsten content was too low for detection (<1 ppm) in keeping with the observations from the cyclooctene recycle experiment conducted previously. Further to this, analysis of the catalyst isolated after the 6th cycle gave a tungsten content of 25.84%, showing a reduction of just 0.16% from the initial value of 26% for unused catalyst, further evidence that catalyst leaching occurring for POM-2.1 is almost negligible.

Table 2.6 Conversion and sulfoxide selectivity values obtained for subsequent catalyst recycles in the oxidation of thioanisole in MeOH catalysed by POM-2.1^a

Run	Conversion ^b	Sulfoxide selectivity ^{b,c}
1	88	92
2	87	92
3	88	92
4	86	91
5	86	90
6	84	88

^aReaction conditions: 0.5 mol% POM-2.1, 1 mmol substrate, 2.5 mmol 35% H₂O₂, 3 mL solvent, RT, 20 min.

^bDetermined by ¹H NMR. ^cSulfoxide selectivity = [%sulfoxide / (%sulfoxide + %sulfone)].

The promising results obtained for the oxidation of various sulfides catalysed by POM-2.1 coupled with the high degree recyclability shows that PIILP supported catalysts are an effective means to achieve mild oxidations, often outperforming other heterogeneous catalysts published in the literature, particularly with regard to the reaction temperature, time and amount of H₂O₂ required. The use of PIILP supports also appears to have a dampening effect on the catalyst activity, which can be greatly advantageous allowing for high selectivity to be achieved for both sulfoxide and sulfone, an aspect which can be fine-tuned through solvent choice or reaction time. Due to the largely industrially relevant nature of both sulfoxides and sulfones, be it in fine chemical production or the purification of crude oil, the use of an efficient environmentally benign, selective catalyst is highly desirable in the scale up of reactions. As such a more in depth study into heterogeneous sulfoxidations using PIILP catalysts and their implementation into continuous flow processes was conducted, full details of which are outlined in chapter 3.

2.3.5. Polymer Support Comparisons

Due to the clear influence of the support morphology and microenvironment over catalyst performance in heterogeneous reactions, an investigation into the effect of the polymer backbone IP-2.1 as a lead was conducted. A range of ionic polymers of varying composition were prepared; this

included varying the ratio of co-monomer to IP-2.1 for a constant average chain length as well as varying the average polymer chain length while retaining the co-monomer to IP-2.1. In this regard, IP-2.2 and IP-2.3 were prepared which consisted of a co-monomer ratio of 1 IL unit every 6 alkyl monomers, with the former having the same average chain length as IP-2.1 of ~50 units, and hence a reduced IL loading, while the latter maintained the same number of IL units but with a longer average chain length of approximately 120 units. Despite the relatively well behaved nature of ROMP elemental analysis obtained for IP-2.2 and IP-2.3 showed that both polymers consisted of an average co-monomer ratio closer to 1 : 5.5 rather than the 1 : 6 proposed by the reaction stoichiometry, corresponding to ionic loadings of 1.08 mmol g⁻¹ and 1.09 mmol g⁻¹, respectively. As the ROMP mechanism is dominated by the relief of ring strain, the incomplete incorporation of cis-cyclooctene in the final polymers may be due to the lower ring strain of the monomer of 7.4 kcal mol⁻¹ compared to that of the norbornene bicyclic of 27.2 kcal mol⁻¹.⁴⁵ While the difference in ring strain did not cause

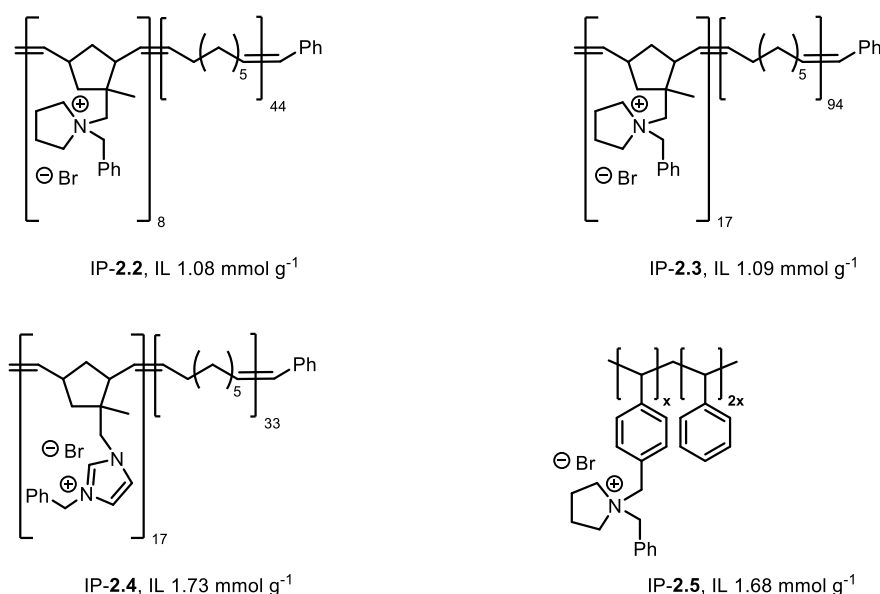
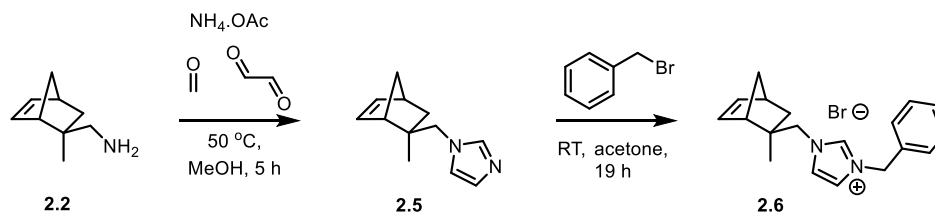


Figure 2.14 IPs 2.2 – 2.5 used to illustrate the effect of different polymer support structure on catalyst performance in H₂O₂-mediated oxidations. In each case the ionic loading (mmol g⁻¹) is shown.

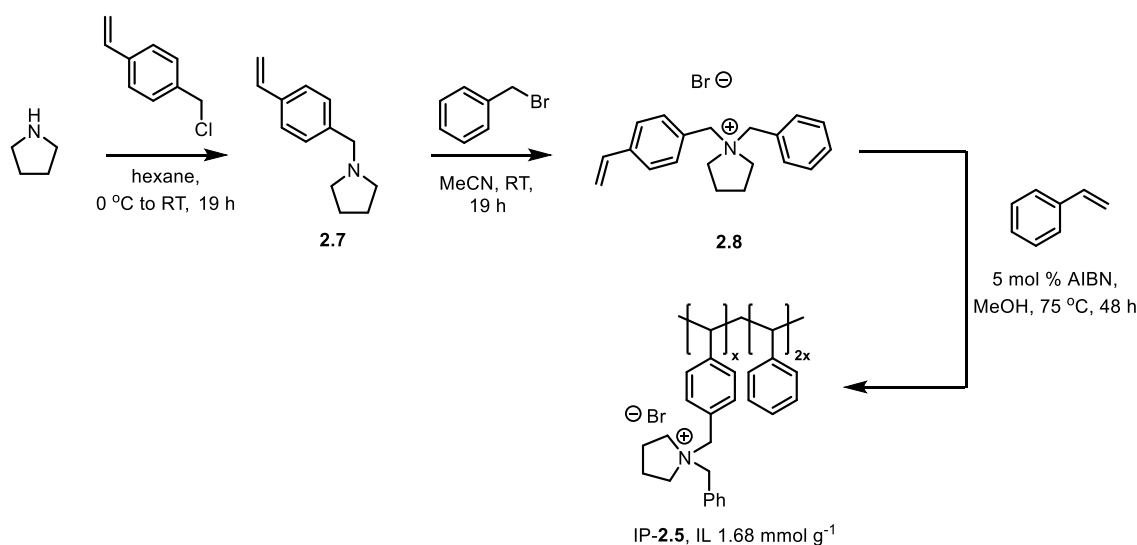
issue in the generation of IP-2.1 with respects to correct co-monomer incorporation, the excess of cis-cyclooctene present in the formulation of IP-2.2 and IP-2.3 appears to exacerbate this difference, leading to incomplete incorporation of cis-cyclooctene. The apparent inability to fully incorporate the desired larger amounts of cis-cyclooctene into produced co-polymers highlights a significant limitation of this particular ROMP system. In order to address this issue it will be necessary to use more reactive metathesis catalysts such as the 2nd generation Grubbs catalyst and/or by using a co-monomer with comparable ring strain to norbornene. However, as these materials were to be used for exploratory work and the co-monomer ratio of 1 : 5 was deemed significantly different to the 1 : 2 ratio of IP-2.1 that they could be used as is. In order to evaluate the effect of the nature of the IL

group present on the polymer support, IP-2.4 was proposed as a direct imidazolium-functionalised comparison to the pyrrolidinium-functionalised IP-2.1. The desired monomer 2.6 was prepared by first constructing the imidazole ring from 2.2 using a modified of the conditions reported by Matsuoka *et al* (scheme 2.6).⁴⁶



Scheme 2.6 Synthesis of the imidazolium bromide-functionalised norbornene monomer 2.6

Following purification by column chromatography the imidazole-functionalised monomer was quaternized with benzyl bromide under the same conditions outlined in scheme 2.2, before undergoing ROMP under the same conditions used for the preparation of IP-2.1. Elemental analysis of IP-2.4 gave an ionic loading of 1.73 mmol g⁻¹, a value consistent with the expected co-monomer ratio of 1 : 2 and confirming that IP-2.4 was a direct analogue of IP-2.1; this would allow for a direct comparison between the pyrrolidinium and imidazolium IL functionalities. Finally a direct styrene-based analogue of IP-2.1 was prepared as a means to assess the relative merits of the two polymerisation methods. The desired pyrrolidinium-tagged styrene monomer 2.8 was prepared through a straightforward two step synthesis starting with the quantitative alkylation of pyrrolidine with 4-vinylbenzyl chloride which was then quaternised with an excess of benzyl bromide

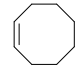
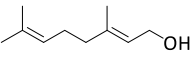
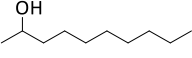
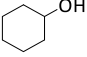
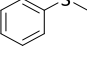
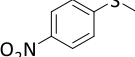


Scheme 2.7 Synthesis of the pyrrolidinium bromide-functionalised styrene monomer 2.8 and subsequent free radical initiated polymerisation to give IP-2.5

as described above (scheme 2.7). The resulting analytically pure monomer was then subjected to free radical-initiated polymerisation in ethanol with 5 mol% azobisisobutyronitrile (AIBN) and two equivalents of styrene as a co-monomer to yield IP-2.5. While the synthesis of **2.8** is considerably more straightforward and higher yielding than its norbornene-based counterpart **2.4**, the need to employ much harsher polymerisation conditions highlights the advantages of using ROMP to prepare PIILP materials. Elemental analysis of IP-2.5 also demonstrated the comparatively uncontrolled way in which free radical polymerisation proceeds, giving an ionic loading which corresponded to a co-monomer ratio of 1 : 2.3 as opposed to the 1 : 2 ratio obtained for the IP-2.1.

Following the preparation of the desired IPs the corresponding catalysts POM-2.2, POM-2.3, POM-2.4 and POM-2.5 were generated through the same H₂O₂-mediated degradation of phosphotungstic acid followed by ion exchange according to the procedure used for POM-2.1. Again all catalysts were obtained as amorphous, insoluble solids which all possessed tungsten loadings consistent with complete ion exchange and the proposed formulation as determined by elemental analysis. The freshly prepared PIILP catalysts were evaluated against a selection of substrates representative of the three different oxidation reactions previously investigated with POM-2.1, the results of which are summarised in table 2.7. The reduction in the ionic loading for a polymer chain of comparable length observed between POM-2.1 and POM-2.2 appears to have no influence on

Table 2.7 Comparison of the catalytic performance of the different prepared PIILP catalysts in select hydrogen peroxide-mediated epoxidations, alcohol oxidations and sulfoxidations

entry	substrate	POM-2.1	POM-2.2	POM-2.3	POM-2.4	POM-2.5
1		98 ^a	96 ^a	83 ^a	97 ^a	96 ^a
2		96 ^a	98 ^a	>99 ^a	>99 ^a	>99 ^a
3		97 ^b	93 ^b	>99 ^b	98 ^b	11 ^b
4		98 ^b	98 ^b	97 ^b	99 ^b	21 ^b
5		88 ^c (84) ^d	94 ^c (64) ^d	85 ^c (61) ^d	97 ^c (68) ^d	74 ^c (97) ^d
6		89 ^c (78) ^d	80 ^c (64) ^d	87 ^c (45) ^d	52 ^c (83) ^d	99 ^c (75) ^d

^aReaction conditions described in table 2.2. Determined by GC of reaction mixture using n-decane as an internal standard. ^bReaction conditions described in table 2.3. Determined by ¹H NMR. ^cReaction conditions described in table 2.5, conducted in MeCN solvent. Determined by ¹H NMR. ^dSulfoxide selectivity = [%sulfoxide / (%sulfoxide + %sulfone)].

catalyst performance in both epoxidation and alcohol oxidation reactions (entries 1 – 4). This effect is also observed for the longer polymer chain of POM-2.3, which also gave a comparable performance except for the epoxidation of cis-cyclooctene which experienced a minor reduction in activity. While the investigation into the oxidation of alcohols showed that there was a strong correlation between

the accessibility of the peroxometalate anion and catalyst performance, the differences in polymer morphology between POM-**2.1-2.3** may not be significant enough to demonstrate this effect. Due to the polynuclear nature of the active peroxometalate there are numerous active sites for each anion; as such the subtle differences in polymer morphology may not prevent effective approach of the substrates to an active site. Interestingly, in the oxidation of 4-nitrothioanisole POM-**2.3** showed markedly different selectivity to POM-**2.1** (entry 6). This increased affinity for the sulfone product could be the result of different pore sizes within the catalysts, retaining the 4-nitrothioanisole substrate in close proximity to the active peroxometalate for longer times. This in turn would help facilitate further reaction by allowing more time for the second oxidation to yield sulfone. This effect on product selectivity is also observed in the oxidation of thioanisole with POM-**2.3** and in both sulfoxidation reactions catalysed by POM-**2.2** albeit to a lesser extent (entries 5 and 6). The higher sulfone selectivity of catalyst based on the two alkyl-rich polymers demonstrates that it should be possible to control product selectivity by altering support morphology, however, the effect appears to be somewhat subtle and substrate specific.

Altering the IL fragment between the analogous supports from pyrrolidinium in POM-**2.1** to imidazolium in POM-**2.4** also appears to have no significant effect on catalyst performance in both epoxidation and alcohol oxidation, again most likely as a result of the multisite nature of the active species. However, aspects of product selectivity are again observed in the sulfoxidation reactions investigated, with POM-**2.4** appearing to be a more efficient catalyst in the oxidation of thioanisole, albeit with poorer sulfoxide selectivity, whilst simultaneously giving a markedly poorer performance for 4-nitrothioanisole when compared to POM-**2.1** (entries 5 and 6). During the electrophilic attack of the substrates during catalysis the cation of the IL fragment will influence the formation of partial charges in the transition state, which is likely to affect the rate of reaction. While having a more profound effect than the structure of the backbone, this difference in rate caused by altering the nature of the ionic liquid cation still appears to remain more subtle and substrate specific. For example, it would be reasonable to assume that the enhancement obtained with the imidazolium decorated PIILP catalyst would extend to a range of sulfides rather than substrate specific to thioanisole. This again shows the incredibly complex relationship between the substrate, catalyst and support material and the need for more thorough studies.

The very minor influence of the structure of the polymer backbone over catalyst behaviour is further highlighted by the performance of POM-**2.5**, the polystyrene-based analogue of POM-**2.1** which gave comparable conversions and product selectivity in epoxidations and sulfoxidations. Despite this, POM-**2.5** performed very poorly for alcohol oxidations and gave very low conversions. This appears to be a direct result of the poor stability of the polystyrene support under the harsher

reaction conditions, as evidenced by the significant clumping of the catalyst material in the reaction vessel post reaction. Despite this, the TGA curve obtained for IP-2.5 showed no significant loss of mass until temperatures approximately 160 °C (figure 2.15); the gradual slight decrease in mass before this point is believed to be solvent trapped within the polymer sample. This would imply that any thermal degradation pathway that is occurring does not result in loss of mass, while no notable exotherms/endotherms were observed in the corresponding DSC.

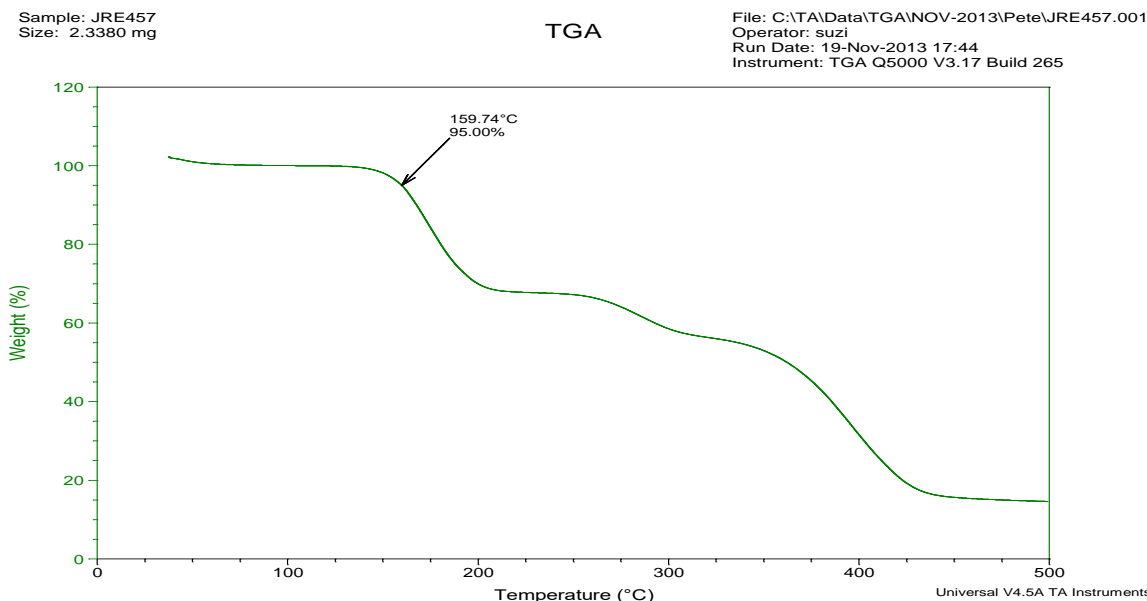


Figure 2.15 TGA curve for POM-2.5 taken with a heating rate of 10 °C min⁻¹

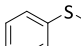
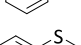
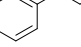
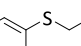
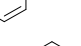
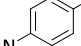
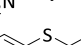
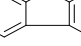
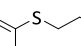
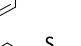
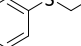
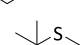

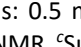
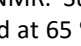

Despite the apparent increased robustness of the polystyrene-based support with regards to higher thermal stability compared to its norbonene-based counterparts, the materials produced through the ROMP process still appear much more appropriate for harsher reaction conditions, and as such can be considered better multipurpose catalyst supports to be used across different reactions. A comparison of the 5 prepared ionic polymer supports demonstrated that it is possible to change the performance of the peroxometalate catalyst by modifying the polymer backbone structure and composition as well as by altering the nature of the cation. With regard to the former, the differences in pore structure arising from the increase in co-monomer content may be responsible for the enhancement in rate as the cavities could effectively retain the substrates in close proximity to the active sites. The relative spacing of the IL moieties will also clearly influence the microenvironment around the active sites making it difficult to rationalise the effect of co-monomer ratio on performance. The differences in reaction rates caused by these structure differences appear to be incredibly subtle and are much more notable in the sulfoxidations in which differences in product selectivity can be observed. While alteration of the IL cation used has a more prominent, albeit substrate specific, effect on catalyst performance the differences are again mostly notable in the

sulfoxidation reactions. With this in mind a more thorough investigation into the role of the polymer support was conducted under sulfoxidation conditions.

2.3.6. Ionic Liquid Functionality Comparisons

In order to more thoroughly investigate the effect on sulfoxidation selectivity of different IL functionalities in PIILP supports a range of different IL-functionalised monomers are required. During the preparation of the norbornene-based monomers **2.4** and **2.6** and the comparative styrene based analogue **2.8** it was noted that the latter was much more straightforward to prepare in high yield. In this regard, styrene-based monomers would be ideal to produce large quantities of different polymer materials for exploratory development type investigations. In the oxidation of thioanisole and 4-nitrothioanisole investigated in table 2.6 the analogous ROMP and polystyrene-based PIILP catalysts POM-2.1 and POM-2.5 showed almost the same behaviour, giving selectivities and yields within 10% of each other. This would imply that the structural difference between the two polymers does not have a significant influence over catalyst performance. As such the evaluation of these two catalysts was extended to the full selection of sulfides from table 2.5 in order to undertake a more thorough comparison between these the two supports (table 2.8).

Table 2.8 Selective oxidation of sulfides to sulfoxides with hydrogen peroxide catalysed by POM-2.1 POM-2.5^a

entry	substrate	solvent	POM-2.1		POM-2.5	
			% Conv. ^b	Sulfoxide selectivity ^{b,c}	% Conv. ^b	Sulfoxide selectivity ^{b,c}
1		MeCN	88	84	74	97
2		MeOH	95	96	99	92
3		MeCN	92	80	77	95
4		MeOH	92	93	97	95
5		MeCN	98 ^d	65 ^d	97 ^d	81 ^d
6		MeOH	99 ^d	98 ^d	89 ^d	79 ^d
7		MeCN	89	88	99	75
8		MeOH	56	95	92	90
9		MeCN	24	88	34	79
10		MeCN ^e	95	19	85	25
11		MeCN	98	58	55	80
12		MeOH	62	90	55	85
13		MeCN	99	76	99	73
14		MeOH	92	98	99	84
15		MeCN ^f	59	98	90	70
16		MeOH ^f	99	78	96	73

^aReaction conditions: 0.5 mol% catalyst, 1 mmol substrate, 2.5 mmol 35% H₂O₂, 3 mL solvent, RT, 15 min.

^bDetermined by ¹H NMR. ^cSulfoxide selectivity = [%sulfoxide / (%sulfoxide + %sulfone)]. ^dDetermined by ¹³C NMR.

^eReaction conducted at 65 °C. ^fReactions conducted in deuteriated solvent for 2 minutes and monitored by ¹H NMR.

Comparison of POM-2.1 and POM-2.5 shows no discernible trend in performance between the two catalysts. Catalysis conducted in MeCN gave comparable conversions and sulfoxide selectivities across the full range of substrates tested, with the exception of ethyl phenyl sulfide which performed more poorly with POM-2.5 (entry 3) and *tert*-butyl methyl sulfide, which gave a conversion of just 59% with POM-2.1 compared to the 90% with POM-2.5 (entry 15). For the latter the incredibly short reaction times required for this substrate will make minor differences in catalyst rates seem much more profound. The most notable difference in catalyst performance was for the oxidation of 4-nitrothioanisole in MeOH with POM-2.1 giving a conversion of just 56% while POM-2.5 gave 92% conversion in the same time. Interestingly, despite the significant difference in rates as evidenced by the conversions, both were highly selective for sulfoxide.

With the exception of a few specific substrate/solvent combinations, the results in table 2.8 strongly suggest that any differences between the structures of the two support materials that may result from the polymerisation method or the nature of the carbon polymer backbone does not have a significant effect on catalyst performance. In keeping with the observations made in table 2.7 it would appear that it is the nature of the IL fragments within the support which has a more significant influence on the performance of POM-based PIILP catalysts. Combining this knowledge with the fact that styrene-based polymers are synthetically more straightforward it was decided to prepare a range of different IL-decorated polystyrene PIILP materials (figure 2.16) in order to investigate the influence of the ionic liquid cation on catalyst performance. . To this end IP-2.6, IP-2.7 and IP-2.8, prepared by A. Clemmet for work conducted as a larger overarching project concerning PIILP, were selected for comparison against the pyrrolidinium-based IP-2.5 (figure 16). As in the analogous synthesis of IP-2.5 polymerisations involving styrene based imidazolium gave materials with less accurate co-monomer

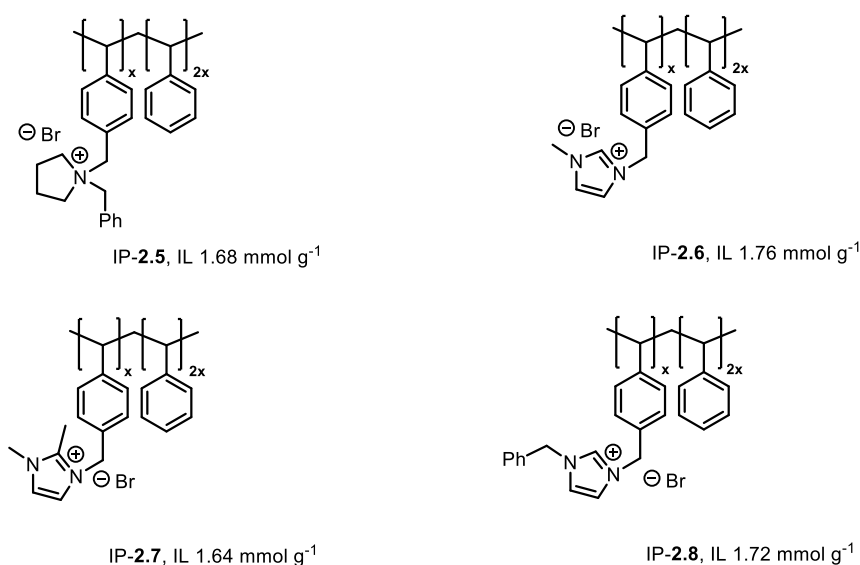


Figure 2.16 Polystyrene-based IPs 2.5 – 2.8 used to illustrate the effect of IL group functionality on catalyst performance in H₂O₂-mediated sulfoxidations. In each case the ionic loading (mmol g⁻¹) is shown

ratios, typically in the region of 1 : 2.3, compared to their ROMP-based PIILP counterparts. Using the same procedure described above for the preparation of 2.5 each of the new ionic polymers were first impregnated with peroxometalate by ion exchange to yield the corresponding POM catalysts as amorphous solids. Despite the inaccuracy in polymer composition which arose from the largely uncontrolled polymerisation method, elemental analysis of POM-2.6 – 2.8 indicated tungsten loadings which corresponded to complete ion exchange, allowing for accurate catalyst loadings to be determined. The performance of the 3 imidazolium-functionalised PIILP catalysts were evaluated against their pyrrolidinium-functionalised counterpart POM-2.5 in the oxidation of the aryl alkyl sulfides (figure 2.17).

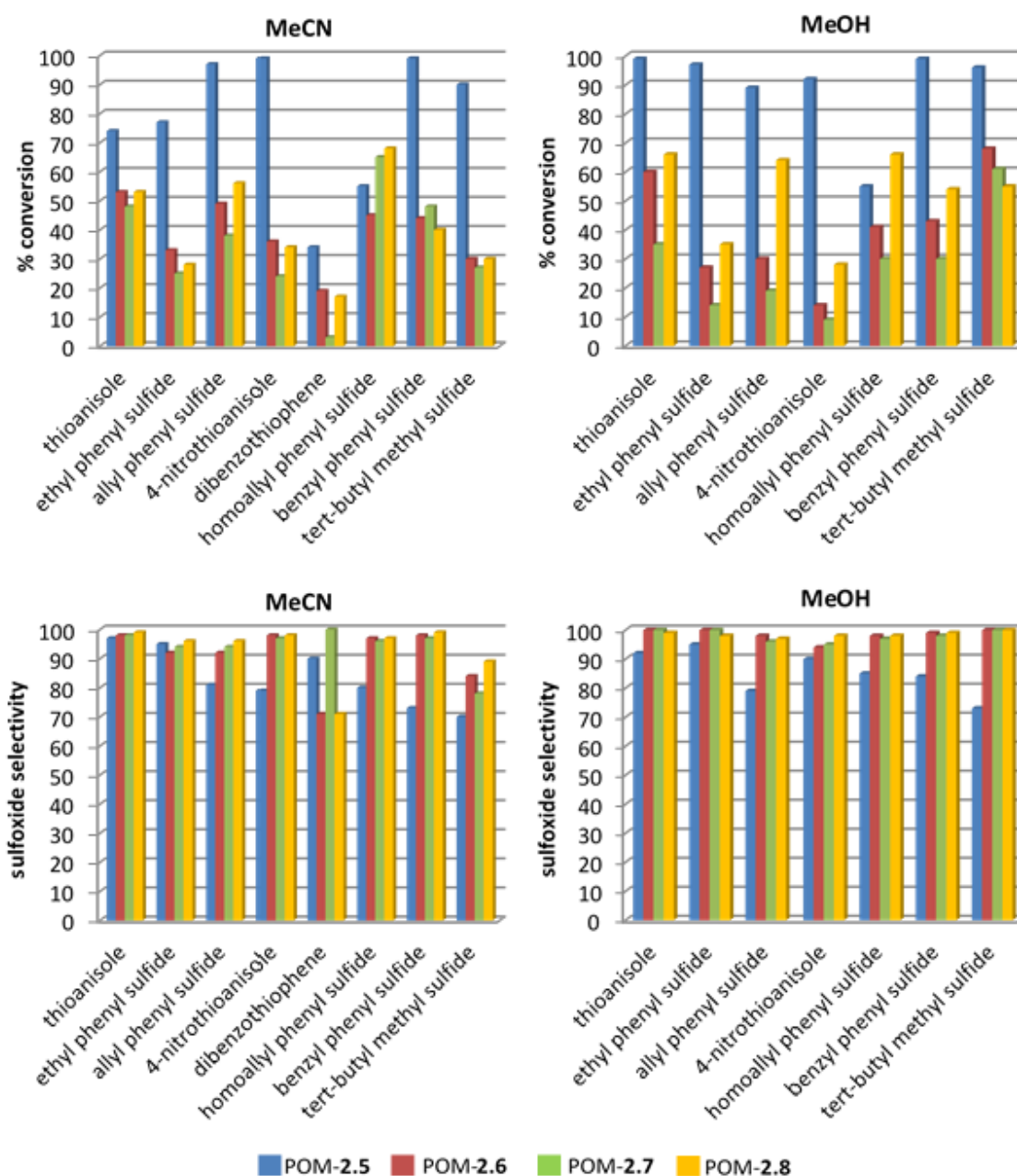


Figure 2.17 Conversion and selectivity profiles for the oxidation of various sulfides catalysed by POM-2.5 – 2.8 under reaction conditions outlined in tables 2.5 and 2.8

General observations show that POM-2.5 far outperforms any of the imidazolium-based catalysts in terms of conversions achieved, however, POM-2.5 consistently produced lower sulfoxide selectivity than its imidazolium-based counterparts across all substrates tested. The most notable outperformance was seen in the oxidation of 4-nitrothioanisole, in which POM-2.5 gave conversions above 90% in both solvents while other catalysts gave only values ranging from 9 to 30%. Interestingly, in contrast to this trend the imidazolium-based systems POM-2.7 and POM-2.8 outperformed POM-2.1 in both solvents (figure 2.18).

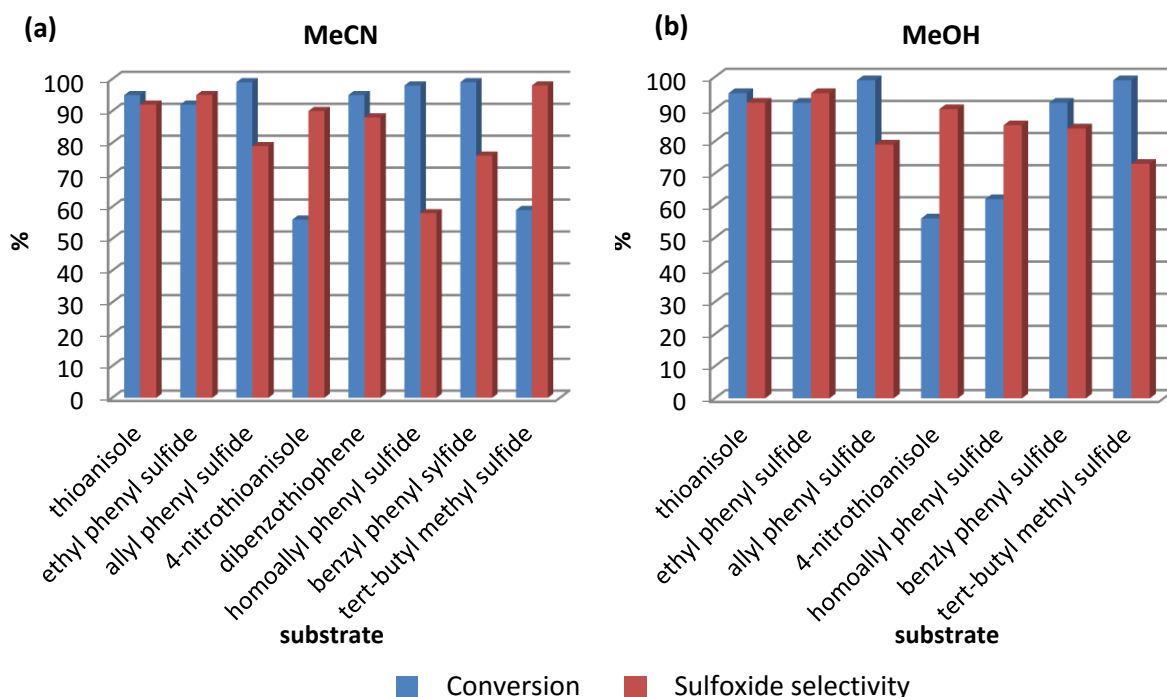


Figure 2.18 Graphical summary of the performance of POM-2.1 in the H₂O₂-mediated oxidation of aryl alkyl sulfides in MeCN and MeOH solvents

This higher activity could be caused by an increase in the affinity of the substrate for the support materials in POM-2.7 and POM-2.8 as a result of the increased hydrophobicity of the imidazolium cation compared with pyrrolidinium.⁴⁷ This effect is most evident with the benzyl side chains in POM-2.8 which could create more hydrophobic regions and effectively retain the homoallyl phenyl sulfide substrate in close proximity to the active centres. This observation, however, does not hold for the highly hydrophobic dibenzothiophene which performed poorly with all three imidazolium-based catalysts. It is likely that the microstructure in these materials gives pore sizes and structures which are not suited for larger substrates. Due to the electrophilic nature of the oxidation mechanism it is likely the presence of an ionic environment could stabilise the forming partial charges in the transition state, and hence facilitate the reaction. In this regard, the delocalised, softer positive charge of the imidazolium groups in POM-2.6 – 2.8 may be unable to achieve this effect to the same

extent of the harder cationic charge of the pyrrolidinium group of POM-2.5, potentially explaining the higher performance of the latter system. Despite the considerable difference in catalyst activity all four catalysts gave similar sulfoxide selectivities. When the sulfoxidation reactions catalysed by POM-2.6 – 2.8 were conducted for longer periods of time in order to increase the conversions achieved, a notable drop in sulfoxide selectivity was also observed, illustrating that the high selectivity initially observed was a product of reduced catalyst activity.

While the results obtained in figure 2.17 highlight that the IL functionality of the PIILP support can exert an incredibly profound effect on catalyst performance (as evidenced by the markedly higher conversions achieved with POM-2.5) it is difficult to infer any significant trend with regard to the nature of cation, its role and the substrate structure. Attributing the differences in activity solely to the nature of the IL cation is most likely an oversimplification as differences in IL structure most likely results in differences in the overall morphology of the catalyst material. These results again highlight the incredibly complex nature of the relationship between catalyst, support and the reacting substrate.

2.4. Conclusions

ROMP has been used to prepare a well-defined IL-decorated polymer support that can be impregnated with the peroxometalate anion $[\text{PO}_4\{\text{WO}(\text{O}_2)_2\}_4]^{3-}$ via anion exchange to give an amorphous, insoluble catalyst POM-2.1. Analysis of this material showed that the catalyst is granular in nature and that complete ion exchange had occurred. This initial PIILP catalyst proved to be highly effective in the mild epoxidation of various substrates, often outperforming comparable heterogeneous catalysts reported in the literature, while also efficiently recycling with almost negligible leaching of the active tungsten species. These promising results show that PIILP catalysis is an effective means to transfer the positive attributes of ILs to well-defined, solid supports to give highly active, environmentally benign catalysts. This observation was further vindicated in the oxidation of various sulfides, which was not only highly active but gave controllable product selectivity. Taking these positive results as a basis, the use of PIILP may be a viable approach to obtaining highly efficient, mild continuous flow processes, as discussed in chapter 3. Unfortunately the oxidation of alcohols revealed one of the major limitations of PIILP catalysis with regard to catalyst clumping and much lower activity under the reaction conditions, although the origin of this poor performance has not been unequivocally established.

Investigations into the effect of the nature of the polymer support on catalysts performance showed that differences in activity and selectivity were largely subtle and somewhat substrate specific, making patterns difficult to predict and rationalise. Although a profound difference in

catalyst activity was observed between systems based on pyrrolidinium and imidazolium IL cations the relationship between support structure and performance still remains incredibly complex. Due to the multisite nature of the active peroxometalate anion the subtle differences in polymer morphology and microstructure may not significantly alter or hinder the approach of different substrates during reaction. Differences in catalyst performance may be much more obvious when investigating more well-defined, single site active species. Although further studies are clearly required to elucidate a full understanding of the complex relationship between the structure and, function of the support and catalyst performance, the well behaved nature of ROMP process used to generate PIILP supports combined with the synthetically diverse, modular means of generating the required monomers will allow systematic modification of the support to explore and develop structure-activity patterns. Taking the promising initial results discussed in this chapter coupled with these considerations, PIILP catalysis can be further exploited and optimised for use as a general tool across the full spectrum of catalysis.

2.5. Experimental

All manipulations involving air-sensitive compounds were carried out using standard Schlenk line techniques under an atmosphere of nitrogen in oven-dried glassware. Chloroform, dichloromethane and methanol were distilled from calcium hydride and diethyl ether and hexane from sodium wire. Dicyclopentadiene was cracked by distillation over Fe_2O_3 powder to give cyclopentadiene which was used without further purification. All reagents were purchased from commercial suppliers and used without further purification. ^1H and $^{13}\text{C}\{^1\text{H}\}$ NMR spectra were recorded on a JEOL ESC-400 instrument. Solid state ^{31}P NMR were recorded at 161.87 MHz using a Varian VNMRS 400 spectrometer and a 4 mm (rotor o.d.) magic-angle spinning probe. They were obtained using cross-polarisation with a 2 s recycle delay, 3 ms contact time, at ambient temperature and at a sample spin-rate of 10 kHz. Between 1000 and 3600 repetitions were accumulated. Spectral referencing was with respect to an external sample of neat tetramethylsilane (carried out by setting the high-frequency signal from adamantane to 38.5 ppm). Gas chromatography-mass spectrometry was performed on a Saturn 2220 GC-MS system using a factorFour VF-5ms capillary column, 30 m, 0.25 mm, 0.25 μm and high resolution mass spectrometry was conducted on a Waters Micromass LCT Premier mass spectrometer. CHN analysis was undertaken using a Carlo-Erba 1100 elemental combustion analyser controlled with CE Eager 200 software and metal analysis was performed using a Perkin-Elmer Optima 4300 ICP-OES analyser. Thermogravimetric analysis (TGA) and Differential Scanning Calorimetry (DSC) was performed using a Ta TGA Q5000, at a heating rate of either 5 $^\circ\text{C min}^{-1}$ or 10 $^\circ\text{C min}^{-1}$. All samples were sealed in a glovebox into aluminium pans. The onset of the weight loss in each thermogram was used as a measure of the decomposition temperature. TEM images were acquired in bright field using a Tecnai 200 kV F20 Transmission Electron Microscope with a Field Emission Gun. A few drops of sample were pipetted onto an Agar holey carbon film copper TEM grids and the prepared grid was set aside for ca. 20 min prior to inserting it into the microscope, in order to allow the solvent to evaporate. Images were taken with a Gatan CCD digital camera attached to the microscope. X-Ray Crystallography data were measured on an Agilent Gemini A Ultra diffractometer at 150 K, with $\text{Mo K}\alpha$ ($\lambda = 0.71073\text{\AA}$) radiation. Semiempirical absorption corrections were applied based on symmetry-equivalent and repeated reflections. Structures were solved by direct methods and refined on all unique F_2 values, with anisotropic non-H atoms and constrained riding isotropic H atoms for carbon atoms; $U(\text{H})$ was set at 1.2 (1.5 for methyl groups) times U_{eq} of the parent atom. Hydrogen atoms for the water molecule were constrained to a distance of 0.94 \AA and $U(\text{H})$ set at 1.2 times U_{eq} of the parent atom. Programs were CrysAlisPro10 for data collection, integration, and absorption corrections and SHELXTL11 for structure solution, refinement, and graphics. FT-IR spectrums were

record on a Varian 800 FT-IR spectrometer system using a pike technologies diamond crystal plate ATR unit. Ionic polymers IP-2.6, IP-2.7 and IP-2.8 were prepared by A. Clemmet and used as is.

2-Methylbicyclohept-5-ene-2-carbonitrile (2.1)¹⁹

A three-neck round bottomed flask was charged with boron trichloride 1M in hexanes (23.0 mL, 23.0 mmol) and cooled to 0 °C after which methacrylonitrile (15.2 mL, 182.0 mmol) was added slowly causing the instant formation of a white solid. After the drop-wise addition of freshly cracked cyclopentadiene (10.0 mL, 151.0 mmol) the white solid redissolved and was allowed to stir for 19 h and warm to room temperature. The resultant pale yellow oil was then poured onto an excess of NaHCO₃ on ice and allowed to stir for approximately 10 mins after which time the product was extracted with diethyl ether (3 X 100 mL) and the combined extracts dried with MgSO₄ before the solvent was removed under reduced pressure to give the product as a pale oil in 72% yield (14.50 g). ¹H NMR (399.78 MHz, CDCl₃, δ): (94 : 6 *endo* : *exo* mixture, major *exo*) 6.25 (dd, *J* = 5.4, 1.9 Hz, 1H, H_aC=CH_b), 5.96 (dd, *J* = 5.4, 1.9 Hz, 1H, H_aC=CH_b), 3.02 (m, 1H, bridgehead), 2.93 (m, 1H, bridgehead) 2.27 (dd, *J* = 13.7, 1.5 Hz, 1H, CH₂), 2.25 (dd, *J* = 13.7, 1.5 Hz, 1H, CH₂), 1.76 (dt, *J* = 14.3, 2.0 Hz, 1H, bridge CH₂), 1.53 (dt, *J* = 14.3, 2.0 Hz, 1H, bridge CH₂), 1.18 (s, 3H, CH₃); ¹³C{¹H} NMR (100.52 MHz, CDCl₃, δ): 138.9, 131.8, 127.3, 52.5, 49.6, 43.2, 40.7, 30.2, 23.9; LRMS (EI⁺) *m/z* 134 [M+H]⁺.

(2-Methylbicyclohept-5-en-2-yl)methylamine (2.2)

A solution of **2.1** (13.48 g, 101.0 mmol) in diethyl ether (*ca.* 20 mL) was added drop-wise to a stirred suspension of lithium aluminium hydride (7.7 g, 202 mmol) in freshly distilled diethyl ether (100 mL) cooled to 0 °C. Upon complete addition of **2.1** the reaction was allowed to warm to room temperature and stirred for a further 20 h. NaOH (1.0 M, 12 mL) was then added drop-wise to the mixture which had again been cooled to 0 °C followed by distilled water (100 mL) and allowed to stir for 1 h after which time the mixture was filtered through celite. After washing celite with diethyl ether (150 mL) the combined organic extract was then treated with HCl (1 M, 180 mL) and extracted with diethyl ether (3 X 75 mL). The resulting aqueous layer was then treated with NaOH solution (1 M) to approximately pH 12. The product was then extracted with diethyl ether (3 X 100mL), dried with MgSO₄ and the solvent removed under reduced pressure to give **2.2** as a yellow-orange oil in 61% yield (8.5 g). ¹H NMR (400 MHz, CDCl₃, δ): 6.08 (dd, *J* = 5.4, 1.9 Hz, 1H, H_aC=CH_b), 6.04 (dd, *J* = 5.4, 1.9 Hz, 1H, =CH), 2.70 (m, 1H, bridgehead), 2.65 (br, 2H, CH_aH_b-NH₂), 2.26 (m, 1H, bridgehead), 1.53 (br d, *J* = 8.2 Hz, 1H, bridge CH), 1.42 (dd, *J* = 13.0, 4.5 Hz, 1H, CH₂), 1.33 (br d, *J* = 8.2 Hz, 1H, bridge CH),

1.15 (br, 2H, NH₂), 0.82 (s, 3H, CH₃), 0.73 (dd, *J* = 13.0, 2.5 Hz, 1H, CH₂); ¹³C NMR (100 MHz, CDCl₃, δ): 136.7, 135.5, 53.2, 48.7, 47.7, 43.3, 43.0, 38.3, 22.7; LRMS (EI⁺) *m/z* 138 [M+H]⁺.

1-(2-Methylbicyclohept-5-en-2-yl)methylpyrrolidine (2.3)⁴⁸

A round bottom flask was charged with **2.2** (5.0 g, 37.0 mmol), 1,4-dibromobutane (4.42 mL, 37.0 mmol), potassium carbonate (10.23 g, 74.0 mmol) and acetonitrile (300 mL) and heated to reflux with rapid stirring under nitrogen for 20 h. The mixture was filtered through a frit to remove excess potassium carbonate and the solvent was removed under reduced pressure. The resultant residue was diluted with diethyl ether (*ca.* 50 mL) followed by the addition of HCl (1.0 M, 74.0 mL, 74.0 mmol). The aqueous layer was extracted with diethyl ether (2 X 70 mL), treated with NaOH solution (1.0 M) until the solution reached pH 12. Product was extracted with diethyl ether (3 X 75 mL) and the combined organic fractions were dried with MgSO₄, filtered and the solvent removed under reduced pressure to give the product as an orange oil in 72% yield (5.09 g). *Exo*-diastereoisomer: ¹H NMR (400 MHz, CDCl₃, δ): 6.06 (br m, 2H, =CH), 2.70 (br s, 1H, bridgehead CH), 2.58 (br m, 5H, pyrrolidine CH₂ + bridgehead CH), 2.42 (br s, 2H, CH₂), 1.70 (br m, 4H, pyrrolidine CH₂), 1.58 (br d, *J* = 8.3 Hz, 1H, bridge CH), 1.51 (dd, *J* = 11.4, 3.6 Hz, 1H, CH₂), 1.29 (br d, *J* = 8.3 Hz, 1H, bridge CH), 0.88 (s, 3H, CH₃), 0.78 (dd, *J* = 11.4, 1.9 Hz, 1H, bridge CH); ¹³C NMR (100 MHz, CDCl₃, δ): 136.6, 135.9, 68.5, 56.6, 50.8, 47.7, 43.5, 42.8, 39.7, 25.0, 23.7; LRMS (EI⁺) *m/z* 192 [M+H]⁺; HRMS (ESI⁺) exact mass calcd for C₁₃H₂₂N [M+H]⁺ requires *m/z* 192.1752, found *m/z* 192.1749; Anal. Calc for C₁₃H₂₁N: C, 81.61; H, 11.06; N, 7.32. Found: C, 81.77; H, 11.34; N, 7.56.

1-Benzyl-1-((2-methylbicyclohept-5-en-2-yl)methyl)pyrrolidinium bromide (2.4)

A round bottom flask was charged with **2.3** (5.09 g, 27.0 mmol), benzyl bromide (12.6 mL, 81.0 mmol) and acetone (30 mL) and the resulting yellow solution was left to stir at ambient temperature for 19 h, during which time a white precipitate formed. The solid was isolated by filtration, washed with hexane (20 mL), diethyl ether (2 X 40 mL) and acetone (20 mL) and dried under high vacuum to give the product as a spectroscopically pure white powder in 73% yield (7.09 g). Crystals suitable for X-ray structure determination were grown by slow diffusion of a chloroform solution layered with hexane at room temperature. *Exo*-diastereoisomer: ¹H NMR (400 MHz, CDCl₃, δ): 7.63 (br d, *J* = 6.4, Hz, 2H, Ar-H), 7.37 (m, 3H, Ar-H), 6.13 (dd, *J* = 5.4, 2.0 Hz, 1H, =CH), 6.00 (dd, *J* = 5.4, 2.0 Hz, 1H, =CH), 5.14 (d, *J* = 12.1 Hz, 1H, N-CH_aH_b-Ph), 4.62 (d, *J* = 12.1 Hz, 1H, NCH_aH_b-Ph), 4.02 (d, *J* = 13.6 Hz, 1H, CMeCH_cH_d-N), 3.93 (m, 1H, pyrrolidine NCH₂CH₂) 3.79 (m, 1H, pyrrolidine NCH₂CH₂), 3.71 (d, *J* = 13.6

Hz, 1H, CMeCH_cH_d-N), 3.70 (m, 2H, pyrrolidine NCH₂CH₂), 2.44 (br s, 1H, bridgehead CH), 2.51 (br s, 1H, bridgehead CH), 2.06 (m, 1H, pyrrolidine NCH₂CH₂), 1.97 (dd, *J* = 11.4, 3.6 Hz, 1H, CH_eH_f), 1.90 (m, 1H, pyrrolidine NCH₂CH₂), 1.73 (m, 2H, pyrrolidine NCH₂CH₂), 1.66 (d, *J* = 9.2 Hz, 1H, bridge CH), 1.27 (br d, *J* = 9.2 Hz, 1H, bridge CH), 1.18 (2, 3H, CH₃), 0.87 (dd, *J* = 11.4, 2.3 Hz, 1H, CH_eH_f); ¹³C NMR (100 MHz, CDCl₃, δ): 138.8, 134.9, 133.2, 130.7, 129.3, 128.2, 72.9, 65.1, 62.8, 60.9, 53.2, 48.1, 44.5, 42.9, 40.5, 25.8, 22.8, 21.8; HRMS (ESI⁺) exact mass calcd for C₂₀H₂₈N [M]⁺ requires *m/z* 282.2222, found *m/z* 282.2221; Anal. Calc for C₂₀H₂₈BrN: C, 66.29; H, 7.79; N, 3.87. Found: C, 66.54; H, 8.13; N, 4.09%.

1-((2-Methylbicyclohept-5-en-2-yl)methyl)imidazole (2.5)⁴⁶

An oven-dried Schlenk flask was charged with ammonium acetate (3.30 g, 42.8 mmol), **2.2** (4.90 g, 35.7 mmol) and MeOH (25 mL) which was allowed to stir and heat to 50 °C. A solution of formaldehyde (37%, 5.35 mL, 71.4 mmol) and glyoxal (40%, 8.15 mL, 71.4 mmol) in MeOH (25 mL) was then added drop wise to the stirred solution which was subsequently allowed to stir at 50 °C for 20 h. Upon cooling to room temperature the solvent was removed under reduced pressure and the resulting residue was washed with 2 M KOH (500 mL) before the product was extracted with dichloromethane (3 X 50 mL), dried with MgSO₄ and the solvent removed under reduced pressure to give the crude product. Purification was achieved via column chromatography with a 40 : 1 dichloromethane : MeOH eluent to give the product as a dark brown oil in 60 % yield (4.05 g). *Exo*-diastereoisomer: ¹H NMR (400 MHz, CDCl₃, δ): 7.46 (s, 1H, N=CH-N), 7.04 (m, 1H, H_aC=CH_b imidazole), 6.91 (m, 1H, H_aC=CH_b imidazole), 6.15 (dd, *J* = 5.4, 1.9 Hz, 1H, H_aC=CH_b), 6.02 (dd, *J* = 5.4, 1.9 Hz, 1H, H_aC=CH_b), 3.97 (m, 2H, C-CH₂-N), 2.86 (m, 1H, CH bridgehead), 2.46 (m, 1H CH bridgehead), 1.60 (m, 2H, CH₂ bridge, CH-CH₂-C), 1.48 (m, 2H, CH₂ bridge, CH-CH₂-C), 0.83 (s, CH₃). ¹³C NMR (100 MHz, CDCl₃, δ): 138.1, 137.2, 135.1, 128.8, 120.5, 58.0, 49.1, 47.4, 43.5, 43.2, 38.9, 24.1. HRMS (ESI⁺) exact mass calcd for C₁₂H₁₆N₂ [M]⁺ requires *m/z* 188.2682, found *m/z* 188.2678.

3-Benzyl-1-((2-methylbicyclohept-5-en-2-yl)methyl)imidazolium bromide (2.6)

A round bottom flask was charged with **2.5** (3.84 g, 20.4 mmol), benzyl bromide (7.78 mL, 50.0 mmol) and toluene (150 mL) and allowed to stir under ambient conditions for 24 h, after which time the resulting fine precipitate was isolated by filtration. The product was then washed with diethyl ether (*c.a.* 150 mL) before drying under high vacuum to give a white powder in 44 % yield (3.23 g). *Exo*-diastereoisomer: ¹H NMR (400 MHz, CDCl₃, δ): 10.70 (s, 1H, N=CH-N), 7.50 (m, 2H, H_aC=CH_b imidazolium), 7.45 (m, 1H, Ar-H), 7.38 (m, 1H, Ar-H), 7.32 (m, 3H, Ar-H), 6.13 (dd, *J* = 5.4, 1.9 Hz, 1H,

$H_aC=CH_b$), 5.98 (dd, $J = 5.4, 1.9$ Hz, 1H, $H_aC=CH_b$), 5.61 (m, 2H, N- CH_2 -Ph), 4.35 (m, 2H, C- CH_2 -N), 2.85 (m, 1H, CH bridgehead), 2.43 (m, 1H, CH bridgehead), 2.46 (m, 1H CH bridgehead), 1.60 (m, 2H, CH_2 bridge, CH- CH_2 -C), 1.48 (m, 2H, CH_2 bridge, CH- CH_2 -C), 0.85 (s, CH_3). ^{13}C NMR (100 MHz, $CDCl_3$, δ): 137.7, 137.6, 138.7, 133.4, 129.5, 129.1, 123.7, 121.8, 60.4, 53.2, 49.4, 47.8, 43.7, 43.0, 38.6, 23.8. HRMS (ESI⁺) exact mass calcd for $C_{19}H_{23}N_2$ [M]⁺ requires m/z 279.3984, found m/z 279.3989.

General Procedure for the Ring-Opening Metathesis Polymerisation of cis-cyclooctene with Cationic Monomers 2.4 and 2.6

In a typical procedure a flame-dried Schlenk flask was charged with dry chloroform (80 mL), the specified amount of *cis*-cyclooctene and the cationic monomer (11.7 mmol). To the stirred solution was added the appropriate amount of $[RuCl_2(PCy_3)_2(=CHPh)]$ in chloroform (*ca.* 10 mL) and the resulting mixture was heated to 40 °C and left to stir for 19 h. Upon completion the reaction was allowed to cool to room temperature, ethyl vinyl ether (10 eq with respects to Grubbs catalyst) added and the solution stirred for an additional hour at 40 °C. Upon cooling to room temperature the polymer was precipitated by the slow addition of the reaction mixture to rapidly stirred diethyl ether (*ca.* 600 mL); after stirring for 60 minutes the polymer was isolated by filtration using a sintered glass frit, washed with diethyl ether and dried to give a pale green solid. A solution of tris-(hydroxymethyl)-phosphine was prepared by degassing 2-propanol (90 mL) with nitrogen for 30 min before adding tetrakis(hydroxymethyl)phosphonium chloride (25 eq with respects to Grubbs catalyst). Potassium hydroxide pellets (25 eq with respects to Grubbs catalyst) were added slowly to the vigorously stirred solution over the course of 15 minutes during which time a white precipitate formed. The mixture was allowed to stir for a further 10 min and then added to a solution of the polymer in chloroform (*ca.* 100-150 mL). After heating at 60 °C for 19 h, NaBr (250 eq with respects to Grubbs catalyst) was added and the mixture stirred for an additional hour at 60 °C. The mixture was then filtered, washed rigorously with distilled water (3 X 50 mL) and the resultant organic layer was added drop-wise to vigorously stirred diethyl ether (*ca.* 500 mL) to induce precipitation of the polymer. After stirring for approximately 60 min the polymer was allowed to settle, isolated by filtration through a frit, washed with diethyl ether (2 X 50 mL) and dried under high vacuum.

1-(4-Vinylbenzyl)pyrrolidine (2.7)

An oven-dried Schlenk flask was charged with hexane (25 mL) and 4-vinylbenzyl chloride (4.6 mL, 32.8 mmol) and cooled using ice water. Pyrrolidine (5.4 mL, 65.6 mmol) was added to the cooled

mixture over the course of 1 h causing an instant colour change of cloudy white to clear yellow. Following the complete addition of pyrrolidine the reaction vessel was removed from the ice water and allowed to stir for 19 h at room temperature after which time the mixture was filtered and the solvent removed under reduced pressure to give the product as a yellow oil in 98% yield (6.02 g). ¹H NMR (400 MHz, CDCl₃, δ): 7.31 (m, 4H, Ar-H), 6.66 (dd, *J* = 17.4, 10.6 Hz, 1H, H_aC=CH_bH_c), 5.71 (d, *J* = 17.4 Hz, 1H, H_aC=CH_bH_c), 5.16 (d, *J* = 10.5 Hz, 1H, H_aC=CH_bH_c), 3.56 (s, 2H, Ar-CH₂-N), 2.46 (m, 4H, N-CH₂), 1.73 (m, 4H, pyrrolidine N-CH₂-CH₂). ¹³C NMR (100 MHz, CDCl₃, δ): 139.03, 136.55, 128.93, 125.97, 113.20, 60.33, 54.05, 23.34.

1-Benzyl-1-(4-vinylbenzyl)pyrrolidin-1-ium bromide (2.8)

A round bottom flask was charged with **2.7** (3.38 g, 18.0 mmol), benzyl bromide (4.2 mL, 27.0 mmol) and acetonitrile (20 mL). The yellow solution was allowed to stir at room temperature for 19 h after which time the reaction mixture was added drop-wise to vigorously stirred diethyl ether (*ca.* 500 mL) to induce precipitation of the product. The resultant yellow-white solid was isolated by filtration, washed with diethyl ether and dried under high vacuum to give **2.8** as a yellow-white powder in 82% yield (5.32 g). ¹H NMR (400 MHz, CDCl₃, δ): 7.57 (m, 4H, Ar-H), 7.39 (m, 5H, Ar-H), 6.66 (dd, *J* = 17.4, 10.6 Hz, 1H, H_aC=CH_bH_c), 5.79 (d, *J* = 17.4 Hz, 1H, H_aC=CH_bH_c), 5.34 (d, *J* = 10.6 Hz, 1H, H_aC=CH_bH_c), 5.04 (s, 4H, Ar-CH₂-N), 3.68 (m, 4H, N-CH₂), 2.04 (m, 4H, pyrrolidine N-CH₂-CH₂). ¹³C NMR (100 MHz, CDCl₃, δ): 139.59, 135.48, 133.46, 133.22, 130.49, 129.15, 127.71, 126.92, 126.75, 116.12, 63.31, 57.64, 21.28.

Radical Initiated Polymerisation of 1-benzyl-1-(4-vinylbenzyl)pyrrolidin-1-ium bromide with styrene (IP-2.5)

An oven-dried Schlenk flask was charged with **2.8** (1.5 g, 4.2 mmol), azobisisobutyronitrile (0.1g, 0.6 mmol), and styrene (0.96 mL, 8.4 mmol) before the mixture was diluted with dry methanol (20 mL). The resulting reaction mixture was degassed using the freeze/thaw method with liquid nitrogen (after 3 cycles no more escaping gas was observed). Upon warming to room temperature the reaction mixture was heated to 75 °C and allowed to stir for 48 h, after which time the mixture was added drop-wise to rapidly stirred diethyl ether (*ca.* 100 mL) to induce precipitation of the product. The resulting white solid was isolated by filtration, washed with hexane and diethyl ether and dried under high vacuum to give IP-**2.5** as a white powder (2.6 g). Anal. Calc for C₃₆H₄₀NBr: C, 76.31; H, 7.12; N, 2.47. Found: C, 77.01; H, 7.14; N, 2.36.

Synthesis of Polymer Supported peroxophosphotungstates

A hydrogen peroxide solution (35% w/w, 9.7 mL, 100 mmol) was added to phosphotungstic acid (1.73 g, 0.6 mmol) dissolved in a minimum volume of water and stirred at room temperature for 30 min. After this time, a solution of the ionic polymer (1.8 mmol, based on polymer repeat unit) in the minimum volume of ethanol was added, which resulted in the immediate precipitation of an amorphous white solid. The mixture was cooled to 0 °C, filtered through a sintered glass frit and the precipitate washed with water (2 × 10 mL) and diethyl ether (3 × 75 mL) and dried under vacuum to afford the desired supported peroxophosphotungstate catalyst. FT-IR (KBr plates): $\tilde{\nu}$ = 1086, 1058, 1028 (P-O), 957 (W=O), 837 (O-O), 585, 535 $W(O_2)_{\text{asym,sym}}$.

General Procedure for Catalytic Epoxidations

A Schlenk flask was charged with substrate (1.0 mmol), catalyst (2 mol% based on W) and acetonitrile (3 mL) and the resulting mixture was heated to 50 °C with rapid stirring. The reaction was initiated by the addition of hydrogen peroxide (35% solution, 0.18 mL, 2.0 mmol) and allowed to stir for the allocated time. Upon cooling to room temperature decane (0.195 mL, 1.0 mmol) was added as an internal standard and the resulting mixture was diluted with diethyl ether (25 mL) and washed with water. The organic layer was separated, dried with $MgSO_4$, concentrated under reduced pressure and analyzed by GC-MS to determine conversion before being purified by column chromatography.

General Procedure for Epoxidation Recycle Experiments

An oven dried Schlenk flask charged with polymer supported catalyst (0.0405 g, 1.5 mol %) and acetonitrile (12 mL) was heated to 60 °C. Cyclooctene (0.40 mL, 3.0 mmol) was added, the reaction initiated by the addition of hydrogen peroxide (35% solution, 0.75 mL, 6.0 mmol) and the resulting mixture left to stir at 60 °C for 3 hours. After this time, decane (0.195 mL, 1.0 mmol) was added as internal standard, the solution centrifuged (10 min, 12000 rpm), decanted and the remaining catalyst washed with water and diethyl ether and dried prior to reuse under the same conditions.

***Trans-2,3-epoxyhexan-1-ol*⁴⁹**

¹H NMR (400 MHz, $CDCl_3$, δ): 3.91 (m, 1H), 3.60 (m, 1H), 2.92 (m, 2H), 1.77 (t, J = 6.2 Hz, 1H), 1.44 (m, 4H), 0.95 (t, J = 7.1 Hz, 3H); ¹³C NMR (100 MHz, $CDCl_3$, δ): 61.6, 58.2, 55.7, 33.5, 19.2, 13.8.

*Cis-2,3-epoxyhexen-1-ol*⁵⁰

¹H NMR (399.78 MHz, CDCl₃, δ): 3.81 (dd, *J* = 12.2, 3.9 Hz, 1H), 3.60 (dd, *J* = 12.2, 7.0 Hz, 1H), 3.20-3.13 (m, 1H), 3.07-3.00 (m 1H), 2.14-2.03 (m 1H), 1.61-1.39 (m 4H), 1.05-0.99 (m, 3H); ¹³C{¹H} (100 MHz, CDCl₃, δ): 61.1, 57.4, 56.8, 30.1, 19.9, 14.2.

*3-Methyl-2,3-epoxybutan-1-ol*⁵¹

¹H NMR (400 MHz, CDCl₃, δ): 3.83 (m, 1H), 3.65 (m, 1H), 2.95 dd, *J* = 6.5, 2.5 Hz, 1H), 1.78 (m, 1H), 1.31 (s, 3H), 1.29 (s, 3H); ¹³C NMR (100 MHz, CDCl₃, δ): 63.8, 61.2, 58.7, 24.5, 18.6.

*2,3-Epoxy-3,7-dimethyl-6-octene-1-ol*⁵²

¹H NMR (300 MHz, CDCl₃, δ): 5.11 (br t, *J* = 7.1 Hz, 1H), 3.72 (dd, *J* = 12.2, 4.2 Hz, 1H), 3.60, dd, *J* = 12.2, 6.8 Hz, 1H), 2.99 (dd, *J* = 6.6, 4.2 Hz, 1H), 2.04 (m, 2H), 1.70 (s, 3H), 1.63 (s, 3H). 1.31 (s, 3H); ¹³C NMR (100 MHz, CDCl₃, δ): 132.1, 123.2, 63.1, 61.4, 61.0, 33.1, 25.4, 24.2, 17.7, 16.5.

*Trans-3,4-epoxyhexan-1-ol*⁴⁹⁻⁵⁰

¹H NMR (400 MHz, CDCl₃, δ): 3.71 (d, *J* = 6.1 Hz, 2H), 2.79 (ddd, *J* = 7.6, 4.4, 2.2 Hz, 1H), 2.71 (dt, *J* = 5.4, 2.3 Hz, 1H), 2.15 (s, 1H), 1.91-1.80 (m, 1H), 1.66-1.54 (m, 1H), 1.58-1.43 (m, 2H), 0.91 (t, *J* = 7.7 Hz, 3H); ¹³C NMR (100 MHz, CDCl₃, δ): 62.4, 50.0, 56.2, 33.9, 19.7, 14.1.

Cis-cyclooctene epoxide^{26a, 53}

¹H NMR (400 MHz, CDCl₃, δ): 2.88 (m, 2H), 2.12 (m, 2H), 1.65-1.42 (m, 8H), 1.22 (m, 2H); ¹³C{¹H} (100 MHz, CDCl₃, δ): 55.6, 26.5, 26.2, 25.7. GC-MS (EI), *m/z* = 126 [M⁺].

*Cyclohexene epoxide*⁵⁴

¹H NMR (400 MHz, CDCl₃, δ): 3.11 (s, 2H), 1.95-1.72 (m, 4H), 1.44-1.12 (m, 4H); ¹³C NMR (100 MHz, CDCl₃, δ): 52.2, 24.7, 19.6.

*2,3-Epoxybicyclo[2.2.1]heptanes*⁵⁴

¹H NMR (400 MHz, CDCl₃, δ): 3.01 (s, 2H), 2.38 (br s, 2H), 1.45-1.40 (m, 2H), 1.30-1.25 (m, 1H), 1.18-1.12 (m, 2H), 0.64 (d, *J* = 9.8 Hz, 1H); ¹³C MNR (100 MHz, CDCl₃, δ): 51.2, 36.5, 26.1, 24.9.

*Styrene epoxide*⁵⁵

¹H NMR (400 MHz, CDCl₃, δ): 7.30 (m, 5H), 3.82 (dd, *J* = 4.1, 2.5 Hz, 1H), 3.11 (dd, *J* = 5.4, 4.1 Hz, 1H), 2.77 (dd, *J* = 5.2, 2.5 Hz, 1H); ¹³C{¹H} (100 MHz, CDCl₃, δ): 137.4, 128.2, 128.0, 125.4, 52.2, 51.3.

General Procedure for Catalytic Oxidation of Alcohols

A Schlenk flask was charged with substrate (1.0 mmol), catalyst (2 mol %) and acetonitrile (3 mL) and the resulting mixture was heated to 80 °C with rapid stirring. The reaction was initiated by the addition of hydrogen peroxide (35% solution, 0.58 mL, 6.0 mmol) and allowed to stir for 24 h. Upon cooling to room temperature the reaction mixture was diluted with diethyl ether (25 mL) and washed with water. The organic layer was separated, dried with MgSO₄, filtered, and the solvent removed *in vacuo*. The resulting residue was analyzed by ¹H and ¹³C NMR spectroscopy to determine conversion before being purified by column chromatography.

*2-Decanone*⁵⁶

¹H NMR (400 MHz, CDCl₃, δ): 2.41 (t, 2H, *J* = 7.6 Hz), 2.13 (s, 3H), 1.60-1.53 (m, 2H), 1.25 (bs, 10H), 0.88 (t, 3H, *J* = 7.0 Hz); ¹³C NMR (100 MHz, CDCl₃, δ): 209.3, 43.9, 32.0, 29.8, 29.7, 29.5, 29.5, 29.4, 29.2, 23.9, 22.7, 14.1.

*4-Decanone*⁹

¹H NMR (500 MHz, CDCl₃, δ): 2.40-2.36 (m, 4H), 1.63-1.53 (m, 4H), 0.92-0.86 (m, 6H); ¹³C NMR (100 MHz, CDCl₃, δ): 211.55, 44.78, 42.93, 31.71, 29.03, 23.91, 22.60, 17.39, 14.11, 13.85.

*Acetophenone*⁵⁶

¹H NMR (CDCl₃, 400 MHz, δ): 7.97 (d, *J* = 8.2 Hz, 2H), 7.57 (t, *J* = 7.4 Hz, 1H), 7.48 (t, *J* = 7.6 Hz, 2H), 2.61 (s, 3H). ¹³C NMR (CDCl₃, 100 MHz, δ): 198.0, 136.9, 133.0, 128.4, 128.2, 26.5.

*2,2-Dimethylbutan-2-one*⁵⁷

¹H NMR (200 MHz, CDCl₃, δ): 2.15 (s, 3H), 1.14 (s, 9H); ¹³C NMR (50 MHz, CDCl₃, δ): 214.4, 44.4, 26.5, 24.81.

*Cyclohexanone*⁵⁸

¹H NMR (400 MHz, CDCl₃, δ): 2.36-2.32 (t, 4H), 1.90-1.84 (m, 4H), 1.75-1.70 (m, 2H); ¹³C NMR (400 MHz, CDCl₃, δ): 212.37, 41.97, 27.00, 24.89.

General Procedure for Catalytic Oxidations of Sulfides

An oven-dried schlenk was charged sequentially with sulfide (1 mmol), catalyst (0.013 g, 0.005 mmol) and solvent (3 mL), the reaction was then activated by the addition of 35% H₂O₂ (0.24 mL, 2.5 mmol) and allowed to stir at room temperature for 15 min. The reaction mixture was then diluted with CH₂Cl₂ (25 mL) and washed with water (*c.a.* 50 mL) before the organic extract was dried with MgSO₄ and the solvent removed under reduced pressure. The resulting residue was analysed by ¹H NMR. Relative percentages of starting material and products was determined using integrals in the ¹H NMR spectra.

General Procedure for Kinetic Monitoring of Sulfide Oxidation

An oven-dried Schlenk flask was charged with sulfide (4 mmol) and either MeCN or MeOH (12 mL for 4-nitrothioanisole and 16 mL for dibenzothiophene) and allowed to stir for approximately 5 min to ensure that the solution was homogeneous. The solid catalyst (0.02 mmol based on catalyst repeat unit) was then added, washing the sides of the vessel with the reaction mixture to ensure that no material remained out of the reaction mixture. After the activation of the reaction by the addition of 35% H₂O₂ (0.86 mL, 10 mmol) 0.2 mL aliquots were taken via syringe at the designated times and added to sample vials containing dichloromethane (5 mL) and distilled water (10 mL). After shaking vigorously the dichloromethane layer was decanted and dried with MgSO₄ before the solvent was removed and the resulting residues were analysed by ¹H NMR in order to determine the relative composition of the aliquot.

*Methyl phenyl sulfoxide*⁴⁰

¹H NMR (400 MHz, CDCl₃, δ): 7.69-7.62 (m, 2H), 7.50-7.41 (m, 2H), 7.36-7.30 (m, 1H), 2.73 (s, 3H); ¹³C NMR (100.5 MHz, CDCl₃, δ): 145.42, 130.95, 128.63, 123.54, 43.93.

*Methyl phenyl sulfone*⁴⁰

¹H NMR (400 MHz, CDCl₃, δ): 7.95-7.87 (m, 2H), 7.71-7.61 (m, 2H), 7.59-7.52 (m, 1H), 3.02 (s, 3H); ¹³C NMR (100.5MHz, CDCl₃, δ): 137.44, 133.21, 128.54, 126.23, 44.88.

*Ethyl phenyl sulfoxide*⁴⁰

¹H NMR (400 MHz, CDCl₃, δ): 7.84-7.49 (m, 2H), 7.48-7.13 (m, 3H), 2.91 (q, 1H, *J* = 6.61 Hz), 2.78-2.69 (q, 1H, *J* = 6.61 Hz), 1.23 (t, 3H, *J* = 6.61 Hz); ¹³C NMR (100.5 MHz, CDCl₃, δ): 145.69, 131.47, 129.85, 125.42, 47.19, 10.39.

*Ethyl phenyl sulfone*⁴⁰

¹H NMR (400 MHz, CDCl₃, δ): 7.99 (m, 2H), 7.59 (m, 3H), 3.09 (q, 2H, *J* = 7.11 Hz), 1.30 (t, 3H, *J* = 7.11 Hz); ¹³C NMR (100.5 MHz, CDCl₃, δ): 138.31, 133.47, 128.92, 127.86, 50.28, 7.34.

*Allyl phenyl sulfoxide*⁴⁰

¹H NMR (400 MHz, CDCl₃, δ): 7.64-7.60 (m, 2H), 7.39-7.36 (m, 2H), 7.31-7.26 (m, 1H), 5.44 (ddt, 1H, *J* = 7.11, 10.22, 17.10 Hz), 5.16 (dq, 1H, *J* = 1.12, 10.22 Hz), 5.01 (dq, 1H, *J* = 1.42, 17.10 Hz), 3.43 (dt, 2H, *J* = 7.11, 1.12 Hz); ¹³C NMR (100.5 MHz, CDCl₃, δ): 142.13, 131.24, 129.06, 125.09, 124.71, 117.93, 60.63.

*Allyl phenyl sulfone*⁴⁰

¹H NMR (400 MHz, CDCl₃, δ): 7.95-7.91 (m, 2H), 7.69-7.62 (m, 2H), 7.37-7.44 (m, 1H), 5.63 (ddt, 1H, *J* = 7.19, 10.31, 17.21 Hz), 5.18 (dq, 1H, *J* = 1.22, 10.31 Hz), 5.02 (dq, 1H, *J* = 1.48, 17.21 Hz), 3.91 (dt, 2H, *J* = 7.19, 1.22 Hz); ¹³C NMR (100 MHz, CDCl₃, δ): 138.27, 133.74, 129.02, 128.88, 124.63, 117.51, 60.67.

*4-Nitro-methylphenyl sulfoxide*⁵⁹

¹H NMR (400 MHz, CDCl₃, δ): 8.39 (d, *J* = 8.0 Hz, 2H), 7.90 (d, *J* = 7.5 Hz, 2H), 2.85 (s, 3H); ¹³C NMR (100 MHz, CDCl₃, δ): 152.4, 150.0, 126.2, 125.8, 43.5.

*4-Nitro-methylphenyl sulfone*⁶⁰

¹H NMR (400 MHz, CDCl₃, δ): 8.43 (d, *J* = 8.8 Hz, 2H), 8.16 (d, *J* = 8.8 Hz, 2H), 3.12 (s, 3H); ¹³C NMR (100 MHz, CDCl₃, δ): 150.9, 145.9, 129.0, 124.6, 44.3.

*Dibenzothiophene sulfoxide*⁴⁰

¹H NMR (400 MHz, CDCl₃, δ): 7.98-7.91 (m, 4H), 7.75-7.71 (m, 2H), 7.59-7.52 (m, 2H); ¹³C NMR (100.5 MHz, CDCl₃, δ): 143.33, 132.67, 129.83, 126.37, 124.16, 123.45.

*Dibenzothiophene sulfone*⁴⁰

¹H NMR (400 MHz, CDCl₃, δ): 7.85-7.77 (m, 4H), 7.66-7.61 (m, 2H), 7.55-7.51 (m, 2H); ¹³C NMR (100.5 MHz, CDCl₃, δ): 137.62, 133.77, 131.53, 130.16, 121.97, 121.54.

*Homoallyl phenyl sulfoxide*⁶¹

¹H NMR (300 MHz, CDCl₃, δ): 7.75-7.55 (m, 5H), 6.04-5.90 (m, 1H), 5.31-5.20 (m, 2H), 2.98-2.83 (m, 2H), 2.73-2.68 (m, 1H), 2.50-2.45 (m, 1H); ¹³C NMR (100 MHz, CDCl₃, δ): 135.4, 130.4, 129.0, 124.1, 117.0, 56.2, 26.3.

*Homoallyl phenyl sulfone*⁶²

¹H NMR (400 MHz, CDCl₃, δ): 7.89-7.87 (m, 2 H), 7.65-7.62 (m, 1H), 7.56-7.53 (m, 2 H), 5.73-5.64 (m, 1 H), 5.04-4.99 (m, 2 H), 3.15-3.11 (m, 2 H); 2.46-2.40 (m, 2H); ¹³C NMR (100 MHz, CDCl₃, δ) 138.9, 133.7, 133.6, 129.2, 128.0, 117.1, 55.3, 26.7

*Benzyl phenyl sulfoxide*⁴⁰

¹H NMR (400 MHz, CDCl₃, δ): 7.55-7.42 (m, 2H), 7.36-7.17 (m, 3H), 7.11-6.63 (m, 5H), 3.98 (s, 2H); ¹³C NMR (100.5 MHz; CDCl₃, δ): 142.59, 130.83, 130.26, 128.87, 128.57, 128.24, 128.15, 124.21, 63.44.

*Benzyl phenyl sulfone*⁴⁰

¹H NMR (400 MHz, CDCl₃, δ): 7.74-7.65 (m, 2H), 7.41-7.32 (m, 3H), 7.14-7.06 (m, 5H), 4.41 (s, 2H); ¹³C NMR (100.5 MHz; CDCl₃, δ): 137.49, 133.44, 130.53, 128.61, 128.47, 128.39, 128.31, 62.53.

*tert-butyl methyl sulfoxide*⁶³

¹H NMR (300 MHz, CDCl₃, δ): 2.42 (s, 3H), 1.37 (s, 9H); ¹³C NMR (100 MHz; CDCl₃, δ): 57.80, 36.68, 26.60.

*tert-Butyl methyl sulfone*⁶⁴

¹H NMR (300 MHz, CDCl₃, δ): 2.70 (s, 3H), 1.41 (s, 9H); ¹³C NMR (100 MHz; CDCl₃, δ): 50.51, 32.05, 23.25.

2.6. References

1. a) D. Betz, P. Altmann, M. Cokoja, W. A. Herrmann and F. E. Kühn, *Coord. Chem. Rev.*, 2011, **255**, 1518-1540; b) J. Muzart, *Adv. Synth. Catal.*, 2006, **348**, 275-295.
2. a) A. Corma and H. Garcia, *Top. Catal.*, 2008, **48**, 8-31; b) L. Protesescu, M. Tudorache, S. Neatu, M. N. Grecu, E. Kemnitz, P. Filip, V. I. Parvulescu and S. M. Coman, *J. Phys. Chem. C*, 2011, **115**, 1112-1122.
3. a) M. T. Pope and A. Müller, *Angew. Chem. Int. Ed.*, 1991, **30**, 34-48; b) J. T. Rhule, C. L. Hill, D. A. Judd and R. F. Schinazi, *Chem. Rev.*, 1998, **98**, 327-358.
4. a) N. Mizuno, K. Kamata and K. Yamaguchi, *Top. Catal.*, 2010, **53**, 876-893; b) I. V. Kozhevnikov, *Chem. Rev.*, 1998, **98**, 171-198.
5. M. V. Vasylev and R. Neumann, *J. Am. Chem. Soc.*, 2004, **126**, 884-890.
6. a) C. Venturello and R. D'Aloisio, *J. Org. Chem.*, 1988, **53**, 1553-1557; b) C. Venturello, R. D'Aloisio, J. C. J. Bart and M. Ricci, *J. Mol. Catal.*, 1985, **32**, 107-110; c) R. Neumann and A. M. Khenkin, *J. Org. Chem.*, 1994, **59**, 7577-7579; d) L. Salles, C. Aubry, R. Thouvenot, F. Robert, C. Doremieux-Morin, G. Chottard, H. Ledon, Y. Jeannin and J. M. Bregeault, *Inorg. Chem.*, 1994, **33**, 871-878; e) D. C. Duncan, R. C. Chambers, E. Hecht and C. L. Hill, *J. Am. Chem. Soc.*, 1995, **117**, 681-691.
7. a) L. Liu, C. Chen, X. Hu, T. Mohamood, W. Ma, J. Lin and J. Zhao, *New J. Chem.*, 2008, **32**, 283-289; b) L. Gharnati, O. Walter, U. Arnold and M. Döring, *Eur. J. Inorg. Chem.*, 2011, **2011**, 2756-2762.
8. S.-S. Wang, W. Liu, Q.-X. Wan and Y. Liu, *Green Chem.*, 2009, **11**, 1589-1594.
9. Y. M. A. Yamada, C. K. Jin and Y. Uozumi, *Org. Lett.*, 2010, **12**, 4540-4543.
10. X. Lang, Z. Li and C. Xia, *Synth. Commun.*, 2008, **38**, 1610-1616.
11. C. Aubry, G. Chottard, N. Platzler, J. Brégeault, R. Thouvenot, F. Chauveau, C. Huet and H. Ledon, *Inorg. Chem.*, 1991, **30**, 4409-4415.
12. a) P. Schwab, R. H. Grubbs and J. W. Ziller, *J. Am. Chem. Soc.*, 1996, **118**, 100-110; b) R. H. Grubbs, *Angew. Chem. Int. Ed.*, 2006, **45**, 3760-3765; c) T. M. Trnka and R. H. Grubbs, *Acc. Chem. Res.*, 2000, **34**, 18-29; d) F. N. Tebbe, G. W. Parshall and D. W. Ovenall, *J. Am. Chem. Soc.*, 1979, **101**, 5074-5075.
13. a) S. T. Nguyen, L. K. Johnson, R. H. Grubbs and J. W. Ziller, *J. Am. Chem. Soc.*, 1992, **114**, 3974-3975; b) C. W. Bielawski and R. H. Grubbs, *Prog. Polym. Sci.*, 2007, **32**, 1-29.
14. a) B. F. Straub, *Angew. Chem. Int. Ed.*, 2005, **44**, 5974-5978; b) K. Getty, M. U. Delgado-Jaime and P. Kennepohl, *J. Am. Chem. Soc.*, 2007, **129**, 15774-15776.
15. P. E. Romero and W. E. Piers, *J. Am. Chem. Soc.*, 2005, **127**, 5032-5033.

16. a) T. J. Clark, N. J. Robertson, H. A. Kostalik, T. J. Clark, P. F. Mutolo, H. D. Abruña and G. W. Coates, *J. Am. Chem. Soc.*, 2009, **131**, 12888-12889; b) N. J. Robertson, H. A. Kostalik, T. J. Clark, P. F. Mutolo, H. D. Abruña and G. W. Coates, *J. Am. Chem. Soc.*, 2010, **132**, 3400-3404.
17. I. Biondi, G. Lauenczy and P. J. Dyson, *Inorg. Chem.*, 2011, **50**, 8038-8045.
18. W. L. Dilling, R. D. Kroening and J. C. Little, *J. Am. Chem. Soc.*, 1970, **92**, 928-948.
19. A. Borosy, G. Frater, U. Müller and F. Schröder, *Tetrahedron*, 2009, **65**, 10495-10505.
20. R. L. Pederson, I. M. Fellows, T. A. Ung, H. Ishihara and S. P. Hajela, *Adv. Synth. Catal.*, 2002, **344**, 728-735.
21. a) C. Larroche, J. P. Laval, A. Lattes and J. M. Basset, *J. Org. Chem.*, 1984, **49**, 1886-1890; b) N. Seehof, S. Grutke and W. Risse, *Macromolecules*, 1993, **26**, 695-700; c) J. P. Mathew, A. Reinmuth, J. Melia, N. Swords and W. Risse, *Macromolecules*, 1996, **29**, 2755-2763; d) P. S. Wolfe and K. B. Wagener, *Macromolecules*, 1999, **32**, 7961-7967; e) J. D. Rule and J. S. Moore, *Macromolecules*, 2002, **35**, 7878-7882; f) Y. S. Vygodskii, A. S. Shaplov, E. I. Lozinskaya, O. A. Filippov, E. S. Shubina, R. Bandari and M. R. Buchmeiser, *Macromolecules*, 2006, **39**, 7821-7830; g) S. Sutthasupa, M. Shiotsuki and F. Sanda, *Polym J*, 2010, **42**, 905-915.
22. a) E. L. Dias, S. T. Nguyen and R. H. Grubbs, *J. Am. Chem. Soc.*, 1997, **119**, 3887-3897; b) M. S. Sanford, J. A. Love and R. H. Grubbs, *J. Am. Chem. Soc.*, 2001, **123**, 6543-6554.
23. J. G. Hamilton, K. J. Ivin and J. J. Rooney, *J. Mol. Catal.*, 1986, **36**, 115-125.
24. M. V. Vasylyev and R. Neumann, *J. Am. Chem. Soc.*, 2003, **126**, 884-890.
25. K. Yamaguchi, C. Yoshida, S. Uchida and N. Mizuno, *J. Am. Chem. Soc.*, 2005, **127**, 530-531.
26. a) L. Plault, A. Hauseler, S. Nlate, D. Astruc, J. Ruiz, S. Gatard and R. Neumann, *Angew. Chem. Int. Ed.*, 2004, **43**, 2924-2928; b) S. Nlate, L. Plault and D. Astruc, *Chem. Eur. J.*, 2006, **12**, 903-914.
27. H. Li, Z. Hou, Y. Qiao, B. Feng, Y. Hu, X. Wang and X. Zhao, *Catal. Commun.*, 2010, **11**, 470-475.
28. A. J. Stapleton, M. E. Sloan, N. J. Napper and R. C. Burns, *Dalt. Trans.*, 2009, 9603-9615.
29. X. Lang, Z. Li and C. Xia, *Synth. Commun.*, 2008, **38**.
30. a) M. C. Carreno, *Chem. Rev.*, 1995, **95**, 1717-1760; b) I. Fernández and N. Khiar, *Chem. Rev.*, 2003, **103**, 3651-3706; c) S. Caron, R. W. Dugger, S. G. Ruggeri, J. A. Ragan and D. H. B. Ripin, *Chem. Rev.*, 2006, **106**, 2943-2989; d) R. Bentley, *Chem. Soc. Rev.*, 2005, **34**, 609-624.
31. a) W.-Y. Qi, T.-S. Zhu and M.-H. Xu, *Org. Lett.*, 2011, **13**, 3410-3413; b) S.-S. Jin, H. Wang and M.-H. Xu, *Chem. Comm.*, 2011, **47**, 7230-7232; c) J. Chen, J. Chen, F. Lang, X. Zhang, L. Cun, J. Zhu, J. Deng and J. Liao, *J. Am. Chem. Soc.*, 2010, **132**, 4552-4553; d) Q.-A. Chen, X. Dong,

- M.-W. Chen, D.-S. Wang, Y.-G. Zhou and Y.-X. Li, *Org. Lett.*, 2010, **12**, 1928-1931; e) F. Lang, D. Li, J. Chen, J. Chen, L. Li, L. Cun, J. Zhu, J. Deng and J. Liao, *Adv. Synth. Catal.*, 2010, **352**, 843-846; f) L. Du, P. Cao, J. Xing, Y. Lou, L. Jiang, L. Li and J. Liao, *Angew. Chem. Int. Ed.*, 2013, **52**, 4207-4211.
32. a) H. Li, L. He, J. Lu, W. Zhu, X. Jiang, Y. Wang and Y. Yan, *Energy Fuels*, 2009, **23**, 1354-1357; b) W. Zhu, H. Li, X. Jiang, Y. Yan, J. Lu, L. He and J. Xia, *Green Chem.*, 2008, **10**, 641-646; c) D. Huang, Y. J. Wang, L. M. Yang and G. S. Luo, *Ind. Eng. Chem. Res.*, 2006, **45**, 1880-1885; d) H. Li, X. Jiang, W. Zhu, J. Lu, H. Shu and Y. Yan, *Ind. Eng. Chem. Res.*, 2009, **48**, 9034-9039; e) W. Huang, W. Zhu, H. Li, H. Shi, G. Zhu, H. Liu and G. Chen, *Ind. Eng. Chem. Res.*, 2010, **49**, 8998-9003; f) Y. Ding, W. Zhu, H. Li, W. Jiang, M. Zhang, Y. Duan and Y. Chang, *Green Chem.*, 2011, **13**, 1210-1216; g) W. Zhu, Y. Ding, H. Li, J. Qin, Y. Chao, J. Xiong, Y. Xu and H. Liu, *RSC Adv.*, 2013, **3**, 3893-3898; h) E. Lissner, W. F. de Souza, B. Ferrera and J. Dupont, *ChemSusChem*, 2009, **2**, 962-964.
33. X. Shi, X. Han, W. Ma, J. Wei, J. Li, Q. Zhang and Z. Chen, *J. Mol. Catal. A: Chem.*, 2011, **341**, 57-62.
34. F. Rajabi, S. Naserian, A. Primo and R. Luque, *Adv. Synth. Catal.*, 2011, **353**, 2060-2066.
35. P. Zhao, M. Zhang, Y. Wu and J. Wang, *Ind. Eng. Chem. Res.*, 2012, **51**, 6641-6647.
36. X. Xue, W. Zhao, B. Ma and Y. Ding, *Catal. Comm.*, 2012, **29**, 73-76.
37. B. Karimi and M. Khorasani, *ACS Catal.*, 2013, **3**, 1657-1664.
38. A. Pourjavadi, S. H. Hosseini, F. Matloubi Moghaddam, B. Koushki Foroushani and C. Bennett, *Green Chem.*, 2013, **15**, 2913-2919.
39. a) S. P. Das, J. J. Boruah, H. Chetry and N. S. Islam, *Tetrahedron Lett.*, 2012, **53**, 1163-1168; b) F. Gregori, I. Nobili, F. Bigi, R. Maggi, G. Predieri and G. Sartori, *J. Mol. Catal. A*, 2008, **286**, 124-127; c) E. Baciocchi, M. F. Gerini and A. Lapi, *J. Org. Chem.*, 2004, **69**, 3586-3589; d) B. M. Choudary, B. Bharathi, C. V. Reddy and M. L. Kantam, *J. Chem. Soc., Perkin Trans.*, 2002, 2069-2074.
40. J. J. Boruah, S. P. Das, S. R. Ankireddy, S. R. Gogoi and N. S. Islam, *Green Chem.*, 2013, **15**, 2944-2959.
41. S. P. Das, J. J. Boruah, N. Sharma and N. S. Islam, *J. Mol. Catal. A: Chem.*, 2012, **356**, 36-45.
42. X. Shi, X. Han, W. Ma, J. Wei, J. Li and Q. Zhang, *J. Mol. Catal. A*, 2011, **341**, 57-62.
43. G. P. Romanelli, P. I. Villabrilie, C. V. Cáceres, P. G. Vázquez and P. Tundo, *Catal. Comm.*, 2011, **12**, 726-730.
44. a) R. D. Chakravarthy, V. Ramkumar and D. K. Chand, *Green Chem.*, 2014, **16**, 2190-2196; b) K. Kamata, T. Hirano and N. Mizuno, *Chem. Comm.*, 2009, 3958-3960.
45. R. Walker, R. M. Conrad and R. H. Grubbs, *Macromolecules*, 2009, **42**, 599-605.

46. Y. Matsuoka, Y. Ishida, D. Sasaki and K. Saigo, *Tetrahedron*, 2006, **62**, 8199-8206.
47. J. Ranke, A. Othman, P. Fan and A. Müller, *Int. J. Mol. Sci.*, 2009, **10**, 1271-1289.
48. C. Da, Z. Han, M. Ni, F. Yang, D. Liu, Y. Zhou and R. Wang, *Tetrahedron: Asymm.*, 2003, **14**, 659-665.
49. H. Adolfsson, C. Copéret, J. P. Chiang and A. K. Yudin, *J. Org. Chem.*, 2010, **65**, 8651-8658.
50. K. Kamata, K. Yonehara, Y. Sumida, K. Yamaguchi, S. Hikichi and N. Mizuno, *Science*, 2003, **300**, 964-966.
51. X. Li and B. Borhan, *J. Am. Chem. Soc.*, 2008, **130**, 16126-16127.
52. J. M. Schomaker, V. R. Pulgam and B. Borhan, *J. Am. Chem. Soc.*, 2004, **126**, 13600.
53. A. Murphy, A. Pace and T. D. P. Stack, *Org. Lett.*, 2004, **6**, 3119-3122.
54. B. Kang, M. Kim, J. Lee, Y. Do and S. Chang, *J. Org. Chem.*, 2006, **71**, 6721-6727.
55. a) A. Piccinini, S. A. Kavanagh, P. B. Connon and S. J. Connon, *Org. Lett.*, 2010, **12**, 608-611;
b) K. Huang, H. Wang, V. Stepanenko, M. De Jesús, C. Torruellas, W. Correa and M. Ortiz-Marciales, *J. Org. Chem.*, 2011, **76**, 1883-1886.
56. M. B. T. Thuong, A. Mann and A. Wagner, *Chem. Comm.*, 2012, **48**, 434-436.
57. S. Pääkkönen, J. Pursiainen and M. Lajunen, *Tetrahedron Lett.*, 2010, **51**, 6695-6699.
58. L. Di and Z. Hau, *Adv. Synth. Catal.*, 2011, **353**, 1253-1259.
59. P. Gogoi, M. Kalita, T. Bhattacharjee and P. Barman, *Tetrahedron Lett.*, 2014, **55**, 1028-1030.
60. G. Yuan, J. Zheng, X. Gao, X. Li, L. Huang, H. Chen and H. Jiang, *Chem. Comm.*, 2012, **48**, 7513-7515.
61. J. Skarzewski, E. Wojaczyńska and I. Turowska-Tyrk, *Tetrahedron: Asymm.*, 2002, **13**, 369-375.
62. S. Mannathan and C.-H. Cheng, *Chem. – Eur. J.*, 2012, **18**, 11771-11777.
63. M. H. Ali and S. Stricklin, *Synth. Commun.*, 2006, **36**, 1779-1786.
64. B. J. McNelis, D. D. Sternbach and A. T. MacPhail, *Tetrahedron*, 1994, **50**, 6767-6782.

Chapter 3

PIILP Continuous Flow Oxidation Chemistry

This chapter is based on the publication:

S. Doherty, J. G. Knight, M. A. Carroll, J. R. Ellison, S. J. Hobson, S. Stevens, C. Hardacre and P. Goodrich, "Efficient and Selective Hydrogen Peroxide-Mediated Oxidation of Sulfides in Segmented and Continuous Flow using a Peroxometalate-Based Polymer Immobilised Ionic Liquid Phase Catalyst", *Green Chem.*, 2015, **17**, 1559 – 1571

Table of Contents:

3.1.	Abstract	99
3.2.	Introduction	99
3.3.	Results and Discussion	101
	3.3.1. <i>Batch Optimisation</i>	101
	3.3.2. <i>Segmented Flow Experiments</i>	105
	3.3.3. <i>Continuous Flow, Scale Up and Sequential Reactions</i>	114
3.4.	Conclusions	119
3.5.	Experimental	121
3.6.	References	124

3.1. Abstract

The oxidation of aryl alkylsulfides catalysed by the highly efficient, mild oxidation catalyst POM-2.1, prepared in chapter 2, was further investigated in order to fully determine the extent of chemoselectivity possible. Through control of the reaction time, temperature and solvent high selectivity (c.a. >80%) for both sulfoxide and sulfone across the full range of substrates tested was achieved. Reduction of the catalyst loading enabled high turnover frequencies (TOF) to be achieved, showing that the active species remains productive through extensive catalytic cycles. Coupling this knowledge with the promising catalyst recycle data obtained in the oxidation of thioanisole, which showed negligible deterioration in conversion and product selectivity upon successive recycles, POM-2.1 was identified as an ideal candidate for developing continuous flow processes. Using a cartridge packed with POM-2.1 and silica an operationally straightforward system was designed which, through segmented flow experiments, gave controllable product selectivity as a function of residence time and solvent choice. High conversions and selectivity for either the sulfoxide (92% in methanol at 96% conversion at a residence time of 4 minutes) or sulfone (96% in acetonitrile at 96% conversion and a residence time of 15 minutes) was achieved for thioanisole; similar activity/selectivity profiles were obtained for the five substrates investigated. The immobilised catalyst also remained active for 8 hours under continuous flow operation for the oxidation of thioanisole, showing little drop in either activity or selectivity over time; this allowed for the processing of 6.5 g of substrate corresponding to a turnover number of c.a. 46,000. Use of a single catalyst cartridge for the consecutive oxidation of multiple substrates gave activity-selectivity profiles that matched closely those obtained with fresh catalyst, further confirming the long term stability of the catalyst under reaction conditions.

3.2. Introduction

As discussed in chapter 2 the efficient, mild and selective oxidation of sulfides to yield either sulfoxide or sulfone is of particular interest due to their diverse applications across the chemical industry, including the production of fine chemicals, bioactive compounds and agrochemicals.¹ To this end traditional oxidants, such as nitric acid or KMnO_4 which suffer from low yields, extremely harsh reaction conditions and poor E-factors² have fallen out of favour. Other oxidants such as *m*-chloroperbenzoic acid,³ NaIO_4 ,⁴ and oxone⁵ also suffer from high cost, the need for a large excess of oxidant to be used and the requirement for complicated handling procedures. Again, as discussed in chapter 2 the use of hydrogen peroxide as an oxidant is highly favourable due to the mild conditions required to achieve reaction and the production of H_2O as the sole by-product, in particular when used in conjunction with polyoxometalate catalysts. The initial extensive evaluation of the supported

peroxometalate $[\text{PO}_4\{\text{WO}(\text{O}_2)_2\}_4]^{3-}$ PIILP catalyst POM-2.1 in chapter 2 showed that these systems were highly active and selective under incredibly mild conditions while also being highly recyclable, making them ideal candidates for the use in scaled up, heterogeneous synthesis. In recent years continuous flow chemistry has been extensively investigated as a means to achieve effective reaction scale up and as an intermediary between bench top chemistry and manufacturing scales. The implementation of flow conditions affords numerous advantages over the obvious use of heterogeneous catalyst, which predominantly arise from the unique reaction environment. Conducting the reaction under microfluidic conditions the narrow channels in which the reaction occurs significantly increase the surface area to volume ratio (illustrated with 1 cm³ volume in figure 3.1). This high ratio greatly assists heat transfer, allowing for more rapid, efficient and uniform heating to occur in the reaction media. When fluids pass through the confined regions in a microfluidic reactor two predominant modes of flow may occur, laminar and turbulent flow. The former system tends to occur at slower velocities and results in the formation of a series of parallel layers.⁶ Under these conditions mixing is radial and diffusion is limited, however, due to the small reactor size radial diffusion is extremely rapid.⁶ This highly ordered system allows for incredibly uniform and efficient mixing of reaction constituents, which in turn can lead to higher degrees of product purity.⁷ The sealed nature of the flow systems under pressure also allows for superheating of solvents, giving access to novel reaction conditions which could drastically improve traditional synthesis.⁸ To this end continuous flow systems have been successfully employed across a range of different chemistry both with and without catalysis, delivering products of high purity under reproducible conditions.⁷

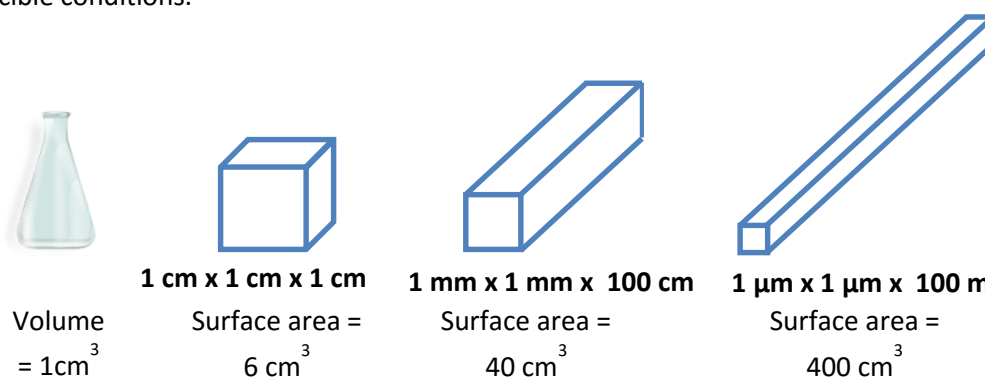


Figure 3.1 Representation of the increasing surface area to volume ratio present in microfluidic systems

As discussed in chapter 1, ILs have been successfully employed to immobilise catalysts in continuous flow reactors across the full spectrum of chemistry, either as co-solvents in biphasic systems or in the form of SILP and PIILP type systems. While dramatically improving the green credentials of these transformations problems often remain with regards to catalyst leaching and lower catalyst activities. To this end the highly efficient, well-defined PIILP catalysts prepared in

chapter 2 are ideal candidates for implementation under continuous flow conditions; our exploratory studies in this area are presented herein.

3.3. Results and Discussion

3.3.1. Batch Optimisation

Out of the 8 catalysts prepared in chapter 2 the pyrrolidinium-functionalised ROMP-based system POM-2.1 was the most extensively investigated and demonstrated promising recycle properties in the epoxidation of cis-cyclooctene and the oxidation of thioanisole, with almost negligible tungsten leeching and very little reduction in reactivity across successive cycles. Initial studies concerning sulfoxidation reactions with this catalyst showed strong aspects of product selectivity as a function of solvent choice, allowing for high yields of either the sulfoxide or sulfone to be obtained under mild conditions and in short times. Though MeCN was shown to an effective solvent for the sulfoxidation of various aryl alkyl sulfides in chapter 2, it's use is considered to be less than environmentally benign, with simple alcohols such as MeOH and EtOH exhibiting much greater green credentials.⁹ In order to further optimise this catalytic system with regard to tuneable product selectivity and the overall green credentials of the reaction a full solvent screen was conducted for the oxidation of thioanisole under optimum conditions established in the previous chapter (table 3.1). As discussed previously, the use of protic solvents heavily favours the formation of the sulfoxide through hydrogen bond

Table 3.1 Oxidation of thioanisole catalysed by POM-2.1 conducted in varying solvents^a

entry	solvent	% Conv. ^b	% sulfoxide ^b	% sulfone ^b	Sulfoxide selectivity ^{b,c}
1	MeCN	88	74	14	84
2	MeOH	95	91	4	96
3	EtOH	85	71	14	84
4	i-PrOH	52	52	0	100
5	EG ^d	21	21	0	100
6	PC ^e	75	56	16	78

^aReaction conditions: 0.5 mol% catalyst, 1 mmol substrate, 2.5 mmol 35% H₂O₂, 3 mL solvent, room temperature, 15 min. ^bDetermined by ¹H NMR. ^cSulfoxide selectivity = [%sulfoxide / (%sulfoxide + %sulfone)] x 100%. ^dEG = ethylene glycol. ^ePC = propylene carbonate.

interactions which slow the second oxidation to the sulfone.¹⁰ This effect was observed across the three alcohols tested, however, the increase in aliphatic character seen between MeOH, EtOH and i-PrOH clearly has a deleterious effect on catalyst performance (entries 2-4). Interestingly, ethylene glycol gave incredibly poor conversion (entry 5), which may due to catalyst clumping, in much the same manner as described for the oxidation of alcohols outlined in chapter 2, which would render active sites of the catalyst inaccessible. Propylene carbonate was selected as an environmentally benign alternative solvent due to its highly polar aprotic nature and green credentials arising from its

synthesis from epoxides and captured CO₂.¹¹ The synthesis of propylene carbonate from CO₂ gives the solvent an added desirable aspect for the scaling up of reactions under flow conditions with regard to a sustainable chemical feedstock, while also potentially providing a viable means of capturing CO₂ and reducing greenhouse gas emissions.¹² Gratifyingly POM-2.1 performed well in all solvents except ethylene glycol, however, MeCN and MeOH were identified as the optimum solvents for this study. As such these two solvents were more thoroughly investigated, however, future work conducted with PIIIP catalysts for use in continuous flow applications will focus on modification of the polymer support in order to increase catalyst performance in alternative solvents, such as propylene carbonate, further increasing the overall green credentials of these mild heterogeneous oxidation systems.

Following the promising results reported in chapter 2 for the oxidation of various sulfides to yield high sulfoxide selectivity, more forcing reaction conditions were employed to also demonstrate that it is possible to achieve high selectivity for sulfone, as these are also incredibly versatile and useful compounds. As part of the preliminary study conducted in chapter 2 using thioanisole as a benchmark substrate (table 2.4), 5 equivalents of H₂O₂ were observed to significantly increase reaction selectivity towards the sulfone product (entry 5). As such these conditions were selected to monitor the conversion-selectivity profile of the oxidation as a function of time and temperature in both MeCN and MeOH (figure 3.2). Unsurprisingly sulfone selectivity was observed to increase with

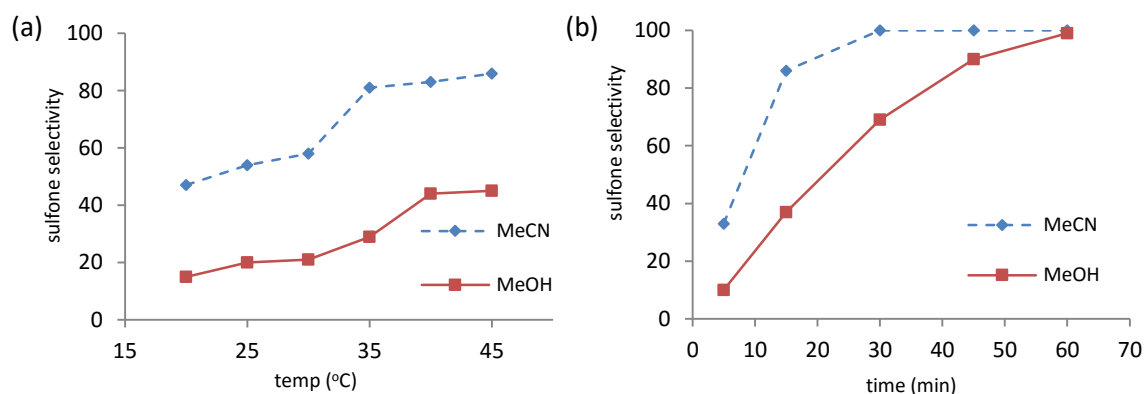


Figure 3.2 Influence of reaction conditions on the selectivity for methyl phenyl sulfone in the hydrogen peroxide-mediated oxidation of thioanisole catalysed by 0.5 mol% POM-2.1. Influence of (a) temperature at a reaction time of 15 min (b) reaction time at 45 °C. Reaction conditions: 1 mmol thioanisole, 5 mmol 35% H₂O₂, 3 mL solvent.

an increase in reaction temperature, reaching a maximum value at a temperature 45 °C in both MeCN and MeOH. The data shown in figure 3.2 (a) also highlight the solvent dependent chemoselectivity, with the protic nature of MeOH significantly slowing the second oxidation to give a maximum sulfone selectivity of just 39%, compared to the 86% in MeCN under the same conditions. Taking 45 °C as an optimum temperature for sulfone selectivity the influence of reaction time was investigated. Again

the disparate difference in the rate of the second oxidation in both solvents is clearly evident, with the reaction reaching completion in just 30 minutes in MeCN as opposed to 60 minutes in MeOH. Gratifyingly, while MeOH proved to be the poorer of the two solvents investigated, similarly high sulfone selectivity was achieved for the oxidation of thioanisole in MeOH catalysed by the IL functionalised $[C_4mim]_3[PMo_{12}O_{40}]$ under comparable conditions.¹³ This similar performance further highlights the highly efficient nature of the heterogeneous POM-**2.1** catalyst. The preference for these systems to form sulfone in MeCN has been previously observed, both in chapter 2 and with similar polymer-immobilised peroxotungstate anions reported in the literature.¹⁴ To further illustrate the high efficiency of POM-**2.1** the catalyst loading was reduced to just 0.025 mol% under optimum conditions of 45 °C in MeCN. Under these conditions a total turnover number of 3960 mole sulfone per catalyst was achieved, however, a prolonged reaction time of 6 hours was required.

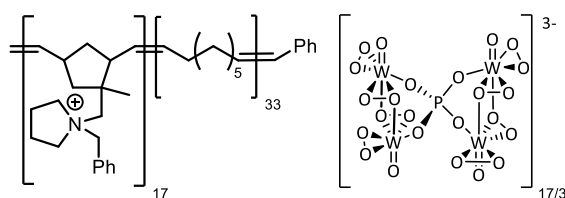
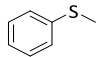
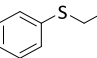
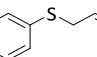
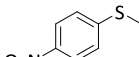
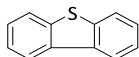
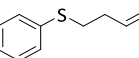
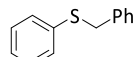


Figure 3.3 PIILP-immobilised peroxometalate catalyst POM-**2.1**

Having identified the optimum reaction conditions with regards to sulfone selectivity as 45 °C and MeCN as the solvent the full scope of sulfides investigated in chapter 2, with the exception of *tert*-butyl methyl sulfide, were tested. A reaction time of 15 minutes was selected in order to effectively highlight the differences in product selectivity between substrates (table 3.2). Under these conditions complete conversion was achieved for all substrates, except dibenzothiophene, with high levels of sulfone selectivity ranging from 77% for 4-nitrothioanisole to 100% with ethyl phenyl sulfide. As with the sulfoxide selective reaction conditions used previously the variation in performance, with regard to selectivity for the desired product, appears to be a direct reflection of the nucleophilicity of the reacting sulfide, which again supports an electrophilic mechanism.¹⁴⁻¹⁵ While POM-**2.1** performed relatively poorly in the oxidation of dibenzothiophene under these optimum conditions, as evidenced by the TOF of just 280 h⁻¹ (entry 5), the results obtained in the previous chapter (table 2.5 entry 10) demonstrated that it is possible to achieve TOFs comparable to the other substrates as well as high sulfone selectivity by increasing the reaction temperature to 65 °C. Though conducted under harsher conditions the TOF of 760 h⁻¹ achieved for the oxidation of dibenzothiophene to the corresponding sulfone at this temperature is a marked improvement over analogous heterogeneous polyoxometalate-based catalysts reported in the literature. For example, a temperature responsive phase transfer system $[(C_{18}H_{37})_2(CH_3)_2N]_7[PW_{11}O_{39}]$ gave a turnover frequency of just 248 h⁻¹ at 60 °C,^{15a} while similar polymer immobilised peroxotungstates gave a TOF of just 9 h⁻¹ at 78 °C.¹⁴ This poorer performance appears to be somewhat more frequent in the literature, with the IL-immobilised

V₂O₅/[C₁₂mim][HSO₄] giving 4 h⁻¹ at a temperature of 45 °C¹⁶ and a commercially available Merrifield resin supported peroxomolybdenum which gave a TOF of 7.2 h⁻¹ at 78 °C.¹⁷ The results obtained in table 3.2 not only illustrate that very high degrees of sulfone selectivity can be achieved alongside the high sulfoxide selectivity discussed in chapter 2, under relatively mild reaction conditions, but also further highlight the incredibly high efficiency of POM-2.1 compared to other reported heterogeneous oxidation catalysts in the literature. It is also important to note that even under these harsher oxidation conditions of increased temperature and H₂O₂ concentration complete chemoselectivity for oxidation of the sulphur is retained, as evidenced by the complete absence of epoxide in the oxidation of allyl and homoallyl phenyl sulfide (entries 3 and 6).

Table 3.2 Selective oxidation of sulfides to sulfones with hydrogen peroxide catalysed by POM-2.1^a

entry	substrate	% Conv. ^b	% sulfoxide ^b	% sulfone ^b	Sulfoxide selectivity ^{b,c}	TOF ^d
1		100	14	86	86	688
2		100	0	100	100	800
3		99 ^e	1 ^e	98 ^e	99 ^e	792
4		100	33	77	77	616
5		68	33	35	51	280
6		100	3	97	97	776
7		100	4	96	96	768

^aReaction conditions: 0.5 mol% POM-2.1, 1 mmol substrate, 5 mmol 35% H₂O₂, 3 mL MeCN, 45 °C, 15 min.

^bDetermined by ¹H NMR. ^cSulfoxide selectivity = [%sulfoxide / (%sulfoxide + %sulfone)]. ^dTOF = moles sulfide consumed per mole catalyst per hour. ^eDetermined by ¹³C NMR.

Encouraged by the high activity and selectivity for both products and the promising recycle data obtained in chapter 2, further studies were conducted to illustrate the positive effect of the IL functionality within the PIILP support of POM-2.1. To this end the homogeneous analogue of POM-2.1, [nBu₄]₃[PO₄{WO(O₂)₂}]₄ (POM-TBA) was absorbed onto silica for comparison as a heterogeneous SILP type catalyst. The recycle study was then repeated for the oxidation of thioanisole in order to obtain a direct comparison between the two catalysts (table 3.3). Although POM-TBA immobilised on silica was initially more efficient in terms of conversion and sulfoxide selectivity a considerable reduction in conversion was observed upon successive recycles, such that the system was completely inactive after the third cycle. ICP-OES analysis of the combined aqueous and organic phases taken after the first run showed that 23% of the tungsten from the catalyst had either been removed or extracted from the silica support. This level of catalyst leaching can be directly linked to the poor performance of POM-TBA/SiO₂ which, when compared to the high recyclability of POM-2.1 highlights

the positive effect of the ionic liquid support. Furthermore, analysis of POM-2.1 by IR after the 6th recycle showed characteristic bands at 1079 cm⁻¹ ν (P-O), 957 cm⁻¹ ν (W=O), 585 cm⁻¹ ν_{asym} (W-O₂) and 531 cm⁻¹ ν_{sym} (W-O₂), reported in the literature,¹⁸ implying that here was no significant change to the peroxometalate anion during the reaction. The IR spectrum also showed no evidence for oxidation of the benzylic group of the IL within the PIILP support to the corresponding benzoyl pyrrolidinium cation, indicating that no significant changes occurred to the support structure. This observation was further confirmed by a benchmark oxidation of thioanisole in the presence of ethylbenzene, which also showed that benzylic oxidation did not occur under the mild reaction conditions.

Table 3.3 Conversion and sulfoxide selectivity values obtained for subsequent catalyst recycles in the oxidation of thioanisole in MeOH catalysed by POM-2.1 and POM-TBA immobilised on silica^a

Run	POM-2.1		POM-TBA/SiO ₂	
	Conversion ^b	Sulfoxide selectivity ^{b,c}	Conversion ^b	Sulfoxide selectivity ^{b,c}
1	88	92	99	97
2	87	92	44	97
3	88	92	14	96
4	86	91	--	--
5	86	90	--	--
6	84	88	--	--

^aReaction conditions: 0.5 mol% catalyst, 1 mmol substrate, 2.5 mmol 35% H₂O₂, 3 mL solvent, RT, 20 min.

^bDetermined by ¹H NMR. ^cSulfoxide selectivity = [%sulfoxide / (%sulfoxide + %sulfone)].

The additional studies conducted in this chapter confirm that POM-2.1 is a highly active catalyst for the oxidation of sulfides, whilst also demonstrating that high product selectivity for either sulfoxide or sulfone can be achieved under relatively mild reaction conditions, often greatly outperforming similar heterogeneous catalysts reported in the literature. The positive influence of the IL functionality present within the PIILP support is further highlighted by the high recyclability of POM-2.1, with no detectable catalyst leeching or structural/chemical alterations observed to the catalyst under the reaction conditions. These considerations strongly confirm that POM-2.1, and by extension the PIILP methodology, are ideal tools for use in continuous flow processes centred around mild, efficient heterogeneous catalysis and product scale up. To this end a full investigation into the use of POM-2.1 in a bespoke mild continuous flow oxidation system was conducted.

3.3.2. Segmented Flow Experiments

Following the successful implementation of POM-2.1 in mild, recyclable batch sulfoxidation reactions an operationally straightforward flow set-up was designed using a Uniqsis FlowSyn reactor (figure 3.4). Due to the highly active nature of POM-2.1 as illustrated in the batch studies above and in chapter 2 it was decided to minimise the amount of catalyst used. It was also deemed necessary to ensure sufficient surface area in the solid reactor bed as a means to provide an effective reaction

environment. To this end 0.1 g of POM-2.1 was diluted by mixing with 2.0 g of silica before packing in the cartridge reactor. Two separate reagent reservoirs for the sulfide and hydrogen peroxide were utilized, each with an individual pump. Through a selection valve both pumps can switch to a communal solvent reservoir which acts as the mobile phase. Using this set-up mixing of the two reagents was achieved at a T-piece before the mixture passed through the catalyst cartridge mounted in a heating mantle. The reaction stoichiometry was controlled through the concentration of each reagent reservoir rather than altering the amount of solution each pump processes, ensuring that each pump operates under the same flow rate, removing an extra aspect of variability and error within the system. Following reaction, the reagent stream passes through a backpressure regulator before collection and processing using the same work-up conditions as for the batch sulfoxidation reactions.

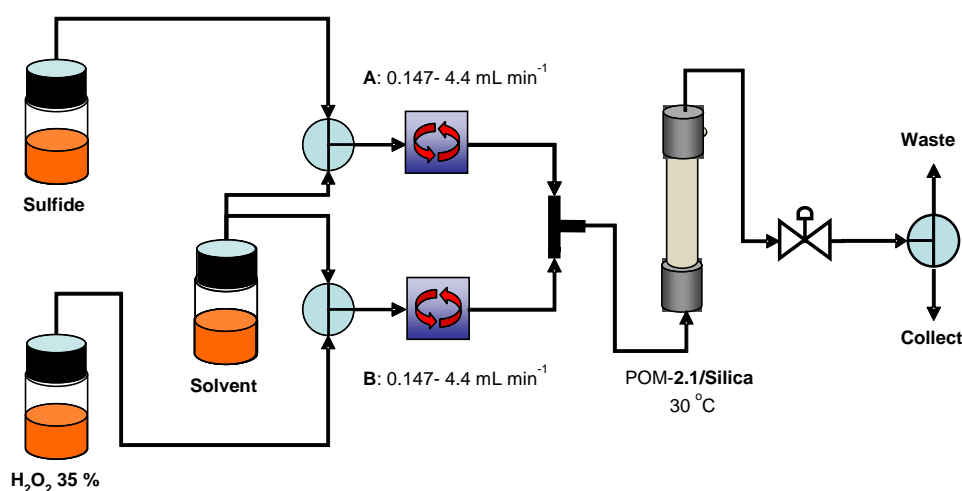


Figure 3.4 Schematic representation of the UniQsis FlowSyn set-up used in the segmented and continuous flow sulfoxidation reactions catalysed by a cartridge of POM-2.1 mixed in silica

One of the limiting drawbacks of continuous flow operation arises when establishing optimum conditions for new/developing chemical reactions. Reaching the steady state, in which variations in flow rate, substrate mixing and heat transfer need no longer be considered, under continuous flow conditions is time consuming. Typically five times the residence time, R_t , the time which reagents remain in contact with the reactor, is required to achieve the steady state and hence remove any variability in experimental throughput.¹⁹ In this regard optimisation is often less than ideal when numerous reaction components such as stoichiometry, residence time and temperature, must be considered. As continuous flow experiments must, by their nature, be conducted sequentially optimisation can become very time consuming while also requiring vast amounts of solvent and reagent. To this end the use of segmented flow conditions in which a specific volume of the effective reaction mixture is passed through the flow system by a transport solvent is often utilized for rapid and efficient reaction screening and optimisation. Conducting investigations in this manner allows a small volume of 'reaction mixture' to be effectively exposed to varying conditions in

a rapid manner while utilizing significantly less reagent. As such the initial optimisation of the newly designed flow system was conducted under segmented flow conditions.

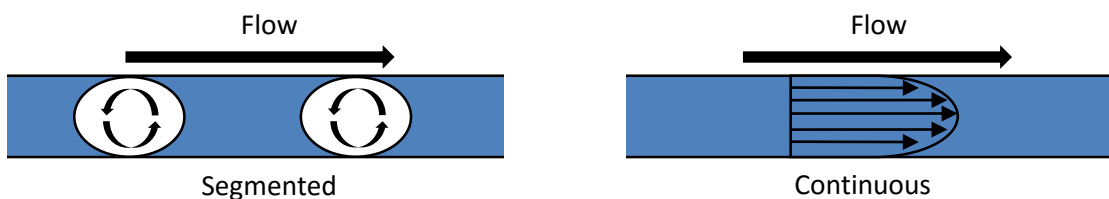


Figure 3.5 Schematic representation of the modes of mixing observed in segmented and continuous laminar flow conditions

From the solvent screening study conducted under batch conditions in table 3.1 MeCN and MeOH were identified as the optimum solvents and as such were also used for all flow investigations, under the rationale that once the ideal operating parameters were identified the polymer properties could then be altered to improve performance in greener solvents. Again thioanisole was selected as a benchmark substrate and using the identified batch conditions as a lead the effect of residence time (R_t), temperature and equivalents of H_2O_2 were investigated. Initially, the effect of temperature was studied using 3 equivalents of H_2O_2 and a flow rate of 1.1 mL min^{-1} ; this corresponded to a residence time of 4 minutes (figure 3.6).

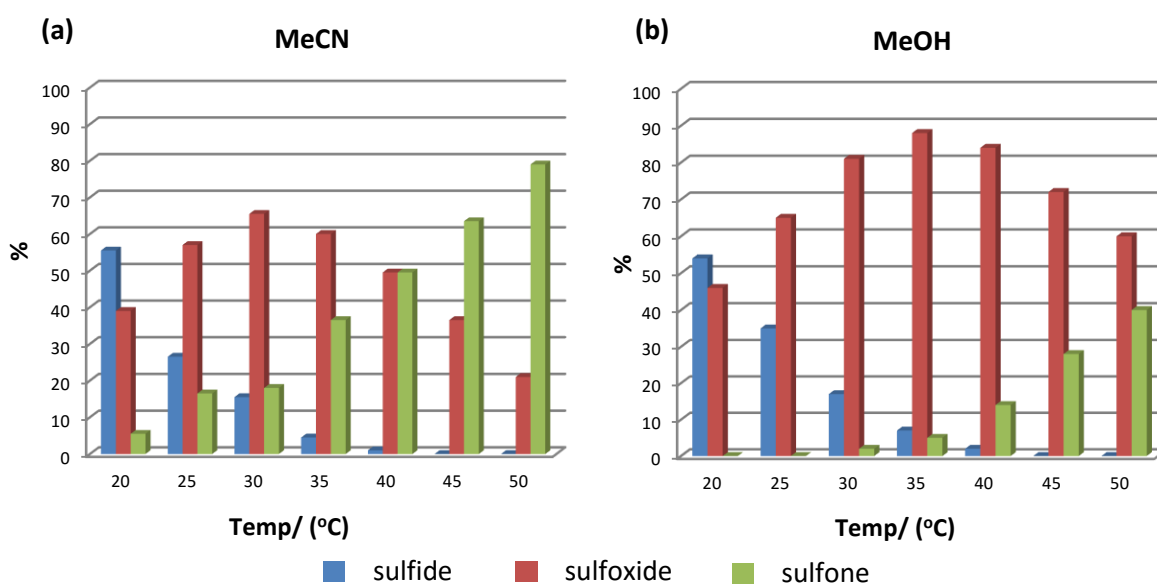


Figure 3.6 Conversion-selectivity profile as a function of reaction temperature in the segmented flow oxidation of thioanisole catalysed by POM-2.1 in MeCN and MeOH solvents

When reactions were conducted in MeCN conversions steadily increased with increasing temperature from 44% at 20 °C up to 100% at temperatures above 45 °C, while a corresponding increase in sulfone selectivity was also observed as expected (figure 3.6 (a)). In contrast, the sulfoxide selectivity obtained in MeOH remained high even at higher temperatures and decreased by only 10%, which is entirely in keeping with this solvents ability to retard the second oxidation to the sulfone. A

comparable increase in conversion to that obtained in MeCN was also observed as a function of temperature when reactions were conducted in MeOH, ranging from just 24% at 20 °C to 88% at 50 °C (figure 3.6 (b)). The lower activity but considerably higher sulfoxide selectivity in MeOH over MeCN is again in keeping with observations made in previous batch studies. From the results obtained in both studies a temperature of 30 °C was identified as the optimum condition that gave the best compromise between conversion and sulfoxide selectivity.

Following identification of an optimum reaction temperature the effect of varying residence time was investigated. As anticipated a gradual increase in conversion was observed with increasing residence time. Using MeCN as the solvent rapid initiation of the reaction was observed to give a conversion of 21% and high sulfoxide selectivity after a residence time of only 0.5 minutes (figure 3.7 (a)). This high selectivity was maintained up to a residence time of 4 minutes, over this time conversions increased up to 90%. However, a subsequent increase in reaction time significantly reduced sulfoxide selectivity, such that the sulfone was obtained as the major product with 96% selectivity at a residence time of 15 minutes. Comparative studies conducted in MeOH showed a similar conversion-selectivity profile. However the optimum balance between conversion and sulfoxide selectivity of 96% and 92%, respectively, was obtained at a residence time of 5 minutes, rather the 4 minutes observed in MeCN in keeping with the slower oxidation in the former solvent (figure 3.7 (b)). The second oxidation is again observed to be much slower in MeOH, as evidenced by the maximum sulfone selectivity of 63% ($R_t = 15$ min) compared to the 96% achieved at the same residence time in MeCN. The data summarised in figure 3.5 clearly shows that a high degree of control over product selectivity is achievable under flow conditions through careful selection of solvent and residence time.

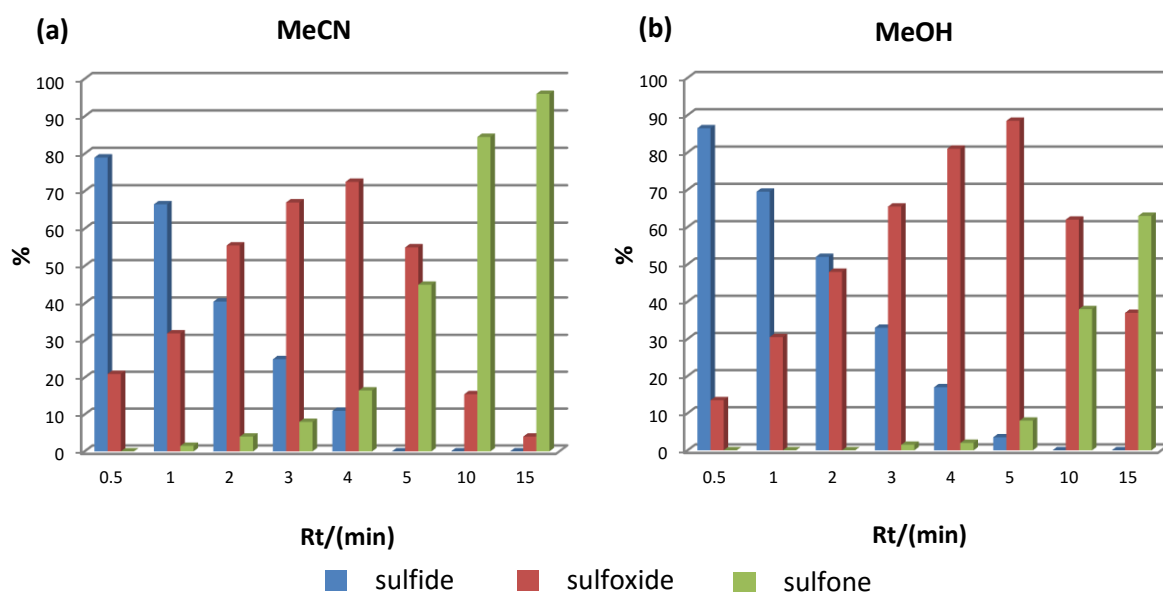
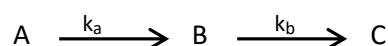


Figure 3.7 Conversion-selectivity profile as a function of residence time (R_t) in the segmented flow oxidation of thioansiole catalysed by POM-2.1 in MeCN and MeOH solvents

A study conducted on the effect of H₂O₂ concentration on conversion and product selectivity as a function of residence time showed markedly different behaviour in each solvent. Concentration was varied from 2 through to 20 equivalents of H₂O₂ for the oxidation of thioanisole with residence times between 0.5 and 15 minutes and in each case both solvents exhibited conversion-selectivity profiles similar to those obtained in figure 3.6 (results shown in Appendix A.1). Interestingly for MeCN a strong dependence of rate on [H₂O₂] was observed up to 12 equivalents of H₂O₂, with a further increase to 20 equivalents having limited effect on rate. In contrast, similar experiments conducted in MeOH showed a much less pronounced dependence of [H₂O₂] on rate corresponding to approximately zero order behaviour. Due to the apparent saturation kinetics observed in MeCN, approximate rate constants for the formation of the sulfoxide (k_a) and the sulfone (k_b) were estimated through fitting the concentration-time profile for the consumption of sulfide and the formation of product through pseudo steady state analysis. Using consecutive elementary reaction kinetics (figure 3.8) the relationships between the rate constants k_a and k_b were used to simulate reaction profiles. Initial estimates for the values of k_a and k_b were obtained by determining approximate half-lives from the experimental sulfoxide and sulfone curves respectively, these values were then used in equations 1-3 to generate the data. The values for k_a and k_b were then adjusted appropriately in order to give the simulated data a good fit with the experimental values (results for 12 eq H₂O₂ shown in figure 3.9). Equations 4 and 5 were used to determine the maximum concentration of sulfoxide and the time at which it occurred as an additional means of confirming the accuracy of the simulated data.



1. $[A]_t = [A]_0 e^{-k_a t}$
2. $[B]_t = \left(\frac{[A]_0 k_a}{k_b - k_a} \right) (e^{-k_a t} - e^{-k_b t})$
3. $[C]_t = [A]_0 \left\{ 1 + \frac{1}{k_a - k_b} (k_b e^{-k_a t} - k_a e^{-k_b t}) \right\}$
4. $[B]_{max} = [A]_0 \left(\frac{k_b}{k_a} \right)^{\frac{k_b}{k_a - k_b}}$
5. $t_{max} = \frac{\ln\left(\frac{k_b}{k_a}\right)}{k_b - k_a}$

Figure 3.8 Equations 1-5 used to estimate rate constants through pseudo steady state analysis for consecutive elementary reactions

As 2.5 equivalents of H₂O₂ are consumed in the complete oxidation to sulfone only the derived rate constants for systems with a large excess of H₂O₂ were calculated, *i.e.* 12 and 20 equivalents in MeCN and MeOH (table 3.4, plots shown in figure 3.9 and Appendix A.2, respectively). The rate constants k_a and k_b were calculated assuming a first order dependence on the sulfide and

sulfoxide respectively. Interestingly they appear to show that the solvent has a much more profound effect on the rate of the first oxidation compared to the second oxidation. It is possible that the observed weaker dependence on $[H_2O_2]$ in MeOH may be a direct result of the solvent's increased hydrogen bonding capability facilitating more effective solvation of the oxidised products and/or the H_2O_2 , thereby reducing interaction with the catalyst surface/active sites. Interestingly, the results in table 3.4 seem to show a reduction in rate constant with increasing H_2O_2 concentration. It is possible that this difference could be the result of experimental error due to the approximation which occurs during the steady state analysis of the reaction.

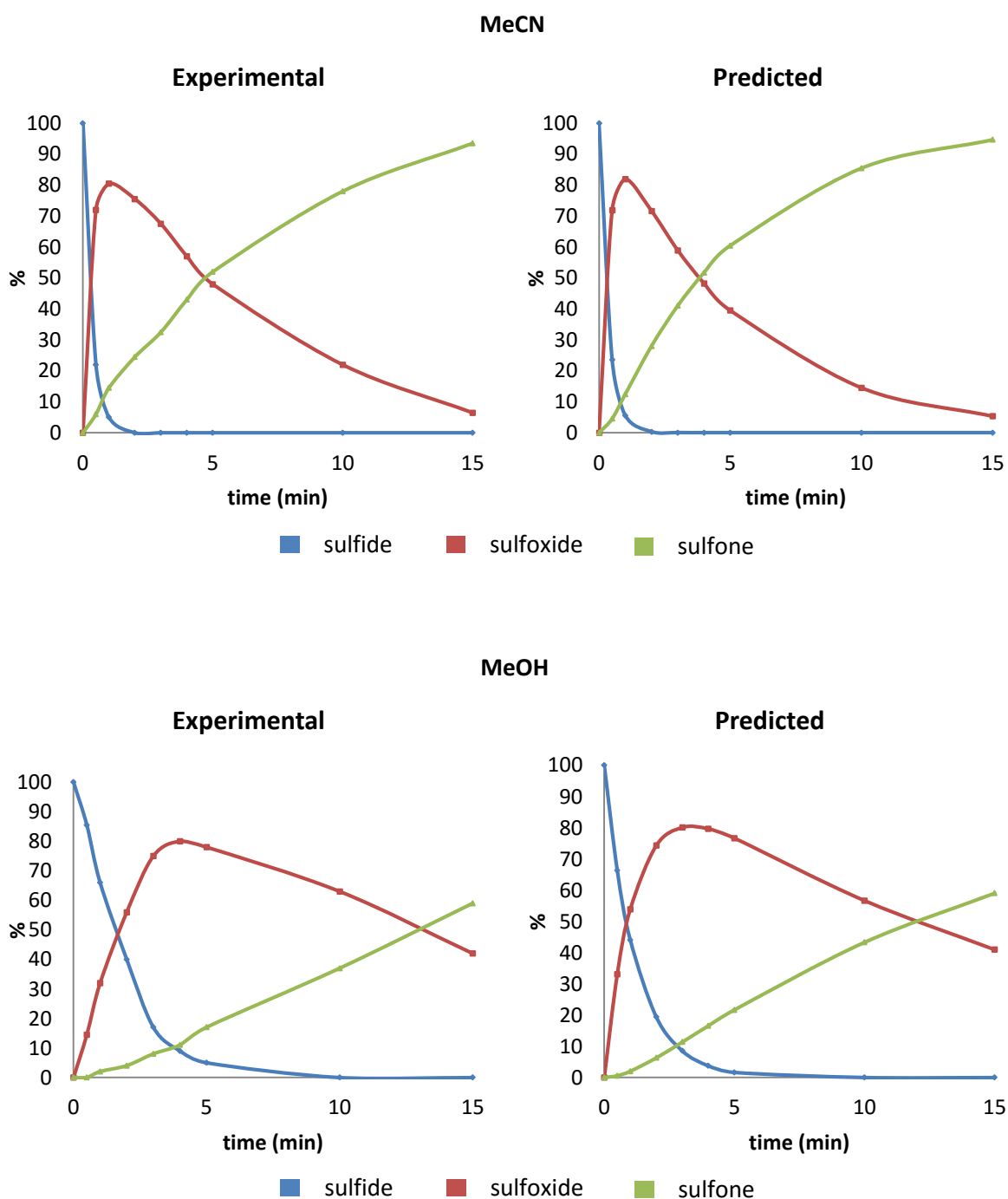


Figure 3.9 Kinetic plots obtained through equations 1-3 for the oxidation of thioanisole with 12 eq H_2O_2 in MeCN and MeOH

Table 3.4 Estimated rate constants for the formation of methyl phenyl sulfoxide (k_a) and methyl phenyl sulfone (k_b) in MeCN and MeOH^a

Entry	Eq. H ₂ O ₂	MeCN		MeOH	
		k_a	k_b	k_a	k_b
1	12	2.89	0.2	0.82	0.07
2	20	2.68	0.17	0.55	0.11

^aData obtained using 0.2 M thioanisole and 2.4 M or 4.0 M solutions of H₂O₂ with flow rates between 0.293 mL min⁻¹ and 8.8 mL min⁻¹ at 30 °C.

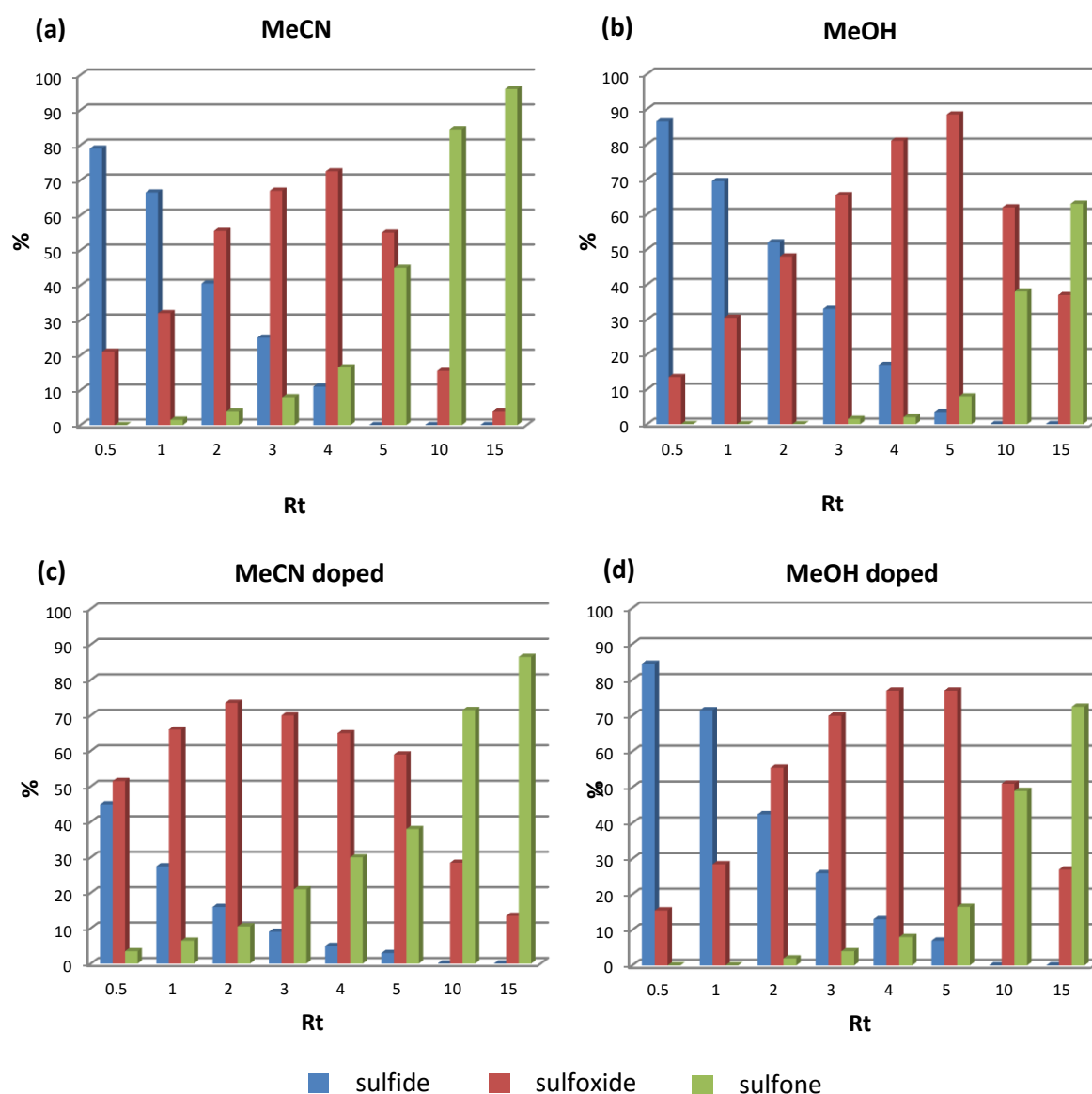


Figure 3.10 Comparison of the conversion-selectivity profiles obtained in the segmented flow oxidation of thioanisole conducted in MeCN and MeOH with and without doping with an extra equivalent of H₂O₂

As the investigated reactions were conducted using a solution prepared from aqueous H_2O_2 , increasing the peroxide concentration will also increase the water content of the reaction. The increased hydrogen bonding capacities of these systems as a result of the increased water content could potentially have an effect on the two oxidation rates. To this end doping experiments were conducted using 3 equivalents H_2O_2 as well as the corresponding system doped with an amount of water representative of the extra amount present with 6 equivalents of H_2O_2 (figure 3.9). Interestingly, doping with additional water caused a notable increase in the rate of the first oxidation when reactions were conducted in MeCN while also causing a slight decrease in the rate of the second oxidation to sulfone. In contrast, when the reactions were conducted in MeOH there was only a minor change in the rate of both oxidations. The enhancement in the rate of the first oxidation in the water-doped MeCN system could possibly be attributed to the formation of a hydrogen bond network which could facilitate access of the substrate to the active peroxometalate within the catalyst surface. These hydrogen bond interactions would also serve to slow the second oxidation in a similar fashion to that observed in MeOH described above. Due to the small impact on the MeOH system caused by the addition of water, and in an attempt to further improve the green credentials of the PIILP flow system the amount of water was further increased. To this end a dual solvent system was designed, consisting of an aqueous H_2O_2 reservoir and methanolic thioanisole. Under analogous conditions to those conducted in MeOH (figure 3.6) a high degree of activity and sulfoxide selectivity was retained with the addition of extra water to the solvent (figure 3.10). Under these conditions optimum performance with regards to a balance between conversion and sulfoxide selectivity was observed

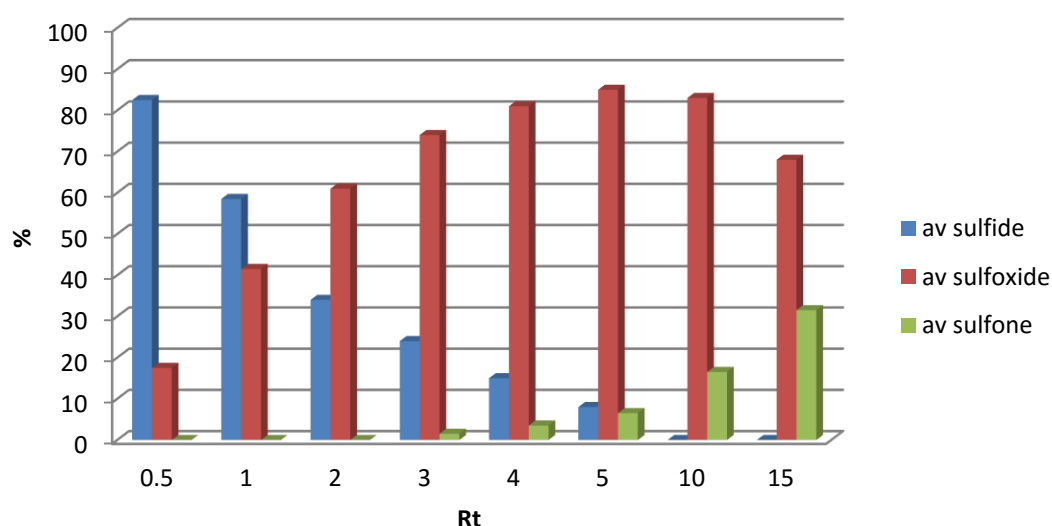
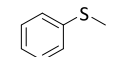
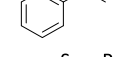
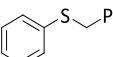
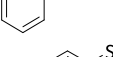
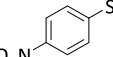
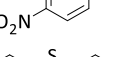
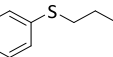
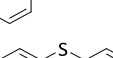
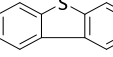
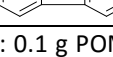


Figure 3.11 Conversion-selectivity profile as a function of residence time for the segmented flow sulfoxidation of thioanisole in MeOH- H_2O (1 : 1, v/v) at 30 °C with 3 equivalents of H_2O_2 catalysed by POM-2.1

at a flow rate of 0.88 mL min^{-1} ($R_t = 5 \text{ min}$), giving 93% and 92% respectively; this performance is a significant improvement on those obtained by varying the H_2O_2 concentration. In comparison, when

the analogous solvent system was transferred to the batch oxidation of thioanisole under the sulfoxide selective conditions a conversion of just 22% was achieved with a catalyst loading of 0.5 mol%, 2.5 equivalents H₂O₂ and a reaction time of 15 minutes. This poor performance was attributed to agglomeration of the catalyst during the reaction which further highlights the significant potential of utilizing PIILP catalysts under flow conditions.

Table 3.5 Summary of the optimum sulfoxide and sulfone selectivity for the segmented flow sulfoxidations of selected aryl sulfides catalysed by POM-2.1^a

entry	substrate	R _t	solvent	% Conv. ^b	Sulfoxide selectivity ^{b,c}	Sulfone selectivity ^{b,d}
1		4	MeOH	83	98	--
2		15	MeCN	100	--	96
3		4	MeOH	93	90	--
4		15	MeCN	100	--	79
5		4	MeOH	61	90	--
6		15	MeCN	100	--	75
7		4	MeOH	80	89	--
8		15	MeCN	100	--	89
9		--	MeOH	--	--	--
10		15	MeCN	76	--	76

^aReaction conditions: 0.1 g POM-2.1/2.0 g silica, 0.2 M aryl sulfide, 0.6 M 35% H₂O₂, residence time 0.5 – 15 min. 30 °C. ^bDetermined by ¹H NMR spectroscopy. ^csulfoxide selectivity = [%sulfoxide/%sulfone + %sulfoxide] x 100%. ^dsulfone selectivity = [%sulfone/%sulfone + %sulfoxide] x 100%.

Following the optimisation process conducted with thioanisole, a reaction temperature of 30 °C and 3 equivalents of H₂O₂ were identified as the optimum balance between high catalyst activity and product selectivity under the mildest conditions possible. As such the substrate scope was extended in order to establish the full extent of the efficiency of this system under these conditions. Conversion-selectivity profiles for residence times between 0.5 and 15 minutes, similar to those shown in figure 3.6, were produced for each substrate in MeCN and MeOH and table 3.5 shows a summary of the optimum product selectivities achieved (the associated conversion-selectivity profiles are shown in appendix A.3). For all substrates, similar selectivity profiles to those shown above for thioanisole were obtained, and, as with thioanisole the selectivity for the sulfoxide was much higher at any given residence time when the reaction was conducted in MeOH compared with MeCN. In the majority of cases the optimum compromise between conversion and sulfoxide selectivity was achieved at a flow rate of 1.1 mL min⁻¹ (R_t = 4 minutes), with the exception of 4-nitrothioanisole which required a slightly longer residence time of 5 minutes. Under the investigated reaction conditions sulfoxide selectivities as high as 90% were obtained across the substrate scope with moderate to high conversion (61-93%). As above sulfone selectivity was generally higher in MeCN with an increase in residence time resulting in an increase in sulfone selectivity, reaching 75-89% at complete conversion. Unfortunately, oxidation of dibenzothiophene under these conditions

proved to be more challenging than other substrates and its limited solubility prevented oxidation under flow conditions in MeOH.

3.3.3. Continuous Flow, Scale Up and Sequential Reactions

Encouraged by the performance of POM-2.1 under mild, segmented flow conditions across a range of aryl sulfides, as well as the promising recyclability data obtained under batch conditions a series of comparative scale-up continuous flow studies were conducted. To this end, the optimum conditions identified under segmented flow of 30 °C and 3 equivalents of H₂O₂ were selected to evaluate the long term stability of POM-2.1 in both MeCN and MeOH, again using thioanisole as a benchmark substrate. For this study, a flow rate of 1.1 mL min⁻¹ (R_t = 4 min), was identified from the data above as the optimum flow rate with regard to the balance between conversion and sulfoxide selectivity. Under these conditions, a 0.2 M solution of thioanisole was continuously processed for 8 hours at this flow rate, with 1 mL samples taken once every hour and analysed by ¹H NMR spectroscopy to evaluate the catalyst performance (figure 3.12). When MeCN was used as the solvent (figure 3.12 (a)) the resulting time-performance profile showed a slight but steady reduction in activity over time, as highlighted by the decrease in conversion of 89% to 79%, accompanied by a decrease in sulfone composition from 29% to just 16% over the 8 hour period. While these results are in keeping with the minor decrease in catalyst performance observed over successive cycles in the batch recycle studies described in chapter 2 and table 3.3, the effect appeared to be much more pronounced under flow conditions. Again, from the recycle studies conducted it was shown that an almost negligible level of tungsten leaching occurred with POM-2.1, as such it was inferred that the deactivation observed under flow conditions could not solely be attributed to loss of the active tungsten species. Evaluation of the set up described in figure 3.3 highlighted that a possible decomposition of the H₂O₂ present in the reagent reservoir could occur over prolonged periods of time as the vessel, whilst protected from sunlight, was standing under ambient conditions, rather than the 2 to 8 °C storage suggested by the supplier. As such the experiment was repeated but the apparatus was stopped after 4 h and the H₂O₂ reservoir replaced with a fresh sample (figure 3.12 (b)). Under this revised procedure the steady minor decline in activity was no longer observed, instead catalyst performance with regard to conversion and sulfoxide selectivity remained relatively consistent within experimental error throughout the 8 hour operating time. Interestingly, when MeOH was used as the solvent, much more profound variations in both the conversion and product selectivity were observed with prolonged continuous usage of POM-2.1 (figure 3.12 (c) and (d)). As with the corresponding MeCN system replenishment of the H₂O₂ reservoir after 4 h reduced this effect, offering additional stability with regard to the absolute change in conversion and selectivity, however, despite this improvement a

profound decrease in performance over time was still observed (figure 3.12 (d)). While the batch recycle studies discussed previously indicated that the IL fragments within the PIILP framework effectively retained the active peroxometalate anion, catalyst leaching would effectively explain the apparent decrease in catalyst performance over time in MeOH. As such ICP-OES analysis was conducted on the hourly aliquots taken in the continuous experiments described by figure 3.12 (b) and (d). Interestingly, despite there being little observable difference in performance over time in

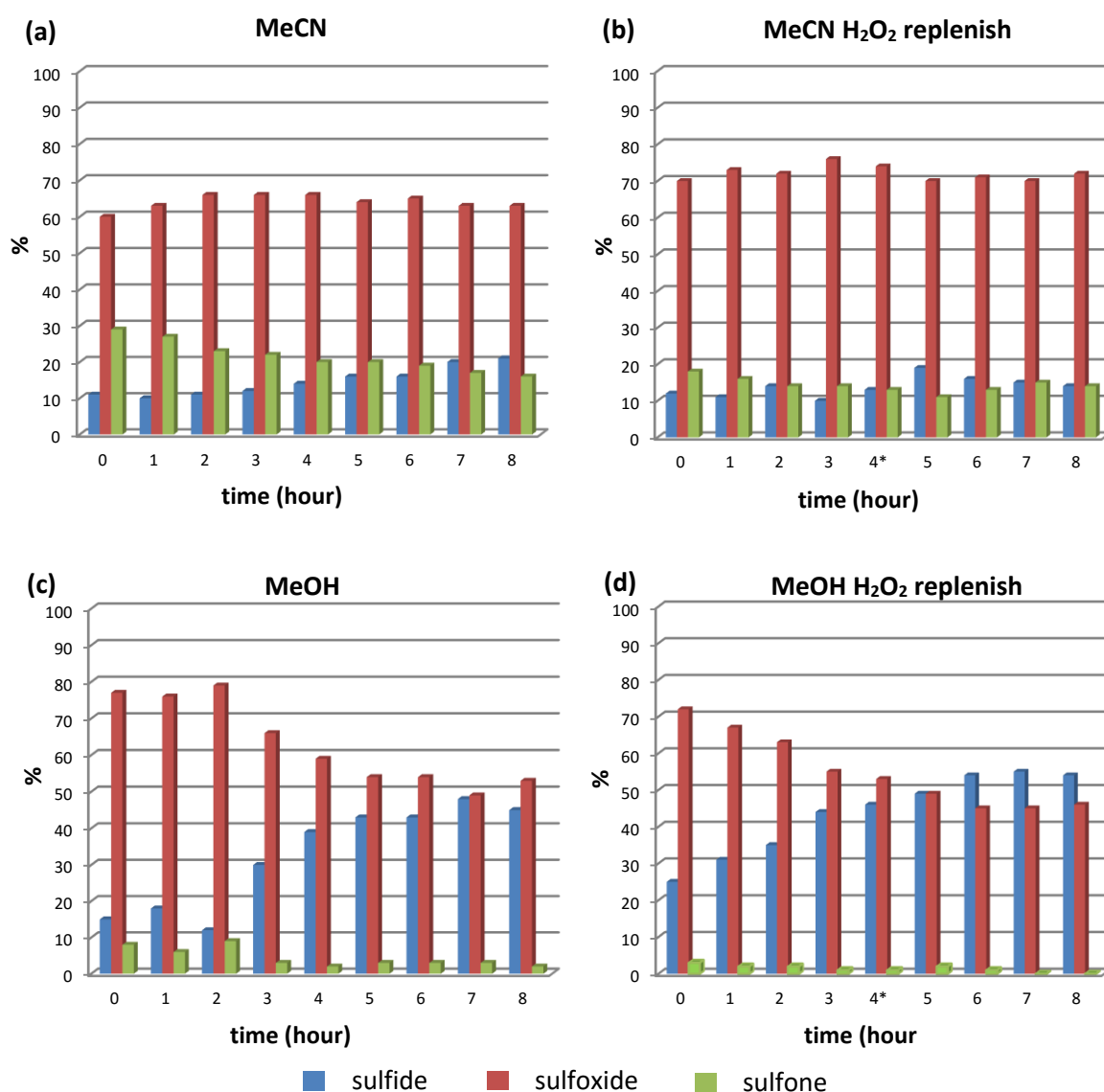


Figure 3.12 Conversion-selectivity profile as a function time for an 8 hour continuous flow sulfoxidation of thioanisole catalysed by POM-2.1 at 30 °C with a residence time of 4 minutes in (a) MeCN, (b) MeCN with replenishment of the H₂O₂ reagent stream after 4 hours (*), (c) MeOH and (d) MeOH with replenishment of the H₂O₂ reagent stream after 4 hours (*)

in performance over time in MeCN, analysis of these aliquots corresponded to a loss of 4.3% of the total tungsten used in the system. Similar analysis for the corresponding MeOH system indicated a total loss of 21% W over the 8 hour period. The significantly higher degree of W leaching observed in MeOH aligns with the prominent decrease in catalyst performance observed in figure 3.12 (c) and (d),

and can be attributed to the hydrogen bonding capability of the solvent, which would result in improved solubility of the charged tungsten species present in the catalyst cartridge. Analysis of POM-2.1 by solid state ^{31}P NMR (see chapter 2) indicated that while the peroxometalate anion $[\text{PO}_4\{\text{WO}(\text{O}_2)_2\}_4]^{3-}$ was the major species, numerous other phosphorous-containing compounds were also present. The H_2O_2 -mediated degradation of phosphotungstic acid has been well-documented to produce numerous different possible tungsten species,²⁰ some of which will not be catalytically active. This could explain the almost negligible change in catalyst performance over time observed when MeCN is used as the solvent despite the leaching of 4.3% of the total W content, with the detected tungsten possibly corresponding to smaller, non-active species formed as by-product during catalyst generation. Taking this consideration into account, it is likely that the decrease in catalyst performance as a function of operation time observed in MeOH is the result of a combination of factors, not just solely leaching of inactive tungsten species. One possible additional factor again arises from the hydrogen bonding capability of MeOH. In this regard the relatively low polarity of the thioanisole starting material will lead to poorer solubility compared to the corresponding sulfoxide and sulfone. This could result in the deposition and gradual build-up of thioanisole over time in the catalyst/silica surface, which could in turn progressively block active catalyst sites within the material. Again this potentially complex relationship highlights a major limitation of POM-2.1 when used with polar protic solvents over prolonged reaction time. One possible solution to this issue would be modification of the polymer morphology and ionic microenvironment in order to limit the support-starting material interaction which might allow for the successful use of PIILP catalysts under continuous operation in greener, protic solvents such as EtOH.

A semi-quantitative repeat of the continuous flow experiments under the conditions corresponding to figure 3.12 (b) and (d) showed that a total of 6.5 g of thioanisole could be processed over an 8 hour period (0.81 g h^{-1}) with a conversion of 88% and a sulfoxide selectivity of 78% when the reaction was conducted in MeCN. While the corresponding MeOH system gave a conversion of just 52% a sulfoxide selectivity of 98% was achieved. Fine tuning of the PIILP architecture will again allow for further optimisation of these catalytic systems to achieve more efficient substrate processing. By way of comparison, a recent study reported that a polystyrene supported benzenesulfonic acid Amberlite IR 120 H catalysed the oxidation of sulfides under continuous flow conditions and gave high sulfoxide selectivity at 22 °C with excellent long term catalyst stability, albeit with a catalyst to substrate ratio of 0.3.²¹ This again highlights the efficiency of POM-2.1 and its high turnover capability under relatively mild conditions.

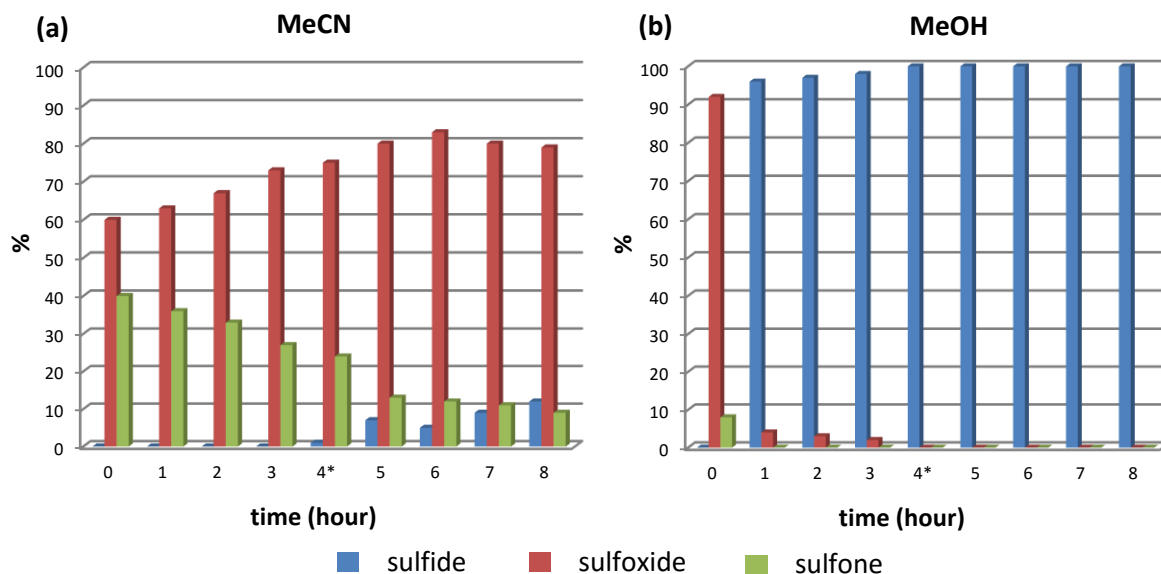


Figure 3.13 Conversion-selectivity profile as a function of time for an 8-hour continuous flow sulfoxidation of thioanisole catalysed by POM-TBA at 30 °C with a residence time of 4 minutes in (a) MeCN and (b) MeOH with replenishment of the H₂O₂ reagent stream after 4 hours (*)

In order to further highlight the positive effect associated with the presence of the ionic microenvironment in the PIILP support of POM-2.1 a comparative set of lifetime studies were conducted using TBA-POM. In this respect an amount of TBA-POM, representative of the total amount of W present in the catalyst cartridge loaded with POM-2.1, was absorbed on silica to give a comparative reactor volume to that described above. Under the same conditions described in figure 3.12 (b) and (d) the POM-TBA based catalyst exhibited considerably higher initial activity than POM-2.1, however, gratifyingly, a dramatic decrease in performance was observed in both solvents (figure 3.13). When MeCN was used as the solvent quantitative conversion of the sulfide was achieved for the first 3 hours, however, a steady decrease in conversion and a corresponding increase in sulfoxide selectivity from 60% to 90% was observed; the end performance was comparable to the corresponding profile observed for POM-2.1 shown in figure 3.7 (a) at a residence time of 4 minutes (figure 3.13 (a)). ICP analysis of aliquots taken corresponded to a tungsten leaching of 7% which was considerably higher than the 4.3% observed for POM-2.1 in MeCN. However, this increase in tungsten leaching does not account for the considerable decrease in performance observed for POM-TBA over the 8-hour period, again highlighting the complex nature of the PIILP support with regard to interactions with the catalyst and substrates. This result would imply that additional stabilisation effects are present when using PIILP supports over time, and as such further studies will be necessary to fully determine the nature of this positive effect. When MeOH was used as the solvent an almost complete drop off in catalyst activity was observed after just one hour of operation. Analysis of the aliquot taken after this hour showed that 21% of the total tungsten had been removed from the

catalyst bed, again partially accounting for the dramatic loss in activity. One possible additional explanation for this pronounced reduction in catalyst activity could be attributed to the long term stability of the active peroxometalate anion. In this regard the initial H₂O₂ formation of the anion from phosphotungstic acid yields a variety of different W-based species. It is therefore plausible that prolonged exposure of the catalytic anion to large quantities of H₂O₂ and MeOH solvent whilst in close proximity to the mildly acidic silica surface could facilitate degradation into different, catalytically inactive polyanions. Again this would imply the positive influence of the PIILP support in POM-**2.1**, which seemingly provides an additional stabilisation effect to the peroxometalate anion as evidenced by the less pronounced drop off in catalyst performance over time in MeOH (figure 3.12 (d)).

Encouraged by the promising long term stability of POM-**2.1** under continuous flow oxidation of thioanisole, a study was conducted to determine if the same PIILP loaded catalyst column could be used consecutively for the oxidation of different substrates. To this end a proof of principle exercise was conducted by processing thioanisole under the optimum segmented flow conditions described above in triplicate at residence times of 5 and 15 minutes. Upon completion of the last experiment the system was purged using the appropriate carrier solvent at a flow rate of 1 mL min⁻¹ for 5 minutes to remove any residual sulphur containing material before switching the reagent reservoir for a different substrate and repeating the process. Reassuringly the conversion-selectivity profiles obtained through this procedure in MeCN were similar to those obtained from the corresponding individual segmented flow experiments conducted on the same substrates (figure 3.14). Gratifyingly, even though the substrate sequence of thioanisole, 4-nitrothioanisole and finally dibenzothiophene

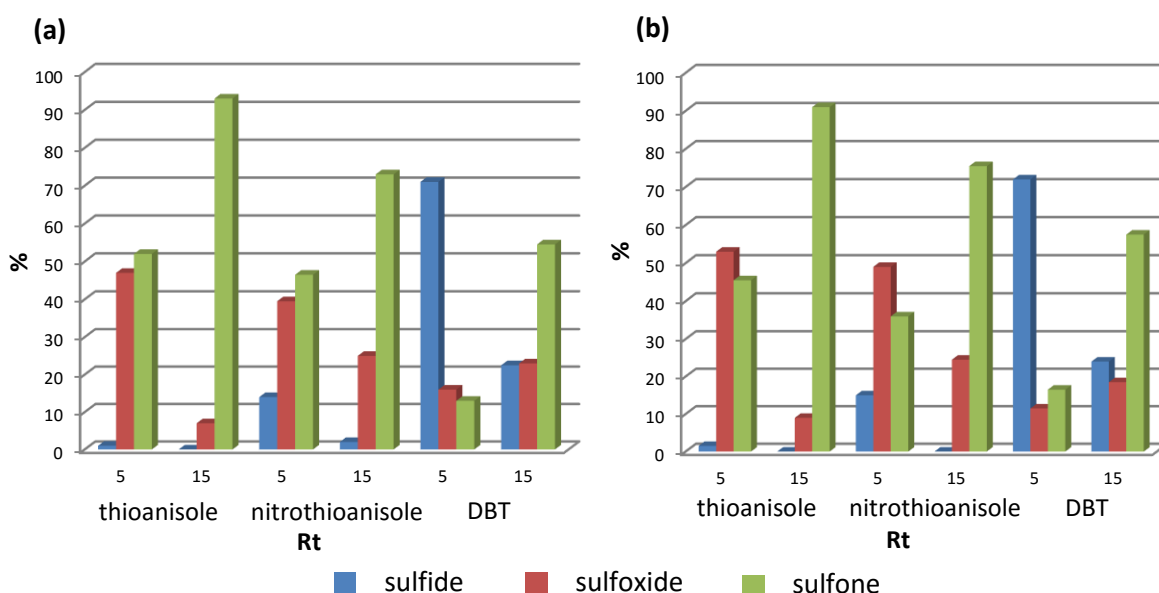


Figure 3.14 (a) Conversion-selectivity profile at residence times of 5 and 15 minutes for segmented flow POM-**2.1** catalysed consecutive sulfoxidation of three different substrates using the same catalyst cartridge. (b) Conversion-selectivity profile at residence times of 5 and 15 minutes for segmented flow POM-**2.1** catalysed consecutive sulfoxidation of three different substrates using fresh catalyst

decreased in relative reactivity, POM-2.1 still achieved the same high activity, further highlighting the stability of the supported catalyst. A similar effect was also observed when the procedure was repeated using MeOH as solvent, although it was again not possible to process dibenzothiophene due to its limited solubility. These results would imply that a fully optimized PIILP catalyst could be a viable fixed-bed catalyst for a general purpose continuous flow system, which could be used for numerous different substrates without the need for any modification to the system.

3.4. Conclusions

The heterogeneous oxidation of various sulfides catalysed by the PIILP-based POM-2.1 under mild conditions was further investigated. While not quite as effective as in MeCN and MeOH, high catalyst performance is achievable in a variety of different alternative solvents, implying that further optimisation of the catalyst material could enable highly efficient, environmentally benign oxidation systems to be developed. Alteration of the batch reaction conditions showed that it is possible to achieve high conversion to the sulfone under relatively mild conditions which further highlighting the efficiency of the immobilised peroxometalate. Extension of the use of the PIILP catalyst to flow systems showed that the highly active behaviour of the catalyst transferred effectively, with observations about catalyst behaviour observed under batch conditions seemingly mirrored in both segmented and continuous flow conditions. In particular, the efficiency and stability of POM-2.1 was demonstrated for the continuous flow oxidation of thioanisole which processed 6.5 g of material, corresponding to a turnover number of 46,428. As under batch conditions, POM-2.1 remains less active than the homogeneous counterpart POM-TBA, however, the long term stability of the former gave a constant performance over time under continuous operation whereas the activity and selectivity of the latter gradually decreased over the same time scale. While this could be due in part to enhanced retention of the active peroxometalate species by the polymer immobilised ionic liquid support, the degrees of tungsten leaching determined by ICP analysis for both the POM-2.1 and POM-TBA systems do not appear to correspond to the significant differences in performance. Again this highlights the complex nature of the relationship between the catalyst, support and reacting substrate, illustrating the necessity for further investigations into the true nature of the catalyst and its surrounding environment. As with the batch studies reported in chapter 2 it will be challenging yet necessary to fully study and understand the nature of this relationship if the PIILP methodology is to be utilized to its full potential. Despite the apparent limitations of POM-2.1 the promising initial results suggest that PIILP materials could be a viable means of generating highly active and stable catalysts for use under mild conditions, as such both the substrate and reaction scope under continuous flow should be extended to fully evaluate the merits of PIILP supports. The processes

described in this chapter are by no means ideal, for example in the continuous flow sulfoxidation an aqueous work up is still required; highlighting that there is significant room for improvement and optimisation. Despite this the performance of POM-2.1 under continuous flow conditions shows that the PIILP methodology could be applied to industrially relevant processes. For example, if chiral functionality were incorporated into the polymer backbone it would be possible to prepare chiral oxidation catalysts which were highly active and selective under mild conditions, allowing for the continuous flow generation of chiral sulfoxides which act as valuable intermediates in the synthesis of pharmaceuticals. As well as this, the setup described in figure 3.4 could be modified as illustrated in Figure 3.15 to develop operationally straightforward and environmentally benign process for the oxidative desulfurization of crude oil.

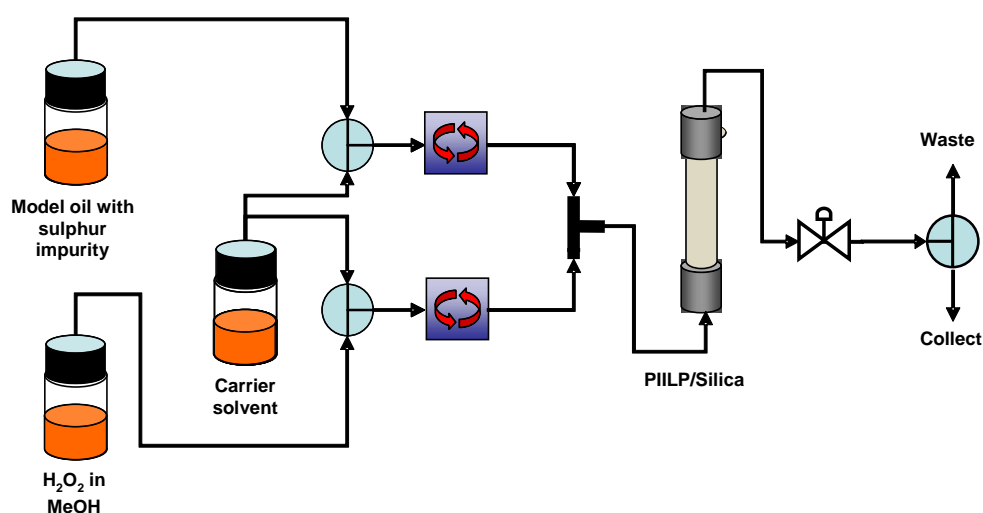


Figure 3.15 Proposed continuous flow setup for the PIILP catalysed oxidative desulfurization of crude oils

3.5. Experimental

All reagents were purchased from commercial suppliers and used without further purification. POM-2.1 and TBA-POM were prepared as described previously in chapter 2. ^1H and $^{13}\text{C}\{^1\text{H}\}$ NMR spectra were recorded on JEOL LAMBDA-500 or ECS-400 instruments. Metal analysis was performed using a Perkin-Elmer Optima 4300 ICP-OES analyser. FT-IR spectrums were record on a Varian 800 FT-IR spectrometer system using a pike technologies diamond crystal plate ATR unit. Flow reactions were performed using a Uniqsis FlowSyn Maxi using PTFE fittings supplied by Uniqsis.

Synthesis of $[n\text{Bu}_4\text{N}]_3[\text{PO}_4\{\text{WO}(\text{O}_2)_2\}_4]/\text{SiO}_2$

An oven-dried Schlenk flask was charged with $[n\text{Bu}_4\text{N}]_3[\text{PO}_4\{\text{WO}(\text{O}_2)_2\}_4]$ (0.094 g, 0.05 mmol) and dichloromethane (6 mL) with the resulting mixture allowed to stir for 15 min before the addition of 1.0 g Geduran[®] Si60 (43-60 μm) followed by a further 2 h stirring at room temperature. The dichloromethane solvent was then removed under high vacuum to afford a free flowing powder. FT-IR (KBr plates): $\tilde{\nu}$ = 1086, 1058, 1028 (P-O), 957 (W=O), 837 (O-O), 585, 535 $\text{W}(\text{O}_2)_{\text{asym, sym}}$. The tungsten loading was confirmed to be 0.19 mmol of W g^{-1} of silica by ICP-OES analysis.

General Procedure for Catalytic Sulfide Batch Oxidations

An oven-dried Schlenk was charged sequentially with sulfide (1 mmol), catalyst (0.013 g, 0.005 mmol) and solvent (3 mL), the reaction was then activated by the addition of 35% H_2O_2 (0.24 mL, 2.5 mmol) and allowed to stir at room temperature for 15 min. The reaction mixture was then diluted with CH_2Cl_2 (25 mL) and washed with water (*c.a.* 50 mL) before the organic extract was dried with MgSO_4 and the solvent removed under reduced pressure. The resulting residue was analysed by ^1H NMR. Relative percentages of starting material and products were determined using integrals in the ^1H NMR spectra.

General Procedure for Catalytic Sulfoxidation Recycle Studies

An oven-dried Schlenk was charged sequentially with sulfide (1 mmol), polymer immobilised catalyst POM-2.1 (0.039 g, 0.015 mmol) or $[n\text{Bu}_4\text{N}]_3[\text{PO}_4\{\text{WO}(\text{O}_2)_2\}_4]$ (100 mg, 6.5 wt% W) and solvent (9 mL), the reaction was then activated by the addition of 35% H_2O_2 (0.72 mL, 7.5 mmol) and allowed to stir at room temperature for 20 min. After this time the solution was centrifuged (10 min, 12000 rpm), decanted using a pipette and the catalyst washed with the reaction solvent (10 mL) and dried under

high vacuum prior to reuse under the same conditions. The remaining solution was subjected to the same work up and analysis described above.

General Procedure for Flow Oxidations

Two reservoirs were charged with sulfide (5.0 mmol) dissolved in the appropriate solvent (total volume of 25 mL, 0.2 M) and hydrogen peroxide 35% (1.46 mL, 15.0 mmol) in the same. A Uniqsis FlowSyn reactor was used to pump 1 mL of each reagent with total flow rates between 0.293 mL min⁻¹ and 8.8 mL min⁻¹ (using either MeCN or MeOH as an appropriate stock solvent) through a T-piece mixer to combine the two streams. The reaction stream was then flowed through a Uniqsis glass/PEEK column reactor (10 mm id) packed with 0.1 g of POM-**2.1** and 2.0 g of SiO₂ (Geduran® Si60 (43-60 μm)) with a volume of 4.4 mL. The column was mounted in the FlowSyn column heater to achieve the desired reaction temperature. The exiting stream was passed through a back pressure regulator (BPR) and 2 mL fractions were collected into separate vials with a 2 mL post-collect to ensure that no sulfide material remained on the column. Each sample was diluted with dichloromethane (10 mL), washed with water (c.a. 15 mL), the organic extract dried over MgSO₄, the solvent removed under reduced pressure and the resulting residue analysed by ¹H NMR to quantify the composition of starting material and products.

General Procedure for Continuous Flow Oxidations

Two reservoirs of thioanisole (6.20 mL, 52.8 mmol) and hydrogen peroxide (7.69 mL, 79.2 mmol) in the appropriate solvent (total volumes of 264 mL, 0.2 M and 132 mL, 0.6 M respectively) were run at a constant total flow rate of 1.1 mL min⁻¹ (R_t of 4 min) for 4 h through the set-up described previously, collecting 1 mL samples every hour. Upon reaching the 4 h mark the apparatus was stopped and the hydrogen peroxide reservoir was replenished before resuming flow for a further 4 h. After a total of 8 h of collecting the combined reagent streams the system was flushed with the solvent at a flow rate of 1 mL min⁻¹ for 15 min to ensure that no sulfide material remained on the column. The collection vessel, which had been cooled to 0 °C, containing the sample run through the 8 h was then diluted with dichloromethane (c.a. 500 mL) and washed with water (c.a. 500 mL). The organic extract was dried over MgSO₄, the solvent removed under reduced pressure and the resulting residue weighed and analysed by ¹H NMR to quantify both the yield of material collected and the composition of starting material and products. The 1 mL samples collected each hour were diluted with 70 % nitric

acid (5 mL) and allowed to stand overnight before being diluted to a volume of 15 mL with distilled water and analysed by ICP in order to determine the extent of tungsten leaching.

General Procedure for Flow Oxidations Using varying substrates

Using the FlowSyn set-up described previously, experiments at residence times of 5 min and 15 min were conducted in triplicate using thioanisole. The sulfide reagent stream was then replaced with a different sulfide solution of the same concentration. After priming the reagent line with the new sulfide for 5 min at a flow rate of 1 mL min⁻¹ and subsequently washing the column with solvent for a further 5 min at 1 mL min⁻¹ the experiments at different residence times were repeated for the new substrate. This cycle could be repeated numerous times provided there was a sufficient supply of hydrogen peroxide in the corresponding reservoir. Samples collected were analysed by ¹H NMR spectroscopy.

*Methyl phenyl sulfoxide*¹⁷

¹H NMR (400 MHz, CDCl₃, δ): 7.69-7.62 (m, 2H), 7.50-7.41 (m, 2H), 7.36-7.30 (m, 1H), 2.73 (s, 3H); ¹³C NMR (100.5 MHz, CDCl₃, δ): 145.42, 130.95, 128.63, 123.54, 43.93.

*Methyl phenyl sulfone*¹⁷

¹H NMR (400 MHz, CDCl₃, δ): 7.95-7.87 (m, 2H), 7.71-7.61 (m, 2H), 7.59-7.52 (m, 1H), 3.02 (s, 3H); ¹³C NMR (100.5MHz, CDCl₃, δ): 137.44, 133.21, 128.54, 126.23, 44.88.

*4-nitro-methylphenyl sulfoxide*²²

¹H NMR (400 MHz, CDCl₃, δ): 8.39 (d, *J* = 8.0 Hz, 2H), 7.90 (d, *J* = 7.5 Hz, 2H), 2.85 (s, 3H); ¹³C NMR (100 MHz, CDCl₃, δ): 152.4, 150.0, 126.2, 125.8, 43.5.

*4-nitro-methylphenyl sulfone*²³

¹H NMR (400 MHz, CDCl₃, δ): 8.43 (d, *J* = 8.8 Hz, 2H), 8.16 (d, *J* = 8.8 Hz, 2H), 3.12 (s, 3H); ¹³C NMR (100 MHz, CDCl₃, δ): 150.9, 145.9, 129.0, 124.6, 44.3.

*Dibenzothiophene sulfoxide*¹⁷

¹H NMR (400M Hz, CDCl₃, δ): 7.98-7.91 (m, 4H), 7.75-7.71 (m, 2H), 7.59-7.52 (m, 2H); ¹³C NMR (100.5 MHz, CDCl₃, δ): 143.33, 132.67, 129.83, 126.37, 124.16, 123.45.

*Dibenzothiophene sulfone*¹⁷

¹H NMR (400 MHz, CDCl₃, δ): 7.85-7.77 (m, 4H), 7.66-7.61 (m, 2H), 7.55-7.51 (m, 2H); ¹³C NMR (100.5 MHz, CDCl₃, δ): 137.62, 133.77, 131.53, 130.16, 121.97, 121.54.

*Homoallyl phenyl sulfoxide*²⁴

¹H NMR (300 MHz, CDCl₃, δ): 7.75-7.55 (m, 5H), 6.04-5.90 (m, 1H), 5.31-5.20 (m, 2H), 2.98-2.83 (m, 2H), 2.73-2.68 (m, 1H), 2.50-2.45 (m, 1H); ¹³C NMR (100 MHz, CDCl₃, δ): 135.4, 130.4, 129.0, 124.1, 117.0, 56.2, 26.3.

*Homoallyl phenyl sulfone*²⁵

¹H NMR (400 MHz, CDCl₃, δ): 7.89-7.87 (m, 2 H), 7.65-7.62 (m, 1H), 7.56-7.53 (m, 2 H), 5.73-5.64 (m, 1 H), 5.04-4.99 (m, 2 H), 3.15-3.11 (m, 2 H); 2.46-2.40 (m, 2H); ¹³C NMR (100 MHz, CDCl₃, δ) 138.9, 133.7, 133.6, 129.2, 128.0, 117.1, 55.3, 26.7

*Benzyl phenyl sulfoxide*¹⁷

¹H NMR (400 MHz, CDCl₃, δ): 7.55-7.42 (m, 2H), 7.36-7.17 (m, 3H), 7.11-6.63 (m, 5H), 3.98 (s, 2H); ¹³C NMR (100.5 MHz; CDCl₃, δ): 142.59, 130.83, 130.26, 128.87, 128.57, 128.24, 128.15, 124.21, 63.44.

*Benzyl phenyl sulfone*¹⁷

¹H NMR (400 MHz, CDCl₃, δ): 7.74-7.65 (m, 2H), 7.41-7.32 (m, 3H), 7.14-7.06 (m, 5H), 4.41 (s, 2H); ¹³C NMR (100.5 MHz; CDCl₃, δ): 137.49, 133.44, 130.53, 128.61, 128.47, 128.39, 128.31, 62.53.

3.6. References

1. a) M. C. Carreno, *Chem. Rev.*, 1995, **95**, 1717-1760; b) I. Fernández and N. Khiar, *Chem. Rev.*, 2003, **103**, 3651-3706; c) S. Caron, R. W. Dugger, S. G. Ruggeri, J. A. Ragan and D. H. B. Ripin, *Chem. Rev.*, 2006, **106**, 2943-2989; d) R. Bentley, *Chem. Soc. Rev.*, 2005, **34**, 609-624.
2. a) T. Durst, *J. Am. Chem. Soc.*, 1969, **91**, 1034-1035; b) G. W. Gokel, H. M. Gerdes and D. M. Dishong, *J. Org. Chem.*, 1980, **45**, 3634-3639.
3. a) N. K. Jana and J. G. Verkade, *Org. Lett.*, 2003, **5**, 3787-3790; b) R. J. Griffin, A. Henderson, N. J. Curtin, A. Echalié, J. A. Endicott, I. R. Hardcastle, D. R. Newell, M. E. M. Noble, L.-Z. Wang and B. T. Golding, *J. Am. Chem. Soc.*, 2006, **128**, 6012-6013.
4. R. S. Varma, R. K. Saini and H. M. Meshram, *Tetrahedron Lett.*, 1997, **38**, 6525-6528.
5. B. Yu, A.-H. Liu, L.-N. He, B. Li, Z.-F. Diao and Y.-N. Li, *Green Chem.*, 2012, **14**, 957-962.
6. F. A. Morrison, *An Introduction to Fluid Mechanics*, Cambridge University Press, 2013.

7. C. Wiles and P. Watts, *Green Chem.*, 2012, **14**, 38-54.
8. a) L. Kong, X. Lv, Q. Lin, X. Liu, Y. Zhou and Y. Jia, *Org. Process Res. Dev.*, 2010, **14**, 902-904; b) A. Manvar and A. Shah, *Org. Biomol. Chem.*, 2014, **12**, 8112-8124.
9. C. Capello, U. Fischer and K. Hungerbuhler, *Green Chem.*, 2007, **9**, 927-934.
10. S. P. Das, J. J. Boruah, H. Chetry and N. S. Islam, *Tetrahedron Lett.*, 2012, **53**, 1163-1168.
11. a) H.-J. Buysch, in *Ullmann's Encyclopedia of Industrial Chemistry*, Wiley-VCH Verlag GmbH & Co. KGaA, 2000; b) D. Stoye, in *Ullmann's Encyclopedia of Industrial Chemistry*, Wiley-VCH Verlag GmbH & Co. KGaA, 2000.
12. a) X. Zhao, N. Sun, S. Wang, F. Li and Y. Wang, *Ind. Eng. Chem. Res.*, 2008, **47**, 1365-1369; b) M. North and R. Pasquale, *Angew. Chem. Int. Ed.*, 2009, **48**, 2946-2948; c) E. Da Silva, W. Dayoub, G. Mignani, Y. Raoul and M. Lemaire, *Catal. Comm.*, 2012, **29**, 58-62.
13. P. Zhao, M. Zhang, Y. Wu and J. Wang, *Ind. Eng. Chem. Res.*, 2012, **51**, 6641-6647.
14. S. P. Das, J. J. Boruah, N. Sharma and N. S. Islam, *J. Mol. Catal. A*, 2012, **356**, 36-45.
15. a) X. Xue, W. Zhao, B. Ma and Y. Ding, *Catal. Comm.*, 2012, **29**, 73-76; b) B. M. Choudary, B. Bharathi, C. V. Reddy and M. L. Kantam, *J. Chem. Soc., Perkin Trans.*, 2002, 2069-2074.
16. Y.-L. Hu, X.-B. Liu and D. Fang, *Catal. Sci. Technol.*, 2014, **4**, 38-42.
17. J. J. Boruah, S. P. Das, S. R. Ankireddy, S. R. Gogoi and N. S. Islam, *Green Chem.*, 2013, **15**, 2944-2959.
18. a) N. J. Campbell, A. C. Dengel, C. J. Edwards and W. P. Griffith, *J. Chem. Soc., Dalton Trans.*, 1989, 1203-1208; b) A. J. Bailey, W. P. Griffith and B. C. Parkin, *J. Chem. Soc., Dalton Trans.*, 1995, 1833-1837; c) A. C. Dengel, W. P. Griffith and B. C. Parkin, *J. Chem. Soc., Dalton Trans.*, 1993, 2683-2688; d) E. Radkov and R. H. Beer, *Polyhedron*, 1995, **14**, 2139-2143; e) C. Rocchiccioli-Deltcheff, M. Fournier, R. Franck and R. Thouvenot, *Inorg. Chem.*, 1983, **22**, 207-216.
19. A. Pashkova and L. Greiner, *Chem. Ing. Tech.*, 2011, **83**, 1337-1342.
20. a) C. Venturello and R. D'Aloisio, *J. Org. Chem.*, 1988, **53**, 1553-1557; b) C. Venturello, R. D'Aloisio, J. C. J. Bart and M. Ricci, *J. Mol. Catal.*, 1985, **32**, 107-110; c) R. Neumann and A. M. Khenkin, *J. Org. Chem.*, 1994, **59**, 7577-7579; d) L. Salles, C. Aubry, R. Thouvenot, F. Robert, C. Doremieux-Morin, G. Chottard, H. Ledon, Y. Jeannin and J. M. Bregeault, *Inorg. Chem.*, 1994, **33**, 871-878; e) D. C. Duncan, R. C. Chambers, E. Hecht and C. L. Hill, *J. Am. Chem. Soc.*, 1995, **117**, 681-691.
21. R. Maggi, S. Chitsaz, S. Loebbecke, C. G. Piscopo, G. Sartori and M. Schwarzer, *Green Chem.*, 2011, **13**, 1121-1123.
22. P. Gogoi, M. Kalita, T. Bhattacharjee and P. Barman, *Tetrahedron Lett.*, 2014, **55**, 1028-1030.

23. G. Yuan, J. Zheng, X. Gao, X. Li, L. Huang, H. Chen and H. Jiang, *Chem. Comm.*, 2012, **48**, 7513-7515.
24. J. Skarzewski, E. Wojaczyńska and I. Turowska-Tyrk, *Tetrahedron: Asymm.*, 2002, **13**, 369-375.
25. S. Mannathan and C.-H. Cheng, *Chem. – Eur. J.*, 2012, **18**, 11771-11777.

Chapter 4

PIILP Lewis-Acid Catalysed Carbon-Carbon Bond Formation

This chapter is based on the publication:

S. Doherty, J. G. Knight, J. R. Ellison, P. Goodrich, L. Hall, C. Hardacre, M. J. Muldoon, S. Park, A. Ribeiro, C. A. N. de Castro, M. J. Lourenço and P. Davey,
“An efficient Cu(II)-bis(oxazoline)-based polymer immobilised ionic liquid phase catalyst for asymmetric carbon-carbon bond formation”, *Green Chem.*,
2014, **16**, 1470 – 1479

Table of Contents:

4.1.	Abstract	129
4.2.	Introduction	129
4.3.	Results and Discussion	130
	<i>4.3.1. Polymer and Catalyst Synthesis</i>	130
	<i>4.3.2. Copper Bis(oxazoline) Catalysed Diels-Alder Reactions</i>	132
	<i>4.3.3. Copper Bis(oxazoline) Catalysed Mukaiyama-Aldol Reactions</i>	140
4.4.	Conclusions	142
4.5.	Experimental	144
4.6.	References	151

4.1. Abstract

A range of linear and cross-linked ionic polymers based on materials generated by both Ring-Opening Metathesis and free radical initiated polymerisation were prepared as PIILP supports to immobilise copper (II)-bis(oxazoline) catalysts. The resulting heterogeneous catalysts were evaluated in the asymmetric Diels-Alder reaction between N-acryloyloxazolidinone and cyclopentadiene and the Mukaiyama-aldol reaction between methylpyruvate and 1-phenyl-1-trimethylsilyloxyethane; both systems revealed that selectivity and ee were heavily influenced by the polymer used and its microenvironment. A range of analogous SILP heterogeneous catalysts based on more conventional supports, such as silica and their homogeneous counterparts, were also tested in order to evaluate the relative merits of PIILP and SILP in asymmetric heterogeneous catalysis.

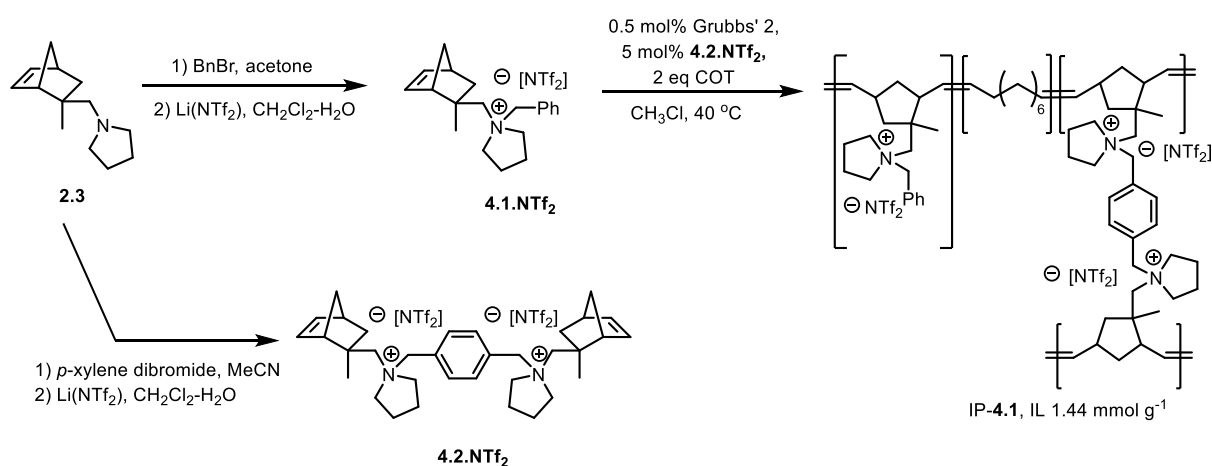
4.2. Introduction

Encouraged by the positive results observed using PIILP in both batch and continuous flow oxidations it was decided to extend the use of this concept into other catalytic systems, in particular in asymmetric catalysis. Aside from the use of enzymatic reactions, the industrial applications of asymmetric catalysts remains rather limited with most examples concerning hydrogenations due largely to the relatively high cost of metal-based systems.¹ In this regard, research over the past two decades has concerned the immobilisation of transition metal-based catalysts using ionic liquids.² The selection of SILP-type immobilisation methods published have also illustrated modification of the activity and selectivity of the catalyst as a result of conformational limitations imposed by the support material, restricting the possible pathways available for reagents to attack.^{3,4,5} Whilst polymer supports with chirality incorporated in their backbone have been widely studied in a range of metal-catalysed asymmetric C-C bond forming reactions, including Diels-Alder cycloadditions, oxidations and hydrogenations,^{6,7,8,9} the use of polyelectrolyte PIL and PIILP-type materials has been less thoroughly investigated.^{10,11} Extensive work conducted previously by the group demonstrated the positive effect of the immobilisation of the Lewis-acidic chiral bis(oxazoline) complexes on a range of transition metals in Diels-Alder cycloadditions through the use of both modified ionic liquids and SILP supports.¹² As a result of this work, and in order to extend the scope of the application of the PIILP methodology, it was decided to undertake a collaborative project with Queen's University Belfast into the immobilisation of chiral copper(II) bis(oxazoline) catalysts using PIILP systems similar to those outlined in chapters 2 and 3.

4.3. Results and Discussion

4.3.1. Polymer and Catalyst Synthesis

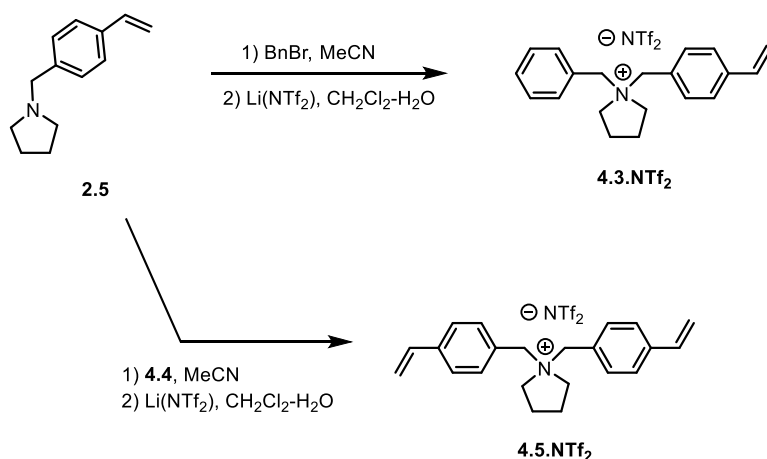
As a result of the successful use of the pyrrolidinium-based ROMP polymer IP-2.1 described in chapters 2 and 3 as a support for the immobilisation of peroxometalate catalysts this system was selected as an initial template for the desired PIILP material. Due to the lack of a large counter anion as with the previous peroxometalate catalyst it was decided that a degree of cross-linking should be introduced into the polymer in order to yield a more robust, insoluble material whilst also affording an additional means to control the pore size and morphology of the polymers produced. To this end the pyrrolidine-based **2.3**, prepared as in chapter 2, underwent alkylation with half an equivalent of *p*-xylylene dibromide to yield the dicationic cross-linker **4.2**. In previous chapters the PIILP materials consisted of a bromide counterion; however, it has been well documented that during catalysis the active Cu(II) bis(oxazoline) forms a complex with the reacting dienophile acting as a two-point binding chelate.^{2a, 13} As such it is necessary to have poorly coordinating, more labile counterions in order to allow this complex to form readily, meaning that halide counterions would act to poison the supported Cu catalyst.¹⁴ In this regard, Cu(OTf)₂ has been widely used as the source of Cu(II) in bis(oxazoline) complexes, however, it was believed that the ionic liquid fragments within the polymer architecture will behave in a similar fashion to bulk ionic liquids and replace the triflate counterions of the copper complex. Based on previous observations in which the less coordinating bistriflimide anion led to a marked improvement in catalyst performance¹⁵ it was decided to convert compounds **4.1** and **4.2** into their corresponding bistriflimide forms through metathesis with an excess of lithium bis((trifluoromethyl)sulfonyl)imide.



Scheme 4.1 Synthesis norbornene-based ionic monomers and ring-opening metathesis polymerisation catalysed by Grubbs 2nd generation catalyst to yield IP-4.1, ionic loading (mmol g⁻¹) is shown.

Once the two desired cationic monomers were obtained they underwent ROMP with cis-cyclooctene as the co-monomer, as described in chapter 2, however, the reaction was instead

catalysed by 2 mol% Grubbs' 2nd generation catalyst. Due to a sterically hindered environment being formed as a result of polymer cross-linking a more reactive catalyst was required. As discussed in previous chapters Grubbs' 2nd generation catalyst has been reported to be much better suited to transformations involving sterically demanding and deactivated olefins.¹⁶ Despite having a slower rate of initiation, the 2nd generation catalyst has a much higher affinity for olefinic substrates over the labile phosphine ligand, resulting in preferential binding of the catalyst to propagating species.¹⁷ Polymerisation of a 1 : 2 ratio of cation to neutral co-monomer together with a cross-linker content of 5 mol% yielded IP-**4.1** in 78% yield, with the elemental analysis obtained for the sample consistent with the expected ratio of each monomer, corresponding to an IL loading of 1.44 mmol g⁻¹.



Scheme 4.2 Synthesis of styrene-based ionic monomers **4.3.NTf₂** and **4.5.NTf₂**

As with chapter 2, in order to evaluate the relative merits of ROMP in the production of PIILP based supports an analogous polystyrene-based system was required. The co-monomer and dicationic cross-linker required to synthesise IPs were prepared by quaternisation of **2.5** with benzyl bromide and 4-vinylbenzyl bromide, respectively. Due to the widely used nature of divinyl benzene as a cross-linker in polystyrene-based materials it was also decided to generate a range of ionic polymers with varying amounts of either DVB or **4.5.NTf₂** as the cross-linker. In this regard, it was hoped that it would be possible to evaluate the effect a neutral and cationic cross-linker would have on polymer microstructure. As such the ionic polymers IP-**4.2** –**4.5** (figure 4.1) were synthesised by the AIBN-initiated radical co-polymerisation of **4.3.NTf₂** with styrene and the desired amount of cross-linker in methanol at 70 °C for 48 h.

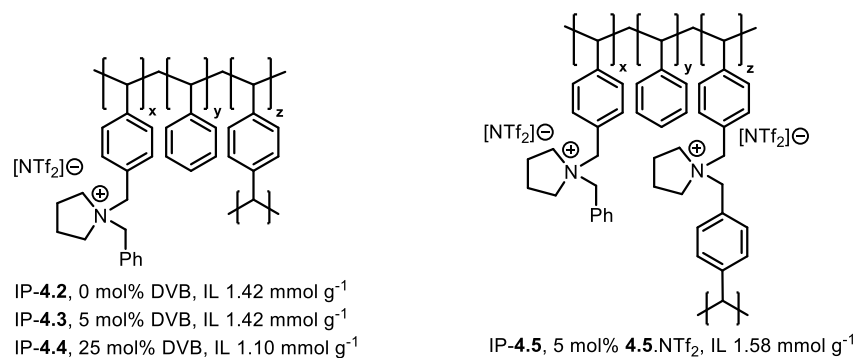
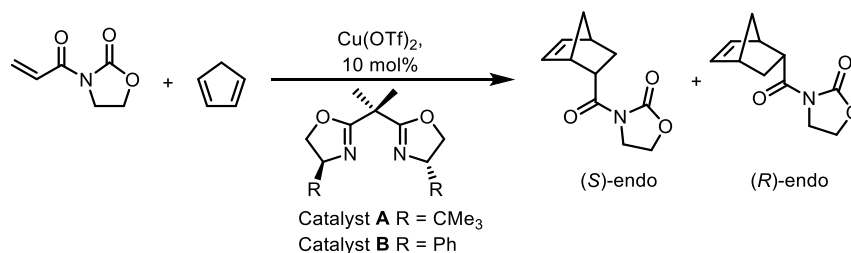


Figure 4.1 IPs 4.2-4.5 used in the immobilisation of Cu(II)-bis(oxazoline) catalysts for the asymmetric Diels-Alder reaction. In each case the degree of cross-linking and ionic loading (mmol g⁻¹) is shown.

4.3.2. Copper Bis(oxazoline)-Catalysed Diels-Alder Reactions

The benchmark Diels-Alder reaction between *N*-acryloyloxazolidinone and cyclopentadiene (Scheme 4.3) has previously been investigated extensively under both homogeneous and heterogeneous conditions with a range of metal (II) bis(oxazoline) catalysts¹² and was therefore selected as an initial reaction with which to test the newly prepared PIILP-systems. In order to fully evaluate these new heterogeneous catalysts the reaction was first conducted in dichloromethane, diethyl ether and the ionic liquid 1-ethyl-3-methylimidazolium bis(trifluoromethyl)sulfonylimide ([C₂mim][NTf₂]) under homogeneous conditions, and in the case of diethyl ether heterogeneous conditions (table 4.1). With the exception of diethyl ether catalyst **A** consistently outperformed catalyst **B** with higher ee's and endo selectivities as a result of the bulky *t*-butyl groups. The presence of ionic liquid, either as an additive or as a bulk solvent, led to a marked improvement in both conversion and ee for both catalysts under the same conditions in molecular solvents, a result in keeping with previous observations by the group.¹²



Scheme 4.3 Diels-Alder reaction between *N*-acryloyloxazolidinone and cyclopentadiene catalysed by 10 mol% Cu(OTf)₂/bis(oxazoline) complexes

In order to compare the efficiency of our PIILP-supports to more conventional SILP-systems, catalysts **A** and **B** were also supported on silica, multi-walled carbon nanotubes (CNT) and a commercially available polystyrene through wet impregnation with dichloromethane and [C₂mim][NTf₂] as the ionic liquid. In an attempt to minimize leaching of both the catalyst and the IL

the reactions were conducted in diethyl ether due to the relatively low solubility of [C₂mim][NTf₂] within this solvent compared to dichloromethane. As with the homogeneous conditions, significant improvements in both conversion and ee were observed for reactions conducted in the presence of SILP catalysts compared to the corresponding support with no IL present. Interestingly, for polystyrene with no IL no reaction was observed even after aging the catalyst for 3 hours (entry10). It is possible that this is a result of poorer binding of the Cu(II) complexes on the non-ionic surface of the polystyrene which was, at least in part, supported by ICP analysis of the etheral phase of the reaction mixture which indicated that up to 50% of the copper had been removed. For the silica support (entries 6 and 7) the low conversion and ee could be attributed to the formation of the cyclopentadiene dimer, facilitated by the surface silanols, which can coordinate to the active copper centre resulting in a non-chiral catalyst.¹⁸ For all supports examined the configuration of the Diels-Alder adduct was the same as those obtained under homogeneous conditions in both molecular solvents and in ionic liquids. As such it would appear that the heterogenisation of a chiral catalyst does not significantly alter its chiral environment, whilst immobilisation in an ionic environment can lead to a marked performance improvement when compared to homogeneous and non-ionic heterogeneous analogues. This enhancement effect, however, appears to be catalyst specific as illustrated by the poor ees obtained for catalyst **B**. While support effects could contribute to these observations the enhancements obtained in the presence of [C₂mim][NTf₂], both as a solvent and in SILP, could possibly be attributed to the less coordinating nature of [NTf₂]⁻ compared with [OTf]⁻ in the original catalyst.¹⁵ By being less coordinating the bistriflimide anions in the copper-ligand complex can dissociate or be displaced more readily in the formation of the chelate transition state with the *N*-acryloyloxazolidinone substrate.

Table 4.1 Comparison of the Diels-Alder reaction between *N*-acryloyloxazolidinone and cyclopentadiene catalysed by 10 mol% Cu(OTf)₂/bis(oxazoline) complexes in Et₂O, CH₂Cl₂ and [C₂mim][NTf₂] under homogeneous conditions and on SiO₂, CNT- and polystyrene-SILP under heterogeneous conditions

Entry	Solvent/ support	Time (min)	Catalyst A			Catalyst B		
			% conv. ^{a,b}	<i>endo</i> ee ^b	% <i>endo</i> ^b	% conv. ^{a,b}	<i>endo</i> ee ^b	% <i>endo</i> ^b
1	CH ₂ Cl ₂	15	78	70(<i>S</i>)	88	44	16(<i>R</i>)	82
2	Et ₂ O	15	32	14(<i>S</i>)	87	38	15(<i>R</i>)	80
3	IL	1	100	90(<i>S</i>)	89	100	19(<i>R</i>)	88
4	IL/Et ₂ O	5	100	91(<i>S</i>)	89	100	18(<i>R</i>)	78
5	CH ₂ Cl ₂ /IL	5	64	82(<i>S</i>)	96	100	16(<i>R</i>)	70
6	SiO ₂	5	32	16(<i>S</i>)	88	76	4(<i>R</i>)	84
7	SiO ₂ /IL	5	100	87(<i>S</i>)	85	100	8(<i>R</i>)	84
8	CNT	5	64	66(<i>S</i>)	87	44	20(<i>R</i>)	83
9	CNT/IL	5	100	92(<i>S</i>)	87	100	3(<i>R</i>)	80
10	PS	5	0	0	0	0	0	0
11	PS/IL	5	74	84(<i>S</i>)	88	100	30(<i>R</i>)	73

^a Conversion at 20 °C. ^b Determined by HPLC, ee's based on the *endo* isomer were calculated from the HPLC profile

To further evaluate the in-house generated PIILP support materials, the commercially available IP-4.6 and IP-4.7 were also converted to the bistriflimide form and used to support catalysts **A** and **B**. Significant conversions were obtained for systems based on IP-4.1- 4.7 which, when compared to the inactivity achieved with the non-ionic polystyrene support, illustrates the positive role that the ionic environment has on catalytic systems and their immobilisation (table 4.2). Gratifyingly, in agreement with previous studies conducted on these type of copper systems in ionic liquid solvents,^{12a} the active bis(oxazoline) complex formed after only 5 minutes stirring of the Cu(OTf)₂ precursor and the ionic polymer supports, as indicated by the distinct green colour. In contrast, considerably longer catalyst aging times (*c.a.* 3 hours) have been reported to be necessary to achieve efficient and reproducible catalysis in molecular solvents in the absence of added ionic liquid.² This further highlights that the ionic liquid moieties present within the ionic polymer architectures behave in a similar fashion to their homogeneous counterparts in bulk ionic liquids either as a solvent or additive.

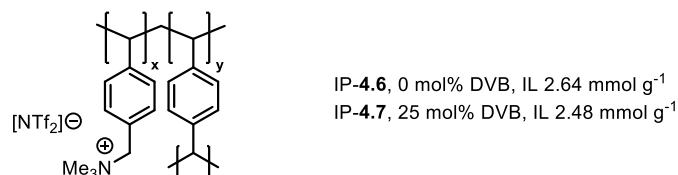


Figure 4.2 The commercially available IPs 4.6 and 4.7 used in the immobilisation of Cu(II)-bis(oxazoline) catalysts for the asymmetric Diels-Alder reaction. In each case the degree of cross-linking and ionic loading (mmol g⁻¹) is shown

The ROMP-generated IP-4.1 achieved high ees (entries 1 and 2) but with a considerably lower conversion compared to its polystyrene-based counterparts, highlighting the important role of the support microenvironment on catalysis. Reassuringly both catalysts **A** and **B** gave high ees when immobilised on the in-house synthesised polystyrene-based polymers IP-4.2-4.5 compared to their commercially available counterparts IP-4.6 and IP-4.7. IP-4.5 proved to be the most efficient system for both catalysts **A** and **B** giving cycloadduct *endo*-(2*S*) in 99% ee and *endo*-(2*R*) in 41% ee at 100% conversion, respectively, with the former result being the highest ee reported to date for this reaction under either heterogeneous or homogeneous conditions (entry 9). Further to this, the ee of 90% (*S*) obtained using IP-4.2 in combination with **A** matched the results obtained using both neat IL and IL-diethyl ether in table 4.1, illustrating that the positive effects associated with bulk ionic liquids can be successfully utilized in solid supports.

Due to the positive influence of a thin film of IL on activity and selectivity for the various heterogeneous supports used in table 4.1, the effect of combining IPs 4.1-4.7 with [C₂mim][NTf₂] was also investigated. Interestingly, the introduction of ionic liquid gave varying results amongst the polymer samples and the two catalysts. In some cases a marked improvement in catalyst performance was observed, most notably with IP-4.1 and IP-4.7 which gave improvements of 43% to

89% and 47% to 91% (entries 1, 2, 13 and 14), respectively, in terms of conversion. IP-4.7 also exhibited a significant increase in the ee from 44(S) to 84(S) upon the introduction of an IL film. Enhancements in ee were also observed with catalyst **A** immobilised on IP-4.2 and IP-4.4, in particular IP-4.4 which showed an increase of 41% (entries 7 and 8), however, very little change in both the *endo/exo*-selectivity and conversion was observed. In contrast, IP-4.6 exhibited a significant increase in conversion upon the introduction of [C₂mim][NTf₂] but without any significant change in ees which consistently remained very poor. Conversely the introduction of a thin film of ionic liquid to systems based on IP-4.3 and IP-4.5 led to significant reductions in both ee and *endo* selectivity. Whilst systems based on catalyst **B** performed consistently well in terms of conversion for all ionic polymers both with and without [C₂mim][NTf₂] there appears to be more discrepancy in terms of the ees and *endo/exo* selectivities, with the former showing very little change and the latter showing considerable variations in the presence of an IL film when compared to catalyst **A** under the same conditions. Interestingly, for all ionic polymers the introduction of IL caused catalyst **B** to give a considerable reduction in ee as opposed to systems using catalyst **A**, with the exception of IP-4.3, which experienced an increase (entry 6). Despite this reduction in ee, all combinations of PIILP catalysts and ionic liquid gave either a higher or equivalent ee when compared to the homogeneous system in dichloromethane (table 4.1).

Table 4.2 Comparison of the Diels-Alder reaction between *N*-acryloyloxazolidinone and cyclopentadiene catalysed by 10 mol% Cu(OTf)₂/bis(oxazoline) complexes immobilised onto a range of polymer supports and polymer-IL supports

Entry	polymer	solvent	Catalyst A			Catalyst B		
			% conv. ^{a,b}	<i>endo</i> ee ^b	% <i>endo</i> ^b	% conv. ^{a,b}	<i>endo</i> ee ^b	% <i>endo</i> ^b
1	IP-4.1	Et ₂ O	43	83(S)	92	100	45(R)	76
2	IP-4.1	Et ₂ O/IL	89	95(S)	97	100	25(R)	73
3	IP-4.2	Et ₂ O	86	90(S)	88	100	35(R)	78
4	IP-4.2	Et ₂ O/IL	100	99(S)	95	100	27(R)	76
5	IP-4.3	Et ₂ O	80	48(S)	92	100	32(R)	79
6	IP-4.3	Et ₂ O/IL	65	31(S)	85	100	26(R)	74
7	IP-4.4	Et ₂ O	69	28(S)	86	100	38(R)	73
8	IP-4.4	Et ₂ O/IL	77	69(S)	89	100	15(R)	76
9	IP-4.5	Et ₂ O	100	99(S)	93	100	41(R)	76
10	IP-4.5	Et ₂ O/IL	60	80(S)	91	100	31(R)	73
11	IP-4.6	Et ₂ O	27	7(S)	88	100	16(R)	92
12	IP-4.6	Et ₂ O/IL	98	9(S)	88	100	18(R)	79
13	IP-4.7	Et ₂ O	47	44(S)	84	100	38(R)	80
14	IP-4.7	Et ₂ O/IL	91	84(S)	91	99	18(R)	91
15	PS	Et ₂ O	0	0	0	0	0	0
16	PS	Et ₂ O/IL	74	84(S)	88	100	30(R)	73

^a Conversion at 20 °C after 5 minutes. ^b Determined by HPLC, ee's based on the *endo* isomer were calculated from the HPLC profile

Whilst it is possible to achieve high ees, selectivities and conversions with most of the ionic polymer supports, the apparent unpredictable variations in enantioselectivity and *endo/exo* selectivity as a function of both catalyst and the support system highlights the need for a rational understanding of how catalyst-support interactions influence catalysis. One possible explanation for some of these observations relates to the extent of swelling of the polymer support under the reaction conditions, with less swelling resulting in poorer access to catalytic sites within the porous structure of the polymer.¹⁹ The negligible swelling of the IPs in diethyl ether and subsequent catalyst inaccessibility could account for some of the low conversions observed when using catalyst **A**, however, this explanation does not hold for catalyst **B** which exhibits high activity and conversions under the same conditions. In order to address the potential swelling problem dichloromethane and toluene were employed as reaction solvents in an attempt to deliberately swell the polymer supports. This, however, led to a complete stripping of the catalyst from the PIILP support as confirmed by ICP analysis, showing that while the effect of solvent on the polymer structure is clearly an important factor the solvent choice is limited for systems employing ionic immobilisation rather than covalent tethering. Another likely cause of the somewhat erratic variations in conversion and ee for catalyst **A** is the geometric constraints imposed on the complex upon confinement within the porous network of the polymer support. Due to the bulky (*S,S*)-*t*-Bu-Box ligand the square planer geometry adopted by the active complex is much more sensitive to geometric changes than the much smaller and more flexible (*S,S*)-Ph-Box in catalyst **B**,^{12b,20} leading to an equilibrium between the bis(oxazoline) complex and the non-chiral catalytically active ligand free copper.²¹ A similar effect has been highlighted in a recent study in which a chiral Cu(Box) complex immobilised on laponite was used to catalyse the Mukaiyama-Michael reaction between *N*-(*E*)-but-2-enoyloxazolidinone and 2-(trimethylsilyloxy)furan.²² The authors speculated that the immobilisation of the copper catalyst on the support surface eliminates the C_2 symmetry of the complex which effectively increases the number of possible coordinations of the bidentate dienophile. Placement of the large oxazolidinone ring in the Michael acceptor Cu-Box complex close to the surface would lead to a large increase in steric hindrance already imposed by the bulky ligand substituents and hence enhance the enantioselectivity effect even further. However, due to the decrease in enantioselectivity observed it was believed that the disposition with the less hindered double bond close to the surface was in fact the more likely case as this would result in both faces of the double bond being shielded by either the oxazolidinone ring or the support surface. The imposition of these geometric constraints on catalyst **A** would appear to be most evident for IPs **4.1**, **4.4** and **4.7**, with the former only effecting conversion and not enantioselectivity. It is possible that this poor conversion is a result of the equilibrium between complexed and ligand-free copper discussed above and the polymer morphology leading to catalyst inaccessibility while the chiral centre in the monomeric pyrrolidinium

units help to maintain a chiral environment and hence give the observed high ee. For IP-**4.4** and IP-**4.7** the high degree of cross-linking could disrupt the square planar geometry and lead to the poor catalyst selectivity. Catalysts derived from both **A** and **B** have been prepared from bis(oxazoline)s grafted to polymers and used in the cyclopropanation of styrene with diethyl azoacetate; in this study the introduction of cross-linking led to a significant reduction in both the *cis/trans* selectivity and the enantioselectivity compared with their homogeneous counterparts.²³ This drop in activity and selectivity was again attributed to the support morphology which resulted in poor accessibility to the tethered bis(oxazoline) ligand which restricted interaction with the Cu(OTf)₂. Using a Nafion support as a benchmark system it was seen that catalyst **A** also suffered from additional steric hindrance between the chiral ligand and the material's surface, resulting in a shift in the metal-ligand equilibrium in favour of the free metal and a subsequent reduction in enantioselectivity when compared to the homogeneous analogue. In contrast, the corresponding Nafion-immobilised catalyst **B** exhibited a much smaller reduction in ee as a result of a more favourable metal-ligand equilibrium due to the smaller (*S,S*)-Ph-Box ligand. As such it is possible that the enhancement in performance achieved upon addition of ionic liquid to catalyst **A** with IPs **4.1**, **4.4** and **4.7** could be the result of metal/ligand leaching, as migration of the catalyst away from the polymer surface into the thin IL layer could reduce unfavourable steric interactions between the support surface and the ligand of the catalyst. Further to this, ionic liquids have been shown to swell polymers, this would in turn give improved access to the active catalytic sites within the polymer microstructure which were previously inaccessible.²⁴

For catalyst **B**, smaller changes in enantioselectivity across the range of ionic polymers used were observed. Similar Lewis acid catalysts using Mg(II) have been previously documented to exist as an equilibrium of numerous different geometries which can all act as an active catalyst during the reaction, essentially giving a mixture of *R*- and *S*- catalyst-substrate complexes.²⁵ It can therefore be inferred that a similar case is possible for the Cu(II) metal centre, with the labile bistriflimide anion present completing the octahedral type geometry (figure 4.3). The presence of multiple active geometries could be the cause of the considerably higher conversions achieved with catalyst **B** when compared to catalyst **A** as well as the possibility of forming Diels-Alder adducts with the opposite configuration reducing the product enantioselectivity. The large amount of active geometries present may also be the source of the differences in *endo* selectivity (*c.a.* Δ20%), a result which has not been previously observed in work conducted by the group previously using silica and carbon-based SILP supports.^{12b}

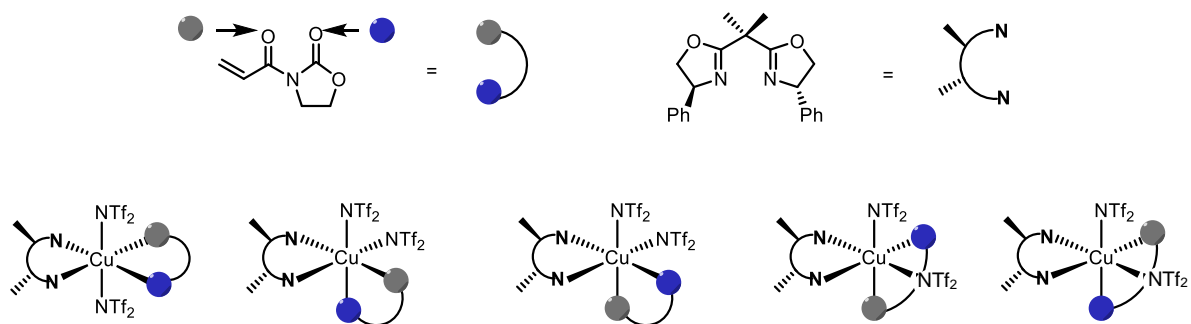


Figure 4.3 Possible geometries of catalyst **B** based on those proposed by G. Desimoni *et al.* for Mg(II) bis(oxazoline) complexes²⁵

In SILP, an ionic environment is required for high catalyst performance, as such it is also possible that the concentration and distribution of the ionic sites within the polymers used as PIILP supports may also influence the selectivity of the reaction.²⁶ In this regard, the loading of Cu in each PIILP system of approximately 0.1 mmol g⁻¹ is considerably lower than the relative concentration of bistriflimide anions present, which generally ranged from approximately 5 to 10 times as high. If the anion present had a major effect in determining the selectivity of the reaction it stands to reason that higher concentrations of bistriflimide could result in higher enantioselectivities; however, the opposite of this appears to be true, with the highest ee's being achieved with IP-4.2 and IP-4.5 which have relatively low [NTf₂]⁻ concentrations of 1.42 mmol g⁻¹ and 1.58 mmol g⁻¹, respectively, compared to IP-4.6 and IP-4.7 which have markedly higher loadings of 2.64 mmol g⁻¹ and 2.48 mmol g⁻¹. This provides further evidence that it is the more complex relationship between the structure of the support and its subsequent interaction with the catalyst and the IL which is responsible for changes in activity and selectivity. Despite the apparent limitations imposed on selectivity and its complex relationship as a function of the support material higher conversions were obtained for all PIILP and PIILP-IL combinations when compared to analogous homogeneous conditions, highlighting the positive/synergistic effect of the catalyst-polymer-IL interaction.

Encouraged by the largely positive results obtained using PIILP supports and reasoning that the immobilised ionic liquid phase within the polymer microstructure would sufficiently retain the catalyst in diethyl ether, a series of recycle experiments were conducted. In order to determine the effect of cross-linking on catalyst recyclability the linear IP-4.2 and the highly cross-linked IP-4.7 were selected as well as the silica support as a benchmark, all with and without ionic liquid present (table 4.3). For all PIILP systems used the catalyst recycled incredibly poorly with a considerable and rapid drop in both conversion and enantioselectivity, while the silica supported system recycled much more efficiently; most notably the silica SILP was used for three successive runs with only a very minor reduction in conversion and ee (entries 12-14). ICP analysis of the diethyl ether layer used to extract the product between each recycle determined that for IP-4.2 and IP-4.7 only 4.2% and 8.0%, respectively, of the copper was removed, whilst HPLC analysis showed that only 10.2% and 14.3% of

the ligand had leached. As in table 4.2 the addition of a thin layer of IL led to an increase in enantioselectivity and conversion as well as a significant reduction in copper leaching to just 0.2% for both ionic polymers as well as ligand leaching which was below the level of quantification by HPLC. Whilst some catalyst/ligand leaching occurred the low levels observed do not correlate to the significant drop in both enantioselectivity and conversion. Further to this, no significant alteration in the polymer structures is observable by FT-IR spectroscopy upon recycle (figure 4.4).

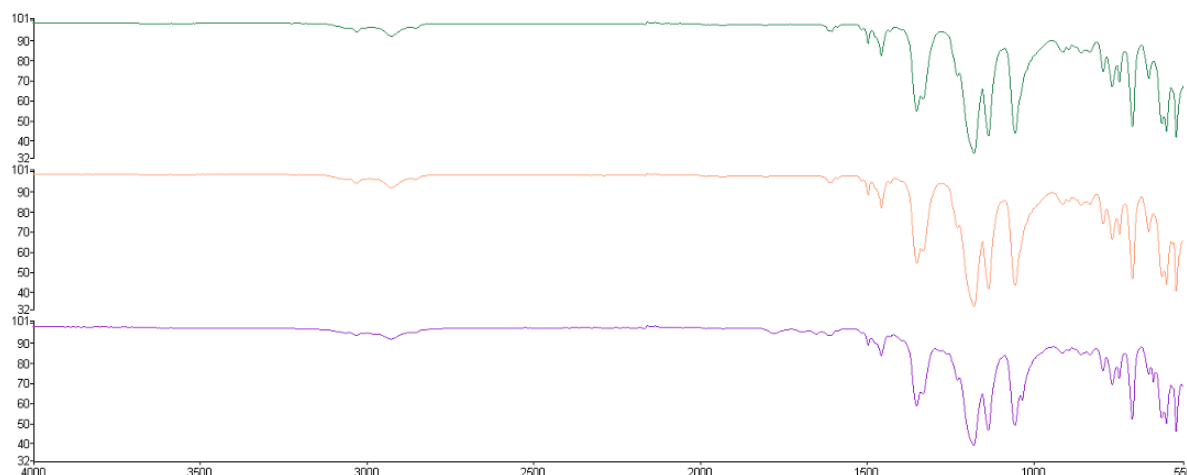


Figure 4.4 IR spectrum of IP-4.2 (green), IP-4.2-catalyst A (orange) and IP-4.2-catalyst A after use (purple) in a Diels-Alder reaction

Based on previous observations by the group when using other SILP materials in Diels-Alder reactions, it is believed that the drop in catalyst efficiency is a result of the build-up of cyclopentadiene dimer on the support surface.^{12b,27} In order to test this theory dicyclopentadiene (10 molar equivalents with respects to substrate) was added to the ethereal layer of a freshly prepared

Table 4.3 Recycle of the Diels-Alder reaction between *N*-scryloyloxazolidinone and cyclopentadiene using catalyst A immobilised on IPs and SiO₂ with and without additional IL.

Entry	Support	Run	Conv. ^{a,b}	<i>endo</i> ee ^b	% <i>endo</i> ^b
1		1	86	90(S)	88
2	IP-4.2	2	68	73(S)	86
3		3	30	7(S)	85
4	IP-4.2/IL	1	100	99(S)	95
5		2	98	74(S)	77
6	IP-4.7	1	47	44(S)	86
7		2	-	No RXN	-
8	IP-4.7/IL	1	91	84(S)	91
9		2	41	88(S)	92
10	SiO ₂	1	90	54(S)	85
11		2	83	43(S)	84
12		1	100	87(S)	86
13	SiO ₂ /IL	2	100	84(S)	85
14		3	93	81(S)	86

^a Conversion at 20 °C after 5 minutes. ^b Determined by HPLC, ee's based on the *endo* isomer were calculated from the HPLC profile

sample of IP-4.2-catalyst **A**; this resulted in a drop in conversion from 86% to 32% and a reduction in ee from 90% to 19%. The ability of the silica-based SILP system to maintain high conversions and ee's upon recycle could be the result of more efficient removal of the cyclopentadiene dimer due to the hydrophilic surface of the silica, as opposed to the more hydrophobic alkyl nature of the PIILP systems. In this regard, it should be possible to enhance the recyclability of our PIILP supports by increasing the hydrophilicity of the polymer architecture, either by incorporation of polyethylene glycol-derived co-monomers or by functionalising the existing pyrrolidinium monomers with PEG motifs (figure 4.5).

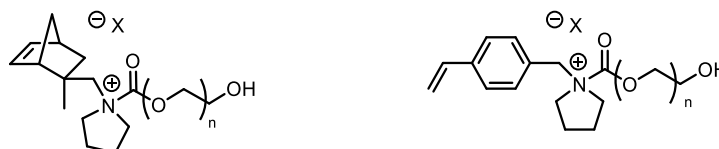
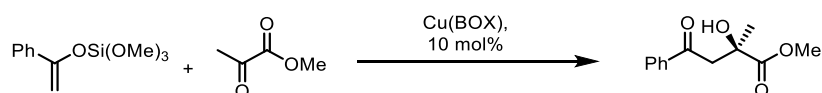


Figure 4.5 Proposed structures of potential PEG-functionalised cationic monomers based on compounds **2.4** and **2.6**

4.3.3. Copper Bis(oxazoline)-Catalysed Mukaiyama-Aldol Reactions

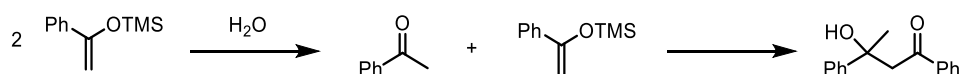
While there are clearly limitations imposed on the effectiveness of the PIILP-type supports by catalyst poisoning with regards to the build-up of the cyclopentadiene dimer, solvent choice and the support structure, it is still possible to achieve results which are comparable or better than those obtained under homogeneous and SILP conditions. Encouraged by this fact and by previous work by the group using SILP systems²⁸ it was decided to investigate the Mukaiyama-aldol reaction between 1-phenyl-1-trimethylsiloxyethene and methyl pyruvate (scheme 4.4) catalysed by 10 mol% catalyst **A** under homogeneous conditions in different solvents, as well as under analogous SiO₂ and CNT-based SILP and selected PIILP conditions (table 4.4).



Scheme 4.4 Mukaiyama-aldol reaction between 1-phenyl-1-trimethylsiloxyethene and methyl pyruvate catalysed by 10 mol% Cu(OTf)₂/bis(oxazoline) complexes

In a similar fashion to the Diels-Alder reaction discussed previously, a significant increase in the rate of reaction is observed under homogeneous conditions upon the addition of ionic liquid, either as a bulk or co-solvent, with the reaction reaching completion in just 1 or 5 minutes for IL and IL/Et₂O, respectively, as opposed to the low conversions obtained after 15 minutes in both dichloromethane and diethyl ether. Further to this, the use of IL as the bulk solvent gave a noticeably higher ee than in either diethyl ether and dichloromethane, however, this also led to the formation of a minor amount (*c.a.* 10%) of the 3-hydroxy-1,3-diphenyl-butan-1-one side product identified by

^1H NMR spectroscopy. This by-product has been previously identified as the result of a Mukaiyama-aldol reaction between 1-phenyl-1-trimethylsiloxyethene and acetophenone, which is generated by hydrolysis of the 1-phenyl-1-trimethylsiloxyethene facilitated by trace amounts of water in the IL.²⁸ Interestingly this hydrolysis only occurs in reactions conducted in ionic liquid. No by-product was observed when using SILP, PIILP and PIILP/IL systems. One possible explanation is that the trace amounts of water present are absorbed onto the support surface rendering them inaccessible for the hydrolysis of 1-phenyltrimethoxysilane to generate the acetophenone required for this side reaction.



Scheme 4.5 Hydrolysis and subsequent Mukaiyama-aldol reaction of 1-phenyltrimethoxysilane to yield 3-hydroxy-1,3-diphenylbutan-1-one by-product.

Both SILP systems based on SiO_2 and CNT gave complete conversions after only 5 minutes with only a slight reduction in ee when compared to the use of bulk IL as the solvent (entries 3, 5 and 6). In contrast, the ees obtained using PIILP and PIILP/IL systems were generally considerably lower than under homogeneous conditions, with the exception of IP-4.3 which gave a comparable ee of 86% (*S*) without a thin layer of IL and 90% (*S*) in the presence of IL (entries 9 and 10). Despite the comparable ees obtained, IP-4.3 gave significantly lower conversions than the analogous homogeneous systems (entry 1 to 3). As previously discussed it is likely that poor catalyst access and stability in the PIILP systems could be responsible for the poor conversions and enantioselectivities. In this regard, it would be reasonable to suggest that an increase in cross-linking could result in a more confining polymer microenvironment. This effect has been reported in a recent study on the effect of the degree of support cross-linking on the ees obtained in the chiral Lewis acid-catalysed asymmetric Mukaiyama-Aldol reactions between silyl ethers and aldehydes, in which the authors noted decreases in catalyst performance with an increase in cross-linking.²⁹ Interestingly, in our study the opposite appears to be true, the performance of IP-4.2 was poorer than the cross-linked IP-4.3 which further highlights the complex relationship between the catalyst, support and substrates involved in the reaction. As previously observed in the Diels-Alder study, the non-ionic environment provided by the polystyrene support proved to yield a completely inactive system, again this could possibly be attributed to a high affinity for the phenyl ring of 1-phenyltrimethoxysilane with the hydrophobic surface of the polymer in a similar fashion to cyclopentadiene discussed previously. Oddly, however, the addition of a thin layer of IL yielded no improvement to the polystyrene support which remained completely inactive, whilst the addition of IL to the IP supports appears to have a dramatic effect, albeit varied and erratic. Again this further highlights the complex, reaction-specific nature of these supported catalysts.

Table 4.4 Mukaiyama-aldol reaction between 1-phenyltrimethoxysilane and methyl pyruvate using catalyst **A** under homogeneous, SILP and PIILP conditions

Entry	system	Time (min)	% conv. ^a	ee ^b
1	CH ₂ Cl ₂	15	43	82(S)
2	Et ₂ O	15	32	80(S)
3	IL	1	100	89(S)
4	IL/Et ₂ O	5	100	84(S)
5	SiO ₂ /IL	5	100	86(S)
6	CNT/IL	5	100	85(S)
7	IP-4.2	5	49	24(S)
8	IP-4.2/IL	5	47	11(S)
9	IP-4.3	5	63	86(S)
10	IP-4.3/IL	5	56	90(S)
11	IP-4.5	5	56	13(S)
12	IP-4.5/IL	5	69	48(S)
13	IP-4.7	5	36	40(S)
14	IP-4.7/IL	5	55	63(S)
15	PS	5	0	-
16	PS/IL	5	0	-

^a Conversion at 20 °C after 5 minutes. ^b Determined by HPLC, ees based on the *endo* isomer were calculated from the HPLC profile

While all the IP supports used performed relatively poorly in terms of conversion it is possible to achieve ees that compare favourably to those obtained under homogeneous conditions using ILs as the bulk solvent, for instance using the combination of IP-4.3 and catalyst **A**. A similar observation has been demonstrated in the Mukaiyama-aldol reaction between ketene thioacetal and methyl pyruvate, in which heterogeneous conditions using an insoluble polymer-bound copper(II)-bis(oxazoline) catalyst gave an ee comparable to that obtained under homogeneous conditions but at the cost of markedly longer reaction times that were required to achieve similar conversions.³⁰

4.4. Conclusions

Through the catalyst screening results obtained by collaborators at Queens' University Belfast it is clear that there are limitations in the application of PIILP-type supports in the immobilisation of copper(II)-bis(oxazoline) catalysts. Despite this, PIILP based copper bis(oxazoline) systems have been identified that either compare with or outperform their homogeneous counterparts as catalysts for the asymmetric Diels-Alder and Mukaiyama-aldol reaction. Immobilisation of the catalyst *via* ionic association rather than covalent tethering limits the deleterious geometric constraints imposed on catalyst, whilst proximity to the support surface can still limit the approach of the reagents and enhance enantioselectivity. For the Diels-Alder reaction catalysts based on in-house synthesised polystyrene-based IPs 4.2-4.6 were notably more active and selective than the commercially available IP-4.6 and IP-4.7 and, in some cases produced higher *endo* selectivities and ees compared to those

obtained under homogeneous and SILP conditions. The poor performance of the ROMP-derived IP-4.1 highlights the sensitivity of these catalytic systems to the polymer support morphology; an effect which is evident from the markedly different performance of IP-4.3 which was designed to be a direct styrene-based counterpart to the norbornene-based IP-4.1. For the Mukaiyama-aldol reaction using catalyst **A**-based systems the in-house synthesised ionic polymers performed much more poorly with only IP-4.3 producing yields comparable to those obtained under homogeneous and SILP conditions. The contrasting performance in terms of conversion and yields for both these reactions highlights the complex nature of the non-covalent immobilisation of the copper catalysts under PIILP conditions. From selected results, it can be seen that under the right conditions the ionic environment of the support material is the determining factor in the catalysts efficiency and stability, rather than simple ionic solvation of the metal triflate complexes in a bulk IL or under SILP conditions as previously encountered by the group. To this end, tailoring of the ionic environment of the PIILP materials should be sufficient to maximise both catalyst efficiency and stability and, in this regard, the use of ROMP-based systems might perhaps be more appropriate. Although IP-4.1 proved to be a poorer support and the monomers required to produce it are more challenging to prepare than their styrene-based counterparts, the living, reproducible nature of the ROMP process affords much more control over the formation of the polymer microstructure, while the mild, functional group-tolerant reaction conditions allow for easier incorporation of catalysis-enhancing motifs in the polymer architecture. Using the norbornene unit as a basic motif for ROMP-suitable ionic monomers also affords alternate methods to improve the selectivity of supported chiral catalysts. For instance, the use of a chiral Lewis acid in the Diels-Alder reaction to prepare the norbornene will afford an enantiopure ionic monomer which, through ROMP, could be used to generate a well-defined short-chain polymer with chiral functionality incorporated in the architecture.

Whilst it will be challenging to achieve, it will be necessary to develop a full understanding of how the polymer's ionic microenvironment interacts with both the chiral catalyst and the reagents if the application of PIILP in asymmetric catalysis is to be implemented to its full potential.

Although the majority of the PIILP systems used showed good initial results for activity and selectivity, deleterious results were observed upon the recycling of the catalysts which was attributed to unfavourable interactions between the polymer structure and the reagents used. Again, in this regard it should be possible to minimize these negative interactions and maximize the performance and recyclability of the catalysts through efficient tailoring of the ionic polymer architecture.

4.5. Experimental

All manipulations involving air-sensitive compounds were carried out using standard Schlenk line techniques under an atmosphere of nitrogen in oven dried glassware. Diethyl ether and dichloromethane were dried and degassed prior to use. Unless otherwise stated all reagents were used as received. 1-Ethyl-3-methylimidazolium bis((trifluoromethyl)sulfonyl)imide, [C₂mim][NTf₂], was prepared in house after drying for 24 h at 60 °C under a high vacuum whilst stirring and found to contain <0.10 wt% water, determined by Karl-Fischer analysis and <10 ppm halide, determined by suppressed ion chromatography.³¹ SI1320 silica support was obtained from GRACE Davison and calcined at 400 °C prior to use. Carbon nanotubes were obtained from Bayer Material Science. Commercial polymers IRA-400 and IRA-900 were purchased from Aldrich as Cl⁻ salts and exchanged into the [NTf₂]⁻ form using LiNTf₂. All polymers were ground using a pestle and mortar and particles of <250 μm were used for catalyst immobilisation. ¹H and ¹³C{¹H} spectra were recorded on a JEOL LAMDA 500 or a ESC-400 instrument. Thin-layer chromatography (TLC) was performed on alumina sheets pre-coated with silica gel 60F 254 and column chromatography was performed using Merck Kieselgel 60. CHN analysis was undertaken using a Carlo-Ebra 1100 elemental combustion analyser controlled with CE Eager 200 software and metal analysis was performed using a Perkin-Elmer Optima 4300 ICP-OES analyser. High resolution mass spectrometry was conducted on a Waters Micromass LCT Premier mass spectrometer. For SEM examination, samples were mounted upon aluminium stubs with carbon tape and analysed using a FEI Quanta 250 FEG SEM at 20kV. The non-ionic sample was coated with Au in order to prevent charging before being mounted on carbon tape. ATR IR spectra were recorded using a Perkin Elmer 100 with a horizontal plate containing a ZnSe crystal. The spectra were recorded with a wavenumber resolution of 4 cm⁻¹ following 16 scans accumulated for a single spectrum. The working temperature was 25 °C. HPLC analysis was conducted using an Agilent 1100 equipped with an UV Diode Array detector.

For the copper-catalysed Diels-Alder reaction the *endo* selectivity and conversions were determined by HPLC and the ees based on the *endo* isomer were calculated from the HPLC profile using a Chiralcel OD-H column hexane : propan-2-ol 90 : 10 flow rate 1 cm³ min⁻¹ at 210 nm. The retention times of the *endo* enantiomers were major (2*S*)-enantiomer *t_R* ~ 18 min and minor (2*R*)-enantiomer *t_R* ~ 20 min.

For the Mukaiyama-aldol reaction, conversions and selectivities were determined by ¹H NMR spectroscopy. Enantioselectivity was calculated from the HPLC profile using a Chiralcel OD-H column hexane : propan-2-ol 96 : 4 flow rate 1 cm³ min⁻¹ at 254 nm. The retention times of the enantiomers were major (2*S*)-enantiomer *t_R* ~ 23 min and minor (2*R*)-enantiomer *t_R* ~ 19 min.

1,4-Bis(1-((2-methylbicyclohept-5-en-2-yl)methyl)pyrrolidinium)benzene dibromide (4.2.Br)

A mixture of **2.3** (4.3 g, 22.5 mmol) and *p*-xylylene dibromide (2.97 g, 11.2 mmol) in acetonitrile (140 mL) was allowed to stir at 50 °C for 48 h after which time the resulting precipitate was isolated by filtration and washed with acetone (*c.a.* 100 mL) followed by diethyl ether (*c.a.* 100 mL). Drying under high vacuum gave the product as a brown-white powder in 64% yield (4.60 g). ¹H NMR (400 MHz, D₂O, δ): 7.85 (m, 4H, Ar-*H*), 7.24 (s, 4H, Ar-CH₂-N), 6.22 (dd, *J* = 5.4, 2.0 Hz, 2H, =CH), 6.21 (dd, *J* = 5.4, 2.0 Hz, 2H, =CH), 5.56 (d, *J* = 7.11 Hz, 2H, N-CH₂-C), 5.05 (d, *J* = 7.11 Hz, 2H, N-CH₂-C), 4.18-3.60 (m, 4H, N-CH₂ pyrrolidinium), 2.97 (m, 2H, CH₂-CH-CH bridgehead), 2.57 (m, 2H, C-CH-CH bridgehead), 2.54-1.91 (m, 12H, CH-CH₂-CH bridge and -CH₂-CH₂- pyrrolidinium), 1.60 (s, 6H, Me), 1.59-1.45 (m, 2H, C-CH₂-CH), 1.23-1.17 (m, 2H, C-CH₂-CH); ¹³C NMR (100 MHz, D₂O, δ): 138.0, 134.9, 133.9, 133.7, 130.9, 72.8, 65.1, 63.5, 61.1, 52.3, 47.4, 44.0, 42.2, 40.4, 24.5, 22.1, 21.6. HRMS (ESI⁺) exact mass calcd for C₃₄H₅₀N₂ [M]⁺ requires *m/z* 486.7722, found *m/z* 486.7717.

1-Benzyl-1-((2-methylbicyclohept-5-en-2-yl)methyl)pyrrolidinium bis((trifluoromethyl)sulfonyl)imide (4.1.NTf₂)

A solution of lithium bis((trifluoromethyl)sulfonyl)imide (2.67 g, 9.3 mmol) in distilled water (10 mL) was added drop-wise to a rapidly stirred solution of **4.1.Br** (1.12 g, 3.1 mmol) in dichloromethane (20 mL) and allowed to stir under ambient conditions for 30 min. The organic layer was then extracted and washed with distilled water (10 mL) repeatedly, checking washings for bromide content with AgNO₃. After the third wash the aqueous layer did not become turbid upon the addition of AgNO₃, the organic layer was then dried *in vacuo* to give a viscous clear oil in 92% yield (1.60 g). 7.63 (br d, *J* = 6.4, Hz, 2H, Ar-*H*), 7.37 (m, 3H, Ar-*H*), 6.13 (dd, *J* = 5.4, 2.0 Hz, 1H, =CH), 6.00 (dd, *J* = 5.4, 2.0 Hz, 1H, =CH), 5.14 (d, *J* = 12.1 Hz, 1H, N-CH₃H_b-Ph), 4.62 (d, *J* = 12.1 Hz, 1H, NCH_aH_b-Ph), 4.02 (d, *J* = 13.6 Hz, 1H, CMeCH_cH_d-N), 3.93 (m, 1H, pyrrolidine NCH₂CH₂), 3.79 (m, 1H, pyrrolidine NCH₂CH₂), 3.71 (d, *J* = 13.6 Hz, 1H, CMeCH_cH_d-N), 3.70 (m, 2H, pyrrolidine NCH₂CH₂), 2.44 (br s, 1H, bridgehead CH), 2.51 (br s, 1H, bridgehead CH), 2.06 (m, 1H, pyrrolidine NCH₂CH₂), 1.97 (dd, *J* = 11.4, 3.6 Hz, 1H, CH_eH_f), 1.90 (m, 1H, pyrrolidine NCH₂CH₂), 1.73 (m, 2H, pyrrolidine NCH₂CH₂), 1.66 (d, *J* = 9.2 Hz, 1H, bridge CH), 1.27 (br d, *J* = 9.2 Hz, 1H, bridge CH), 1.18 (2, 3H, CH₃), 0.87 (dd, *J* = 11.4, 2.3 Hz, 1H, CH_eH_f); ¹³C NMR (100 MHz, CDCl₃, δ): 138.8, 134.9, 133.2, 130.7, 129.3, 128.2, 72.9, 65.1, 62.8, 60.9, 53.2, 48.1, 44.5, 42.9, 40.5, 25.8, 22.8, 21.8; ¹⁹F NMR (376.17 MHz, CDCl₃, δ): -78.67 (s, NTf₂); HRMS (ESI⁺) exact mass calcd for C₂₀H₂₈N [M]⁺ requires *m/z* 282.2222, found *m/z* 282.2221; Anal. Calc for C₂₀H₂₈BrN: C, 66.29; H, 7.79; N, 3.87. Found: C, 66.54; H, 8.13; N, 4.09%.

1,4-Bis(1-((2-methylbicyclohept-5-en-2-yl)methyl)pyrrolidinium)benzene bis{(trifluoromethyl)sulfonyl}imide (4.2.NTf₂)

A solution of lithium bis{(trifluoromethyl)sulfonyl}imide (2.76 g, 9.6 mmol) in distilled water (10 mL) was added drop-wise to a rapidly stirred solution of **4.2.Br** (1.00 g, 1.6 mmol) in dichloromethane (30 mL) and allowed to stir under ambient conditions for 30 min. The organic layer was then extracted and washed with distilled water (10 mL) repeatedly, checking washings for bromide content with AgNO₃. After the third wash the aqueous layer did not become turbid upon the addition of AgNO₃, the organic layer was then dried *in vacuo* to give a fine white powder in 81% yield (1.32 g). Complete ion exchange was confirmed by the ratio of C and N present in the sample. ¹H NMR (400 MHz, D₂O, δ): 7.85 (m, 4H, Ar-H), 7.24 (s, 4H, Ar-CH₂-N), 6.22 (dd, *J* = 5.4, 2.0 Hz, 2H, =CH), 6.21 (dd, *J* = 5.4, 2.0 Hz, 2H, =CH), 5.56 (d, *J* = 7.11 Hz, 2H, N-CH₂-C), 5.05 (d, *J* = 7.11 Hz, 2H, N-CH₂-C), 4.18-3.60 (m, 4H, N-CH₂ pyrrolidinium), 2.97 (m, 2H, CH₂-CH-CH bridgehead), 2.57 (m, 2H, C-CH-CH bridgehead), 2.54-1.91 (m, 12H, CH-CH₂-CH bridge and -CH₂-CH₂- pyrrolidinium), 1.60 (s, 6H, Me), 1.59-1.45 (m, 2H, C-CH₂-CH), 1.23-1.17 (m, 2H, C-CH₂-CH); ¹³C NMR (100 MHz, D₂O, δ): 138.0, 134.9, 133.9, 133.7, 130.9, 72.8, 65.1, 63.5, 61.1, 52.3, 47.4, 44.0, 42.2, 40.4, 24.5, 22.1, 21.6. ¹⁹F NMR (376.17 MHz, CDCl₃, δ): -78.67 (s, NTf₂); HRMS (ESI⁺) exact mass calcd for C₃₄H₅₀N₂ [M]⁺ requires *m/z* 486.7722, found *m/z* 486.7717.

Ring-Opening Metathesis Polymerisation of 1-benzyl-1-((bicyclohept-5-en-2-yl)methyl)pyrrolidinium bis{(trifluoromethyl)sulfonyl}imide (4.1.NTf₂) with cis-cyclooctene and cross-linker (4.2.NTf₂)

An oven-dried Schlenk flask was charged with **4.1.NTf₂** (1.39 g, 2.5 mmol), **4.2.NTf₂** (0.39 g, 0.38 mmol), cyclooctene (0.65 mL, 5.0 mmol) and CHCl₃ (20 mL) and allowed to stir for approximately 15 minutes. Once all reagents were dissolved a solution of Grubbs 2nd generation catalyst (0.032g, 0.038 mmol) in CHCl₃ (5 mL) was added to the mixture which was subsequently allowed to stir at 40 °C for 18 h, after which time a brown precipitate was observed. Ethyl vinyl ether (0.37 mL, 3.75 mmol) was then added to the mixture which was then refluxed for 2.5 h. After cooled to room temperature the resulting green solid was isolated by filtration and washed with ethyl vinyl ether (*c.a.* 50 mL) to remove the liberated Ru-containing species followed by Et₂O (*c.a.* 100 mL). After drying under high vacuum the polymer was isolated as an off-white powder (1.84 g). Anal. Calcd for C₄₄H₆₄N₃S₃O₅F₈ (polymer repeat unit): C, 54.87; H, 6.70; N, 4.36. Found: C, 56.19; H, 6.84; N, 4.04.

1-Benzyl-1-(4-vinylbenzyl)pyrrolidinium bis{(trifluoromethyl)sulfonyl}imide (4.3.NTf₂)

A solution of lithium bis{(trifluoromethyl)sulfonyl}imide (4.82 g, 16.8 mmol) in distilled water (30 mL) was added drop-wise to a rapidly stirred solution of **4.3.Br** (3.00g, 8.4 mmol) in dichloromethane (30 mL) and allowed to stir under ambient conditions for 30 min. The organic layer was then extracted and washed with distilled water (20 mL) repeatedly, checking washings for bromide content with AgNO₃. After the third was the aqueous layer did not become turbid upon the addition of AgNO₃, the organic layer was then dried *in vacuo* to give a yellow/white crystalline solid in 92% yield (4.32 g). ¹H NMR (399.78 MHz, CDCl₃, δ): 7.57 (m, 4H, Ar-H), 7.39 (m, 5H, Ar-H), 6.66 (dd, *J* = 17.4, 10.6 Hz, 1H, H_{C_a}=CH_bH_c). 5.79 (d, *J* = 17.4 Hz, H_{C_a}=CH_bH_c), 5.34 (d, *J* = 10.6 Hz, H_{C_a}=CH_bH_c), 5.04 (s, 4H, Ar-CH₂-N), 3.68 (m, 4H, N-CH₂), 2.04 (m, 4H, pyrrolidine N-CH₂-CH₂); ¹³C{¹H} NMR (100.52 MHz, CDCl₃, δ): 139.59, 135.48, 133.46, 133.22, 130.49, 129.15, 127.71, 126.92, 126.75, 116.12, 63.31, 57.64, 21.28; ¹⁹F NMR (376.17 MHz, CDCl₃, δ): -78.67 (s, NTf₂); Anal. Calcd for C₂₂H₂₄F₆N₂O₄S₂: C, 47.31; H, 4.31; N, 5.02. Found C, 47.49; H, 4.67; N, 5.33; HRMS (ESI⁺): exact mass calcd for C₂₀H₂₄N [M⁺] *m/z* 278.19009, found *m/z* 278.1904.

4-Vinylbenzyl bromide (4.4)

A round bottom flask was charged with 4-vinylbenzyl chloride (0.93 mL, 6.6 mmol), ^tbutyl-catechol (0.0033 g, 0.2 mmol), sodium bromide (2.72 g, 26.4 mmol) and acetone (30 mL). The resulting mixture was brought to reflux and allowed to stir for 19 hours after which time the reaction mixture was filtered and the solvent removed *in vacuo* to give a yellow oil. Analysis by ¹H NMR spectroscopy showed that the sample still contained approximately 50 % of the chloride starting material, the reflux was therefore repeated for a further 19 hours. After filtration and drying the resultant yellow oil was again analysed by ¹H NMR spectroscopy showing that the reaction had gone to 94% completion. ¹H NMR (399.78 MHz, CDCl₃, δ): 7.39 (m, 4H, Ar-H), 6.76 (dd, *J* = 17.4, 10.6 Hz, 1H, H_aC=CH_bH_c), 5.78 (d, *J* = 17.4 Hz, 1H, H_aC=CH_bH_c), 5.29 (d, *J* = 10.6 Hz, 1H, H_aC=CH_bH_c), 4.58 (s, 2H, Ar-CH₂-Cl), 4.48 (s, 2H, Ar-CH₂-Br). ¹³C{¹H} NMR (100.52 MHz, CDCl₃, δ): 137.51, 137.43, 136.32, 129.14, 126.78, 114.39, 33.62.

1,1-Bis(vinylbenzyl)pyrrolidinium bromide (4.5.Br)

A round bottom flask was charged with **2.5** (0.66 g, 3.5 mmol), 4-vinylbenzyl bromide (0.82 g, 4.2 mmol) and acetonitrile (4 mL), the mixture was then allowed to stir under ambient conditions for 18 h. The product was precipitated by the drop-wise addition of the reaction mixture into rapidly stirred diethyl ether (*ca.* 100 mL) and then isolated by filtration and dried under high vacuum to give **4.5.Br** as a yellow/white powder in 74% yield (1.00 g). ^1H NMR (399.78 MHz, CDCl_3 , δ): 7.55 (m, 4H, Ar-H), 6.67 (dd, $J = 17.4, 10.6$ Hz, 2H, $H_a\text{C}=\text{CH}_b\text{H}_c$), 5.81 (d, $J = 17.4$ Hz, $\text{HC}_a=\text{CH}_b\text{H}_c$), 5.34 (d, $J = 10.6$ Hz, $\text{HC}_a=\text{CH}_b\text{H}_c$), 5.03, (s, 4H, Ar- CH_2 -N), 3.47 (m, 4H, CH_2 -N- CH_2), 2.05 (m, 4H, pyrrolidine N- CH_2 - CH_2); $^{13}\text{C}\{^1\text{H}\}$ NMR (100.52 MHz, CDCl_3 , δ): 139.6, 135.5, 133.5, 126.9, 126.8, 116.2, 63.1, 57.6, 21.3; Anal. Calcd for $\text{C}_{22}\text{H}_{26}\text{NBr}$: C, 68.75; H, 6.82; N, 3.64. Found: C, 69.08; H, 7.11; N, 3.89; HRMS (ESI $^+$): exact mass calcd for $\text{C}_{22}\text{H}_{26}\text{N}$ [M^+] m/z 304.2065, found m/z 304.2054.

1,1-Bis(4-vinylbenzyl)pyrrolidinium bis{(trifluoromethyl)sulfonyl}imide (4.5.NTf₂)

A solution of lithium bis{(trifluoromethyl)sulfonyl}imide (1.12 g, 3.9 mmol) in distilled water (5 mL) was added drop-wise to a rapidly stirred solution of **4.5.NTf₂** (0.5 g, 1.3 mmol) in dichloromethane (5 mL) and allowed to stir under ambient conditions for 30 min. The organic layer was then extracted and washed with distilled water (10 mL) repeatedly, checking washings for bromide content with AgNO_3 . After the third wash the aqueous layer did not become turbid upon the addition of AgNO_3 , the organic layer was then dried *in vacuo* to give an off-white crystalline solid in 92% yield (0.69 g). ^1H NMR (399.78 MHz, CDCl_3 , δ): 7.55 (m, 4H, Ar-H), 6.67 (dd, $J = 17.4, 10.6$ Hz, 2H, $H_a\text{C}=\text{CH}_b\text{H}_c$), 5.81 (d, $J = 17.4$ Hz, $\text{HC}_a=\text{CH}_b\text{H}_c$), 5.34 (d, $J = 10.6$ Hz, $\text{HC}_a=\text{CH}_b\text{H}_c$), 5.03, (s, 4H, Ar- CH_2 -N), 3.47 (m, 4H, CH_2 -N- CH_2), 2.05 (m, 4H, pyrrolidine N- CH_2 - CH_2); $^{13}\text{C}\{^1\text{H}\}$ NMR (100.52 MHz, CDCl_3 , δ): 139.5, 135.4, 133.6, 126.8, 126.75, 126.7, 116.4, 63.2, 57.7, 21.5; ^{19}F NMR (376.17 MHz, CDCl_3 , δ): -78.67 (s, NTf_2); Anal. Calcd for $\text{C}_{22}\text{H}_{26}\text{F}_6\text{N}_2\text{O}_4\text{S}_2$: C, 49.31; H, 4.48; N, 4.79. Found: C, 49.77; H, 4.67; N, 5.09; HRMS (ESI $^+$): exact mass calcd for $\text{C}_{22}\text{H}_{26}\text{N}$ [M^+] m/z 304.2065, found m/z 304.2054.

General procedure for radical initiated polymerisations of 1-benzyl-1-(4-vinylbenzyl)pyrrolidinium bis{(trifluoromethyl)sulfonyl}imide with styrene and cross-linker

In a typical procedure, an oven-dried Schlenk flask was charged with the 1-benzyl-1-(4-vinylbenzyl)pyrrolidinium monomer **4.3.NTf₂** (5.2 mmol), styrene (10.3 mmol) and the specified amounts of azobisisobutyronitrile and corresponding cross-linker. After dilution with dry methanol (50 mL) the resulting reaction mixture was degassed with 5 freeze/thaw cycles using liquid nitrogen. Upon

warming to room temperature the reaction mixture was heated to 75 °C and allowed to stir for 48 h. In the case of insoluble polymers the solvent was decanted and the resulting precipitate washed with hexane and diethyl ether before drying under high vacuum, whereas the reaction mixture containing soluble polymers was added drop-wise to rapidly stirring diethyl ether to induce precipitation. The product was subsequently isolated by filtration and washed with diethyl ether before drying under high vacuum. Each of the polymers was isolated as an off white crystalline solid.

General procedure for anion exchange for the commercial resins

A solution of lithium bis{(trifluoromethyl)sulfonyl}imide (1.00 g, 3.49 mmol) in distilled water (30 mL) was added drop-wise to a rapidly stirred slurry of the IRA resins (2.00 g) and allowed to stir under ambient conditions overnight. The aqueous layer was then removed and the resin was stirred for a further 1 h in fresh distilled water (20 mL). This process was repeated twice more with fresh water before drying the resin *in vacuo* at 60 °C for 48 h. The resulting ionic polymer was then used as a heterogeneous support for the Diels-Alder reaction.

General procedure for the homogeneous Lewis acid catalysed Diels-Alder and Mukaiyama-aldol reaction in 1-ethyl-3-methylimidazolium bis{(trifluoromethyl)sulfonyl}imide ([C₂mim][NTf₂])

A flame-dried Schlenk flask was charged with ligand (0.011 mmol), Cu(OTf)₂ (0.010 mmol, 10 mol%) and dichloromethane (5 mL) and the resulting solution stirred at room temperature for 3 h to afford a clear green solution. Thereafter, *N*-acryloyloxazolidinone (0.0143 g, 0.1 mmol) was added followed by freshly distilled cyclopentadiene (50 μL). For the Mukaiyama-aldol reaction, methyl pyruvate (0.0102 g, 0.1 mmol) followed by 1-phenyl-1-trimethylsiloxyethene. The reaction mixture was stirred at the desired temperature for the specified amount of time and then diluted with 5 mL of 1 : 1 ethyl acetate-hexane.

Following concentration of the Diels-Alder reaction mixture, the crude adduct was dissolved in diethyl ether (5 mL) and filtered through a small plug of silica gel to afford unpurified product which was analysed directly.

Following concentration of the Mukaiyama-aldol reaction mixture, the residual oil was redissolved in THF (5 mL) and the corresponding silyl-adduct was hydrolysed by stirring for 1 h in the presence of 2 M HCl (10 mL). The THF was removed under vacuum and the keto-alcohol was extracted from the aqueous phase by washing with diethyl ether (3 x 5 mL). The crude product was analysed directly.

For reactions conducted in diethyl ether, the catalyst was activated in dichloromethane the solvent was then removed under vacuum and diethyl ether added (5 mL); the resulting mixture was stirred for 30 min after which time the substrates were added. The reaction was worked up as previously described to afford the unpurified product which was analysed directly.

General procedure for the liquid-liquid biphasic Lewis acid catalysed Diels-Alder and Mukaiyama reactions in [C₂mim][NTf₂]/diethyl ether

A flame-dried Schlenk flask was charged with ligand (0.011 mmol) and metal(II) triflate (0.010 mmol, 10 mol%). To this was added dichloromethane (5 mL) and [C₂mim][NTf₂] (0.15 g, 0.23 mL) and the resulting solution stirred at room temperature for 5 min. The dichloromethane was then removed under high vacuum for one hour leaving the active catalyst dissolved in the ionic liquid. Thereafter, diethyl ether (5 mL) was added followed by the Diels-Alder or Mukaiyama-aldol substrates. The resulting mixture was stirred at the desired temperature for the specified amount of time after which the diethyl ether was removed and the remaining ionic liquid was extracted with diethyl ether (2 × 10 mL) in air. The Diels-Alder or Mukaiyama-aldol products were worked up as previously described to afford the unpurified product which was analysed directly.

General procedure for the heterogeneous Lewis acid catalysed Diels-Alder and Mukaiyama-aldol reactions in diethyl ether/support

A flame-dried Schlenk flask was charged with ligand (0.011 mmol), metal(II) triflate (0.010 mmol, 10 mol%) and dichloromethane (5 mL) and the resulting solution stirred at room temperature for 5 min. To the resulting green solution was added silica, carbon or ionic polymer support (0.1 g) and for catalysis using a supported ionic liquid film, 0.1 mL of ionic liquid was also added. (For the non-ionic polystyrene support the resulting metal triflate-ligand solution was stirred for 3 h before the addition of the polymer support). After stirring for 5 min, the dichloromethane was removed under vacuum for one hour to afford a free flowing powder after which the flask was charged with diethyl ether (5 mL) followed by the Diels-Alder or Mukaiyama-aldol substrates. The reaction mixture was stirred at room temperature for the specified amount of time after which the silica was extracted with diethyl ether (3 × 5 mL) in air. The reaction was worked up as previously described to afford the unpurified products which was analysed directly.

Procedure for the recycle of heterogeneously catalysed reactions

The catalyst/ether slurry solution was left to settle in order to separate the phases after which the ethereal layer was removed by pipette and the heterogeneous catalyst was further extracted with diethyl ether (2 × 5 mL). After extraction fresh diethyl ether (5 mL) was added to the heterogeneous catalyst and the resultant slurry was charged with further portions of Diels-Alder substrate. ICP analysis was conducted on a portion of the supernatant phase between recycles.

*(R)-methyl 2-hydroxy-2-methyl-4-oxo-4-phenylbutanoate*³²

¹H NMR (400 MHz, CDCl₃, δ): 7.94-7.97 (m, 2H), 7.57-7.61 (m, 1H), 7.47-7.49 (m, 2H), 3.78 (s, 3H), 3.67 (d, *J* = 17.9 Hz, 1H), 3.36 (d, *J* = 17.6 Hz, 1H), 1.52 (s, 3H).

*1,3-diphenyl-3-hydroxy-1-butanone*³³

¹H NMR (500 MHz, CDCl₃, δ): 7.89-7.91 (d, *J* = 8.0 Hz, 2H), 7.56-7.58 (t, *J* = 7.0 Hz, 1H), 7.44-7.49 (m, 4H), 7.30-7.33 (t, *J* = 8.0 Hz, 2H), 7.20-7.22 (t, *J* = 7.0 Hz, 1H), 4.87 (s, 1H), 3.77-3.80 (d, *J* = 17.0 Hz, 1H), 3.32-3.36 (d, *J* = 17.0 Hz, 1H), 1.62 (s, 3H).

4.6. References

1. H.-U. Blaser and E. Schmidt, in *Asymmetric Catalysis on Industrial Scale*, Wiley-VCH Verlag GmbH & Co. KGaA, 2004, pp. 1-19.
2. a) D. A. Evans, S. J. Miller and T. Lectka, *J. Am. Chem. Soc.*, 1993, **115**, 6460-6461; b) D. A. Evans, M. C. Kozlowski and J. S. Tedrow, *Tetrahedron Lett.*, 1996, **37**, 7481-7484.
3. J. M. Thomas and R. Raja, *Acc. Chem. Res.*, 2008, **41**, 708-720.
4. S. Taylor, J. Gullick, P. McMorn, D. Bethell, P. C. Bulman Page, F. E. Hancock, F. King and G. J. Hutchings, *J. Chem. Soc., Perkin Trans. 2*, 2001, 1714-1723.
5. R. S. Varma, *Tetrahedron*, 2002, **58**, 1235-1255.
6. a) C. A. McNamara, M. J. Dixon and M. Bradley, *Chem. Rev.*, 2002, **102**, 3275-3300; b) N. E. Leadbeater and M. Marco, *Chem. Rev.*, 2002, **102**, 3217-3274.
7. A. Puglisi, M. Benaglia and V. Chiroli, *Green Chem.*, 2013, **15**, 1790-1813.
8. a) B. M. L. Dioso, I. F. J. Vankelecom and P. A. Jacobs, *Adv. Synth. Catal.*, 2006, **348**, 1413-1446; b) S. Itsuno, K. Watanabe, T. Koizumi and K. Ito, *React. Polym.*, 1995, **24**, 219-227.

9. H. W. Bae, J.-S. Han, S. Jung, M. Cheong, H. S. Kim and J. S. Lee, *Appl. Catal. A*, 2007, **331**, 34-38.
10. P. Barbaro and F. Liguori, *Chem. Rev.*, 2008, **109**, 515-529.
11. J. M. Fraile, J. I. García and J. A. Mayoral, *Chem. Rev.*, 2008, **109**, 360-417.
12. a) P. Goodrich, C. Hardacre, C. Paun, V. I. Pârvulescu and I. Podolean, *Adv. Synth. Catal.*, 2008, **350**, 2473-2476; b) P. Goodrich, C. Hardacre, C. Paun, A. Ribeiro, S. Kennedy, M. J. V. Lourenço, H. Manyar, C. A. Nieto de Castro, M. Besnea and V. I. Pârvulescu, *Adv. Synth. Catal.*, 2011, **353**, 995-1004.
13. a) J. S. Johnson and D. A. Evans, *Acc. Chem. Res.*, 2000, **33**, 325-335; b) D. A. Evans and J. S. Johnson, *J. Am. Chem. Soc.*, 1998, **120**, 4895-4896; c) D. A. Evans, S. J. Miller, T. Lectka and P. von Matt, *J. Am. Chem. Soc.*, 1999, **121**, 7559-7573.
14. D. A. Evans, J. A. Murry, P. von Matt, R. D. Norcross and S. J. Miller, *Angew. Chem. Int. Ed. Engl.*, 1995, **34**, 798-800.
15. J. M. Fraile, J. I. García, C. I. Herrerías, J. A. Mayoral, D. Carrié and M. Vaultier, *Tetrahedron: Asymm.*, 2001, **12**, 1891-1894.
16. B. F. Straub, *Angew. Chem. Int. Ed.*, 2005, **44**, 5974-5978.
17. a) M. S. Sanford, J. A. Love and R. H. Grubbs, *J. Am. Chem. Soc.*, 2001, **123**, 6543-6554; b) M. S. Sanford, M. Ulman and R. H. Grubbs, *J. Am. Chem. Soc.*, 2001, **123**, 749-750.
18. D. Rechavi, B. Albela, L. Bonneviot and M. Lemaire, *Tetrahedron*, 2005, **61**, 6976-6981.
19. B. Corain, M. Zecca and K. Jeřábek, *J. Mol. Catal. A*, 2001, **177**, 3-20.
20. H. Wang, J. Liu, P. Liu, Q. Yang, J. Xiao and C. Li, *Chin. J. Catal.*, 2006, **27**, 946-949.
21. J. M. Fraile, J. I. García, C. I. Herrerías, J. A. Mayoral, S. Gmough and M. Vaultier, *Green Chem.*, 2004, **6**, 93-98.
22. J. M. Fraile, N. García and C. I. Herrerías, *ACS Catalysis*, 2013, **3**, 2710-2718.
23. a) M. J. Fernández, J. M. Fraile, J. I. García, J. A. Mayoral, M. I. Burguete, E. García-Verdugo, S. V. Luis and M. A. Harmer, *Top. Catal.*, 2000, **13**, 303-309; b) J. M. Fraile, J. I. García, C. I. Herrerías, J. A. Mayoral and M. A. Harmer, *J. Catal.*, 2004, **221**, 532-540.
24. P. Izák, Š. Hovorka, T. Bartovský, L. Bartovská and J. G. Crespo, *J. Membr. Sci.*, 2007, **296**, 131-138.
25. G. Desimoni, G. Faita, A. Gamba Invernizzi and P. Righetti, *Tetrahedron*, 1997, **53**, 7671-7688.
26. M. I. Burguete, E. García-Verdugo, I. Garcia-Villar, F. Gelat, P. Licence, S. V. Luis and V. Sans, *J. Catal.*, 2010, **269**, 150-160.
27. Y. Wan, P. McMorn, F. Hancock and G. Hutchings, *Catal Lett*, 2003, **91**, 145-148.

28. S. Doherty, P. Goodrich, C. Hardacre, V. I. Pârvulescu and C. Paun, *Adv. Synth. Catal.*, 2008, **350**, 295-302.
29. S. Itsuno, S. Arima and N. Haraguchi, *Tetrahedron*, 2005, **61**, 12074-12080.
30. S. Orlandi, A. Mandoli, D. Pini and P. Salvadori, *Angew. Chem. Int. Ed.*, 2001, **40**, 2519-2521.
31. C. Villagrán, M. Deetlefs, W. R. Pitner and C. Hardacre, *Anal. Chem.*, 2004, **76**, 2118-2123.
32. J. Sedelmeier, T. Hammerer and C. Bolm, *Org. Lett.*, 2008, **10**, 917-920.
33. C. H. Cheon and H. Yamamoto, *Tetrahedron*, 2010, **66**, 4257-4264.

Chapter 5

PIILP Palladium Nanoparticle Catalysed Carbon-Carbon Bond Formations

Table of Contents:

2.1.	Abstract	156
2.2.	Introduction	156
2.3.	Results and Discussion	160
	2.3.1. <i>Polymer Design and Synthesis</i>	160
	2.3.2. <i>Suzuki-Miyaura Cross-Couplings</i>	171
2.4.	Conclusions	185
2.5.	Experimental	187
2.6.	References	197

5.1. Abstract

Free radical initiated polymerisation was used to prepare two imidazolium chloride functionalised polymers, both with and without a nitrile bearing co-monomer. The resulting materials were used to immobilise sodium tetrachloropalladate through ion exchange and the resulting palladium(II) loaded materials were subsequently reduced by hydrogenation to afford the corresponding polymer immobilised ionic liquid stabilised palladium nanoparticles. With the aim of investigating the potential stabilising effect of the nitrile groups on nanoparticle formation, the materials were analysed by transmission electron microscopy to show both supports gave small, asymmetrically spherical nanoparticles. The observed size distributions for both supports appeared relatively broad, ranging from 1 – 15 nm, however, the presence of the nitrile-functionalised co-monomer gave slightly smaller nanoparticles with a tighter distribution than the unfunctionalised counterpart. The catalytic activity of the two supported nanoparticle catalysts was evaluated in the Suzuki-Miyaura coupling between various aryl bromides and phenylboronic acid in the presence of base, with both catalysts giving moderate to good performance across the substrate scope under mild conditions. Analysis of the catalysts after use showed much smaller nanoparticles with a smaller size distribution, suggesting leaching and redeposition of molecular palladium during the reaction, with the excess of substrate further stabilising smaller nanoparticles towards agglomeration. Comparison of the supported unreduced PdCl₄ precursors showed comparable activity to the pre-reduced nanoparticles, with no induction period required, indicating efficient in situ reduction of the supported Pd species. Mercury poisoning tests suggest that the reaction proceeds, at least in part, through a homogeneous mechanism resulting from leached Pd, again supporting a “catch and release” mechanism.

5.2. Introduction

As previously discussed in chapter 1, the existing precedent for the use of ionic polymer supports in catalysis seemingly favours the stabilisation of transition metal nanoparticles. While metal nanoparticles offer many unique properties which fuel their continued interest across a range of technical applications, including electrochemistry, sensors, opto-electronics, biotechnology as well as catalysis,¹ it is their high surface area to volume ratio which is particularly beneficial in catalysis. In this regard, it is of paramount importance to be able to synthesise nanoparticles with a small, well-defined size distribution in a controlled and reproducible fashion.² While the unique favourable properties of nanoparticles is typically attributed to their small size, the surface energy effects associated with these particles can also be detrimental for their long term stability and usability, with small nanoparticles being kinetically stable and prone to forming thermodynamically favourable

larger particles through agglomeration.³ This thermodynamically-driven spontaneous agglomeration is based on the principle of Ostwald ripening (figure 5.1).⁴ The tendency towards agglomeration arises from the relatively high number of coordinatively unsaturated atoms or molecules present in small particles which are considerably less energetically stable than fully coordinated, well-ordered atoms or molecules present in bulk substances. Conversely larger particles have a much smaller surface area to volume ratio, and therefore possess relatively fewer surface atoms which in turn results in a lower energy state for the particle. As a system attempts to lower its overall energy atoms or molecules will detach from the surface of a particle before diffusing through a solution. These free atoms or molecules then attach to a larger particle, essentially reducing the number of smaller particles whilst increasing the number of larger, more energetically favourable particles in the system.

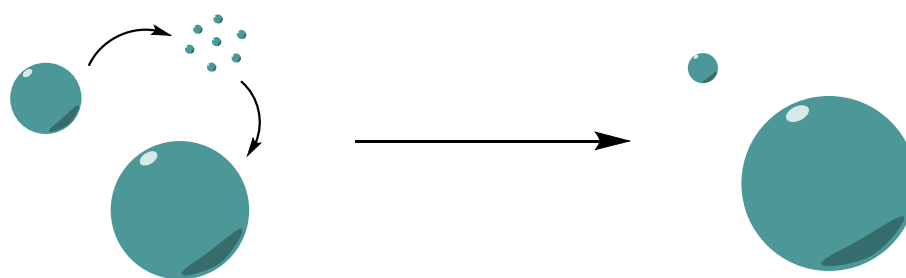


Figure 5.1 Schematic representation of Ostwald ripening

As a means to prolong the life of smaller nanoparticles and prevent agglomeration to their larger counterparts, the kinetically unstable surface sites must be stabilised. In this regard, the addition of protective groups, typically during the formation of the nanoparticles through reductive methods or thermal decomposition, achieves stabilisation through electrostatic or steric forces, or a combination of the two.⁵ Once the nanoparticle is formed various different interactions between the surface sites and the stabiliser can occur via three prominent modes of stabilisation (figure 5.2). Firstly, traditional ligand type interactions, which involve a lone pair from a heteroatom such as thiols and thioethers,⁶ phosphines⁷ and various different N-⁸ and O-donors.⁹ As with molecular catalysis the use of ligands can have a profound effect on performance, with both the electronic and steric properties of the ligands affecting how they interact with the metal surface, while the use of chiral ligands has been shown to influence asymmetric transformations.¹⁰ The second common mode of stabilisation used for metal nanoparticles employs the use of ionic species such as salts, for example the ubiquitous *N*-alkylammonium halides, or surfactants.¹¹ To this end stabilisation is achieved through strong adsorption of a layer of anions to the surface of the metal which in turn necessitates the formation of a layer of counter cations to maintain charge neutrality to afford an ionic double layer surrounding the metal particle (figure 5.2 (B)).^{5a, 11a, 12} The use of charged species in this manner can have a dramatic effect on the metal's behaviour, with both anion and cation playing a key role in the stabilisation. For example, varying the nature of the cation used can alter the phase behaviour of

the catalyst and allow for movement between organic and aqueous media. Additionally the use of certain surfactants can lead to the generation of anisotropically shaped particles such as rods.¹³ Ionic liquids have also been heavily exploited in this fashion, in particular imidazolium-based systems.¹⁴ While stabilisation occurs through the same electrostatic mechanism additional stabilisation may also occur from steric effects, for example long alkyl chain based imidazolium ILs have been shown to provide additional stabilisation.¹⁵ As discussed in chapter 1 however, the complex inter- and intramolecular forces present in ILs make simple electrostatic (i.e. a combination of electronic and steric) interactions an oversimplification. Effects within the IL such as hydrogen bonding and hydrophobicity as well as sterics all potentially have an influence over size, size distribution and shape of metal nanoparticles.¹⁶ The functionalization of ILs can also afford several additional benefits. For example the addition of heteroatom-containing groups to either the anion or cation of the IL can provide additional ligand-type interactions to the metal surface.¹⁷ To this end imidazolium ILs functionalised with thiols,¹⁸ ethers,¹⁹ carboxylic acids,¹⁷ amines,^{17,20} hydroxyls,^{18b,21} and nitriles²² have all been shown to be more efficient stabilisers for noble metal nanoparticles compared to their non-functionalised counterparts. As with most forms of catalysis the use of ILs has also been exploited to yield effective heterogeneous catalysts, either through biphasic media or under SILP conditions, allowing for the stable nanoparticles to be reused for successive cycles. The third mode of stabilisation predominantly employs the use of polymers, such as poly(*N*-vinyl-2-pyrrolidone) (PVP) or poly(vinyl alcohol) (PVA), to coat the surface of the metal particle and provide steric protection from agglomeration (figure 5.2 (C)).²³ Dendrimers, with their well-defined molecular structures and cavities, have also been extensively exploited for this purpose. The use of dendrimers in this manner has the additional benefit of providing a well-defined environment surrounding the nanoparticles, which generally remain encapsulated within the pores and channels of the polymer material. Such porous systems can even control the passage of reactants and products to and from the active species, leading to enhancements in reaction performance.²⁴

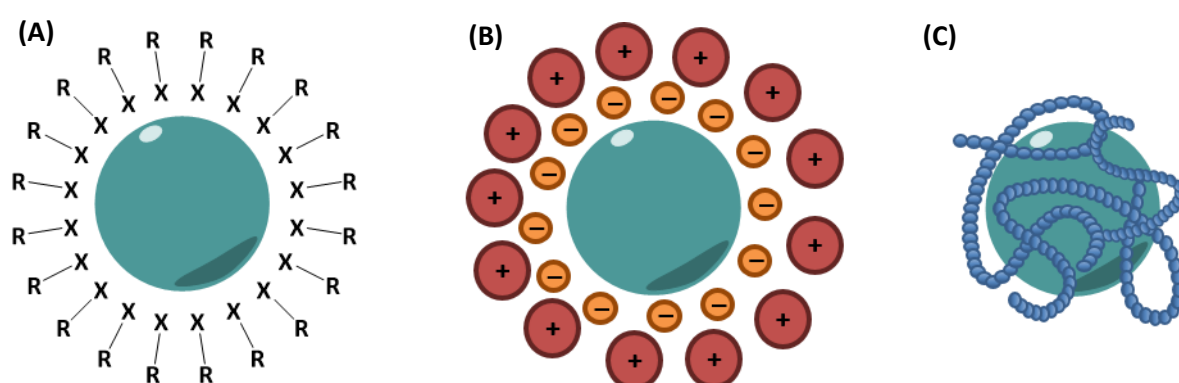


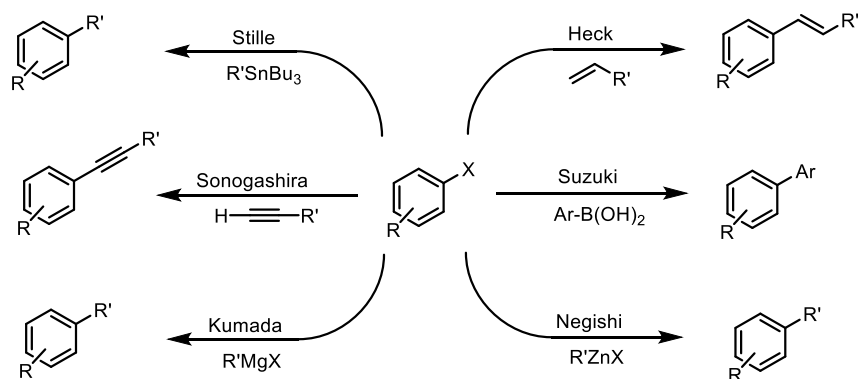
Figure 5.2 Schematic representation of the stabilisation of metal nanoparticles using different types of protective groups: (A) ligands; (B) ionic species such as salts or surfactants; and (C) polymers

While clearly an oversimplification of the complex nature of the relationships between the nanoparticle surface and the capping agent, a heteroatom-modified polymer immobilised ionic liquid support could be considered to combine the three modes of stabilisation outlined in figure 5.2, effectively providing electrosteric stabilisation to agglomeration. Through the tuneable nature of polymer chemistry it could be possible to rationally control the particle size, size distribution and morphology of the desired nanoparticles through careful variations in the charge density, charge distribution, hydrophobicity/hydrophilicity and degree of cross-linking of the polymer support. Further to this, the introduction of functional co-monomers could also allow for additional modification to the particle surface through ligand-like interactions to influence catalyst activity and/or selectivity. Through controlling the phase behaviour, or by preparing insoluble polymers it should also be possible to easily separate and reuse the stabilised catalyst. In this regard, the use of PIILP type supports to stabilise metal nanoparticles is proving to be an increasingly popular and effective strategy across the full spectrum of catalysis. For example, ionic co-polymers consisting of 1-vinyl-3-alkyl imidazolium and *N*-vinyl-2-pyrrolidone functionalities have been prepared to stabilise Rh nanoparticles to combine the beneficial influence of ILs with the commonly used PVP stabiliser. The resulting catalyst showed considerable longevity and total turnover numbers five times greater than those previously observed in the hydrogenation of benzene catalysed by Ir nanoparticles in [C₄mim][PF₆].²⁵ The stabilisation provided by these co-polymers highlighted a synergistic effect between the IL and the polymer, with the reaction proceeding poorly and forming a black precipitate when conducted in the absence of either the co-polymer or [C₄mim][PF₆]. More recently poly(1-vinyl-3-alkyl imidazolium) polymers were used to prepare Ag, Au and Ni nanoparticles, with the alkyl chain length exhibiting a profound effect on the size of the nanoparticle.²⁶ Imidazolium-decorated styrene-based homopolymers have also been shown to stabilise Au, Pt and Pd nanoparticles through a combination of electrosteric effects as well as the formation of micelles. Under these conditions it was also possible to transfer the nanoparticles from the aqueous phase to a hydrophobic IL without any aggregation by performing anion exchange of the chloride-based polymer.²⁷ Similarly, ROMP-based imidazolium-functionalised homopolymers have been used to prepare highly stable Au nanoparticles which proved to be highly active and moderately selective catalysts for the reduction of nitrophenol and cinnamaldehyde.²⁸ Cross-linked dicationic imidazolium polymers have also been used to immobilise Pd nanoparticles for catalytic carbonylative Suzuki couplings. Again the size and dispersion of the nanoparticles could be influenced by varying the composition of the polymer material, while the introduction of cross-linking amine groups proved to be substantially favourable.²⁹ The considerable literature precedent for the positive, often synergistic effect of IL moieties combined with polymer materials clearly indicates that the PIILP principle developed in the previous chapters would be ideal for the preparation of metal nanoparticle for catalysis.

5.3. Results and Discussion

5.3.1. Polymer Design and Synthesis

While PILs and other PIILP-like materials have been extensively used in the preparation of transition metal nanoparticles for a range of applications arguably one of the more versatile, and widely investigated metals is palladium. This interest in Pd catalysts arises from the critical impact traditional homogenous and heterogeneous systems have had on synthetic organic chemistry, in particular, the variety of Pd-catalysed carbon-carbon bond-forming reactions (scheme 5.1).³⁰ In this regard, Pd-catalysed coupling reactions have proved to be widely applicable across chemistry, including the production of pharmaceuticals, agrochemicals, polymers and other high-tech materials.³¹ With these considerations in mind, Pd was selected as the initial catalytic metal of choice for investigating the application of the PIILP methodology in the preparation of stable nanoparticle catalysts.

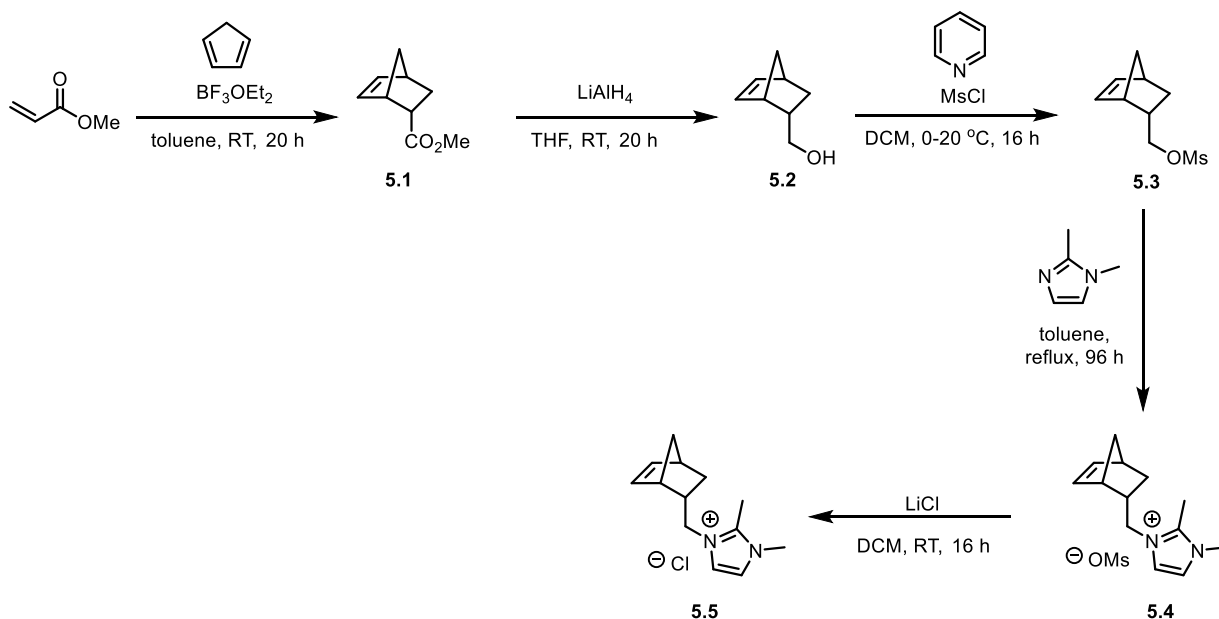


Scheme 5.1 Representative Pd-catalysed cross-coupling reactions to form carbon-carbon bonds

The norbornene framework investigated in chapters 2 and 4 was again initially targeted as a suitable monomer backbone to give well-defined PIILP supports through the ROMP process. The role of the IL fragment in catalysis with metal nanoparticles is potentially more profound than in previous examples, with both the anion and cation of ILs interacting directly with the nanoparticle surface.^{14c} While the pyrrolidinium cation was previously chosen for synthetic convenience, imidazolium was instead selected for the application of PIILP as a stabiliser for metal nanoparticles. In this regard, the imidazolium moiety was selected due to the existing, extensive precedent for their use in metal nanoparticle preparation³² as well as the proven strong interactions between the imidazolium ring and both the nanoparticle surface and cleaved free metal.^{14c, 33} The use of the imidazolium cation could also offer additional control over the size and shape of the supported nanoparticles which, in part, are related to the volume of polar and non-polar nanoregions within ILs and IL-functionalised supports. For example, when ionic metal precursors are used they tend to reside within the polar region, causing the size of the forming nanoparticle to be directly related to the volume of the counter anion of the IL.³⁴ Conversely, when neutral precursors are used they reside in the non-polar regions,

with the size of the forming nanoparticles reported to be directly related to the length of the *N*-alkyl side chain of the imidazolium IL.³⁵ As such the use of the imidazolium cation in PIILP could allow an additional, methodical means to control the prepared nanoparticle properties. In part, the interaction of imidazolium based ILs with metal nanoparticles has been attributed to the formation of *N*-heterocyclic carbenes (NHCs), either through direct oxidative addition of the C(2)-H bond or via deprotonation of the imidazolium.^{33, 36} While this carbene formation has often proven to be advantageous, occasionally even being responsible for the positive IL effects observed, there are also several reports of catalyst deactivation. For example, formation of a stable Pd-imidazolylidene in the Pd-catalysed telomerisation of butadiene-methanol in the presence of [C₄mim][NTf₂] as a co-solvent.³⁷ In order to avoid an extra degree of ambiguity with regards to the environment around the supported Pd nanoparticles it was decided to prevent the formation of NHCs by the PIILP support. To this end we identified C2-methylated methylimidazolium **5.5** as the IL cation, which has also been previously used for the preparation of ROMP-based homopolymers to support water soluble Au nanoparticles.³⁸ As discussed above, the introduction of N-, O-, S- or P-containing functionalities, either as part of the imidazolium side chain or as ligands, can provide extra stabilisation through coordination to the metal surface. This observation also stands for PIILP-type polymer supports, for example when cross-linked dicationic imidazolium-based polystyrene polymers were used in the preparation of Pd nanoparticles for carbonylative Suzuki cross coupling. In this work the authors reported a notable increase in nanoparticle stability accompanied by smaller particle sizes and tighter size distributions upon the introduction of amine functionality to the cross-linked IL units when compared to their unfunctionalised counterparts.²⁹ To this end, it was also decided to introduce a heteroatom-functionalised co-monomer. Numerous different groups which behave like ligands have been employed throughout the literature, however, there has been extensive work conducted by Dyson *et al* introducing nitrile groups into the alkyl chains of pyridinium and imidazolium-based ILs for the stabilisation of Pd nanoparticles. In this regard nanoparticles in the nitrile-functionalised ILs are highly stable and remain active after numerous recycles; this was associated with weak coordination of the nitrile to the metal surface as evidenced by IR spectroscopy. The authors postulated that the nitrile groups form a protective sheath around the nanoparticles which further prevents aggregation.^{22b, 39} As such the nitrile-functionalised co-monomer **5.6** was initially proposed, rationalising that it may be possible to allow for additional modulating of catalyst performance in a similar way to classical organometallic/coordination chemistry. The cationic cross-linker **5.8** was also

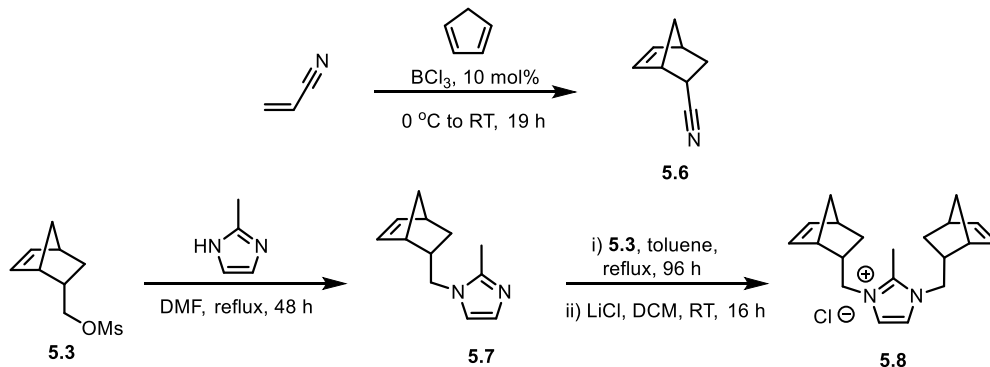
proposed as a means to ensure that the produced PIILP material was both robust and insoluble in a similar fashion to the pyrrolidinium-based counterpart prepared in chapter 4.



Scheme 5.2 Synthesis of the norbornene-based imidazolium chloride monomer **5.5**

As with the norbornene-based monomers prepared in chapters 2 and 4 a modular approach was taken to prepare monomers **5.5**, **5.6** and **5.8**. The imidazolium-functionalised monomer **5.5** was prepared in a similar manner to its pyrrolidinium counterpart (scheme 5.2). This involved a Diels-Alder reaction to give methyl ester-functionalised norbornene **5.1**, which was reduced with LiAlH_4 to afford the corresponding methyl alcohol **5.2**. This was then converted to the corresponding mesylate **5.3**, before quaternisation with 1,2-dimethylimidazole and subsequent ion exchange to give the desired imidazolium monomer **5.5**. The second monomer **5.6** was prepared in one step via a Diels-Alder reaction between cyclopentadiene and acrylonitrile. Unfortunately, the attempted synthesis of cross-linker **5.8** by reaction of 2-methylimidazole and 2 equivalents of the mesylate was unsuccessful, with only the monosubstituted imidazole **5.7** isolated (scheme 5.3). The failure to add the second norbornene unit was attributed to the sterically congested environment around the imidazole ring and, as such, monomer **5.8** was deemed unviable. Formation of a linear polymer using a 2 : 1 ratio of **5.5** to **5.6** was attempted using Grubbs 2nd generation catalyst, however, the reaction was observed to be incredibly slowly, with poor incorporation of the nitrile monomer. This poor polymerisation performance was thought to be caused by coordination of both the imidazolium ring and nitrile group to the Ru metal, leading to catalyst deactivation as discussed in chapter 2. In order to overcome this deactivation effect it would be necessary to prepare **5.5** as the *exo*-isomer rather than the *endo*-form given by the initial Diels-Alder reaction. Although the use of ROMP affords a greater design potential for PIILP based materials, this particular system requires considerable development if it is to be used as a viable means to prepare suitable polymers. Due to the poor performance of the polymerisation reaction, the inability to prepare the desired cationic cross-linker as well as the difficulty in the

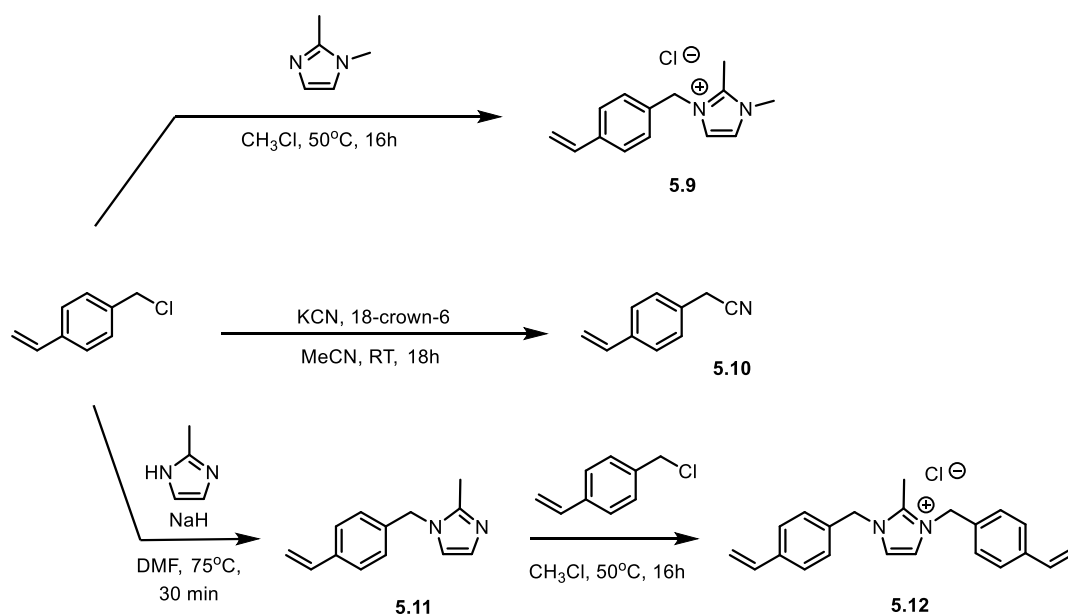
preparation and handling of **5.5**, which was highly hygroscopic as both the mesylate and chloride, it was decided to investigate alternate polymerisation methods. To this end, the implementation of the PIILP concept in the preparation of nanoparticle was to be investigated as a proof of principle exercise, rather than undertaking an extensive polymer development project.



Scheme 5.3 Synthesis of the norbornene-based co-monomer **5.6** and cross-linker **5.8**

In chapters 2 and 4 analogous polystyrene-based PIILP materials were shown to behave similarly to their ROMP-based counterparts and, in the case of Cu-catalysed Diels-Alder reactions, appeared to outperform the ROMP-based systems. Combining these observations with the extensive literature precedent for the use of free-radical initiated polystyrene-based PIL supports the styrene-based analogues of **5.5**, **5.6** and **5.8** were proposed (scheme 5.4). The desired methylimidazolium monomer **5.9** was prepared as an analytically pure white powder in an operationally straightforward single step reaction between 1,2-dimethylimidazole and 4-vinylbenzyl chloride. Similarly the nitrile functionalised co-monomer **5.10** could also be prepared in a single step from 4-vinylbenzyl chloride and potassium cyanide in the presence of 18-crown-6. Through deprotonation of 2-methylimidazole with NaH the intermediate **5.11** was obtained, which was then reacted with a second equivalent of 4-vinylbenzyl chloride to yield the cationic cross-linker **5.12**. The relatively straightforward synthesis of all three functionalised monomers highlights the advantageous nature of polystyrene chemistry as all monomers were obtained in high yield as stable, easy to handle solids, unlike the hygroscopic imidazolium-functionalised norbornene monomers. In addition to the straightforward synthesis, no considerations are needed with regards to *endo*- or *exo*-isomers within the polymer backbone as is the case with norbornene-based PIILP materials.

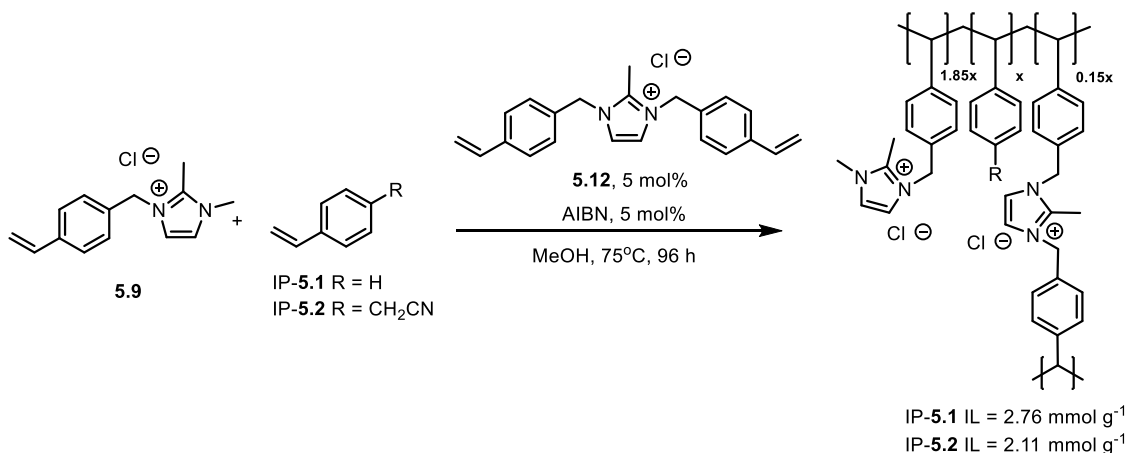
Following the preparation of the three functionalised monomers, two polystyrene-based PIILP supports were prepared through free radical-initiated polymerisation. 5 mol% AIBN was used as the initiator with an imidazolium to co-monomer ratio of 2 : 1, corresponding to an average of 2 IL fragments and 1 heteroatom donor per supported Pd atom in the desired polymer. Commercially available polystyrene-based ion exchange resins have been extensively investigated for the immobilisation of transition metal nanoparticles,⁴⁰ and lightly cross-linked resins were found to



Scheme 5.4 Synthesis of functionalised styrene monomers **5.9**, **5.10** and **5.12** from 4-vinylbenzyl chloride

develop microporous gels structures when swollen by solvent. This tendency to give microporous cavities is particularly suited to accommodate nano-sized materials,⁴¹ as such, a low degree of cross-linking of 5 mol% was selected in order to reproduce this effect (scheme 5.5). Two polymers were prepared in order to evaluate any added effects the presence of the nitrile functionality would have on forming nanoparticles and their catalytic behaviour, one using styrene as the sole co-monomer (IP-**5.1**) and one using **5.10** (IP-**5.2**). Initial attempts at polymerisation were conducted at a temperature of 75°C over 48 hours in the same fashion as the pyrrolidinium-based styrene polymers prepared in previous chapters. However, analysis of the resulting polymers by ¹H NMR spectroscopy showed significant amounts of vinylic protons corresponding to unreacted monomer for both the nitrile-functionalised and unfunctionalised systems. The polymerisations were repeated for an extended reaction time of 96 hours, before the addition of an extra equivalent of AIBN and a further 19 hours reaction. These modified conditions resulted in successful polymerisation of both IP-**5.1** and IP-**5.2**, obtained as white powders, with approximately 15% unreacted monomer present in both cases as evidenced by ¹H NMR. Size exclusion chromatography (SEC) trials were conducted on 200 mg samples of IP-**5.1** and IP-**5.2** in an attempt to remove residual unreacted monomer. Gratifyingly the chromatograms obtained for both polymers indicated largely monomodal molecular weight distributions, suggesting that the polymerisations proceeded with a negligible degree of unwanted termination and chain transfer events (example shown in figure 5.3). Removal of the highly UV active monomer containing fractions by chromatography successfully gave clean samples of both IP-**5.1** and IP-**5.2**, however, because of the large quantities of solvent required as well as the extensive time taken to achieve purification it was deemed unviable to conduct SEC on the larger samples of polymer

produced. To this end, both samples were redissolved and re-precipitated in diethyl ether twice, which reduced the amount of monomer present in both polymers to approximately 5%.



Scheme 5.5 Free-radical initiated polymerisation of **5.9** with functionalised and unfunctionalised co-monomers to give the cross-linked polymers **IP-5.1** and **IP-5.2**

While the presence of free monomer in the polymer samples could affect catalysis by providing different coordination environments for the supported nanoparticles, the small amounts present in the samples of **IP-5.1** and **IP-5.2** were believed to be not present in large enough quantities to significantly affect the supported metal. As well as this, the loading of Pd and subsequent reduction of the metal both involve precipitation steps, which would further reduce the amount of the more soluble monomer. As such the samples **IP-5.1** and **IP-5.2** were used without further purification.

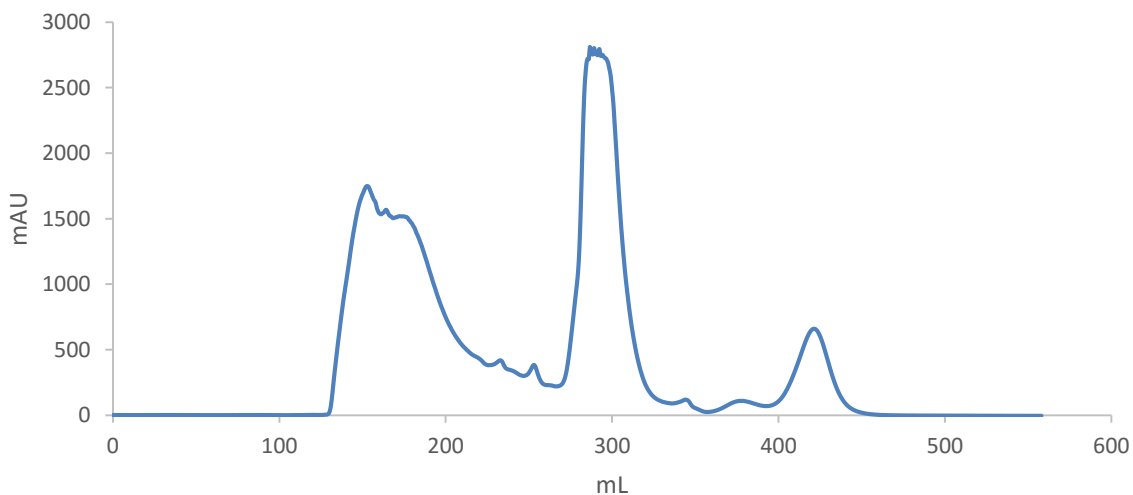


Figure 5.3 Chromatogram obtained at a wavelength of 254 nm for the SEC conducted on a sample of **IP-5.2**. Unreacted monomer was observed in fractions taken around the 300 mL mark and after 400 mL

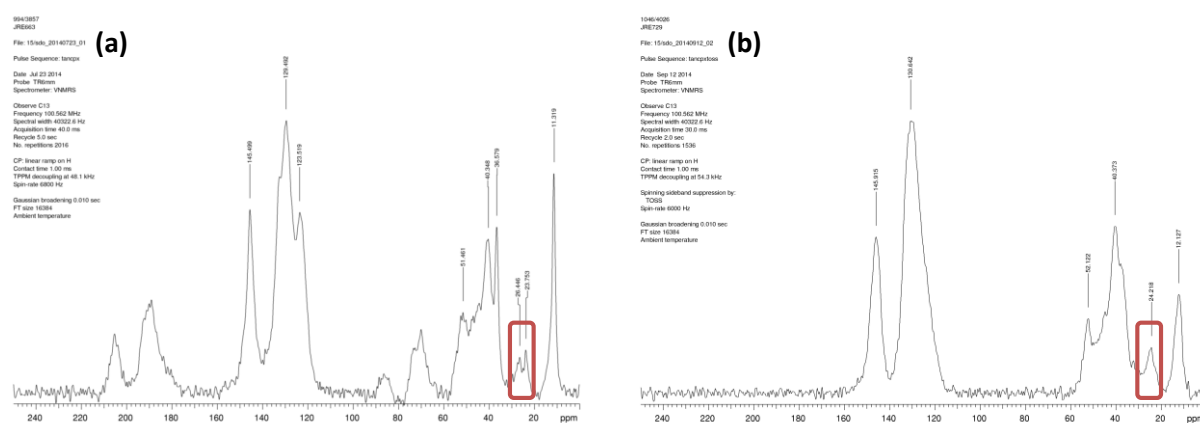
Elemental analysis of **IP-5.1** indicated an ionic liquid loading of 2.76 mmol g^{-1} , corresponding to a ratio of approximately 1.70 imidazolium cations, from both the monomer **5.4** and the cross-linker **5.7** incorporated in the polymer, to one styrene comonomer. Analysis of **IP-5.2** by 1H NMR spectroscopy allowed for comparison between the signals corresponding to the methyl groups of the imidazolium cation and the CH_2 group between the phenyl ring and nitrile group of the functionalised

monomer. Despite the broad nature of the signals in the spectra of the polymers, a ratio of 2.13 : 1 was determined for the imidazolium to nitrile content. Combining this result with the elemental analysis the ionic loading for IP-5.2 was estimated to be 2.11 mmol g⁻¹. Gratifyingly both the nitrile-functionalised system and its unfunctionalised counterpart appear to show good incorporation of all three of the desired co-monomers, however, the discrepancy in the imidazolium to co-monomer ratios observed for IP-5.1 and IP-5.2 again highlights the largely uncontrolled nature of free radical-initiated polymerisations. Due to the structural similarities of the monomer 5.9 and the cross-linker 5.12 it was also not possible to estimate the degree of cross-linking for both polymers. However, analysis of the monomer fractions isolated in the SEC experiments at the 300 mL mark and after 400 mL (figure 5.3) for both polymers suggested that 5.12 and 5.9 were present in similar amounts. As such it can be inferred that both these monomers exhibit similar activity towards polymerisation, and that the degree of cross-linking is of a comparable level to the 5% proposed by the reaction stoichiometry.

The straightforward, high-yielding synthesis of the three styrene-based monomers 5.9, 5.10 and 5.12 proved to be highly advantageous over the production of their norbornene-based analogues, as the latter were difficult to synthesise and handle and appeared to be inactive to the ROMP process. However, the harsh radical initiated polymerisation conditions required to give reasonable levels of reaction may not be able to accommodate more unstable heteroatom-functionalised co-monomers. This would imply that use of these styrene-based systems would not be entirely practical for extensive modification of PIILP in a bid to give optimum nanoparticle catalysts. As previously observed in earlier chapters, the free-radical initiated polymerisation also gives more ill-defined polymer materials, in contrast to the use of ROMP which consistently gave co-monomer ratios in agreement with the proposed formulations. To this end the use of ROMP offers significantly greater design potential as well as seemingly better defined materials, allowing for the methodical, rational and systematic modification of the PIILP support to allow for effective optimisation of the metal nanoparticle catalyst.

Following the preparation and characterisation of IP-5.1 and IP-5.2 the two polymers were to be loaded with a suitable metal precursor. Commonly Pd has been introduced to supports as either the neutral Pd⁰-containing Pd₂(dba)₃ or as Pd^{II} in the form of [PdCl₄]²⁻ which is subsequently reduced to form nanoparticles. While the use of Pd₂(dba)₃ allows for nanoparticle formation with just heating, the often rapid formation under decomposition can lead to larger nanoparticles with broader size distributions.⁴² As such we chose loading the polymer with Na₂PdCl₄ via ion exchange as there are a number of recent literature examples that use this method with similar IL-functionalised supports, including IL-functionalised CNTs,⁴³ cross-linked imidazolium-based microgels⁴⁴ and dicationic

imidazolium-functionalised polymers.²⁹ To this end, samples of IP-5.1 and IP-5.2 underwent complete ion exchange with Na₂PdCl₄. Estimation of the Pd loading by elemental analysis conducted on the resultant IP-5.1-PdCl₄ gave a Pd content of 9 wt%, corresponding to 0.87 mmol of Pd g⁻¹. Similar analysis and estimation of the Pd content of IP-5.2-PdCl₄ gave a Pd loading of 12 wt% corresponding to 1.16 mmol Pd g⁻¹. Interestingly, the presence of the nitrile functionality of IP-5.2 appears to have led to better Pd incorporation than its unfunctionalised counterpart IP-5.1. Solid state ¹³C NMR analysis conducted on IP-5.2 and the corresponding PdCl₄-loaded material (figure 5.4) indicated a direct interaction between the nitrile group and the Pd, as evidenced by the slight downfield shift of the signal corresponding to the CH₂ group adjacent to the nitrile. FT-IR analysis of IP-5.2 and IP-5.2-PdCl₄ further confirmed this by showing an increase in wavenumber for the signal corresponding to the CN stretch from 2254 cm⁻¹ to 2322 cm⁻¹ upon the introduction of PdCl₄. These changes in wavenumber are in agreement with previous observations made in the literature with other nitrile-functionalised ILs and Pd species. For example, a notable increase in the CN stretch wavenumber from 2244-2252 cm⁻¹ to 2319-2326 cm⁻¹ was observed in the immobilisation of PdCl₄ with a range of *N*-butyronitrile pyridinium ILs.^{22b} Similarly, the introduction of Pd(OAc)₂ to nitrile-functionalised



imidazolium ionic liquids showed an increase in the CN stretch from 2251 cm⁻¹ to 2359 cm⁻¹.³⁹

Figure 5.4 Solid state ¹³C NMR spectra for (a) IP-5.2 and (b) IP-5.2-PdCl₄. Signals corresponding to CH₂-CN highlighted for clarity. A shift downfield from 23.753 to 24.218 ppm was observed upon the introduction of Pd

Following the successful preparation and characterisation of IP-5.1-PdCl₄ and IP-5.2-PdCl₄ it was postulated that the ionic environment present in the PIILP supports would stabilise Pd nanoparticles and allow the active catalyst to be stored. To this end initial attempts to reduce the metal-loaded IP-5.1-PdCl₄ and IP-5.2-PdCl₄ were carried out by stirring a methanol suspension of the polymer and NaBH₄. While a colour change from orange to black, indicative of successful reduction of Pd^{II} to Pd⁰, was observed for both polymer supports a white solid by-product was also present. Theorised to be a mixture of NaCl and borates formed from the MeOH solvent these impurities

proved to be difficult to remove due to the partial solubility of the supported catalysts in alcohols and water. Due to the potentially sensitive nature of the supported nanoparticles, with regards to their shape and size, these impurities were deemed to be potentially detrimental as they could coordinate or interact with the metal surface and effect catalysis. Decreasing the solubility of the polymer supports, either by increasing the degree of cross-linking or increasing the hydrophobicity and alkyl character, would allow for easy separation of these borate impurities, however these differences to the polymer architecture will clearly have a profound effect on the nature of the nanoparticles. Issues such as these highlight one of the more limiting factors of the PIILP methodology, illustrating the need to finely balance the physical properties of the material whilst also considering the nature of the microenvironment which surrounds and stabilises the supported catalyst. Despite this fact, the controllable nature of polymer chemistry should allow for suitable alterations to be made in a rational manner, allowing for a highly efficient catalyst with the corresponding desirable material properties to be identified.

In order to obtain supported nanoparticles from IP-5.1-PdCl₄ and IP-5.2-PdCl₄ the reduction was instead conducted under 70 psi of hydrogen in MeOH. Again the colour change to black was observed for both polymer supports suggesting successful reduction of the Pd metal, and, under these conditions the solid white by-product was no longer observed. Elemental analysis of both the supported Pd catalysts after reduction showed little change in the relative ionic loading, implying that negligible leaching occurred during reduction. X-ray photoelectron spectroscopy (XPS) analysis was conducted on IP-5.1-Pd⁰ and IP-5.2-Pd⁰ in order to confirm the oxidation stage of the palladium in the sample (figure 5.5). Peak fitting conducted on the XPS spectra obtained for IP-5.1-Pd⁰ for the 3d_{5/2} and 3d_{3/2} binding energy regions showed that Pd^{II} accounted for 68% of the Pd in the sample indicating that only 32% of the metal had been reduced (figure 5.5 (a)). Interestingly, similar analysis of IP-5.2-Pd⁰ indicated that only 8% of the Pd had been reduced (figure 5.5 (b)). These observations would imply that the presence of the nitrile groups somehow inhibits the reduction, while simultaneously implying a direct interaction between the nitrile group and the Pd metal. The degree of reduction and apparent high composition of Pd^{II} in IP-5.1-Pd⁰ is in agreement with recent studies conducted on polymer supported nanoparticles produced by the NaBH₄ reduction of Na₂PdCl₄.²⁹ In this respect, it is largely accepted that the surface of metal nanoparticles are often functionalised with various different species such as oxides, hydrides and carbenes resulting from the reaction media,⁴⁵ which would in part account for the large amounts of Pd^{II} present in both catalysts. Indeed incomplete reduction of tetrachloropalladate to Pd⁰ during the synthesis of nanoparticles in the presence of polymer networks has been reported previously,⁴⁷ with the authors attributing this effect to poor accessibility of the Pd^{II} sites within the polymeric matrix or to air oxidation of the Pd⁰.⁴⁸

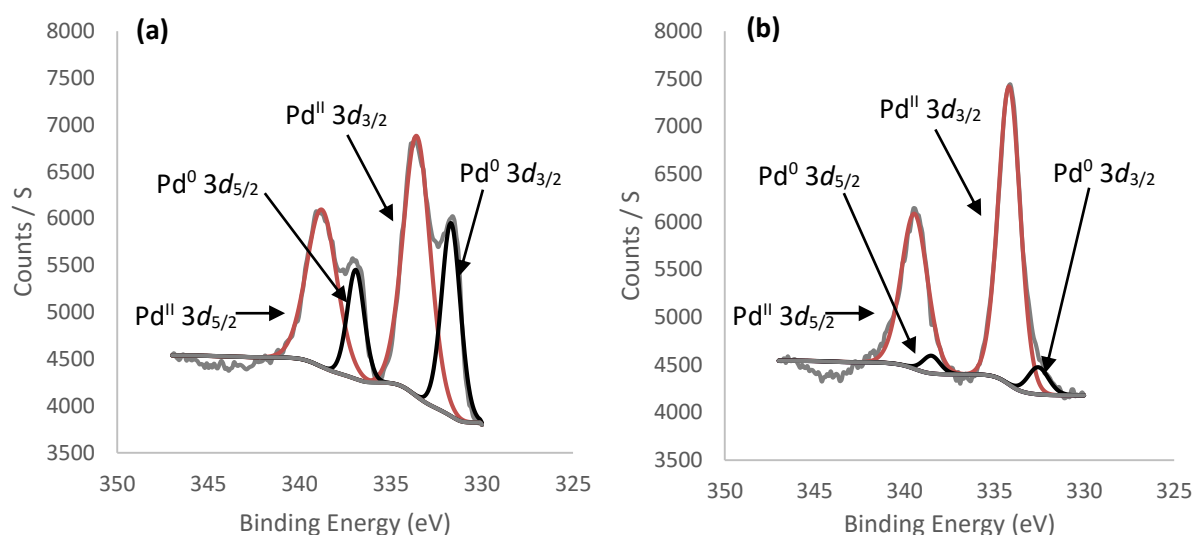


Figure 5.5 XPS spectra and corresponding peak fits for (a) IP-5.1-Pd⁰ and (b) IP-5.2-Pd⁰, assignments based on those recently published by Lemke *et al*⁴⁶

Transmission Electron Microscopy (TEM) images obtained for IP-5.1-Pd⁰ (figure 5.6 (a) and (b)) show the highly contrasting Pd nanoparticles with irregular spherical shapes surrounded by the more poorly contrasting polymer. Interestingly the well-defined particles appear to group together to form small clusters, rather than being dispersed throughout the entire sample (figure 5.6 (a)). This could be due in part to the largely uncontrolled nature in which IP-5.1 formed. In this regard, the random arrangement of monomers throughout each polymer chain could potentially give areas of high charge density due to poorly localised incorporation of the styrene co-monomer. Processing of the images obtained for IP-5.1-Pd⁰ showed a relatively broad, bimodal size distribution between 2 and 15 nm, with a particle size of 5 nm being the most abundant present (figure 5.6 (c)). The irregular spherical shape and size of the nanoparticles in IP-5.1-Pd⁰ is in agreement with general observations about nanoparticles formed by the reduction of Pd(II) with either NaBH₄ or hydrogen in ILs,⁴⁵ indicating that the ionic environment in the PIILP support may provide a similar mode of stabilisation and to comparable degrees to its IL counterpart. TEM images obtained for IP-5.2-Pd⁰ show a similar arrangement of particles (figure 5.6 (d) and (e)), despite the apparent lower content of Pd⁰ as suggested by the XPS analysis. Again the nanoparticles appear roughly spherical and seem to congregate in high concentration regions. Despite these similarities the nanoparticles in IP-5.2-Pd⁰ appear to have a slightly tighter size distribution, ranging from 2 to 11 nm (figure 5.6 (f)). As with IP-5.1-Pd⁰, particles of 5 nm were the most abundant within the sample, however, the size distribution for IP-5.2-Pd⁰ is considerably shifted towards smaller sizes, with a considerably larger proportion of particles between 2 and 4 nm. This shift towards smaller particles in IP-5.2-Pd⁰ could again be an indication that the nitrile groups interact directly with the Pd species and provide additional stabilisation with respect to agglomeration when compared with IP-5.1.

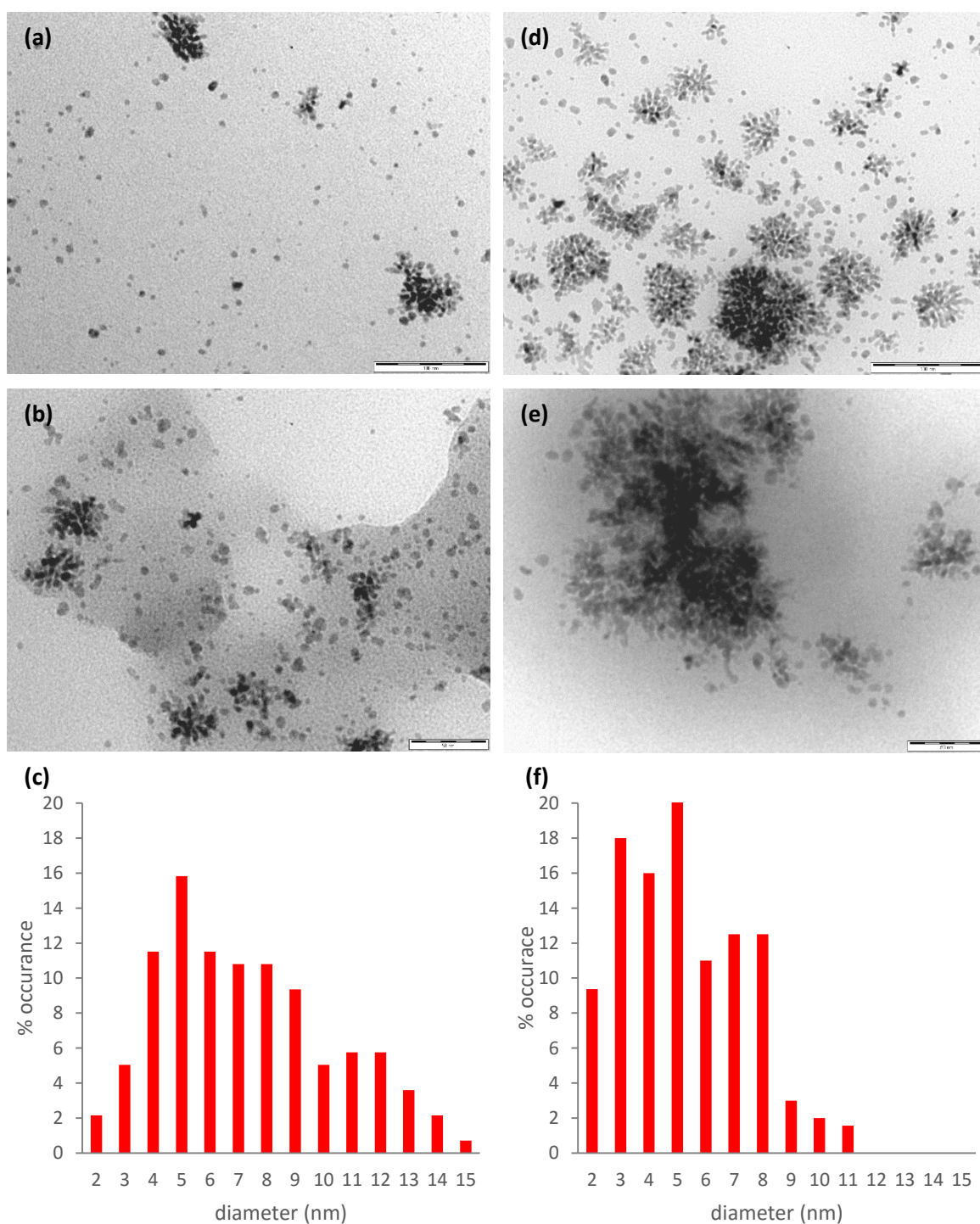


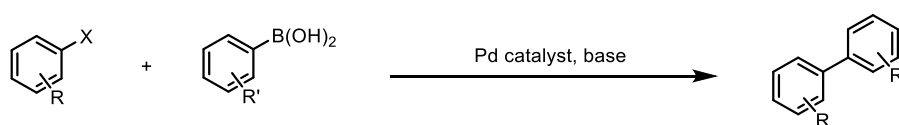
Figure 5.6 TEM images and corresponding size distributions for IP-5.1-Pd⁰ ((a) to (c)) and IP-5.2-Pd⁰ ((d) to (f))

While the nanoparticles present in IP-5.2-Pd⁰ are generally smaller than those in IP-5.1-Pd⁰ both systems exhibit relatively broad size distributions. This is likely due to the largely uncontrolled nature of free radical initiated polymerisation, which results in an ill-defined, random polymer morphology and microenvironment. Again, this highlights the possible benefits of using a well-defined, controlled living polymerisation such as ROMP, however, the synthetic difficulties associated

with these systems must be considered during future development. Interestingly, by comparison, a recent study using Pd supported on dicationic imidazolium divinylbenzene-based polymers for carbonylative Suzuki coupling gave a tight size distribution generally between 2 and 7 nm, with particles as small as 0.5 nm obtained under specific conditions.²⁹ Similarly cross-linked acrylamide-functionalised imidazolium microgels have also been used to generate Pd nanoparticles with tight size distributions.⁴⁴ The authors also reported that using NaBH₄ as the reducing agent gave much smaller nanoparticles as opposed to hydrogen, with the latter system giving an average particle size of 7 nm. Both these literature examples used imidazolium cations with C(2)-H. It is therefore probable that NHC formation occurs during the generation of the supported nanoparticles. While the use of a C(2)-Me group in IP-5.1 and IP-5.2 was proposed as a means to prevent non-innocent cation behaviour during catalysis, the lack of acidic imidazolium protons and the associated NHC formation may be responsible for the formation of slightly larger nanoparticles. This could be confirmed by preparing the corresponding C(2)-H imidazolium based polymers and the corresponding polymer immobilised ionic liquid stabilised palladium and undertaking a comparative study.

5.3.2. Suzuki-Miyaura Cross-Couplings

As discussed above Pd catalysis, in particular when used to achieve carbon-carbon bond formation, is a profoundly versatile, powerful tool throughout synthetic organic chemistry. Amongst the various different couplings possible (scheme 5.1), the Suzuki-Miyaura coupling between an aryl halide and an aryl boronic acid (scheme 5.6) is viewed as one of the most important transformations in biaryl synthesis.⁴⁹ In this regard, biaryls are versatile building blocks in liquid crystal, pharmaceutical, conducting polymer, herbicide and natural product applications.⁵⁰

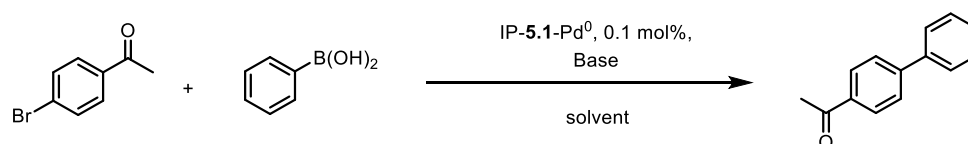


Scheme 5.6 Pd-catalysed Suzuki-Miyaura cross-coupling between aryl halides and aryl boronic acids in the presence of base

Pd nanoparticles have been successfully used as catalysts in Suzuki couplings whilst immobilised on a variety of IL-functionalised supports, for example, in mesoporous silica frameworks functionalised with imidazolium cations⁵¹ and guanidinium-grafted poly(*p*-phenylene) microspheres.⁵² In both cases the authors report efficient, recyclable catalysis across a range of aryl iodides, bromides and even the more challenging chlorides,^{50c} with the former attributing the recyclability of the Pd nanocatalysts to the ordered support structure which acted as a nanoscaffold, effectively catching and releasing active Pd during reaction. More recently highly cross-linked

imidazolium-modified silica was used to give an efficient catalyst which was utilised in a novel, bespoke continuous flow reaction.⁵³ Jiao *et al* have also reported that the ionic loading of dicationic imidazolium divinylbenzene-based polymer supports, as well as the introduction of additional amino groups, has a profound effect on nanoparticle size and performance in carbonylative Suzuki couplings.²⁹ To this end, the Suzuki-Miyaura coupling of arylhalides with boronic acids was identified as an ideal means to evaluate the newly prepared PIILP Pd nanoparticle catalysts.

Initially the evaluation of PIILP nanoparticles focused on the unfunctionalised IP-5.1-Pd⁰, reasoning that this would act as a control and allow the effect of the nitrile groups of IP-5.2 on catalysis to be determined under optimum conditions. In order to screen appropriate conditions the Suzuki coupling between 4-bromoacetophenone and phenylboronic acid (scheme 5.7) was selected as a model reaction for optimisation due to the relatively short reaction times required to achieve high conversion.



Scheme 5.7 Suzuki-Miyaura cross-coupling between 4-bromoacetophenone and phenylboronic acid catalysed by IP-5.1-Pd⁰

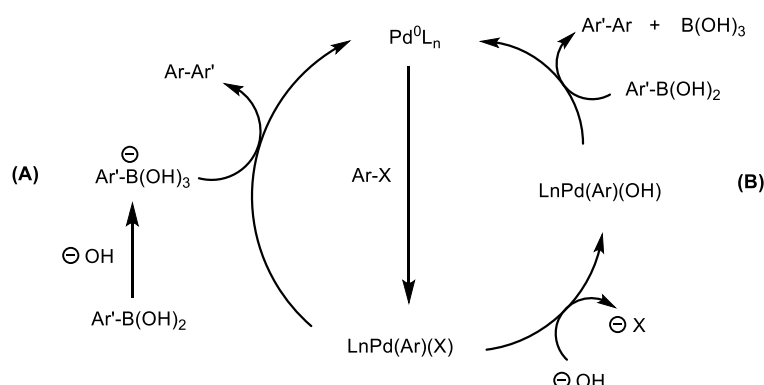
In order to ensure an optimum balance between catalyst performance and the green credentials of the reaction system a full solvent screen was conducted (table 5.1). Poor conversions were obtained in a range of protic and aprotic solvents under mild conditions, with a slight excess of base and phenylboronic acid and a catalyst loading of 0.1 mol% (entries 1-5). Catalyst performance appears to improve in polar, protic solvents with ethylene glycol giving a conversion of 80% under mild conditions in just 30 minutes (entry 6). It is possible that the improvement in performance for reactions conducted in polar protic solvents could, in part, be the result of polymer swelling,

Table 5.1 Solvent effect in the Suzuki-Miyaura coupling of 4-bromoacetophenone and phenylboronic acid catalysed by IP-5.1-Pd^{0a}

entry	solvent	% conv ^b
1	EtOH	36
2	H ₂ O	32
3	toluene	2
4	THF	0
5	DMF	15
6	EG ^c	80
7	EtOH-H ₂ O ^d	88
8	toluene-H ₂ O ^d	7
9	THF-H ₂ O ^d	25
10	EG-H ₂ O ^{c,d}	49

^aReaction conditions: 0.1 mol% catalyst based on repeat unit, 1 mmol 4-bromoacetophenone, 1.13 mmol phenylboronic acid, 1.2 mmol K₂CO₃, 2.4 mL solvent, 30°C, 0.5 h. ^bDetermined by GC of reaction mixture with n-decane as an internal standard. ^cEG = ethylene glycol. ^d50:50 mixture.

allowing ready access to the active Pd centres within the porous polymer network of IP-5.1. Interestingly the addition of water as a co-solvent in a 1 : 1 volume ratio resulted in a significant improvement in catalyst performance, with the exception of ethylene glycol which gave a marked decrease in conversion (entry 10). The most profound increase in performance was observed when EtOH was used as the co-solvent which gave the highest observed conversion of 88%. The optimum performance of the EtOH-H₂O system is in keeping with recent work conducted with highly cross-linked imidazolium supported Pd nanoparticles; in this case the authors attributed the high activity to the co-solvent's ability to effectively dissolve both the organic reagents and the inorganic base.⁵³ In addition to this, investigations into the catalytic cycle involved in traditional Suzuki couplings with homogeneous catalysts in water-containing solvent systems in the presence of base leads to the *in situ* formation of [OH]⁻ anions. The presence of these hydroxide anions is thought to be directly involved in the transmetalation step of the catalytic cycle, either by displacement of the halide species from the Pd(II) centre to give PdOH complexes, or by direct attack to the arylboronic acid (scheme 5.8).⁵⁴ As such it is reasonable to suggest that the water present in the reaction mixtures of table 5.1 play an integral role in catalysis whilst also providing additional reagent solubility effects.



Scheme 5.8 Catalytic cycle for Pd-catalysed Suzuki-Miyaura cross couplings, proceeding through transmetalation via (A) direct attack of hydroxide to the boronic acid, and (B) by generation of a PdOH complex

Following the observed positive role water plays on the performance of IP-5.1-Pd⁰ in the Suzuki coupling of 4-bromoacetophenone an investigation into the effect of water content in EtOH-based solvent systems was undertaken (table 5.2). Catalyst performance increases significantly upon the introduction of water in a 3 : 1 EtOH : H₂O mixture, with the conversion increasing from 36% to 80% (entries 1 and 2); a further increase in conversion to 88% was obtained with the 50 : 50 EtOH : H₂O system. A further increase in the water content of the solvent system had a deleterious effect on catalyst performance and the conversion decreased dramatically to 56% at a water content of 75%. It is likely that the poor results obtained for higher water contents is a direct result of the poor solubility of the organic reagents used, which were observed to not fully dissolve during the reaction.

As such 50 : 50 EtOH : H₂O was identified as the optimum solvent system, and was used for all further Suzuki couplings.

Table 5.2 Effect of water content in the IP-5.1-Pd⁰-catalysed Suzuki coupling of 4-bromoacetophenone and phenylboronic acid in EtOH^a

entry	EtOH : H ₂ O	% conv ^b
1	100 : 0	36
2	75 : 25	80
3	50 : 50	88
4	25 : 75	57
5	0 : 100	32

^aReaction conditions: 0.1 mol% catalyst based on repeat unit, 1 mmol 4-bromoacetophenone, 1.13 mmol phenylboronic acid, 1.2 mmol K₂CO₃, 2.4 mL solvent, 30°C, 0.5 h. ^bDetermined by GC of reaction mixture with n-decane as an internal standard.

The initial evaluation of reaction conditions for the PIILP Pd nanoparticle systems employed potassium carbonate as the base due to its ubiquitous use in Suzuki-Miyaura coupling chemistry.⁵⁵ In order to ensure optimum catalyst performance with regards to conversion additional bases were also screened (table 5.3). Unsurprisingly, and in keeping with literature precedent, the carbonate bases gave the most efficient systems,^{29, 56} with potassium carbonate giving the best conversion (entries 7 to 8). As such potassium carbonate was selected as the base of choice for all further Suzuki couplings.

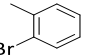
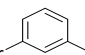
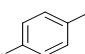
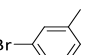
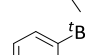
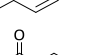
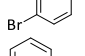
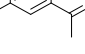
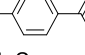
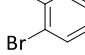
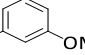
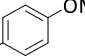
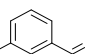
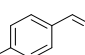
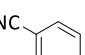
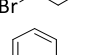
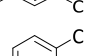
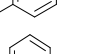
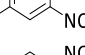
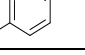
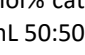

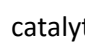
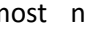
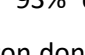
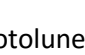




Table 5.3 Effect of base in the IP-5.1-Pd⁰-catalysed Suzuki coupling of 4-bromoacetophenone and phenylboronic acid^a

entry	base	% conv ^b
1	NaOAc	19
2	CsOAc	17
3	NBu ₃	5
4	K ₃ PO ₄	68
5	CsF	43
6	NaHCO ₃	53
7	Na ₂ CO ₃	77
8	K ₂ CO ₃	88
9	Cs ₂ CO ₃	85

^aReaction conditions: 0.1 mol% catalyst based on repeat unit, 1 mmol 4-bromoacetophenone, 1.13 mmol phenylboronic acid, 1.2 mmol base, 2.4 mL 50:50 EtOH:H₂O solvent, 30°C, 0.5 h. ^bDetermined by GC of reaction mixture with n-decane as an internal standard.

With the optimum reaction conditions in hand, the efficiency of IP-5.1-Pd⁰ and IP-5.2-Pd⁰ was evaluated for the coupling between a range of aryl bromides and phenylboronic acid; comparative catalyst testing was also undertaken with the Pd(II) loaded IP-5.1-PdCl₄ and IP-5.2-PdCl₄ (table 5.4). Under mild reaction conditions of 30°C and a catalyst loading of 0.1 mol% with respect to Pd, IP-5.1-Pd⁰ gave varying performance across the range of substrates, varying from very poor to excellent. The initial oxidative addition of the aryl halide to the Pd⁰ centre is largely accepted to be the rate

Table 5.4 Suzuki-Miyaura cross-couplings of arylbromides with phenylboronic acid catalysed by PIIIP catalysts based on IP-5.1 and IP-5.2^a

entry	substrate	time (h)	support	Pd ⁰ Np ^{b,c}	PdCl ₄ ^c
1		16	IP-5.1	43	41
2		16	IP-5.2	44	37
3		6	IP-5.1	66	54
4		6	IP-5.2	69	58
5		6	IP-5.1	58	72
6		6	IP-5.2	66	64
7		19	IP-5.1	38	16
8		19	IP-5.2	41	31
9		19	IP-5.1	41	16
10		19	IP-5.2	49	46
11		16	IP-5.1	35	28
12		16	IP-5.2	34	31
13		19	IP-5.1	2	6
14		19	IP-5.2	9	10
15		0.5	IP-5.1	88	98
16		0.5	IP-5.2	93	91
17		19	IP-5.1	39	78
18		19	IP-5.2	53	71
19		6	IP-5.1	65	66
20		6	IP-5.2	66	66
21		5	IP-5.1	72	74
22		5	IP-5.2	60	54
23		16	IP-5.1	38	81
24		16	IP-5.2	82	70
25		0.5	IP-5.1	96	>99
26		0.5	IP-5.2	99	99
27		4	IP-5.1	74	43
28		4	IP-5.2	77	79
29		4	IP-5.1	79	>99
30		4	IP-5.2	>99	>99
31		0.5	IP-5.1	90	99
32		0.5	IP-5.2	57	92
33		4	IP-5.1	93	>99
34		4	IP-5.2	89	>99
35		4	IP-5.1	95	89
36		4	IP-5.2	94	98

^aReaction conditions: 0.1 mol% catalyst based on repeat unit, 1 mmol arylbromide, 1.13 mmol phenylboronic acid, 1.2 mmol K₂CO₃, 2.4 mL 50:50 EtOH:H₂O solvent, 30°C. ^bNp = nanoparticle. ^cDetermined by GC of reaction mixture with n-decane as an internal standard.

determining step in the catalytic cycle.^{49b} To this end, coupling of electron-deficient aryl halides proceeds efficiently, most notably 4-bromoacetophenone gave 88% conversion while 4-bromobenzonitrile gave 93% conversion in just 30 minutes (entries 15 and 31 respectively). Conversely, mildly electron donating groups on the aryl bromide resulted in deactivation, as shown in the case of 4-bromotoluene which only reached 58% conversion in 6 hours (entry 5). The performance of IP-5.1-Pd⁰ appears to be highly sensitive to steric effects, with *meta*- and, particularly,

ortho-substituents decreasing conversions, for example, the sterically demanding 5-bromo-*m*-xylene gave a conversion of only 38% even after a prolonged reaction time of 19 hours (entry 7). While the activity of IP-5.1-Pd⁰ generally follows the expected trend with regards to the substituent effects of the arylbromide, substrate specific anomalies are apparent. Most notably the Suzuki-Miyaura coupling of 3-bromoacetophenone gave negligible conversion (entry 13) under mild conditions with attempts to improve catalyst performance with elevated reaction temperatures failing.

Interestingly, catalysis conducted with IP-5.2-Pd⁰ appears to proceed very similarly, giving comparable performance and similar reactivity trends across the range of substrates tested, with only a few differences in performance. Most notably IP-5.2-Pd⁰ gave a significantly better performance than its unfunctionalised counterpart in the coupling of 3-bromobenzaldehyde, giving a conversion of 82% compared to just 38% under the same conditions (entries 23 and 24). Similarly IP-5.2-Pd⁰ gave a notable increase in performance for the coupling of 3-bromobenzonitrile which reached complete conversion compared with the 79% achieved using IP-5.1-Pd⁰ (entries 29 and 30). Conversely, a significant decrease in performance was observed in the coupling of 4-bromobenzonitrile as the reaction only reached 57% conversion compared with 90% for IP-5.1-Pd⁰ (entries 31 and 32). Despite an apparent difference in the composition of Pd nanoparticles between IP-5.1-Pd⁰ and IP-5.2-Pd⁰, as evidenced by the lower ratio of Pd⁰ by XPS and the seemingly narrower particle size distribution from the TEM images (figures 5.4 and 5.5, respectively), the presence of the nitrile groups appears to have no overriding influence on catalytic performance. In this regard, the difference in catalyst activity appears to be much more subtle and substrate specific. The similar performance of the seemingly very different nanoparticle catalysts could, in part, be the result of *in situ* reduction of the Pd (II). As such, although it will be extremely challenging, it will be necessary to conduct further studies into the nature of the mechanism and the influence and eventual fate of the Pd within the system if PIILP based catalysts are to be properly utilised.

Although only moderate performance of IP-5.1-Pd⁰ and IP-5.2-Pd⁰ under mild reaction conditions was observed, the two PIILP catalysts appear to compare reasonably favourably with recent reports in the literature. For example, Li and co-workers have reported that Pd nanoparticles immobilised on imidazolium functionalised mesoporous silica networks catalyse the Suzuki coupling of a similar range of aryl bromides under comparable reaction conditions, albeit at higher reaction temperatures and in the presence of more base in water.⁵¹ Similar conversion to both PIILP catalysts were obtained for 4-bromoacetophenone and 4-bromotoluene (entries 5, 6, 13 and 14) but higher reaction temperatures, longer times and a catalyst loading of 0.2 mol% were required. Despite the need for more forcing conditions, these catalysts successfully couple more challenging substrates including a range of aryl chlorides; a feat which has only been achieved by a few solid catalysts.⁵⁷ More

recently highly cross-linked imidazolium networks were reported to catalyse coupling between a range of aryl bromides and iodides under the same reaction conditions used in table 5.4. The catalyst is highly active and required only a slightly elevated temperature of 50°C compared to the 30°C used above.⁵³ However, unlike the two PIILP catalysts reported herein, these systems were able to efficiently catalyse the Suzuki coupling of sterically more demanding substrates such as 2-bromotoluene and 5-bromo-*m*-xylene to near completion.

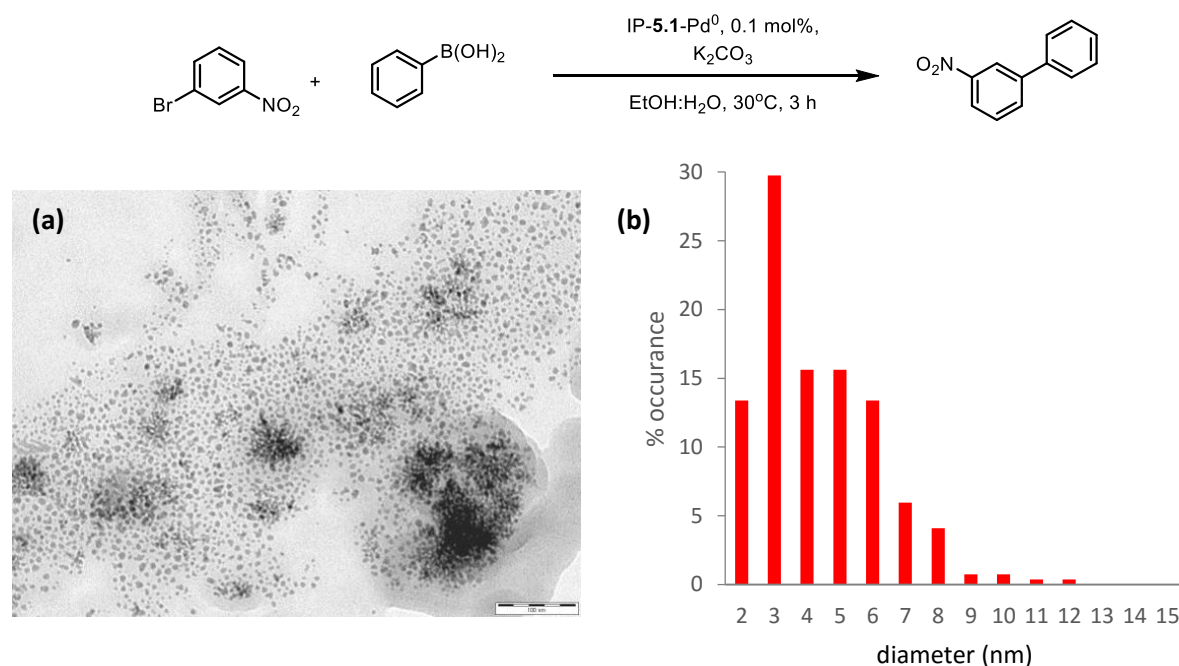


Figure 5.7 TEM image and corresponding nanoparticle size distribution for IP-5.1-Pd⁰ taken after catalysis in the Suzuki coupling of 3-bromonitrobenzene and phenylboronic acid.

In order to determine the influence of the PIILP microenvironment on the supported Pd nanoparticles during catalysis with regards to agglomeration *ex situ* studies were undertaken for the Suzuki coupling of 3-bromonitrobenzene catalysed by IP-5.1-Pd⁰ (table 5.4, entry 33); this reaction was chosen because of the relatively short reaction time and the high solubility of both the reagents and product in the reaction solvent. After a time of 3 hours a small fraction of the reaction mixture was dried and analysed by TEM, the results of which are summarised in figure 5.7. As with the sample of IP-5.1-Pd⁰ analysed before catalysis (figure 5.6), the nanoparticles appear to retain their irregular spherical shape as well as the tendency for individual nanoparticles to cluster in relatively small regions. Interestingly, processing of the TEM image showed that both the modal particle size and the size distribution decreased significantly (figure 5.7 (b)), while the size distribution also appears to be more monomodal. While this apparent decrease in nanoparticle size seems counterintuitive with regards to phenomena like Ostwald ripening, one possible explanation for this observation arises from the catalytic mechanism. The precise nature by which nanoparticles catalyse coupling reactions has been the subject of intense debate over the past decade.⁵⁸ In this regard there are two prevailing

theories; the first involves a heterogeneous mechanism in which both the oxidative addition and transmetalation steps of the catalytic cycle occur on the surface of the nanoparticle.^{52, 58-59} The second possibility involves extraction of active molecular Pd from the nanoparticles which act as a reservoir.^{58, 60} While there have been numerous compelling arguments for both mechanisms, it is likely that both occur simultaneously for a given system, with the reaction conditions used, as well as the nature of the nanoparticle stabilising agent, determining which pathway is dominant (figure 5.8).⁵⁸ When functionalised solid supports, such as the PIILP materials IP-5.1 and IP-5.2, are used the release of molecular Pd is believed to be followed by redistribution to reform the nanoparticles, often described as a “catch and release” system.^{57f, 61} The results obtained from the *ex situ* analysis of IP-5.1-Pd⁰ would indeed suggest such a system is in play, with the excess of substrate present supplying an additional stabilisation effect during the redistribution and reformation of nanoparticles, preventing agglomeration. A similar observation has been made with resin-supported Pd nanoparticles used in the hydrogenation of various industrially relevant substrates, including 3-hexyn-1-ol. The nanoparticles formed by *in situ* reduction of the metal precursor under catalytic conditions were found to be much smaller than those in the pre-reduced catalyst. The authors speculate that the excess of substrate present during catalysis further restricts the growth of the forming nanoparticles.⁶²

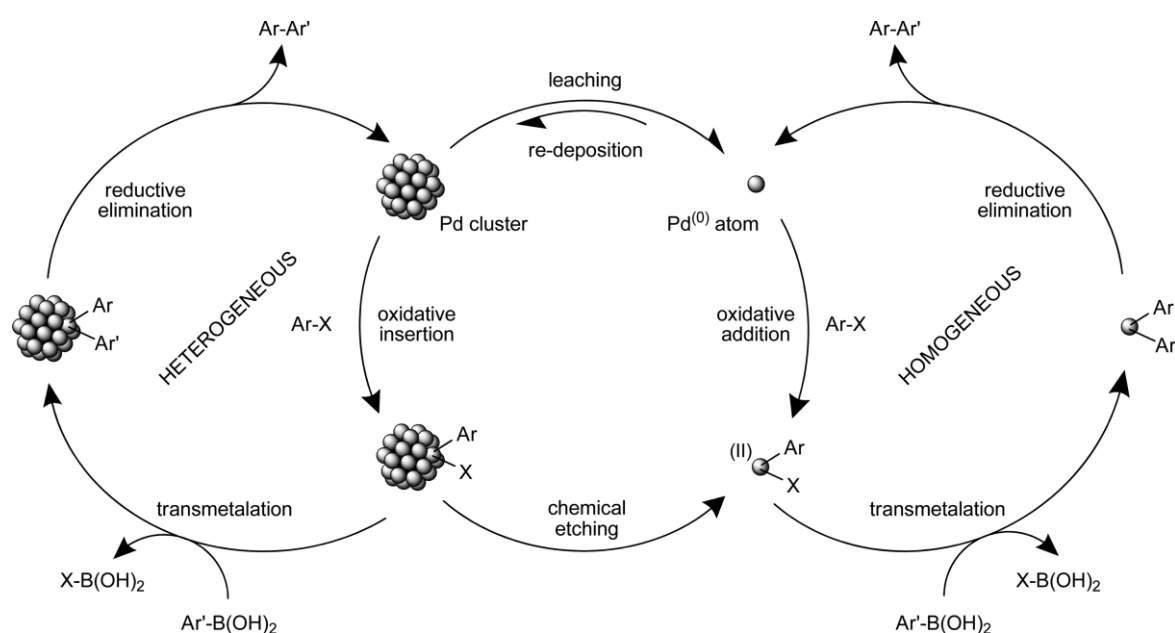


Figure 5.8 Mechanism of the Pd nanoparticle-catalysed Suzuki cross-coupling involving both homogeneous and heterogeneous pathways proposed by Pérez-Lorenzo⁵⁸

The seemingly comparable performance of the two PIILP nanoparticle catalysts, despite the notably different content of Pd⁰, together with the results from the *ex situ* analysis conducted on IP-5.1-Pd⁰ would imply *in situ* reduction of the Pd (II) metal during catalysis, most likely *via* a reductive elimination mechanism with the boronic acid.⁶³ To this end the substrate screen was repeated using catalyst precursors IP-5.1-PdCl₄ and IP-5.2-PdCl₄ (table 5.4). Interestingly, both catalysts gave

comparable performance to their reduced counterparts, showing similar reactivity trends throughout the substrate scope with only a few exceptions. For selected substrates the catalyst generated *in situ* from supported PdCl₄ appears to outperform pre-reduced species, for example, catalyst generated from IP-5.1-PdCl₄ gave 78% conversion for the coupling of 2-bromoanisole, which was a marked improvement on the 39% achieved with IP-5.1-Pd⁰ (entry 17). As the active Pd⁰ centres are generated *in situ* from Pd^{II} it would be reasonable to expect an induction period for reduction of the palladium. This effect would be most evident with shorter reaction times; however, this does not appear to be the case between the supported Pd⁰ and PdCl₄ catalysts. In fact, IP-5.1-PdCl₄ and IP-5.2-PdCl₄ appear to achieve similar degrees of conversion in rapid reactions, such as 4-bromoacetophenone, 4-bromobenzaldehyde and 4-bromobenzonitrile, often even outperforming their pre-reduced counterparts (entries 15, 16, 25, 26, 31 and 32). Similar observations have been reported by Barbaro *et al.* in a series of hydrogenation reactions catalysed by Pd nanoparticles supported on polystyrene-based ion exchange resins.^{62a} The authors postulate that the lack of an induction period when using Pd^{II} as the catalyst is the result of partially reduced Pd species, which are present in minimal amounts and exhibit very high activity during the early stages of reaction. To this end, there is existing literature precedent for the apparent ability of functionalised polymers to stabilise monovalent or mixed-valence metastable Pd species, often dubbed “Pd^{δ+}” or “Pd clusters”.⁶⁴ These partially reduced species often exhibit much higher activity than standard Pd⁰ centres.⁶⁵ As such, it can be argued that the comparable, sometimes enhanced, performance of the two PdCl₄ PIILP catalysts is the result of fast, partial reduction of Pd^{II} to the metastable Pd^{δ+} under the catalytic conditions used in the Suzuki couplings.

While the presence of the nitrile groups of IP-5.2 seemingly had little effect on catalysis, their apparent influence over the formation of Pd nanoparticles from PdCl₄, as evidenced by the XPS and TEM data obtained above, cannot be ignored. To this end, one would expect markedly different catalytic performance as there is strong evidence for the *in situ* reduction and formation of Pd nanoparticles. However, the results obtained in table 5.4 clearly show no distinct trends in activity between the two PIILP catalysts across the substrate range. This in turn highlights the complex nature of the interaction between the Pd metal, ionic microenvironment of the PIILP support and the reacting substrates during the catalytic cycle. In order to further probe the *in situ* reduction of the supported PdCl₄, TEM analysis was conducted on samples of IP-5.1-PdCl₄ and IP-5.2-PdCl₄ exposed to catalytic conditions in the absence of the aryl bromide (figure 5.9). The excess of phenylboronic acid under catalytic conditions with both PIILP supports appears to favour the formation of smaller nanoparticles whilst also giving a significantly narrower size distribution compared to the pre-reduced supported nanoparticles generated by hydrogenation (figure 5.7). Again, these observations are in keeping with a previous report by Barbaro *et al* in which resin-supported Pd nanoparticles formed *in*

situ are notably smaller than their pre-reduced counterparts.^{62a} As with the formation of the PIILP-supported pre-reduced nanoparticles, the presence of the nitrile groups of IP-5.2 appears to have a minor effect on the forming nanoparticles, resulting in a slightly higher proportion of smaller particles compared to those supported by IP-5.1 (figure 5.9 (d) and (c) respectively).

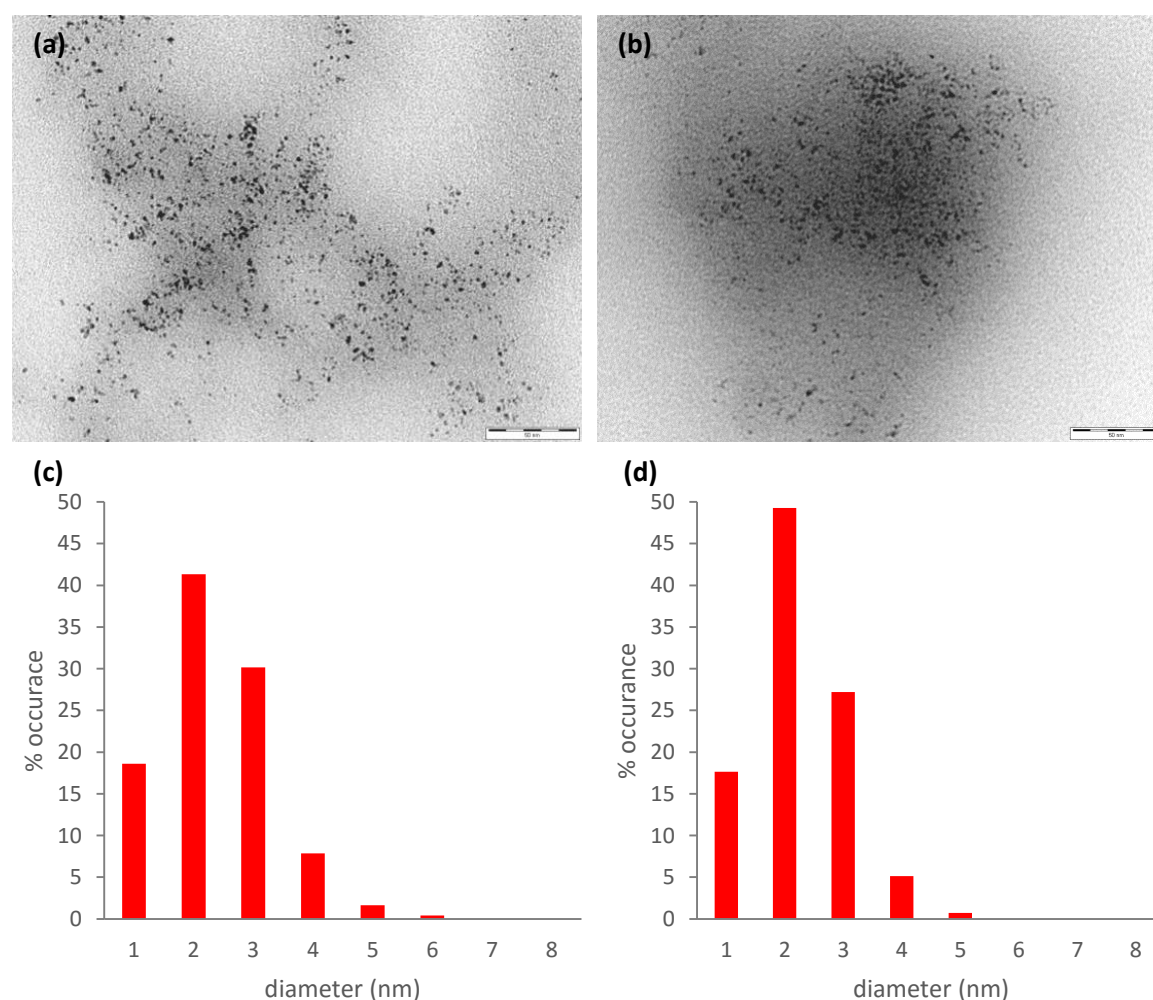


Figure 5.9 TEM images and corresponding size distributions for nanoparticles generated from IP-5.1-PdCl₄ ((a) and (c)) and IP-5.2-PdCl₄ ((b) and (d)) in the presence of phenylboronic acid under catalytic conditions

The evidence gathered from TEM images of the PIILP catalysts, both from the *ex situ* analysis and from the *in situ* nanoparticle formation in the absence of electrophile, clearly shows the formation of Pd⁰ nanoparticles under catalytic conditions. To this end, additional experiments were conducted in order to determine the effect of metal loading and reaction dilution, rationalising that both factors would have an effect on nanoparticle formation, and hence catalyst performance. Again both pre-reduced Pd nanoparticles and the PdCl₄ precursor supported on IP-5.1 were selected as the model systems for this study, with investigations focusing on the Suzuki coupling of 4-bromotoluene. Initially the reaction volume was varied between 0.5 volumes with respect to the standard conditions used above up to 3 volume equivalents (figure 5.10 (a)). For both IP-5.1-PdCl₄ and IP-5.1-Pd⁰ a notable

decrease in performance was observed at lower volumes, which appears to improve to a maximum conversion of about 80% at a volume of 3.6 mL upwards. One possible explanation for this observation is the closer proximity of the Pd metal centres, be it within the PIIIP architecture or in the form of leached species, leading to the formation of a greater proportion of larger, less active Pd nanoparticles. Interestingly, however, the decreased performance at lower volumes is much more profound for the pre-reduced catalysts than the supported PdCl₄, implying that the effect could in fact be due to agglomeration of the Pd⁰ nanoparticles. Furthermore, the performance of both catalysts appears to reach a maximum and shows no obvious decrease at higher reagent dilutions as one would expect. In order to fully investigate these systems it will be necessary to conduct further dilution studies in order to determine the point at which a decrease in catalytic performance is observed.

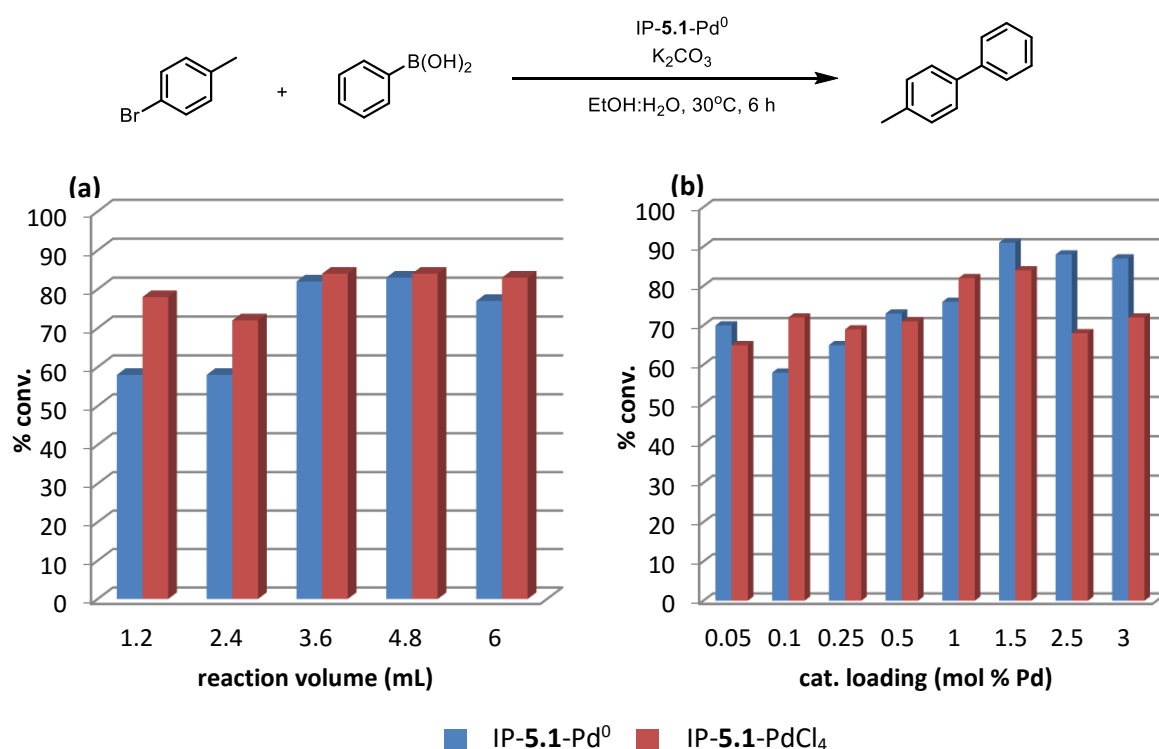


Figure 5.10 Effect of (a) solvent volume and (b) catalyst loading on the Suzuki Miyaura coupling of 4-bromotoluene with phenylboronic acid catalysed by IP-5.1-Pd⁰ and IP-5.1-PdCl₄

In a similar manner the effect of Pd loading was also investigated for both IP-5.1-based catalysts (figure 5.10 (b)). Again, as expected, there appears to be a distinct general increase in conversion with increasing catalyst loading for both systems. However, optimum performance appears to be achieved at a loading of 1.5 mol%, at higher loadings conversions appear to plateau for the pre-reduced catalyst but decrease for the PdCl₄ system. These observations further support the *in situ* reduction of Pd(II) and the aforementioned generation of highly active Pd^{δ+} species.⁶⁵ In this regard, the efficiency of pre-reduced IP-5.1-Pd⁰ drops at lower loadings which may reflect a straightforward dependence on the relative concentration of the active species. Conversely for IP-

5.1-PdCl₄, in which the active species forms *in situ*, increased catalyst loadings appear to have a deleterious effect on performance which may be associated with the formation of larger, less active nanoparticles.

The results gathered in table 5.4 showed that catalysts supported on both PIILP materials IP-5.1 and IP-5.2 gave a comparable, mixed performance over the range of coupling partners investigated, while the Suzuki couplings of more sterically and electronically challenging substrates appears to stall, with no improvement in conversion after prolonged reaction times. In order to determine the nature of the reaction rate for these systems, as well as to probe the differences which occur due to *in situ* nanoparticle formation for the PdCl₄ systems, a series of kinetic studies were undertaken. Again IP-5.1 was selected as the model support and our investigations focussed on the Suzuki-Miyaura coupling of 4-bromotoluene, 4-bromobenzonitrile, 2-bromotoluene and 3-bromonitrobenzene as a representative sample of the full substrate scope. Examples of the data gathered for the two extreme cases, *i.e.* poor performance with 2-bromotoluene and highly efficient coupling with 4-bromobenzonitrile, are shown in figure 5.11, with the full data sets presented in appendix A.4. For both reactions the PdCl₄ catalyst appears to show a more rapid initial rate than its

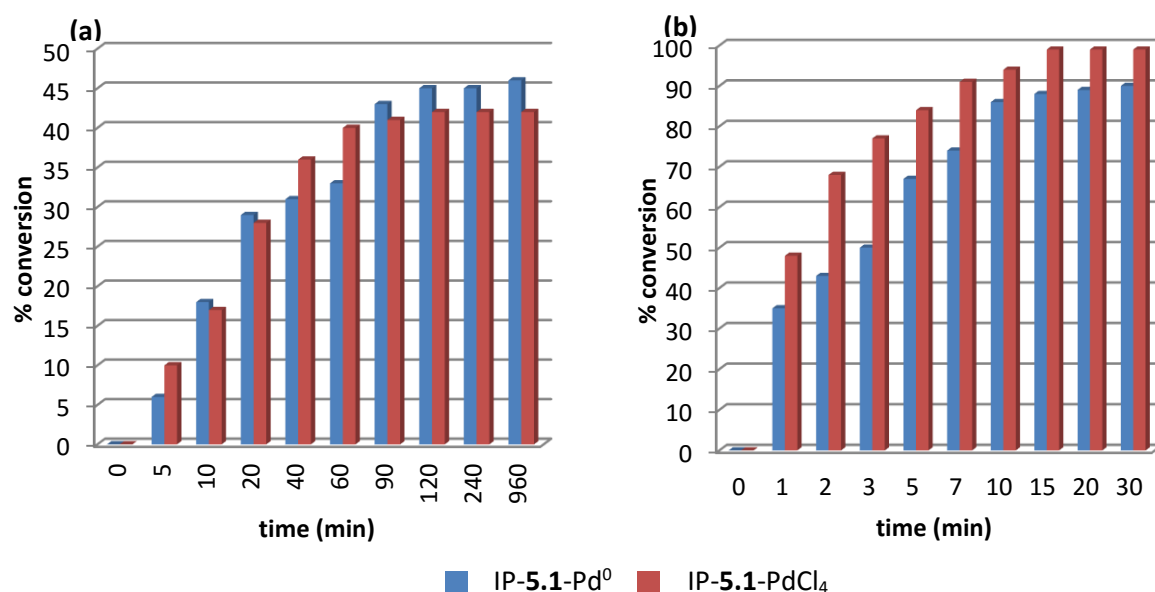


Figure 5.11 Reaction profiles for the Suzuki Miyaura coupling of (a) 2-bromotoluene and (b) 4-bromobenzonitrile with phenylboronic acid catalysed by IP-5.1-Pd⁰ and IP-5.1-PdCl₄

pre-reduced Pd⁰ counterpart. The lack of an induction period and enhanced initial activity observed with PdCl₄ further supports the formation of metastable active Pd^{δ+} species during *in situ* Pd reduction, as discussed previously. Following the formation of Pd⁰ nanoparticles the PdCl₄-based system exhibits very similar reaction profiles to their pre-reduced counterpart, with both IP-5.1-Pd⁰ and IP-5.1-PdCl₄ showing very rapid initial rates during the early stages of the reaction. With regards to the poorly performing coupling, the reaction appears to plateau. For example, the Suzuki coupling

of 2-bromotoluene (figure 5.11 (a)) reaches a maximum conversion of approximately 45% with both catalysts after 90 minutes with no further sign of conversion observed up to a time of 19 hours. One possible explanation for this apparent deactivation effect may be due to the insolubility of many biaryl coupling products in the EtOH-H₂O solvent. In particular, the coupling of 2-bromotoluene results in a slurried reaction mixture, which could in turn lead to mass transport issues after the formation and precipitation of significant product. Additionally, deposition of both the product and reagents onto the polymer support surface over time could lead to a poisoning effect, essentially blocking the active sites within the porous polymer structure. As such the catalyst deactivation effect observed upon the formation of insoluble products could be interpreted to mean either a heterogeneous catalytic mechanism, with the deactivation caused by blocking of the active sites within the PIILP materials, or a homogenous mechanism, with the viscous slurry reaction media leading to poor mass transport of the active molecular Pd species. These seemingly contrasting arguments again highlight the complicated nature by which supported nanoparticle catalysis occurs.

The results obtained from both pre-reduced Pd⁰ and the corresponding PdCl₄ precursor PIILP-supported catalysts could be interpreted as occurring through either a homogeneous or heterogeneous mechanism. With regards to the former, the observed formation of smaller nanoparticles from IP-5.1-Pd⁰ after reaction implies leaching and deposition of molecular Pd through the widely postulated “catch and release” mechanism.^{57f, 61} It is important to note however that the observed smaller nanoparticles may also be the result of reduction of the PdCl₄ present in these systems, as evidenced by the XPS data shown in figure 5.6. In contrast, the poor performance and apparent deactivation observed during the coupling of more challenging substrates could be the result of pore/active site blocking effects within the polymer architecture, suggesting a heterogeneous mechanism. As such, in order to further explore the mechanistic nature of PIILP nanoparticle catalysis it was deemed necessary to undertake further investigations. To this end, the hot filtration test has traditionally been used as a straightforward means of identifying the presence of leached molecular Pd. Removal of the supported catalyst by filtration followed by exposure of the filtrate to the reaction conditions can show a lack of leached Pd, as evidenced by a lack of further conversion. However, despite the seemingly straightforward nature of the hot filtration test there still appears to be some dispute over the meaning of the results obtained, with some authors attributing a lack of catalysis to a number of factors. For example, deactivation of the leached Pd species could occur during the filtration process, either by redeposition of the soluble Pd back onto the solid support, over-coordination of active Pd species or the formation of Pd black.⁵⁸ As such the use of solid, insoluble poisons as a means of identifying the presence of solution phase catalytic species has been widely investigated.⁶⁶ For this, mercury is used as the poison of choice and has been applied across a range of different supported nanoparticle catalysts including different Suzuki

reactions. Despite this, the conclusions drawn are often markedly different, depending on the nature of the system investigated and the reaction conditions.^{57c, 58, 67} Additionally the three-phase test, in which one of the coupling partners is covalently attached to the surface of a suitable support has been used. If leaching of the supported Pd occurs the corresponding biaryl product formed from the anchored reactive group will be observed. Again, the conclusions drawn about the mechanistic nature of the Suzuki coupling appear to be dependent on the particular system investigated.^{57c, 58, 68}

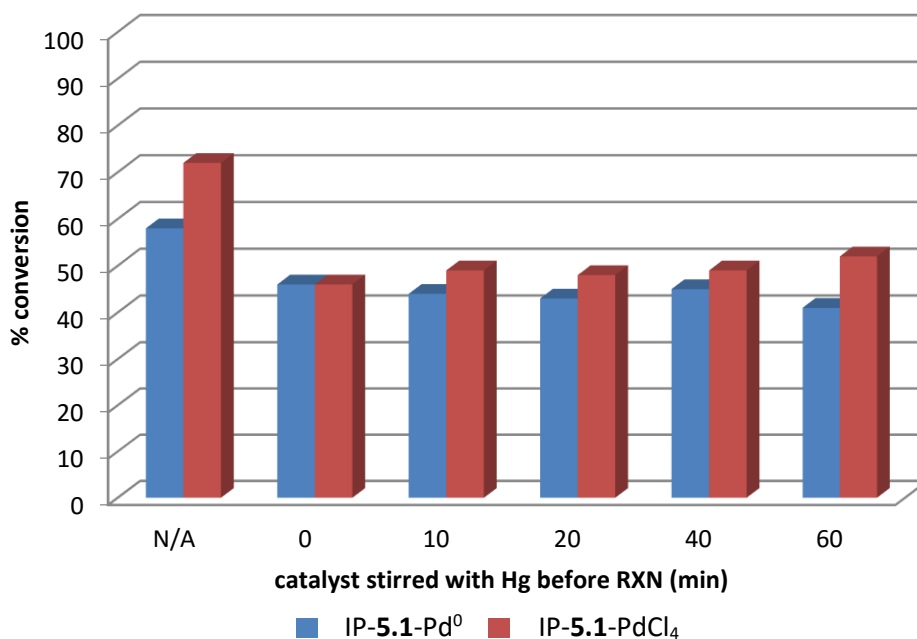


Figure 5.12 Effect of stirring the catalyst with Hg poison before reaction for the Suzuki coupling of 4-bromotoluene with phenylboronic acid catalysed by IP-5.1-Pd⁰ and IP-5.1-PdCl₄, results obtained without Hg are shown for reference

Initially Hg poisoning tests were conducted on the Suzuki coupling of 4-bromotoluene catalysed by IP-5.1-Pd⁰ and IP-5.1-PdCl₄, with the solid catalysts suspended in the reaction solvent and stirred with Hg for varying times before addition of the remaining reagents and heating to reaction temperature (figure 5.12). The addition of Hg before reaction appears to impact the catalytic performance of both the supported Pd⁰ and PdCl₄ systems, reducing the conversions from the 58% and 72%, respectively, achieved in the absence of poison (table 5.4 entry 5). The observed poisoning appears to be more profound for IP-5.1-PdCl₄, however, reasonable conversions were still achieved with both catalysts and, interestingly, aging of the catalyst with the Hg poison for longer periods of time before the reaction appears to have no significant effect on performance. While a slight decrease in performance was observed these results would suggest that the Suzuki couplings proceed, at least in part, via leaching of active Pd species from the support. However, the slight decrease in performance upon the introduction of catalyst poison could suggest that a portion of the reaction does indeed occur via a heterogeneous mechanism, with the Hg blocking a small proportion of the active Pd which has remained encapsulated within the PIILP support. These observations are

in keeping with the mechanism proposed by Pérez-Lorenzo discussed above, in which catalytic activity can be attributed to a combination of both homogeneous and heterogeneous pathways.⁵⁸

5.4. Conclusions

Through straightforward synthesis it is possible to prepare imidazolium-functionalised monomers and cross-linkers, as well as a nitrile-functionalised co-monomer which can be polymerised under standard free radical-initiated conditions. While elevated temperatures and prolonged reaction times are required to achieve high degrees of polymerisations, which in turn may limit the potential polymer functionality scope, both PIILP materials IP-5.1 and IP-5.2 were isolated as air-stable easy to handle solids. Immobilisation of suitable Pd(II) precursor can be achieved through a simple ion exchange procedure with $[\text{PdCl}_4]^{2-}$; reduction of resulting material gave the desired polymer immobilised ionic liquid stabilized PdNPs with a relatively broad size distribution. Although ROMP-based systems proved to be unsuitable for these investigations, due to the difficulties encountered during the monomer synthesis and the poor co-monomer incorporation during the subsequent ROMP, the corresponding synthetically straightforward polystyrene-based counterparts proved to be effective tools in a proof of principle study. The presence of the nitrile co-monomer in IP-5.2 appears to have a minor effect on nanoparticle formation, giving smaller particle sizes and size distribution than the corresponding unfunctionalised system. Despite this difference between the two nanoparticle catalysts, very little difference in activity was observed, with both catalysts showing moderate performance across the substrate scope. The tendency for both supported catalysts to seemingly stall in the Suzuki coupling of sterically and electronically more demanding substrates could be the result of either blocking of the active sites by the product/starting material over time, or by mass transport limitations resulting from the precipitation of many of the products in the reaction mixture. This seemingly raises a degree of ambiguity about the precise mechanism of catalysis, be it either homogeneous or heterogeneous. The Hg poisoning study, however, strongly suggests leaching of molecular Pd, while the TEM images taken after catalysis suggests the smaller nanoparticles may be the result of redeposition, consistent with the “catch and release” mechanism. Leaching of Pd during the reaction could in part explain the seemingly comparable performance of both catalysts despite the clearly different microenvironment provided by IP-5.1 and IP-5.2. Although moderately promising initial results were obtained, it was not deemed practical to perform recycling studies due to the difficulty of retrieving the catalyst from the by-product solids generated during the reaction. One possible way to overcome this issue and evaluate the longevity of PIILP nanoparticle catalysts would be to apply them to continuous flow systems, in a similar fashion to recent work by Pavia *et al.*⁵³ Although the initial results discussed herein are promising, extensive work must still be

conducted if the PIILP methodology is to become a practical tool for nanoparticle catalysis. To this end, it will be necessary to optimise the chemical and physical properties of the desired PIILP supports in order to obtain well-defined nanoparticle distributions in a controlled and rational manner, and to understand how factors such as the ionic microenvironment and the presence of heteroatom donors influence nanoparticle formation and catalyst performance. From the extensive precedent in the literature concerning the enhanced activity of nanoparticles due to the formation of NHCs from imidazolium based ILs, C(2)-H based imidazolium co-monomers would be ideal candidates to enhance the performance of PIILP nanoparticle catalysts. In this regard, current work by the larger research group is investigating PIILP materials analogous to IP-5.1 and IP-5.2 bearing an imidazole co-monomer instead of the nitrile group, as well as phosphine, methoxy and amino containing copolymers, whilst also extending their use to hydrogenation reactions and, eventually, attempting the support of alternative metal nanoparticles such as Ru and Rh.

5.5. Experimental

All manipulations involving air-sensitive compounds were carried out using standard Schlenk line techniques under an atmosphere of nitrogen in oven-dried glassware. Chloroform and dichloromethane were distilled from calcium hydride, methanol from magnesium and diethyl ether and hexane from sodium wire. All reagents were purchased from commercial suppliers and used without further purification. ^1H and $^{13}\text{C}\{^1\text{H}\}$ NMR spectra were recorded on a JEOL ESC-400 instrument. Solid-state ^{13}C NMR spectra were recorded at 100.56 MHz using a Varian VNMRs spectrometer and a 6 mm (rotor o.d.) magic-angle spinning probe. They were obtained using cross-polarisation with a 2 s recycle delay, 3 ms contact time, at ambient probe temperature ($\sim 25^\circ\text{C}$) and at a sample spin-rate of 6 kHz. Between 1000 and 1600 repetitions were accumulated. Spectral referencing was with respect to an external sample of neat tetramethylsilane (carried out by setting the high-frequency signal from adamantane to 38.5 ppm). FT-IR spectrums were record on a Varian 800 FT-IR spectrometer system using a pike technologies diamond crystal plate ATR unit. Gas chromatography was performed using a Shimadzu 2010 series gas chromatograph with a Supelco Beta DEX column. ICP analysis was conducted using a Perkin-Elmer Optima 4300 ICP-OES analyser. TEM images were acquired in bright field using a Tecnai 200 kV F20 Transmission Electron Microscope with a Field Emission Gun. A few drops of sample were pipetted onto an Agar holey carbon film copper TEM grids and the prepared grid was set aside for ca. 20 min prior to inserting it into the microscope, in order to allow the solvent to evaporate. Images were taken with a Gatan CCD digital camera attached to the microscope and processed using Image J software. XPS analysis was performed with a Kratos Axis Nova spectrometer. The solid catalysts were fixed on the support using a carbon double-sided adhesive tape. The spectra were excited by the monochromatized Al Ka source (1486.6 eV) run at 15 kV and 10 mA. For the individual peak regions a pass energy of 20 eV was used. Survey spectrum was measured at 160 eV pass energy. Analysis of the peaks was performed with the CasaXPS software. SEC was conducted on 200 mg of polymer sample dissolved in 5 mL MeOH using an ÄKTA Prime system. UV absorbance chromatograms were collected with PrimeView software v5.0 (GE Healthcare). Note, all solutions used were filtered ($0.45\ \mu\text{m}$) and degassed. Chromatography was typically performed at a flow rate of 1 ml/min. Traces listed were collected at a wavelength of 254 nm.

methyl bicyclo[2.2.1]hept-5-ene-2-carboxylate (5.1)

A solution of methyl acrylate (10.53 mL, 116.2 mmol) in toluene (25 mL) was cooled to 0°C before the slow addition of boron trifluoride etherate (1.43 mL, 11.6 mmol). Freshly cracked cyclopentadiene

(19.54 mL, 232.4 mmol) was then added to the mixture which was subsequently allowed to warm to room temperature and stir for 20 h. The reaction mixture was then quenched by addition to 10% sulphuric acid (100 mL) on ice and stirring for 10 minutes. The organic layer was then extracted before washing with saturated sodium carbonate (100 mL) and brine (100 mL) before drying over MgSO₄. Removal of the solvent under reduced pressure gave the product as a clear yellow oil in 85% yield (14.99 g). ¹H NMR (400 MHz, CDCl₃, δ): 6.19 (m, 1H), 6.14 (m, 1H, CH), 5.97 (m, 1H, CH₂), 3.40 (m, 1H, CH₂), 3.63 (m, 3H), 3.26 (m, 1H, CH), 2.93 (m, 1H, CH), 2.81 (m, 1H, CH), 2.31 (m, 1H, CH), 1.82 (m, 1H, CH₂), 1.45 (m, 1H, CH₂), 1.28 (m, 1H, CH₂), 0.53 (m, 1H, CH₂); ¹³C{¹H} NMR (100.52 MHz, CDCl₃, δ): 181.8, 137.8, 137.7, 132.5, 46.7, 45.6, 43.2, 41.7, 29.1.

(bicyclo[2.2.1]hept-5-en-2-yl)methanol (5.2)

A solution of **5.1** (14.99 g, 98.5 mmol) in THF (50 mL) was added dropwise to a stirred suspension of LiAlH₄ (10.0 g, 263.5 mmol) in THF cooled to 0°C. Following complete addition the reaction mixture was allowed to warm to room temperature before stirring for 19 h. The mixture was then quenched by the addition of water (100 mL) followed by 3M potassium hydroxide (100 mL) whilst cooling to 0°C before stirring for 2 h. Celite was then added to the reaction mixture and the product solution decanted. The celite was then washed exhaustively with Et₂O and the combined organic extract dried over MgSO₄. Removal of the solvent *in vacuo* gave the product as a pale yellow oil in 80% yield (9.73 g). ¹H NMR (400 MHz, CDCl₃, δ): 6.14 (m, 1H, CH), 5.97 (m, 1H, CH₂), 3.40 (m, 1H, CH₂), 3.26 (m, 1H, CH), 2.93 (m, 1H, CH), 2.81 (m, 1H, CH), 2.31 (m, 1H, CH), 1.82 (m, 1H, CH₂), 1.45 (m, 1H, CH₂), 1.28 (m, 1H, CH₂), 0.53 (m, 1H, CH₂); ¹³C{¹H} NMR (100.52 MHz, CDCl₃, δ): 137.5, 136.9, 66.5, 49.6, 45.0, 43.3, 41.7, 28.9.

(bicyclo[2.2.1]hept-5-en-2-yl)methyl methanesulfonate (5.3)

A solution of methanesulfonyl chloride (6.7 mL, 86.2 mmol) in CH₂Cl₂ (25 mL) was added dropwise to a stirred solution of **5.2** (9.73 g, 78.4 mmol) in CH₂Cl₂ cooled to 0°C, with the resulting mixture allowed to warm to room temperature before stirring for 19 h. The reaction mixture was then washed with water (100 mL), 1M HCl (100 mL) then brine (2 × 100 mL) before drying the organic extract over MgSO₄. Removal of the solvent *in vacuo* gave the product as a yellow-orange oil in 75% yield (11.82 g). ¹H NMR (400 MHz, CDCl₃, δ): 6.14 (m, 1H), 5.96 (m, 1H), 2.73 (br s, 1H), 2.64 (br s, 1H), 2.15 (m, 1H), 1.85 (m, 1H), 1.55 (s, 1H), 1.35 (m, 1H), 1.33 (m, 1H), 1.23 (s, 1H), 1.05 and 0.75 (m, 3H), 0.41 (2m, 1H); ¹³C{¹H} NMR (100.52 MHz, CDCl₃, δ): 137.5, 136.9, 66.5, 49.6, 45.0, 43.3, 41.7, 37.9, 28.9.

3-(bicyclo[2.2.1]hept-5-en-2-ylmethyl)-1,2-dimethyl-1H-imidazolium methanesulfonate (5.4)²⁸

A solution of 1,2-dimethylimidazole (4.60 g, 47.9 mmol) in toluene (4 mL) was added to a solution of **5.3** (8.79 g, 43.5 mmol) in toluene (6 mL) before allowing the mixture to stir vigorously under reflux for 48 h. The reaction mixture was then diluted with CH₂Cl₂ (75 mL) before precipitation of the product by addition to Et₂O (500 mL). The resulting precipitate was then isolated by filtration under N₂ as a highly hygroscopic brown powder in 84% yield (10.90 g). ¹H NMR (400 MHz, CDCl₃, δ): 7.35 (m, 1H), 7.23 (m, 1H), 7.22 (m, 1H), 7.06 (m, C-H), 6.34 (m, CH=CH), 6.13 (m, CH=CH), 6.04 (m, CH=CH), 4.30-4.10 (m, 2H, CH₂N,) 3.97 (s, 3H, NCH₃), 3.88-3.77 (m, 5H), 2.94 (m, 1H), 2.88 (m, 1H), 2.79 (m, 1H), 2.74 (s, 3H), 2.71 (s, 3H), 2.69 (s, 3H), 2.55-2.50 (m, 1H), 1.98-1.84 (m, 1H), 1.54-1.26 (m, 2H), 0.67-0.64 (m, 1H); ¹³C{¹H} NMR (100.52 MHz, CDCl₃, δ): 144.1, 139.5, 137.7, 135.6, 123.2, 118.8, 52.6, 49.8, 45.1, 44.1, 41.8, 39.5, 30.9, 11.0.

3-(bicyclo[2.2.1]hept-5-en-2-ylmethyl)-1,2-dimethyl-1H-imidazolium chloride (5.5)

LiCl (10.47 g, 247 mmol) was added to a solution of **5.4** (7.36 g, 24.7 mmol) in CH₂Cl₂ (50 mL) and the resulting slurry was allowed to stir for 16 h at room temperature. The reaction mixture was then filtered and the product precipitated by the dropwise addition of the filtrate to Et₂O (600 mL). The resulting filtrate was then isolated via filtration under N₂ to give the product as a light brown powder in 79% yield (4.64 g). ¹H NMR (400 MHz, CDCl₃, δ): 7.35 (m, 1H), 7.23 (m, 1H), 7.22 (m, 1H), 7.06 (m, C-H), 6.34 (m, CH=CH), 6.13 (m, CH=CH), 6.04 (m, CH=CH), 4.30-4.10 (m, 2H, CH₂O,) 3.97 (s, 3H, NCH₃), 3.88-3.77 (m, 5H), 2.94 (m, 1H), 2.88 (m, 1H), 2.79 (m, 1H), 2.74 (s, 3H), 2.71 (s, 3H), 2.69 (s, 3H), 2.55-2.50 (m, 1H), 1.98-1.84 (m, 1H), 1.54-1.26 (m, 2H), 0.67-0.64 (m, 1H); ¹³C{¹H} NMR (100.52 MHz, CDCl₃, δ): 144.1, 139.5, 137.7, 135.6, 123.2, 118.8, 52.6, 49.8, 44.1, 41.8, 39.5, 30.9, 11.0.

bicyclo[2.2.1]hept-5-ene-2-carbonitrile (5.6)

A three-neck round bottomed flask was charged with boron trichloride 1M in hexanes (15.0 mL, 15.0 mmol) and cooled to 0 °C after which acrylonitrile (7.8 mL, 118.7 mmol) was added slowly causing the instant formation of a white solid. After the drop-wise addition of freshly cracked cyclopentadiene (6.52 mL, 98.5 mmol) the white solid redissolved and was allowed to stir for 19 h and warm to room temperature. The resultant pale yellow oil was then poured onto an excess of NaHCO₃ on ice and allowed to stir for approximately 10 mins after which time the product was extracted with diethyl ether (3 × 100 mL) and the combined extracts dried with MgSO₄ before the solvent was removed

under reduced pressure to give the product as a pale oil in 69% yield (9.76 g). ^1H NMR (399.78 MHz, CDCl_3 , δ): 6.25 (dd, $J = 5.4, 1.9$ Hz, 1H, $\text{H}_a\text{C}=\text{CH}_b$), 5.96 (dd, $J = 5.4, 1.9$ Hz, 1H, $\text{H}_a\text{C}=\text{CH}_b$), 3.02 (m, 1H, bridgehead), 2.93 (m, 1H, bridgehead), 2.54 (m, 1H), 2.27 (dd, $J = 13.7, 1.5$ Hz, 1H, CH_2), 2.25 (dd, $J = 13.7, 1.5$ Hz, 1H, CH_2), 1.76 (dt, $J = 14.3, 2.0$ Hz, 1H, bridge CH_2), 1.53 (dt, $J = 14.3, 2.0$ Hz, 1H, bridge CH_2); $^{13}\text{C}\{^1\text{H}\}$ NMR (100.52 MHz, CDCl_3 , δ): 138.9, 131.8, 127.3, 52.5, 49.6, 43.2, 40.7, 30.2.

1-((bicyclo[2.2.1]hept-5-en-2-yl)methyl)-2-methyl-1H-imidazole (5.7)

A mixture of **5.3** (2.0 g, 9.9 mmol) and 2-methylimidazole (2.44 g, 29.7 mmol) in DMF (10 mL) was heated to reflux and allowed to stir for 48 h. The reaction mixture was then allowed to cool to room temperature before diluting with CH_2Cl_2 (100 mL) and washing with water (3×75 mL). The organic extract was then dried over MgSO_4 before removal of the solvent *in vacuo* to give the product as a brown oil in 63% yield (1.17 g). ^1H NMR (400 MHz, CDCl_3 , δ): 6.87 (m, 1H), 6.79 (m, 1H), 7.22 (m, 1H), 6.13 (m, $\text{CH}=\text{CH}$), 6.04 (m, $\text{CH}=\text{CH}$), 4.30-4.10 (m, 2H, CH_2N), 3.97 (s, 3H, NCH_3), 3.88-3.77 (m, 5H), 2.94 (m, 1H), 2.88 (m, 1H), 2.79 (m, 1H), 2.51 (s, 3H), 2.71 (s, 3H), 2.69 (s, 3H), 2.55-2.50 (m, 1H), 1.98-1.84 (m, 1H), 1.54-1.26 (m, 2H), 0.67-0.64 (m, 1H); $^{13}\text{C}\{^1\text{H}\}$ NMR (100.52 MHz, CDCl_3 , δ): 142.3, 138.9, 131.8, 126.9, 118.5, 48.9, 47.3, 46.9, 42.9, 32.7, 10.3; LRMS (EI^+) m/z 189 [$\text{M}+\text{H}$] $^+$.

1,3-bis((bicyclo[2.2.1]hept-5-en-2-yl)methyl) imidazolium methanesulfonate (5.8)

A solution of **5.7** (4.60 g, 47.9 mmol) in toluene (4 mL) was added to a solution of **5.3** (8.79 g, 43.5 mmol) in toluene (6 mL) before allowing the mixture to stir vigorously under reflux for 48 h. The reaction mixture was then diluted with CH_2Cl_2 (75 mL) before removing the solvent *in vacuo*. Analysis of the resulting brown oil confirmed identity as **5.7**.

General Procedure for the Ring-Opening Metathesis Polymerisation of 5.5 and 5.6

In a typical procedure a flame-dried Schlenk flask was charged with dry chloroform (80 mL), **5.5** (2.38 g, 10 mmol) and the **5.6** (0.60 g, 5 mmol). To the stirred solution was added Grubbs 2nd generation catalyst (0.13 g, 0.15 mmol) in chloroform (*ca.* 10 mL) and the resulting mixture was heated to 40 °C and left to stir for 48 h. Polymerisations were monitored by ^1H NMR.

1,2-Dimethyl-3-(4-vinylbenzyl)imidazolium chloride (5.9)⁶⁹

An oven-dried Schlenk flask was charged with 1,2-dimethylimidazole (5.25 g, 54.6 mmol) and CHCl_3 (50 mL) followed by the slow addition of 4-vinylbenzyl chloride (10 mL, 71.0 mmol) with stirring. The resulting mixture was then heated to 50 °C and allowed to stir for 16 h. Upon cooling back to room temperature the solvent was removed *in vacuo* and the resulting residue washed with ethyl acetate (4 X 50 mL) before drying under high vacuum gave the product as a white powder in 99% yield (13.57 g). ^1H NMR (399.78 MHz, CDCl_3 , δ): 7.67 (dd, $J = 5.4, 1.9$ Hz, 1H, $H_a\text{C}=\text{CH}_b$ imidazolium), 7.29 (m, 4H, Ar-H), 6.58 (dd, $J = 17.4, 10.6$ Hz, 2H, $H_a\text{C}=\text{CH}_b\text{H}_c$), 5.66 (d, $J = 17.4$ Hz, $\text{HC}_a=\text{CH}_b\text{H}_c$), 5.49 (s, 2H, Ar- CH_2 -N), 5.20 (d, $J = 17.4$ Hz, $\text{HC}_a=\text{CH}_b\text{H}_c$), 3.88 (s, 3H, Me (C2 imidazolium)), 2.68 (s, 3H, N-Me); $^{13}\text{C}\{^1\text{H}\}$ NMR (100.52 MHz, CDCl_3 , δ): 144.0, 138.1, 135.6, 132.4, 128.4, 126.9, 122.8, 121.8, 115.1, 51.9, 35.7, 10.7.

2-(4-Vinylphenyl)acetonitrile (5.10)⁷⁰

4-vinylbenzyl chloride (9.86 mL, 70.0 mmol) and potassium cyanide (6.4 g, 100.0 mmol) were added to a solution of 18-crown-6 (0.7 g, 2.8 mmol) in MeCN (55 mL) under Schlenk conditions and the resulting orange mixture was allowed to stir at room temperature for 18 h after which time a colour change to yellow was observed. The solvent was then reduced to a volume of approximately 5 mL under high vacuum before the resulting residue was diluted with distilled H_2O (100 mL) and extracted with Et_2O (2 x 100 mL). The organic extract was then washed with H_2O (50 mL), brine (50 mL), dried with MgSO_4 and finally dried under vacuum to give the product as a yellow oil in 92% yield 9.21 g). ^1H NMR (399.78 MHz, CDCl_3 , δ): 7.38 (m, 4H, Ar-H), 6.66 (dd, $J = 17.4, 10.6$ Hz, 2H, $H_a\text{C}=\text{CH}_b\text{H}_c$), 5.77 (d, $J = 17.4$ Hz, $\text{HC}_a=\text{CH}_b\text{H}_c$), 5.26 (d, $J = 17.4$ Hz, $\text{HC}_a=\text{CH}_b\text{H}_c$), 3.69 (s, 2H, CH_2 -CN); $^{13}\text{C}\{^1\text{H}\}$ NMR (100.52 MHz, CDCl_3 , δ): 137.3, 135.8, 129.2, 128.0, 126.7, 117.7, 114.5, 23.2.

2-Methyl-1-(4-vinylbenzyl)imidazole (5.11)⁷¹

An oven-dried Schlenk flask was charged with sodium hydride (0.73 g, 30.4 mmol) and DMF with the resulting slurry cooled to 0 °C. 2-methylimidazole (3.00 g, 36.5 mmol) was then added to the mixture under N_2 . Once the exotherm had subsided the mixture was heated to 75 °C and allowed to stir for 30 min before the temperature was increased to 95 °C with a further 15 min stirring. The mixture was then once again cooled to 0 °C before the drop-wise addition of 4-vinylbenzyl chloride (4.29 mL, 30.4 mmol) followed by heating to 75 °C and a further 30 min stirring, after which time the mixture was allowed to cool to room temperature before being poured onto H_2O (250 mL). The product was then

extracted with ethyl acetate (2 × 100 mL) with the organic extract then being washed with H₂O (180 mL) and brine (50 mL) before acidification with 6 M HCl (2 × 25 mL). After washing with Et₂O (20 mL) to remove any organic impurities the aqueous layer was neutralised with a NaOH solution (1 M) before the product was finally extracted with Et₂O (3 × 50 mL). After drying with MgSO₄ and removal of the solvent under reduced pressure the product was obtained as a yellow oil in 86% yield (5.18 g). ¹H NMR (399.78 MHz, CDCl₃, δ): 7.26 (m, 2H, Ar-H), 6.88 (m, 2H, Ar-H), 6.81 (d, *J* = 7.6 Hz, 1H, H_aC=CH_b, imidazole), 6.71 (d, *J* = 7.6 Hz, 1H, H_aC=CH_b, imidazole), 6.57 (dd, *J* = 17.4, 10.6 Hz, 4H, 2 × H_aC=CH_bH_c), 5.61 (d, *J* = 17.4 Hz, 2H, 2 × HC_a=CH_bH_c), 5.15 (d, *J* = 17.4 Hz, 2H, 2 × HC_a=CH_bH_c), 4.90 (s, 2H, Ar-CH₂-N), 2.21 (s, 3H, Me); ¹³C{¹H} NMR (100.52 MHz, CDCl₃, δ): 144.8, 137.3, 136.0, 135.6, 127.1, 126.8, 126.6, 119.8, 114.4, 49.4, 12.9.

2-Methyl-1,3-bis(4-vinylbenzyl)imidazolium chloride (5.12)

An oven-dried Schlenk flask was charged with **5.11** (4.00 g, 20.2 mmol) and CHCl₃ (40 mL) followed by the slow addition of 4-vinylbenzyl chloride (3.7 mL, 35.5 mmol) with stirring. The resulting mixture was then heated to 50 °C and allowed to stir for 16 h. Upon cooling back to room temperature the solvent was removed *in vacuo* and the resulting residue washed with ethyl acetate (4 × 50 mL) before drying under high vacuum gave the product as a white powder in 74% yield (5.26g). ¹H NMR (399.78 MHz, CDCl₃, δ): 7.65 (dd, *J* = 5.4, 1.9 Hz, 1H, H_aC=CH_b, imidazolium), 7.24 (m, 8H, Ar-H), 6.62 (dd, *J* = 17.4, 10.6 Hz, 4H, 2 × H_aC=CH_bH_c), 5.69 (d, *J* = 17.4 Hz, 2H, 2 × HC_a=CH_bH_c), 5.49 (s, 4H, 2 × Ar-CH₂-N), 5.23 (d, *J* = 17.4 Hz, 2H, 2 × HC_a=CH_bH_c), 2.71 (s, 3H, N-Me); ¹³C{¹H} NMR (100.52 MHz, CDCl₃, δ): 144.1, 138.2, 135.7, 132.2, 128.4, 127.0, 121.0, 115.2, 51.9, 11.1.

General procedure for radical initiated polymerisations of 1,2-dimethyl-3-(4-vinylbenzyl)imidazolium chloride, 2-methyl-1,3-bis(4-vinylbenzyl)imidazolium and co-monomer

In a typical procedure, an oven-dried Schlenk flask was charged with **5.9** (5.00 g, 20.1 mmol), the cross-linker **5.11** (0.53 g, 1.52 mmol), the appropriate co-monomer (10.9 mmol) and azobisisobutyronitrile (0.25 g, 1.52 mmol). After dilution with dry methanol (100 mL) the resulting reaction mixture was degassed with 5 freeze/thaw cycles using liquid nitrogen. Upon warming to room temperature the reaction mixture was heated to 75 °C and allowed to stir for 96 h after which time the mixture was cooled to room temperature and another equivalent of AIBN was added. After repeating the freeze/thaw degassing the mixture was again heated to 75 °C and allowed to stir for a

further 19 h. Upon cooling to room temperature once more the solvent was removed under high vacuum to yield the desired polymer generally as an off-white brittle powder.

General procedure for the immobilisation of tetrachloropalladate with functionalised cross-linked polymers

In a typical procedure a mixture of palladium (II) chloride (0.319 g, 1.80 mmol), NaCl (1.92 g, 32.8 mmol) in H₂O (30 mL) was allowed to stir at 80 °C for approximately 30 min to give a homogenous orange solution. The appropriate polymer support (0.91 mol eq, based on the mass of the polymer repeat unit) in H₂O (10 mL) was then added to the solution drop wise, causing the instant formation of an orange precipitate, and the resulting slurry allowed to stir under ambient conditions for 5 h. The product was then isolated by filtration and washed with H₂O (50 mL), EtOH (50 mL) and finally Et₂O (100 mL) before drying under high vacuum to give a fine orange powder.

General procedure for the reduction of polymer-immobilised tetrachloropalladate

In a typical procedure the polymer-immobilised palladium species was suspended in EtOH (*c.a.* 60 mL g⁻¹ material) before being placed in a Parr reactor and allowed to stir at 40 °C for 19 h under an H₂ pressure of approximately 70 psi. Once the reaction vessel had cooled and the pressure had been released the resulting black suspension was decanted into a Schlenk flask and the volume reduced to one fifth. After the addition of a large excess of Et₂O to induce precipitation the product was isolated by filtration and washed with Et₂O before drying under high vacuum to give a deep black fine powder.

General procedure for the heterogeneous Pd-catalysed Suzuki Miyaura coupling reactions

An oven-dried Schlenk flask was charged with aryl halide (1 mmol), phenylboronic acid (0.138 g, 1.13 mmol), potassium carbonate (0.166 g, 1.2 mmol) and the catalyst (0.001 mmol, 0.1 mol%, based on mass of polymer repeat unit with assumed complete Pd loading) before being diluted with 50 : 50 EtOH : H₂O (2.4 mL). The reaction mixture was then heated to 30 °C and allowed to stir for the desired amount of time before the addition of the decane standard (0.195 mL, 1 mmol). The mixture was then diluted with Et₂O (10 mL) and H₂O (5 mL) and, after vigorous shaking, the ethereal layer was decanted and passed through a small plug of silica. A small aliquot of the organic extract was then diluted with Et₂O before analysis by GC and the remaining solution dried under reduced pressure with the resulting residue being analysed by ¹H NMR.

*2-Methylbiphenyl*⁷²

¹H NMR (400 MHz, CDCl₃, δ): 7.42 (t, J = 7.4 Hz, 2H), 7.35 (t, J = 7.4 Hz, 3H), 7.31–7.21 (m, 4H), 2.29 (s, 3H).

*3-Methylbiphenyl*⁷³

¹H NMR (400 MHz, CDCl₃, δ): 7.66 (d, J = 7.2 Hz, 2H), 7.46–7.52 (m, 4H), 7.40 (t, J = 7.4 Hz, 2H), 7.25 (d, J = 7.6 Hz, 1H), 2.50 (s, 3H).

*4-Methylbiphenyl*⁷⁴

¹H NMR (400 MHz, CDCl₃, δ): 7.46 (2H, d, J = 7.6 Hz), 7.38 (2H, d, J = 8.0 Hz), 7.32–7.29 (2H, m), 7.20 (1H, t, J = 7.6 Hz), 7.13 (2H, d, J = 7.6 Hz), 2.28 (3H, s).

*3,5-Dimethylbiphenyl*⁷²

¹H NMR (400 MHz, CDCl₃, δ): 7.63 (d, J = 7.4 Hz, 2H), 7.47 (t, J = 7.5 Hz, 2H), 7.37 (t, J = 7.3 Hz, 1H), 7.27 (s, 2H), 7.05 (s, 1H), 2.44 (s, 6H).

*4-(tert-Butyl)-1,1'-biphenyl*⁷⁵

¹H NMR (400 MHz, CDCl₃, δ): 7.71 (d, J = 8.0 Hz, 2H) ; 7.66 (t, J = 6.8 Hz, 2H) ; 7.59 (d, J = 8.0 Hz, 2H); 7.54 (t, J = 7.6 Hz, 2H); 7.43 (t, J = 7.6 Hz, 1H); 1.49 (d, J = 1.6 Hz, 9H).

*1-(Biphenyl-2-yl)ethanone*⁷⁶

¹H NMR (400 MHz, CDCl₃, δ): 7.56–7.49 (m, 2H), 7.43–7.38 (m, 5H), 7.35–7.33 (m, 2H), 2.00 (s, 3H).

*1-(Biphenyl-3-yl)ethanone*⁷⁷

¹H NMR (400 MHz, CDCl₃, δ): 8.18 (s, 1H, ArH), 7.93–7.91 (m, 1H, ArH), 7.77 (d, J = 8.0 Hz, 1H, ArH), 8.00 (s, 2H, ArH), 7.52–7.37 (m, 4H, ArH), 2.64 (s, 3H, CH₃).

*1-(Biphenyl-4-yl)ethanone*⁷⁴

¹H NMR (400 MHz, CDCl₃, δ): 8.03 (2H, d, J = 8.4 Hz), 7.68 (2H, d, J = 8.4 Hz), 7.62 (2H, d, J = 7.6 Hz), 7.48–7.45 (2 H, m), 7.40 (1H, t, J = 7.6 Hz), 2.63 (3H, s).

*2-Methoxybiphenyl*⁷⁴

¹H NMR (400 MHz, CDCl₃, δ): 7.58–7.56 (2H, m), 7.43–7.39 (2H, m), 7.35–7.31 (2H, m), 7.17–7.12 (2H, m), 6.87 (1H, dd, J = 8.4 and 2.4 Hz), 3.82 (3H, s).

*3-Methoxybiphenyl*⁷⁴

¹H NMR (400 MHz, CDCl₃, δ): 7.52 (2H, d, J = 7.2 Hz), 7.40 (2H, t, J = 7.2 Hz), 7.32–7.29 (3H, m), 7.04–6.96 (2H, m), 3.78 (3H, s).

*4-Methoxybiphenyl*⁷⁴

¹H NMR (400 MHz, CDCl₃, δ): 7.59–7.55 (4H, m), 7.44 (2H, t, J = 7.6 Hz), 7.33 (1H, t, J = 7.6 Hz), 7.01 (2H, d, J = 8.8 Hz), 3.87 (3H, s).

*3-biphenylcarbaldehyde*⁷⁷

¹H NMR (400 MHz, CDCl₃, δ): 10.09 (s, 1H, CHO), 8.10 (s, 1H, ArH), 7.86 (d, J = 7.2 Hz, 2H, ArH), 7.62 (d, J = 6.0 Hz, 3H, ArH), 7.49–7.41 (m, 3H, ArH), 7.40 (s, 1H, ArH).

*4-biphenylcarbaldehyde*⁷⁷

¹H NMR (300 Hz, CDCl₃) δ: 9.94 (s, 1H, CHO), 7.83 (d, J = 7.6 Hz, 2H, ArH), 7.64–7.61 (m, 2H, ArH), 7.51 (d, J = 7.6 Hz, 2H, ArH), 7.36–7.34 (m, 3H, ArH).

*2-Biphenylcarbonitrile*⁷⁷

¹H NMR (300 Hz, CDCl₃) δ: 7.76 (dd, $J_1 = 8.0$ Hz, $J_2 = 1.2$ Hz, 1H), 7.64 (td, $J_1 = 7.6$ Hz, $J_2 = 1.2$ Hz, 1H), 7.58 – 7.54 (m, 2H), 7.54 – 7.40 (m, 5H).

*3-Biphenylcarbonitrile*⁷⁸

¹H NMR (300 Hz, CDCl₃) δ: 7.86 (s, 1H), 7.81 (d, $J = 7.7$ Hz, 1H), 7.63 (d, $J = 7.5$ Hz, 1H), 7.57–7.53 (m, 3H), 7.48 (t, $J = 7.4$ Hz, 2H), 7.42 (t, $J = 7.2$ Hz, 1H);

*4-Biphenylcarbonitrile*⁷⁴

¹H NMR (400 MHz, CDCl₃, δ): 7.74–7.67 (4H, m), 7.59 (2H, d, $J = 8.0$ Hz), 7.50–7.41 (3H, m).

*3-Nitrobiphenyl*⁷⁴

¹H NMR (400 MHz, CDCl₃, δ): 8.46 (1H, s), 8.22–8.20 (1H, m), 7.93 (1H, d, $J = 8.0$ Hz), 7.65–7.62 (3H, m), 7.53–7.49 (2H, m), 7.46–7.43 (1H, m).

*4-Nitrobiphenyl*⁷⁴

¹H NMR (400 MHz, CDCl₃, δ): 8.30 (2H, d, $J = 8.8$ Hz), 7.74 (2H, d, $J = 8.8$ Hz), 7.65–7.62 (2H, m), 7.53–7.49 (2H, m), 7.47–7.44 (1H, m).

5.6. References

1. a) N. Tian, Z.-Y. Zhou, S.-G. Sun, Y. Ding and Z. L. Wang, *Science*, 2007, **316**, 732-735; b) R. Sardar, A. M. Funston, P. Mulvaney and R. W. Murray, *Langmuir*, 2009, **25**, 13840-13851; c) H. Jans and Q. Huo, *Chem. Soc. Rev.*, 2012, **41**, 2849-2866; d) J. Dupont, G. S. Fonseca, A. P. Umpierre, P. F. P. Fichtner and S. R. Teixeira, *J. Am. Chem. Soc.*, 2002, **124**, 4228-4229; e) A. R. Tao, S. Habas and P. Yang, *Small*, 2008, **4**, 310-325; f) S. Yang, Z. Peng and H. Yang, *Adv. Funct. Mater.*, 2008, **18**, 2745-2753; g) T. K. Sau, A. L. Rogach, F. Jäckel, T. A. Klar and J. Feldmann, *Adv. Mater.*, 2010, **22**, 1805-1825; h) K. Esumi, R. Isono and T. Yoshimura, *Langmuir*, 2004, **20**, 237-243.
2. a) A.-H. Lu, E. L. Salabas and F. Schüth, *Angew. Chem. Int. Ed.*, 2007, **46**, 1222-1244; b) A. Gedanken, *Ultrason. Sonochem.*, 2004, **11**, 47-55; c) C. N. R. Rao, S. R. C. Vivekchand, K. Biswas and A. Govindaraj, *Dalton Trans.*, 2007, 3728-3749; d) J. Park, J. Joo, S. G. Kwon, Y. Jang and T. Hyeon, *Angew. Chem. Int. Ed.*, 2007, **46**, 4630-4660.
3. M. Kim, V. N. Phan and K. Lee, *CrystEngComm*, 2012, **14**, 7535-7548.
4. F. Caruso, *Colloids and Colloid Assemblies: Synthesis, Modification, Organization and Utilization of Colloid Particles*, Wiley, 2006.
5. a) D. Astruc, F. Lu and J. R. Aranzas, *Angew. Chem. Int. Ed.*, 2005, **44**, 7852-7872; b) C. Pan, K. Pelzer, K. Philippot, B. Chaudret, F. Dassenoy, P. Lecante and M.-J. Casanove, *J. Am. Chem. Soc.*, 2001, **123**, 7584-7593; c) J. D. Aiken and R. G. Finke, *J. Am. Chem. Soc.*, 1999, **121**, 8803-8810.
6. a) M. Brust, M. Walker, D. Bethell, D. J. Schiffrin and R. Whyman, *J. Chem. Soc., Chem. Commun.*, 1994, 801-802; b) L. Seung-Yup, Y. Mami and M. Mikio, *Science and Technology of Advanced Materials*, 2005, **6**, 420; c) F. Lu, J. Ruiz and D. Astruc, *Tetrahedron Lett.*, 2004, **45**, 9443-9445; d) J. Alvarez, J. Liu, E. Roman and A. E. Kaifer, *Chem. Comm.*, 2000, 1151-1152; e) S. Chen, K. Huang and J. A. Stearns, *Chem. Mater.*, 2000, **12**, 540-547; f) M. Ganesan, R. G. Freemantle and S. O. Obare, *Chem. Mater.*, 2007, **19**, 3464-3471.
7. a) M. T. Reetz and J. G. de Vries, *Chem. Comm.*, 2004, 1559-1563; b) Q. Liu, J. C. Bauer, R. E. Schaak and J. H. Lunsford, *Angew. Chem. Int. Ed.*, 2008, **47**, 6221-6224; c) S.-W. Kim, J. Park, Y. Jang, Y. Chung, S. Hwang, T. Hyeon and Y. W. Kim, *Nano Lett.*, 2003, **3**, 1289-1291; d) S. U. Son, Y. Jang, K. Y. Yoon, E. Kang and T. Hyeon, *Nano Lett.*, 2004, **4**, 1147-1151.
8. a) V. Mazumder and S. Sun, *J. Am. Chem. Soc.*, 2009, **131**, 4588-4589; b) A. A. Athawale, S. V. Bhagwat, P. P. Katre, A. J. Chandwadkar and P. Karandikar, *Mater. Lett.*, 2003, **57**, 3889-3894; c) T. Mayer-Gall, A. Birkner and G. Dyker, *J. Organomet. Chem.*, 2008, **693**, 1-3; d) D. I. Gittins and F. Caruso, *Angew. Chem. Int. Ed.*, 2001, **40**, 3001-3004; e) C. J. Serpell, J. Cookson, D. Ozkaya and P. D. Beer, *Nature Chem.*, 2011, **3**, 478-483.

9. a) X. Yang, Z. Fei, T. J. Geldbach, A. D. Phillips, C. G. Hartinger, Y. Li and P. J. Dyson, *Organometallics*, 2008, **27**, 3971-3977; b) J. Amici, M. Sangermano, E. Celasco and Y. Yagci, *Eur. Polym. J.*, 2011, **47**, 1250-1255.
10. a) M. Tamura and H. Fujihara, *J. Am. Chem. Soc.*, 2003, **125**, 15742-15743; b) R. Tatum, T. Akita and H. Fujihara, *Chem. Comm.*, 2006, 3349-3351.
11. a) D. Astruc, *Inorg. Chem.*, 2007, **46**, 1884-1894; b) D. Ghosh and S. Chen, *J. Mater. Chem.*, 2008, **18**, 755-762; c) H. Bönemann, R. Brinkmann and P. Neiteler, *Appl. Organomet. Chem.*, 1994, **8**, 361-378.
12. S. F. L. Mertens, C. Vollmer, A. Held, M. H. Aguirre, M. Walter, C. Janiak and T. Wandlowski, *Angew. Chem. Int. Ed.*, 2011, **50**, 9735-9738.
13. C. Xiao, H. Ding, C. Shen, T. Yang, C. Hui and H. J. Gao, *J. Phys. Chem. C*, 2009, **113**, 13466-13469.
14. a) P. Migowski and J. Dupont, *Chem. – Eur. J.*, 2007, **13**, 32-39; b) R. Venkatesan, M. H. G. Precht, J. D. Scholten, R. P. Pezzi, G. Machado and J. Dupont, *J. Mater. Chem.*, 2011, **21**, 3030-3036; c) A. S. Pensado and A. A. H. Pádua, *Angew. Chem. Int. Ed.*, 2011, **50**, 8683-8687.
15. H. Ishizuka, T. Tano, K. Torigoe, K. Esumi and K. Meguro, *Colloids Surf.*, 1992, **63**, 337-340.
16. B. L. Bhargava, S. Balasubramanian and M. L. Klein, *Chem. Comm.*, 2008, 3339-3351.
17. H. Zhang and H. Cui, *Langmuir*, 2009, **25**, 2604-2612.
18. a) H. Itoh, K. Naka and Y. Chujo, *J. Am. Chem. Soc.*, 2004, **126**, 3026-3027; b) K.-S. Kim, D. Demberelnyamba and H. Lee, *Langmuir*, 2004, **20**, 556-560; c) G. Shuyan, Z. Hongjie, W. Xiaomei, M. Wenpeng, P. Chunyun and G. Liaohai, *Nanotechnology*, 2005, **16**, 1234.
19. H. S. Schrekker, M. A. Gelesky, M. P. Stracke, C. M. L. Schrekker, G. Machado, S. R. Teixeira, J. C. Rubim and J. Dupont, *J. Colloid Interface Sci.*, 2007, **316**, 189-195.
20. R. MARCILLA, D. MECERREYES, I. ODRIOZOLA, J. A. POMPOSO, J. RODRIGUEZ, I. ZALAKAIN and I. MONDRAGON, *Nano*, 2007, **02**, 169-173.
21. a) L. C. Branco, J. N. Rosa, J. J. Moura Ramos and C. A. M. Afonso, *Chem. – Eur. J.*, 2002, **8**, 3671-3677; b) X. Yuan, N. Yan, S. A. Katsyuba, E. E. Zvereva, Y. Kou and P. J. Dyson, *Phys. Chem. Chem. Phys.*, 2012, **14**, 6026-6033.
22. a) D. Zhao, Z. Fei, R. Scopelliti and P. J. Dyson, *Inorg. Chem.*, 2004, **43**, 2197-2205; b) D. Zhao, Z. Fei, T. J. Geldbach, R. Scopelliti and P. J. Dyson, *J. Am. Chem. Soc.*, 2004, **126**, 15876-15882; c) M. H. G. Precht, J. D. Scholten and J. Dupont, *J. Mol. Catal. A: Chem.*, 2009, **313**, 74-78.
23. a) L. D. Rampino and F. F. Nord, *J. Am. Chem. Soc.*, 1941, **63**, 3268-3268; b) N. Toshima and T. Yonezawa, *New J. Chem.*, 1998, **22**, 1179-1201.

24. a) L. Balogh and D. A. Tomalia, *J. Am. Chem. Soc.*, 1998, **120**, 7355-7356; b) L. K. Yeung and R. M. Crooks, *Nano Lett.*, 2001, **1**, 14-17; c) M. V. Gomez, J. Guerra, A. H. Velders and R. M. Crooks, *J. Am. Chem. Soc.*, 2009, **131**, 341-350; d) R. M. Crooks, M. Zhao, L. Sun, V. Chechik and L. K. Yeung, *Acc. Chem. Res.*, 2001, **34**, 181-190; e) L. Wu, B.-L. Li, Y.-Y. Huang, H.-F. Zhou, Y.-M. He and Q.-H. Fan, *Org. Lett.*, 2006, **8**, 3605-3608.
25. G. S. Fonseca, A. P. Umpierre, P. F. P. Fichtner, S. R. Teixeira and J. Dupont, *Chem. – Eur. J.*, 2003, **9**, 3263-3269.
26. K. T. Prabhu Charan, N. Pothanagandhi, K. Vijayakrishna, A. Sivaramakrishna, D. Mecerreyes and B. Sreedhar, *Eur. Polym. J.*, 2014, **60**, 114-122.
27. D. Zhao, Z. Fei, W. H. Ang and P. J. Dyson, *Small*, 2006, **2**, 879-883.
28. I. Biondi, G. Laurenczy and P. J. Dyson, *Inorg. Chem.*, 2011, **50**, 8038-8045.
29. N. Jiao, Z. Li, Y. Wang, J. Liu and C. Xia, *RSC Adv.*, 2015, **5**, 26913-26922.
30. a) J. Tsuji, *Palladium Reagents and Catalysts: Innovations in Organic Synthesis*, Wiley, 1997; b) J. F. Hartwig, *Organotransition Metal Chemistry: From Bonding to Catalysis*, University Science Books, 2010.
31. a) C. Torborg and M. Beller, *Adv. Synth. Catal.*, 2009, **351**, 3027-3043; b) J. Magano and J. R. Dunetz, *Chem. Rev.*, 2011, **111**, 2177-2250.
32. a) P. A. Z. Suarez, J. E. L. Dullius, S. Einloft, R. F. De Souza and J. Dupont, *Polyhedron*, 1996, **15**, 1217-1219; b) Y. Chauvin, L. Mussmann and H. Olivier, *Angewandte Chemie International Edition in English*, 1996, **34**, 2698-2700.
33. L. S. Ott, M. L. Cline, M. Deetlefs, K. R. Seddon and R. G. Finke, *J. Am. Chem. Soc.*, 2005, **127**, 5758-5759.
34. a) E. Redel, R. Thomann and C. Janiak, *Inorg. Chem.*, 2008, **47**, 14-16; b) G. S. Fonseca, G. Machado, S. R. Teixeira, G. H. Fecher, J. Morais, M. C. M. Alves and J. Dupont, *J. Colloid Interface Sci.*, 2006, **301**, 193-204; c) P. Migowski, D. Zanchet, G. Machado, M. A. Gelesky, S. R. Teixeira and J. Dupont, *Phys. Chem. Chem. Phys.*, 2010, **12**, 6826-6833.
35. a) T. Gutel, J. Garcia-Anton, K. Pelzer, K. Philippot, C. C. Santini, Y. Chauvin, B. Chaudret and J.-M. Basset, *J. Mater. Chem.*, 2007, **17**, 3290-3292; b) T. Gutel, C. C. Santini, K. Philippot, A. Padua, K. Pelzer, B. Chaudret, Y. Chauvin and J.-M. Basset, *J. Mater. Chem.*, 2009, **19**, 3624-3631; c) P. Migowski, G. Machado, S. R. Texeira, M. C. M. Alves, J. Morais, A. Traverse and J. Dupont, *Phys. Chem. Chem. Phys.*, 2007, **9**, 4814-4821; d) G. Salas, A. Podgorsek, P. S. Campbell, C. C. Santini, A. A. H. Padua, M. F. Costa Gomes, K. Philippot, B. Chaudret and M. Turmine, *Phys. Chem. Chem. Phys.*, 2011, **13**, 13527-13536.
36. a) J. D. Scholten, G. Ebeling and J. Dupont, *Dalton Trans.*, 2007, 5554-5560; b) M. H. G. Prechtel, P. S. Campbell, J. D. Scholten, G. B. Fraser, G. Machado, C. C. Santini, J. Dupont and

- Y. Chauvin, *Nanoscale*, 2010, **2**, 2601-2606; c) P. S. Campbell, C. C. Santini, D. Bouchu, B. Fenet, K. Philippot, B. Chaudret, A. A. H. Padua and Y. Chauvin, *Phys. Chem. Chem. Phys.*, 2010, **12**, 4217-4223; d) Y. E. Corilo, F. M. Nachtigall, P. V. Abdelnur, G. Ebeling, J. Dupont and M. N. Eberlin, *RSC Adv.*, 2011, **1**, 73-78.
37. L. Magna, Y. Chauvin, G. P. Niccolai and J.-M. Basset, *Organometallics*, 2003, **22**, 4418-4425.
38. I. Biondi, G. Lauenczy and P. J. Dyson, *Inorg. Chem.*, 2011, **50**, 8038-8045.
39. a) C. Chiappe, D. Pieraccini, D. Zhao, Z. Fei and P. J. Dyson, *Adv. Synth. Catal.*, 2006, **348**, 68-74; b) Z. Fei, D. Zhao, D. Pieraccini, W. H. Ang, T. J. Geldbach, R. Scopelliti, C. Chiappe and P. J. Dyson, *Organometallics*, 2007, **26**, 1588-1598.
40. a) P. Barbaro, C. Bianchini, G. Giambastiani, W. Oberhauser, L. M. Bonzi, F. Rossi and V. Dal Santo, *Dalton Trans.*, 2004, 1783-1784; b) P. Barbaro, *Chem. – Eur. J.*, 2006, **12**, 5666-5675; c) P. Barbaro and F. Liguori, *Chem. Rev.*, 2008, **109**, 515-529; d) C. Moreno-Marrodan, F. Liguori, E. Mercade, C. Godard, C. Claver and P. Barbaro, *Catal. Sci. Technol.*, 2015, **5**, 3762-3772.
41. a) B. Corain, M. Zecca and K. Jeřábek, *J. Mol. Catal. A: Chem.*, 2001, **177**, 3-20; b) M. Králik and A. Biffis, *J. Mol. Catal. A: Chem.*, 2001, **177**, 113-138.
42. S. S. Zalesskiy and V. P. Ananikov, *Organometallics*, 2012, **31**, 2302-2309.
43. Y. S. Chun, J. Y. Shin, C. E. Song and S.-g. Lee, *Chem. Comm.*, 2008, 942-944.
44. Y. Zhang, X.-Y. Quek, L. Wu, Y. Guan and E. J. Hensen, *J. Mol. Catal. A: Chem.*, 2013, **379**, 53-58.
45. J. D. Scholten, B. C. Leal and J. Dupont, *ACS Catal.*, 2012, **2**, 184-200.
46. W. M. Lemke, R. B. Kaner and P. L. Diaconescu, *Inorg. Chem. Front.*, 2015, **2**, 35-41.
47. S. Kidambi and M. L. Bruening, *Chem. Mater.*, 2005, **17**, 301-307.
48. R. W. J. Scott, H. Ye, R. R. Henriquez and R. M. Crooks, *Chem. Mater.*, 2003, **15**, 3873-3878.
49. a) N. Miyaura, T. Yanagi and A. Suzuki, *Synth. Commun.*, 1981, **11**, 513-519; b) N. Miyaura and A. Suzuki, *Chem. Rev.*, 1995, **95**, 2457-2483; c) J.-P. Corbet and G. Mignani, *Chem. Rev.*, 2006, **106**, 2651-2710; d) Yin and J. Liebscher, *Chem. Rev.*, 2007, **107**, 133-173; e) F. Bellina, A. Carpita and R. Rossi, *Synthesis*, 2004, 2419-2440; f) D.-H. Lee, J.-H. Kim, B.-H. Jun, H. Kang, J. Park and Y.-S. Lee, *Org. Lett.*, 2008, **10**, 1609-1612.
50. a) L. Pu, *Chem. Rev.*, 1998, **98**, 2405-2494; b) L. F. Tietze, G. Ketschau, U. Heuschert and G. Nordmann, *Chem. – Eur. J.*, 2001, **7**, 368-373; c) A. F. Littke and G. C. Fu, *Angew. Chem. Int. Ed.*, 2002, **41**, 4176-4211.
51. B. Karimi, D. Elhamifar, J. H. Clark and A. J. Hunt, *Chem. – Eur. J.*, 2010, **16**, 8047-8053.
52. S. Li, J. Wang, Y. Kou and S. Zhang, *Chem. – Eur. J.*, 2010, **16**, 1812-1818.

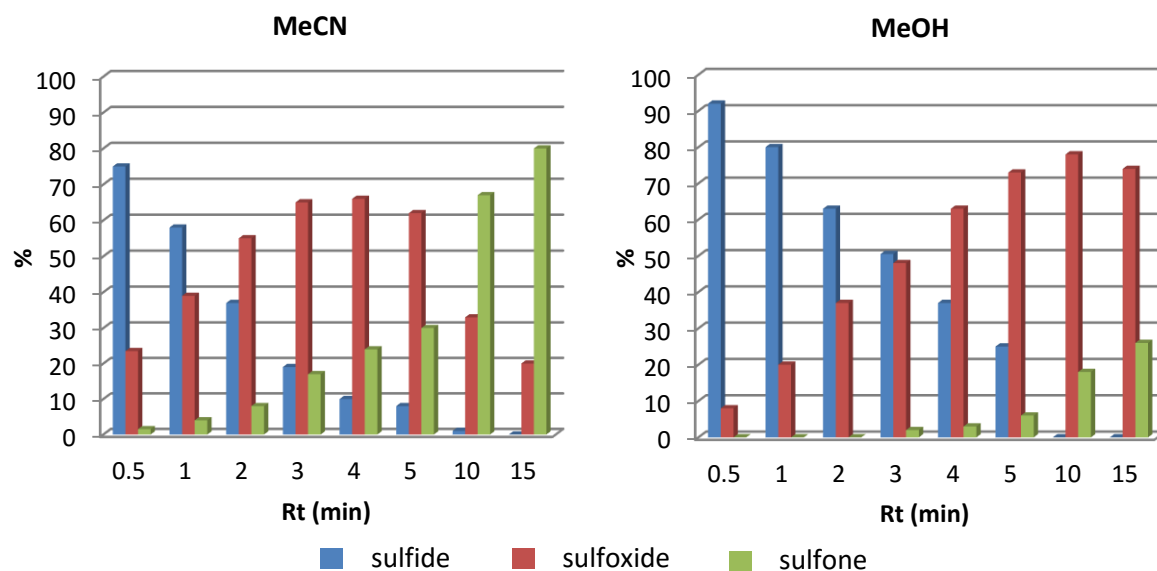
53. C. Pavia, E. Ballerini, L. A. Bivona, F. Giacalone, C. Aprile, L. Vaccaro and M. Gruttadauria, *Adv. Synth. Catal.*, 2013, **355**, 2007-2018.
54. a) B. P. Carrow and J. F. Hartwig, *J. Am. Chem. Soc.*, 2011, **133**, 2116-2119; b) N. Miyaoura, *J. Organomet. Chem.*, 2002, **653**, 54-57; c) A. A. C. Braga, N. H. Morgon, G. Ujaque, A. Lledós and F. Maseras, *J. Organomet. Chem.*, 2006, **691**, 4459-4466; d) L. J. Goossen, D. Koley, H. L. Hermann and W. Thiel, *J. Am. Chem. Soc.*, 2005, **127**, 11102-11114; e) Y. Suzaki and K. Osakada, *Organometallics*, 2006, **25**, 3251-3258.
55. D. D. Dolliver, B. T. Bhattarai, A. Pandey, M. L. Lanier, A. S. Bordelon, S. Adhikari, J. A. Dinsler, P. F. Flowers, V. S. Wills, C. L. Schneider, K. H. Shaughnessy, J. N. Moore, S. M. Raders, T. S. Snowden, A. S. McKim and F. R. Fronczek, *J. Org. Chem.*, 2013, **78**, 3676-3687.
56. a) A. El Kadib, K. McEleney, T. Seki, T. K. Wood and C. M. Crudden, *ChemCatChem*, 2011, **3**, 1281-1285; b) S. MacQuarrie, J. H. Horton, J. Barnes, K. McEleney, H.-P. Looock and C. M. Crudden, *Angew. Chem. Int. Ed.*, 2008, **47**, 3279-3282.
57. a) Y. M. A. Yamada, K. Takeda, H. Takahashi and S. Ikegami, *J. Org. Chem.*, 2003, **68**, 7733-7741; b) R. Nishio, M. Sugiura and S. Kobayashi, *Org. Lett.*, 2005, **7**, 4831-4834; c) C. M. Crudden, M. Sateesh and R. Lewis, *J. Am. Chem. Soc.*, 2005, **127**, 10045-10050; d) W. J. Sommer and M. Weck, *Adv. Synth. Catal.*, 2006, **348**, 2101-2113; e) W. Han, C. Liu and Z. Jin, *Adv. Synth. Catal.*, 2008, **350**, 501-508; f) K. Köhler, R. G. Heidenreich, S. S. Soomro and S. S. Pröckl, *Adv. Synth. Catal.*, 2008, **350**, 2930-2936.
58. M. Pérez-Lorenzo, *J. Phys. Chem. Lett.*, 2012, **3**, 167-174.
59. R. Narayanan and M. El-Sayed, *Top. Catal.*, 2008, **47**, 15-21.
60. a) N. T. S. Phan, M. Van Der Sluys and C. W. Jones, *Adv. Synth. Catal.*, 2006, **348**, 609-679; b) R. Narayanan, C. Tabor and M. El-Sayed, *Top. Catal.*, 2008, **48**, 60-74; c) J. G. de Vries, *Dalton Trans.*, 2006, 421-429.
61. a) Z. Niu, Q. Peng, Z. Zhuang, W. He and Y. Li, *Chem. – Eur. J.*, 2012, **18**, 9813-9817; b) M. I. Burguete, E. García-Verdugo, I. Garcia-Villar, F. Gelat, P. Licence, S. V. Luis and V. Sans, *J. Catal.*, 2010, **269**, 150-160; c) F. Zhao, M. Shirai, Y. Ikushima and M. Arai, *J. Mol. Catal. A: Chem.*, 2002, **180**, 211-219.
62. a) C. M. Marrodan, D. Berti, F. Liguori and P. Barbaro, *Catal. Sci. Technol.*, 2012, **2**, 2279-2290; b) G. Grochola, I. K. Snook and S. P. Russo, *J. Chem. Phys.*, 2008, **129**, 154708; c) É. Ansoborlo, B. Amekraz, C. Moulin, V. Moulin, F. Taran, T. Bailly, R. Burgada, M.-H. Hengé-Napoli, A. Jeanson, C. Den Auwer, L. Bonin and P. Moisy, *C. R. Chim.*, 2007, **10**, 1010-1019.
63. A. R. Siamaki, A. E. R. S. Khder, V. Abdelsayed, M. S. El-Shall and B. F. Gupton, *J. Catal.*, 2011, **279**, 1-11.

64. a) S.-M. Huang, L. Wang and B.-L. He, *React. Polym.*, 1992, **16**, 93-103; b) Z. Karpiński, in *Adv. Catal.*, eds. H. P. D.D. Eley and B. W. Paul, Academic Press, 1990, vol. Volume 37, pp. 45-100.
65. Z. M. Michalska, B. Ostaszewski, J. Zientarska and J. W. Sobczak, *J. Mol. Catal. A: Chem.*, 1998, **129**, 207-218.
66. D. Astruc, *Nanoparticles and Catalysis*, Wiley, 2008.
67. J. M. Richardson and C. W. Jones, *J. Catal.*, 2007, **251**, 80-93.
68. S. J. Broadwater and D. T. McQuade, *J. Org. Chem.*, 2006, **71**, 2131-2134.
69. W. Chen, Y. Zhang, L. Zhu, J. Lan, R. Xie and J. You, *J. Am. Chem. Soc.*, 2007, **129**, 13879-13886.
70. L.-J. Zhao, C. K.-W. Kwong, M. Shi and P. H. Toy, *Tetrahedron*, 2005, **61**, 12026-12032.
71. *United States Pat.*, US4560690 A, 1985.
72. Y. Wu, P. Y. Choy and F. Y. Kwong, *Org. Biomol. Chem.*, 2014, **12**, 6820-6823.
73. H. Liu, B. Yin, Z. Gao, Y. Li and H. Jiang, *Chem. Comm.*, 2012, **48**, 2033-2035.
74. J. Yang and L. Wang, *Dalt. Trans.*, 2012, **41**, 12031-12037.
75. H. Wang, L. Li, X.-F. Bai, W.-H. Deng, Z.-J. Zheng, K.-F. Yang and L.-W. Xu, *Green Chem.*, 2013, **15**, 2349-2355.
76. Z. Liu, H. Tan, L. Wang, T. Fu, Y. Xia, Y. Zhang and J. Wang, *Angew. Chem. Int. Ed.*, 2015, **54**, 3056-3060.
77. H. Yan, P. Chellan, T. Li, J. Mao, K. Chibale and G. S. Smith, *Tetrahedron Lett.*, 2013, **54**, 154-157.
78. R.-J. Tang, Q. He and L. Yang, *Chem. Comm.*, 2015, **51**, 5925-5928.

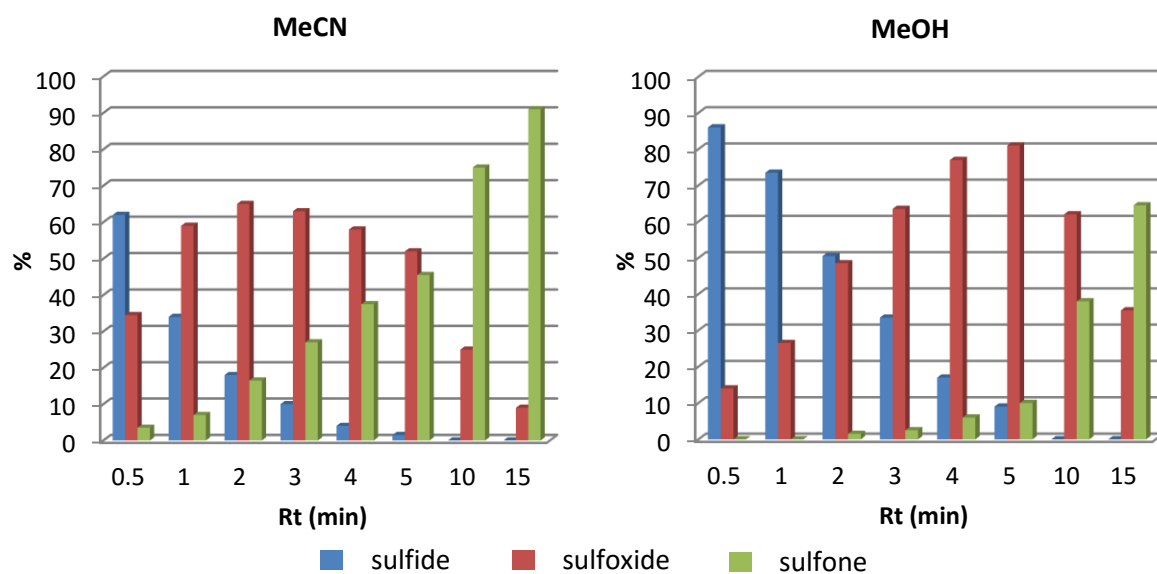
Appendices

A.1. Segmented Flow Oxidation of Thioanisole with Varying H₂O₂ Concentrations

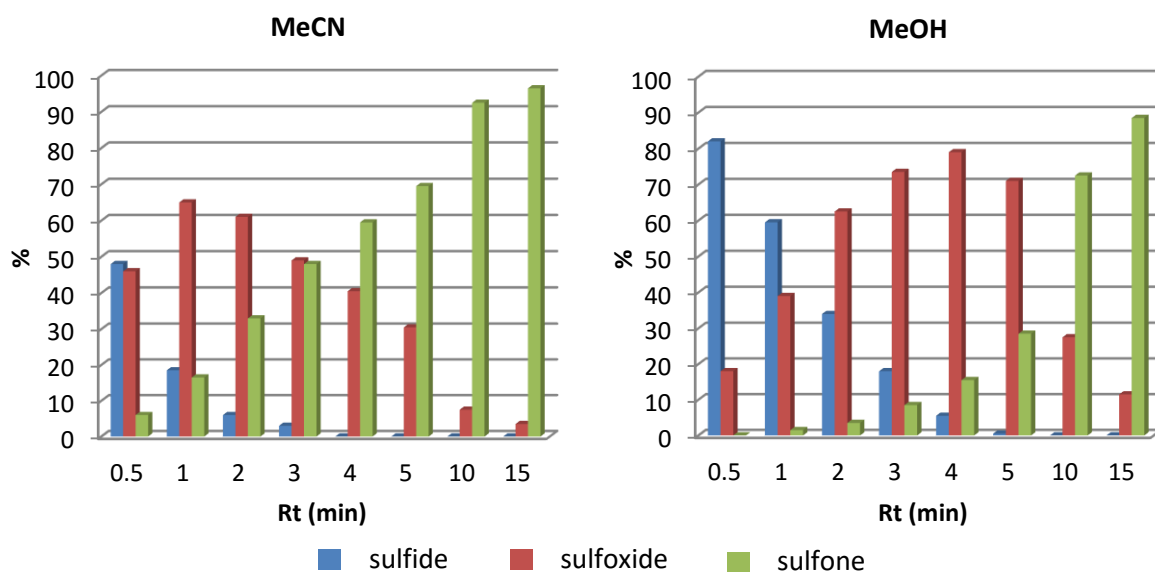
A.1.1. Conversion-selectivity profiles at 30°C with 2 equivalents of H₂O₂



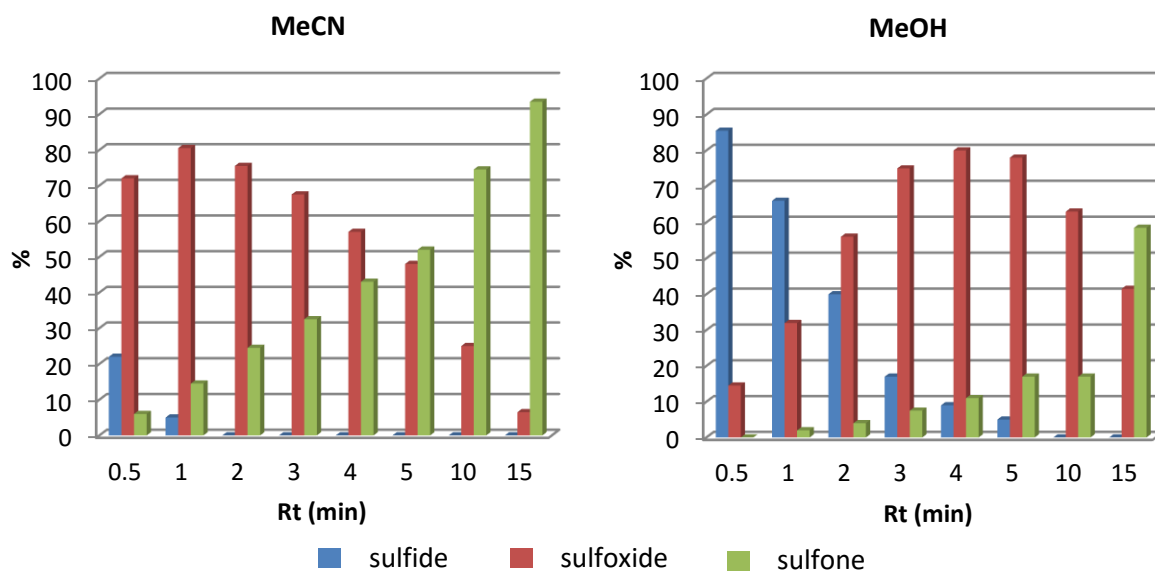
A.1.2. Conversion-selectivity profiles at 30°C with 3 equivalents of H₂O₂



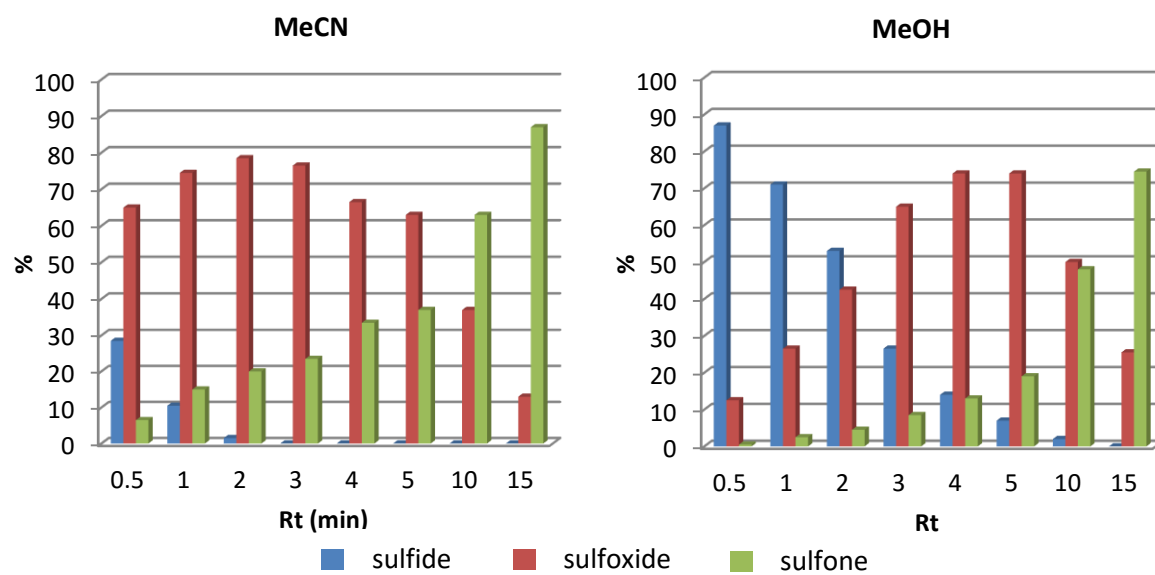
A.1.3. Conversion-selectivity profiles at 30°C with 6 equivalents of H₂O₂



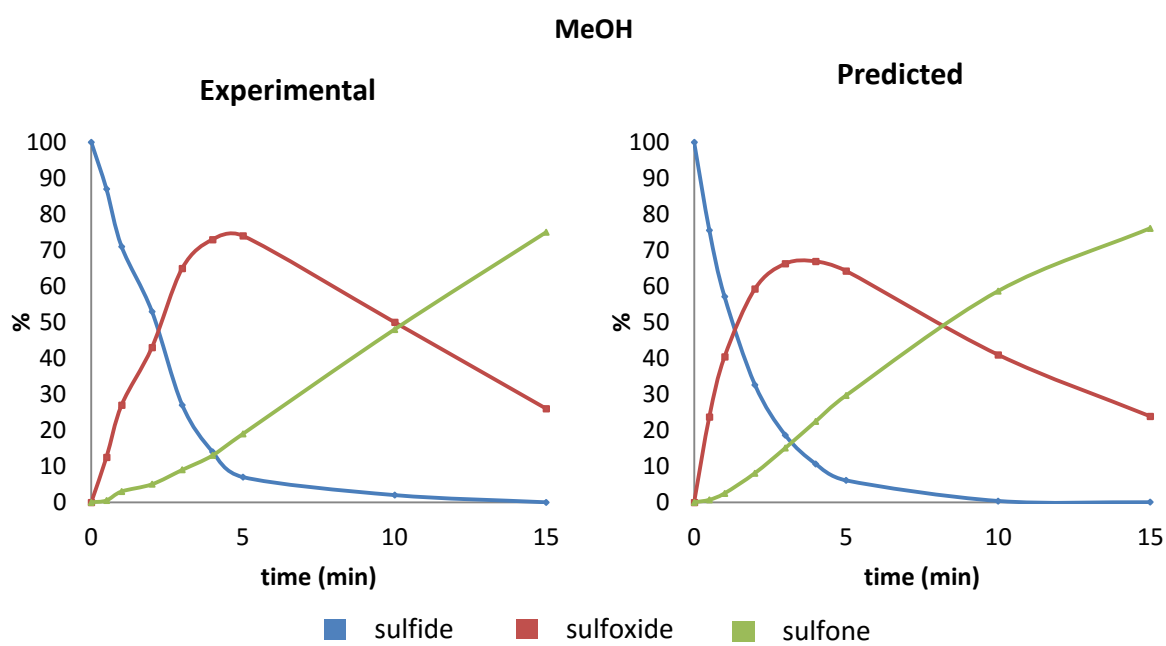
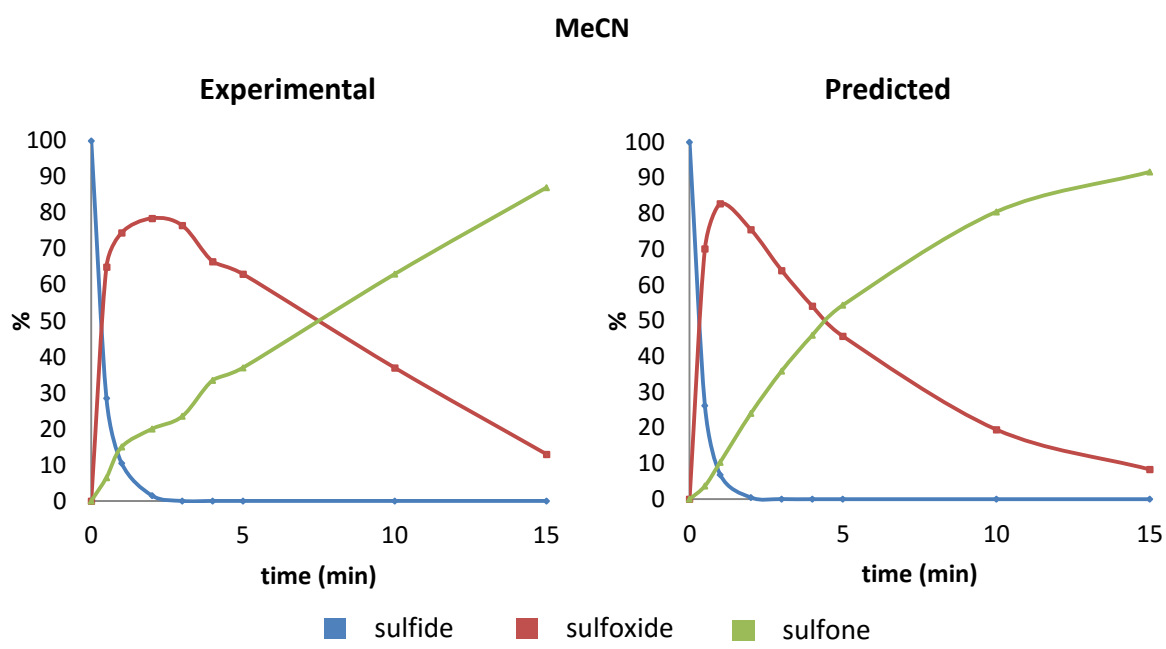
A.1.4. Conversion-selectivity profiles at 30°C with 12 equivalents of H₂O₂



A.1.5. Conversion-selectivity profiles at 30°C with 20 equivalents of H₂O₂

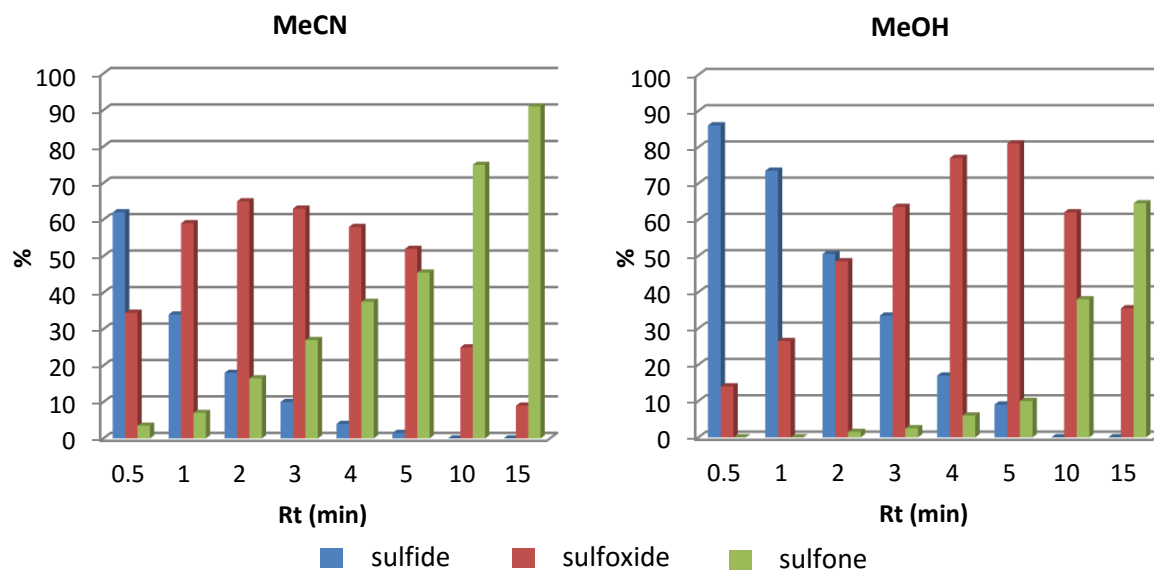


A.2. Kinetic plots for the oxidation of thioanisole using 20 equivalents of H₂O₂ at 30°C

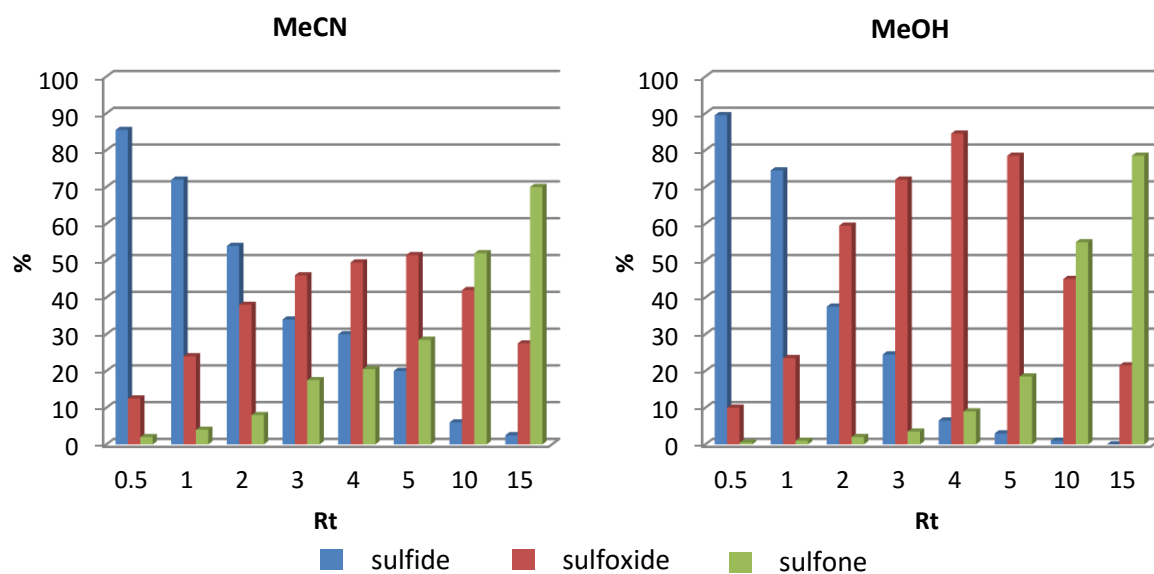


A.3. Conversion-Selectivity Profiles for Segmented Flow Sulfoxidations at 30°C with 3 equivalents of H₂O₂

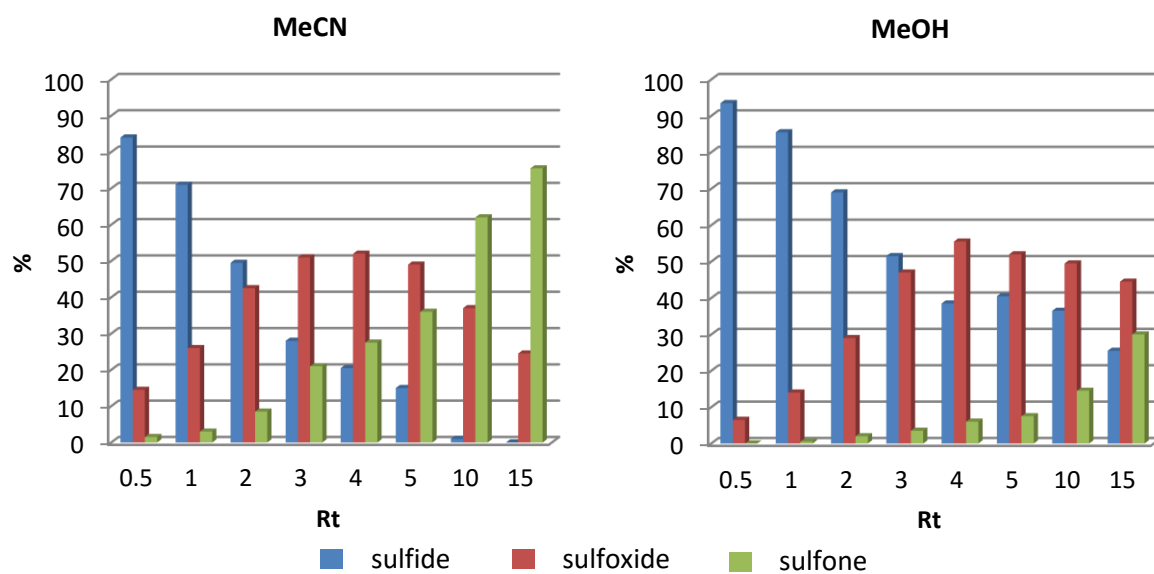
A.3.1. Thioanisole



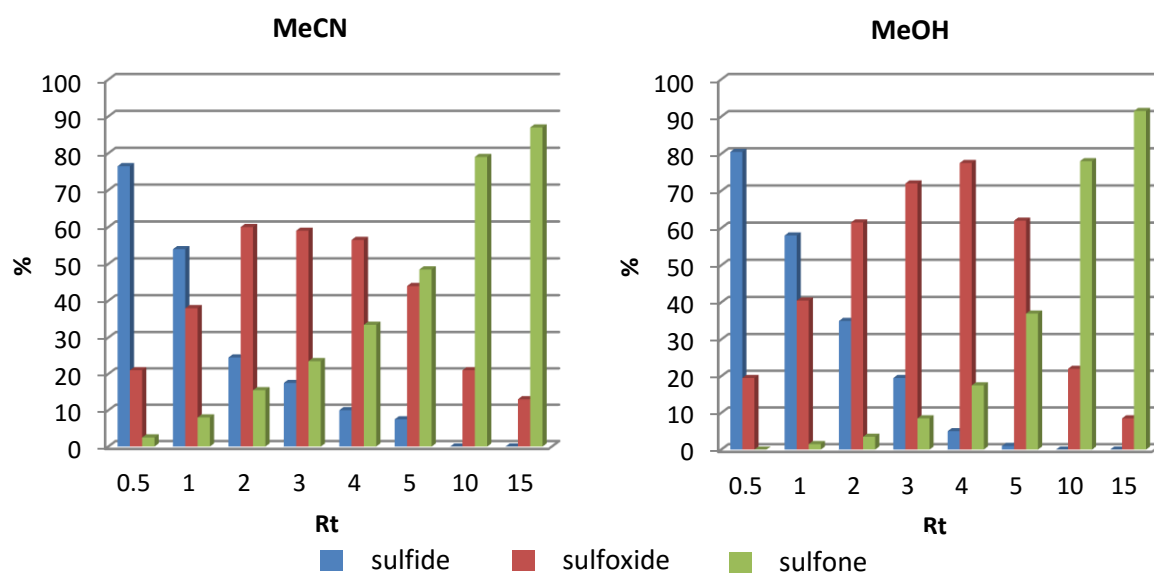
A.3.2. Benzyl phenyl sulfide



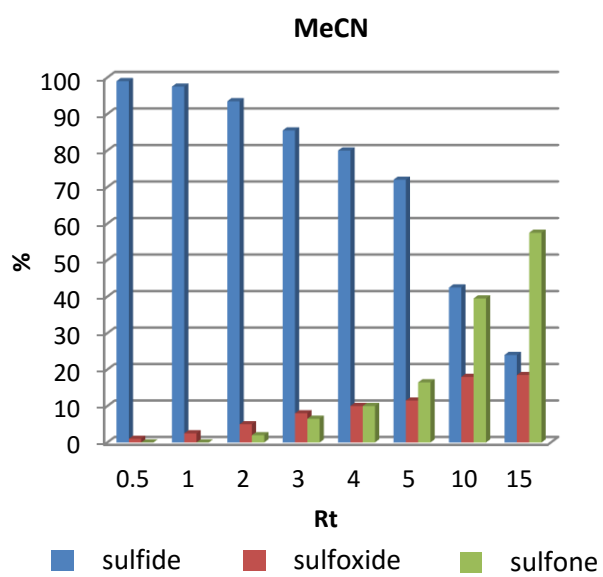
A.3.3. 4-nitrothioanisole



A.3.4. Homoallyl phenyl sulfide

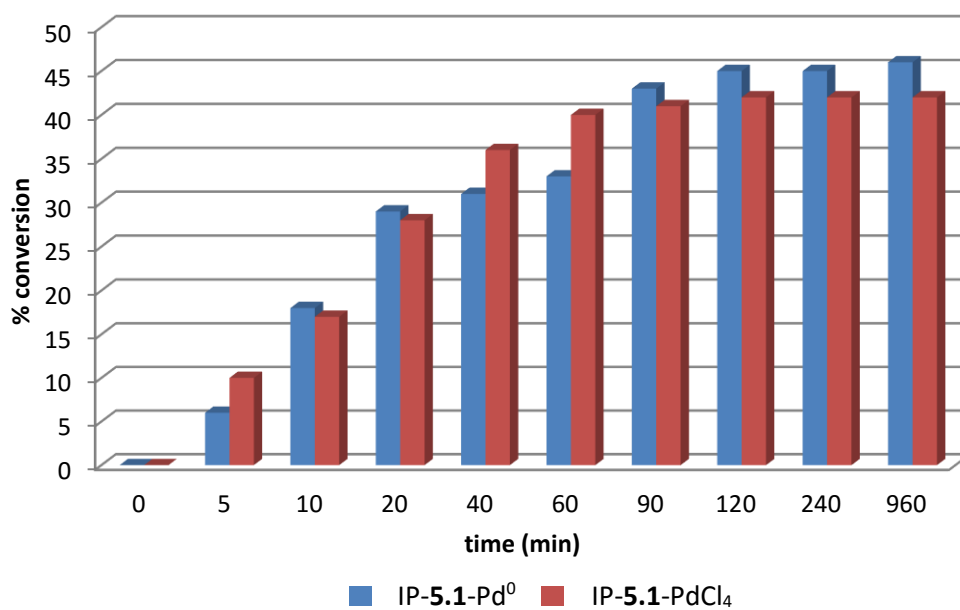


A.3.5. Dibenzothiophene

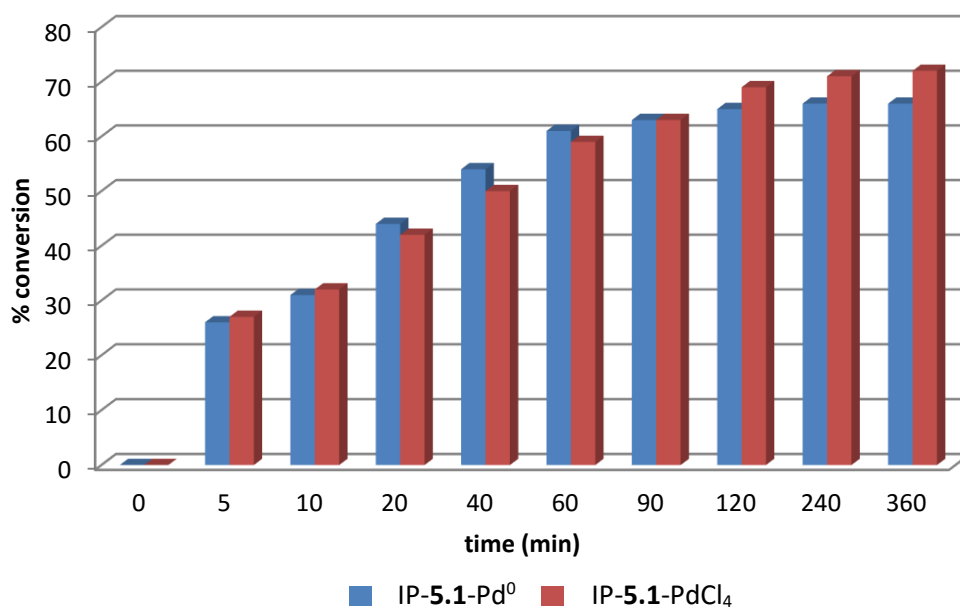


A.4. Reaction Profiles for PIILP Catalysed Suzuki Miyaura Cross-Couplings

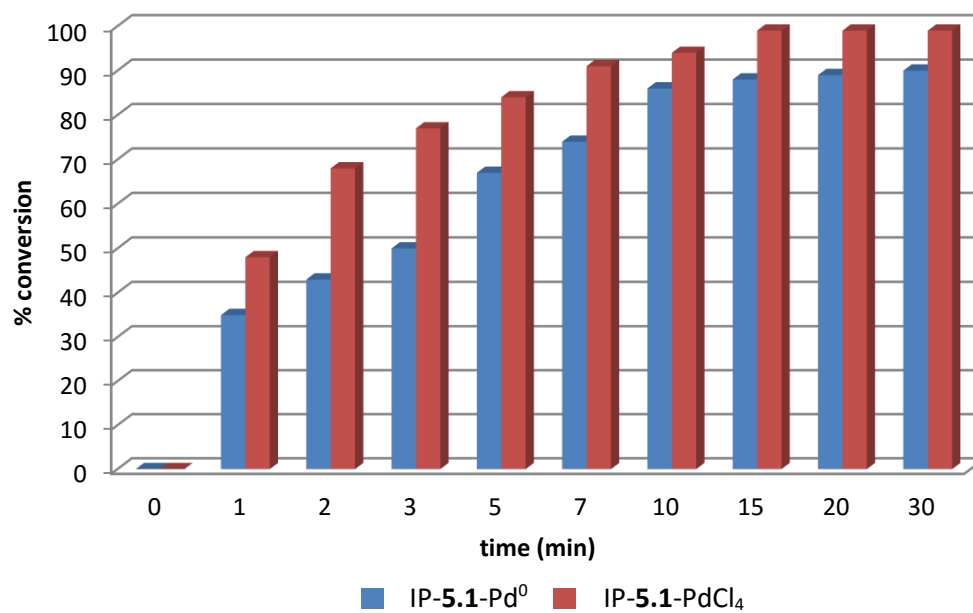
A.5.1. 2-bromotoluene



A.5.2. 4-bromotoluene



A.5.3. 4-bromobenzonitrile



A.5.4. 3-bromonitrobenzene

